HYDROGEOCHEMICAL CHARACTERIZATION OF THE ROCKS OF THE ACCRA PLAINS FOR A RADIOACTIVE WASTE REPOSITORY

ERIC TETTEH GLOVER

(10260486)

DEPARTMENT OF NUCLEAR SCIENCE AND APPLICATIONS

GRADUATE SCHOOL OF NUCLEAR AND ALLIED SCIENCES

UNIVERSITY OF GHANA, LEGON

PhD

JUNE 2013

HYDROGEOCHEMICAL CHARACTERIZATION OF THE ROCKS OF THE ACCRA PLAINS FOR A RADIOACTIVE WASTE REPOSITORY

THIS DISSERTATION IS SUBMITTED TO THE UNIVERSITY OF GHANA, LEGON IN PARTIAL FULFILLMENT OF THE REQUIREMENT FOR THE AWARD OF DOCTOR OF PHILOSOPHY DEGREE IN NUCLEAR AND RADIOCHEMISTRY

ERIC TETTEH GLOVER (10260486)

BSc (Russia), 1994; MSc (Russia), 1996; MSc (UK), 2003

DEPARTMENT OF NUCLEAR SCIENCES AND APPLICATIONS

GRADUATE SCHOOL OF NUCLEAR AND ALLIED SCIENCES

UNIVERSITY OF GHANA

JUNE 2013

DECLARATION

This dissertation is the result of research work undertaken by Eric T. Glover in the Department of Nuclear Science and Applications, Graduate School of Nuclear and Allied Sciences University of Ghana under the supervision of Dr. Thomas Tetteh Akiti and Prof. Shiloh D. Osae, both of the Graduate School of Nuclear and Allied Sciences, University of Ghana

Signature

Eric T. Glover
(Student)

Date

Signature

Dr. Thomas T. Akiti

(Principal Supervisor)

Date

Signature

Professor Shiloh D. Osae

(Co-Supervisor)

Date

ACKNOWLEDGMENT

First and foremost, l would like to give thanks to the Almighty God for Grace and strength which has enabled me accomplish this task. I wish to express my sincere thanks and appreciation to my principal research supervisor, Dr. Thomas Tetteh Akiti, for his time, guidance, encouragement and positive criticisms throughout this study. To my associate supervisor, Prof Shiloh D. Osae, I am grateful for the considerable time he spent having meaningful discussions with me during the course of this research. Results of this dissertation could not have been possible without the assistance of the late Prof Giovanni Maria Zuppi. I am grateful for his assistance in obtaining a fellowship from the International Centre for Theoretical Physics (ICTP) which enabled me carry out analyses of my samples in the Institute of Environmental Geology and Geoengineering (IGAG), National Research Council (CNR) Rome, Itay. I would like to acknowledge the support and encouragement of Prof. John Justice Fletcher, who has been particularly helpful both prior to and during this Ph.D research work. I would like to extend my appreciation to Prof S. Dampare for his comments and suggestions that helped shape my research work.

I am most grateful to the Training and Research in Italian Laboratory Programme of ICTP which funded my 6 months stay in Rome for analyses of my samples. I would like to thank the staff of IGAG especially Dr. Mauro Brilli, Dr. Giovanni Accordi, Dr Girolamo Belardi, Dr. Mario Voltaggio, Dr. Massimo Spadoni, Mr.Marcello Serracino, Mr. Italo Maurizi for their assistance in analyses of my samples.

I would also like to thank my fellow research scientists at Ghana Atomic Energy Commission especially Dr. F. G. Ofosu, Mr. O. C. Oppon, Dr. A. Faanu, Dr. R. J. Fianko, Dr. D. Addotey,

Mr. S. Ganyaglo, Prof. D. Adomako, Mr Felix Aidoo and staff of the National Radioactive Waste Management Centre, who have given me much encouragement and assistance during the course of this research. I would also like to thank staff of the Isotope Hydrology and Atomic Absorption Spectrometry laboratories of the National Nuclear Research Institute.

Finally, l would like to thank my parents and the entire family for their numerous sacrifices and for providing me with the best of education. God richly bless them.

TABLE OF CONTENTS

CHAPTER TWO LITERATURE REVIEW

LIST OF TABLES

Tables in Appendices

LIST OF FIGURES

Figures in Appendices

Abstract

The geological disposal of radioactive waste in well-engineered repositories in stable geological formations has been internationally accepted as a suitable option. The disposal system makes use of both man-made and natural barriers to contain and isolation the radionuclides. Precambrian crystalline rocks are regarded as one of the favourable host rocks for a radioactive waste repository. Hydrogeochemical characterization of the rocks of the Accra Plains, located in the south eastern part of Ghana underlain by crystalline gneisses and schists, has been carried out to determine its suitability for a radioactive waste repository.

The mineralogical analyses of the rock and soil samples collected indicated that feldspars, hornblende, biotite, quartz with minor pyroxenes are the primary minerals with illite, kaolinite, montmorillonite and carbonates occurring as secondary minerals. The accessory minerals present include chlorite, epidote, magnetite, rutile and sphene. The iron rich minerals, magnetite, biotite, chlorite, and amphiboles will create a reducing environment required for a repository.

The pH value of the groundwater at the Valley View University is lower than the recommended pH values (6-10) for a repository environment, making the site unsuitable for a radioactive waste repository. Calcium and magnesium ions which constitute 48% of the total cations in the groundwater will provide a stable chemical environment for a backfill and buffer materials.

The groundwaters of the Accra Plains is composed of three (3) water types. Groundwater Type 1 is composed of Na-Mg-Ca-Cl-HCO_3 and found along the foot of the Akwapim-Togo Mountains. Groundwater Type 2 is composed of Na-Mg-Ca-Cl and found in most parts of the

central area of the Plains whilst groundwater type 3 occur along the coastal zone of the Plains and composed of Na-Ca-Cl.

Silicate mineral weathering is the predominant influence on the composition of the groundwaters. Evaporative enrichment of recharging waters, ion exchange and reverse ion exchange also controls the chemical composition of the groundwater especially along the coastal areas of the Plain.

The stability diagram shows that the chemistry of the groundwater favours the formation of kaolinite and montmorillonite. The long time stability of these minerals together with their ion exchange properties which can retard the migration of long-lived radionuclides makes them a useful backfill and or buffer material for a radioactive waste repository.

The groundwater had an average isotopic value of –3.19‰ for $\delta^{18}O$ and –14.36‰ for $\delta^{2}H$. The groundwaters at Valley View University are more depleted than the other groundwaters in the Plains suggesting that the groundwater was recharge at a high elevation. The Akwapim-Togo Mountains would be the source of these groundwaters, implying there are preferential channels or routes through which waters that are recharged on the Akwapim-Togo Mountains find their way to the university campus. This makes that area unsuitable for a waste repository.

The activity concentration of ^{40}K was found to be higher than the other naturally occurring radionuclides which can be attributed to the abundance of K-feldspar minerals in the geological formation. The highest radionuclide concentrations were measured in the rock samples collected

from GAEC premises whereas the Krobo Mountains samples had the lowest radionuclide concentrations. The relative U enrichment in the GAEC samples suggests reducing condition and precipitation of UO_2. The Ashiaman samples reflected high Th concentration indicating preferential removal of uranium by leaching through groundwater infiltration.

The area between the Akwapim Togo and the Valley View University was found to be unsuitable for a radioactive waste repository due to preferential channels which will easily saturate the repository. Secondly the pH of the groundwaters were lower than the required pH conditions for a radioactive waste repository

The presence of redox-sensitive minerals in the mafic gneisses which will ensure a reducing environment for a radioactive repository makes the hydrogeochemical conditions of the geological formation at Okwenya and the foothills of the Krobo Mountains are favourable for a repository. The presence of montmorillonite clay minerals in these areas will give the repository with a good buffer material which will be stable for a long period of time and also retard the migration of the long live radionuclides.

Chapter One

Introduction

1.1 Background

Radioactive waste materials are generated from applications of radioactive materials in the fields of medicine, agriculture, industry and research as well as from the use of nuclear energy for electricity production. They present a potential hazard to human health and the environment and must be managed safely so as to ensure any associated risks do not exceed acceptable levels both now and in the future. This is required both by law and by the precept that any society which benefited from the use of the radioactive materials should act in a responsible manner with respect to mankind and the environment. Although we can make every effort to minimise the generation of radioactive waste materials and store the waste safely, it is inevitable that there will always remain some waste materials that have to be disposed.

The radioactive waste materials contain radionuclides with half–lives ranging from less than a day to thousands of millions of years. Storage of the waste materials will result in the decay of the short-lived radionuclides to insignificant levels, but the long-lived radionuclides present a long term potential hazard. Indefinite storage of waste materials containing long-lived radionuclides is not the best option, because of the cost involved in monitoring, maintaining and providing security for the storage facility. The radiation doses that would be received in maintaining and refurbishing the storage facilities can be high. Indefinite storage also requires the maintenance of expertise. Adoption of indefinite storage policy will also place an unacceptable burden on future generation from practices that provided benefit to the present

generation. Sustainable operation of a nuclear industry therefore requires an acceptable and safe disposal route for the radioactive waste materials generated.

Nature has proven that geological isolation of radioactive waste is possible through some natural examples (or "analogues"). The most significant example occurred almost 2 billion years ago at Oklo in what is now Gabon in West Central Africa, where sixteen spontaneous nuclear reactors operated within a rich vein of uranium ore. The uranium in the natural reactors occurred as the mineral uranite (UO_2) which is commonly used as a nuclear fuel (Knight, 1998). At that time the concentration of ^{235}U in the natural uranium was about 3.68% enriched to achieve self-sustaining natural fission reaction. These natural nuclear reactors continued operation for about 500,000 years before dying away. They produced all the radionuclides found in High Level Waste (HLW), including over 5 tonnes of fission products and 1.5 tonnes of plutonium, all of which remained at the site and eventually decayed into non-radioactive elements. Despite thousands of centuries of tropical rain and subsurface water, the long-lived radioactive waste from these reactors migrated less than 10 metres (Curtis, 1985). Furthermore, deposits of uranium ore exist underground without any expression of this by release of radionuclides at the surface (e.g. at Cigar Lake in Canada and Olympic Dam in South Australia).

Careful burial of radioactive waste in well-engineered ‘repositories’ in stable geological environments without any economic value, at specially selected sites, at various depths below the land surface depending on the activity of the waste material has been accepted as the favoured disposal solution. This disposal option known as ‘geological disposal’ provides permanent safety not just for the present generation, but also for the future generation. The aims of geological disposal are to:

- Contain the waste until most of the radioactivity and especially those associated with shorter-lived radionuclides has decayed;
- Isolate the waste from the biosphere and substantially reduce the likelihood of inadvertent human intrusion into the waste;
- Delay any significant migration of radionuclides to the biosphere until a time in the very far future when much of the radioactivity will have decayed; and
- Ensure that any levels of radionuclides eventually reaching the biosphere are such that possible radiological impacts in the future are acceptably low.

1.2. Classification of Radioactive Waste Materials

The radioactive waste materials for which disposal is considered cover a wide spectrum of solid, liquid and gaseous forms. On the basis of half-life and type of radioactivity they are classified into six classes of waste as follows (IAEA, 2009)

- Exempt Waste (EW): Waste materials that meet the criteria for clearance, exemption or exclusion from regulatory control for radiation protection purposes as described in the IAEA Safety Standards Series, GSG-1 (IAEA 2009).

- Very Short Lived Waste (VSLW): Waste materials that can be stored for decay over a limited period of up to a few years and subsequently cleared from regulatory control according to arrangements approved by a regulatory body, for uncontrolled disposal, reuse or discharge. This class includes waste containing primarily radionuclides with very short half-lives often used for research and medical purposes. They also consist of

demolished material (such as concrete, plastic, bricks, metal, valves, piping etc.) produced during rehabilitation or dismantling operations on nuclear industrial sites.

- Very Low Level Waste (VLLW): Waste materials that does not necessarily meet the criteria of EW, but that does not need a high level of containment and isolation and, therefore, is suitable for disposal in near surface landfill type facilities with limited regulatory control. Such landfill type facilities may also contain other hazardous waste materials. Typical waste in this class includes soil and rubble with low levels of activity concentration. Concentrations of longer lived radionuclides in VLLW are generally very limited. Industries, such as food processing, chemical, steel, mining etc produce VLLW as a result of the concentration of natural occurring radioactive materials present in certain minerals used in their manufacturing processes.

- Low Level Waste (LLW): Waste materials that are above clearance levels, but with limited amounts of long lived radionuclides. Such waste requires robust isolation and containment for periods of up to a few hundred years and is suitable for disposal in engineered near surface facilities. This class covers a very broad range of waste. They are generated from hospitals and industry, as well as the nuclear fuel cycle. It comprises paper, rags, tools, clothing, filters etc. It comprises 90% of the volume but only 1% of the radioactivity of all radioactive waste materials. To reduce its volume, it is often compacted or incinerated before disposal.

- Intermediate Level Waste (ILW): Waste materials that, because of their content (higher amount of radioactivity), particularly of long lived radionuclides, require a greater

degree of containment and isolation. ILW may contain alpha emitting radionuclides that will not decay to a level of activity concentration acceptable for near surface disposal. Therefore, waste in this class requires disposal at greater depths, of the order of tens of metres to a few hundred metres. However, ILW needs no provision, or only limited provision, for heat dissipation during its storage and disposal. It typically comprises ion-exchange resins, chemical sludges and metal fuel cladding, as well as contaminated materials from reactor decommissioning. Smaller items and any non-solids may be solidified in concrete or bitumen for disposal. It makes up some 7% of the volume and has 4% of the radioactivity of all radioactive waste.

- High Level Waste (HLW): Waste material with levels of activity concentration high enough to generate significant quantities of heat by the radioactive decay process or waste with large amounts of long lived radionuclides that require remote handling. It contains fission products and transuranic elements generated in the reactor core. HLW accounts for over 95% of the total radioactivity produced in the process of electricity generation. There are two distinct kinds of HLW:

  - used fuel itself in fuel rods, or

  - separated waste from reprocessing the used fuel as described below.

  HLW has both long-lived and short-lived components, depending on the length of time it will take for the radioactivity of particular radionuclides to decrease to levels that are considered no longer hazardous for people and the surrounding environment. Disposal in deep, stable geological formations usually several hundred metres or more below the surface is the generally recognized option for disposal of HLW.

Treatment and conditioning processes are used to convert the radioactive waste materials into a form that is suitable for its subsequent management, such as transportation, storage and final disposal. Of these types of wastes produced, HLW are of greatest concern, as they require isolation from the biosphere for periods of thousands of years to allow the intensely radioactive, shorter-lived elements to decay below acceptable levels, followed by continued isolation of up to one million years so that contamination from the long-lived radionuclides does not occur. These dual requirements can be seen in Figure 1.1 which shows the total and individual activities of HLW as a function of time. The most practical method of meeting these requirements involves firstly the incorporation and immobilization of the waste into a solid matrix followed by long-term isolation in a suitable repository.

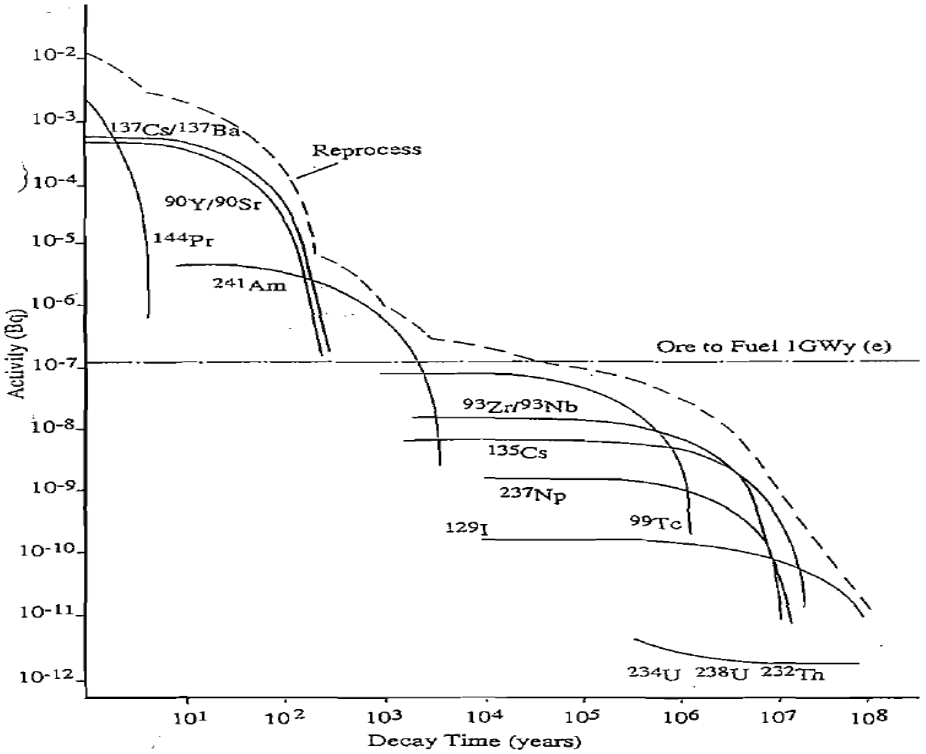

Figure. 1.1. Total and individual activities of waste produced from a 1GWe light Water reactor during one year of operation. (OECD, 1984)

1.3. Radioactive Waste Status in Ghana

Records have it that, the use of radioactive materials in Ghana began in 1952 at the Physics Department of the University College of the Gold Coast now University of Ghana (GAEC Annual Report, 2001). Since then, application of radioactive materials have grown and with it, the general awareness in the country of the numerous economic benefits to be derived from application of radioactive materials. They are being used in the medicine for cancer treatment; industrial radiography for the non-destructive testing of welds; as nuclear gauges in the mining, road construction, breweries, oil and gas exploration and production industries as well as in other petrochemical industries. Food irradiation for shelf life extension and preservation, sterilization of medical products and disinfestations and research and teaching purposes are among the applications of radioactive materials in Ghana.

Ghana Atomic Energy Commission (GAEC) was established in 1963 by an Act of Parliament (Act 204), which has been superseded by the new Atomic Energy Commission Act (Act 588) 2000. The functions of GAEC include the promotion, development and peaceful application of nuclear and biotechnological techniques for economic and social development in Ghana. The following practices are being carried out within the GAEC premises at Kwabenya; utilization of a 30kW research reactor, gamma irradiation facility, non-destructive testing facility, calibration of radiation monitoring equipment using radioactive sources (^{137}Cs and ^{60}Co) and the application of a host of other radioactive sources for research purposes.

The National Radioactive Waste Management Centre (NRWMC) was established by GAEC on behalf of the Government of Ghana to safely manage all radioactive waste materials generated in

the country. The NRWMC operates a Centralized Radioactive Waste Storage facility where all the radioactive waste materials collected are processed and stored.

The over six decades of application of radioactive materials in Ghana has resulted in the generation of a number of radioactive waste materials which are in storage at the facility operated by the NRWMC. There is an increase in the amount and radioactivity of the radioactive waste materials being generated in the country due to increase in use of radioactive materials especially in the mining and petroleum industry. Decommissioning of the 30kW research reactor operated by GAEC will also generate some amount of radioactive waste materials that must be safely and permanently disposed.

Ghana intends to add nuclear power to the country's energy mix. The introduction of nuclear power into the country's energy mix will significantly increase the amount of radioactive waste materials to be managed. Long term storage is not a sustainable option and it will place an unacceptable burden on future generation from practices that provided benefit to the present generation. There is therefore the need for a disposal facility for both the existing and future radioactive waste materials.

1.4. Statement of Problem

Disposal of radioactive wastes in geological repository will add a concentrated source of radioactivity to the natural radioactivity dispersed in the geologic formation. The natural environmental radioactivity and the associated external exposure due to gamma radiation depend

mainly on local geological and geographical conditions, and it is especially related to the rock types as some rock has high natural radioactivity.

The safety and performance of the disposal system must be assured for hundreds of thousands of years into the future because of the long half-lives of some of the radionuclides. The central issue in assessing the long-term performance and safety of a radioactive waste disposal facility is the ability to predict confidently the nature and effect of processes and geological events far into the future. It is not possible to ensure that the radioactive waste disposal system can be developed in an environment where all the components will be thermodynamically stable although the kinetics of the various reactions leading to equilibrium conditions may be very slow (Vandergraaf, 1987).

Over this long disposal period, the barriers will undergo degradation. The degradation mechanism and extent of degradation of the barriers and solubility of the waste form would be influenced by the groundwater chemistry. The solubility and mobilisation of radionuclides in the waste form and their subsequent transport to the biosphere will also be influenced by the groundwater chemistry. The solid mineral phase will also influence the transport of the dissolved substances in the groundwater through various sorption and exchange reactions.

The physicochemical and geochemical characteristics of the geological and hydrogeological environment should tend to limit the release of radionuclides from the disposal facility to the accessible environment or at least to restrict their migration. The Swedish regulations for safe disposal of radioactive waste stipulate that: ‘The repository site and repository depth should be chosen so that the geological formation provides adequate stable and favourable conditions to ensure that the repository barriers perform as intended over an adequate period of time’ (SKI,

2002). Thus the choice of a host rock and surrounding geological environment that has suitable geochemical characteristics and good retardation properties for long lived radionuclides is particularly important in geological disposal. Stable geochemical conditions is mainly described by a reducing environment and a composition controlled by equilibrium between water and rock forming minerals.

Description of the geochemical and hydrochemical conditions of the host rock and the surrounding geological and hydrogeological units of a repository environment should include:

(a) Mineralogical and petrographical composition of the geological media and their geochemical properties;
(b) Groundwater chemistry.

Slow groundwater movement over long periods of time, a positive feature of a suitable disposal environment, results in the development of waters at geochemical equilibrium with the minerals forming the surrounding rock and are therefore good indicators of how chemical conditions, especially pH and redox, are regulated. The chemical condition of the groundwater also reflects the origins of the water. Groundwater chemistry thus provides information on the chemical nature of the groundwater for characterisation of the hydrogeochemical conditions of the aquifer.

1.5. Aim and Objectives of the Research

The aim of this thesis is to contribute to the hydrogeochemical characterisation of the rocks of the Accra Plains and to verify their desired favourable and stable hydrogeochemical conditions for a radioactive waste repository. To achieve this objective requires the:

- Determination of the mineralogical composition of the rocks and deduction of their influence on the groundwater composition
- Understanding of the hydrogeochemical processes that control the groundwater chemistry and determination of the possible future evolution of the groundwater
- Characterization of the groundwater geochemical facies and the geochemical evolution of the groundwater
- Determination of the distribution and abundance of natural occurring radionuclides in the rocks and characterization of their behaviour in the geological environment.

1.6. Scope and Approach

The scope and approach of the research involved literature studies on hydrogeochemical studies carried out on crystalline rock aquifers for the safe disposal of radioactive waste. It also involved field studies carried out on the Accra Plains, laboratory investigations, data analyses and interpretation of the acquired data. Mineralogical analyses of the rocks and soil in the Accra Plains was carried out employing Electron Probe Microanalysis (EPMA), Scanning Electron Microscopy (SEM) and X-ray diffraction techniques (XRD).

The geochemical conditions of the groundwater of the Accra Plains were assessed by considering the abundance and distribution of the physico-chemical parameters (major ions, pH, TDS, EC and environmental stable isotopes (^{2}H and ^{18}O)) in order to characterise the groundwater and relate them to the various hydrogeochemical processes occurring in the rocks. The hydrogeochemical software tool, AQUACHEM, was used for the chemical plots data analyses. The hydrogeochemical model PHREEQC was used to calculate the ion activities and

saturation indices of the mineral phases. Stability diagrams were used for the interpretation of thermodynamic controls on the geological formation.

The description of hydrogeochemical data included statistical studies (Principal Component Analysis (PCA) and cluster analysis) intended to interpret the governing processes through data reduction and classification (Suk and Lee 1999; Meng and Maynard 2001). The Hierarchical cluster analysis method was used to classify the groundwater into distinct groups on the basis of their hydrogeochemical characteristics (dendrogram).The PCA was used to find a new set of independent variables, identify outlier samples and distinguish the contributions of natural processes and anthropogenic inputs to the chemical composition of the groundwater. Correlation analysis (Pearson correlation), a bivariate method, was applied to describe the degree of relation between two hydrochemical parameters.

A Gamma-ray spectrometry was used to determine the abundance and distribution of natural occurring radioactive materials in the soils and rocks. The data was considered in the context of natural geochemical analogues of actinides in the waste materials which may be released into the geological environment and characterization of the natural processes which control their interaction with groundwater.

The combined results derived from the various methods were employed in the characterization of the hydrogeochemical condition occurring in the Accra Plains and to verify the desired favourable, stable hydrogeochemical conditions for a radioactive waste repository.

The research work presented in this dissertation has been organized into eight major chapters including this overview. Chapter 2 (literature review) first looked at hydrogeochemical research activities carried out on Precambrian crystalline formations in some countries. Secondly it looked at hydrogeochemical processes which control groundwater chemistry. It also reviewed the geochemical behaviour of some naturally occurring radionuclides (uranium-238 and thorium-232) as useful analogues of the actinides which may be present in the disposed radioactive waste. Chapter 3 described the materials and methods used in the investigations. In Chapter 4, the petrography and mineralogy of the rocks of Accra Plains was discussed. In Chapter 5, the hydrogeochemical conditions of the Accra Plains were assessed by considering the abundance and distribution of the major ions in the groundwaters. In Chapter 6 the environmental stable isotopes (^{18}O, ^{2}H) of water was used to investigate the origin and recharge conditions of the groundwater. Chapter 7 described the concentration and distribution of natural occurring radionuclides in the rocks and identified the geochemical processes which might have resulted in the observed radionuclide distribution. Chapter 8 presents the summarized conclusions from this work and recommendations for further studies in this field of research.

1.7. Study Area

Precambrian crystalline rocks are regarded as one of the favourable host rock for the long-term disposal of radioactive wastes due to their stability in terms of tectonic effects characterised by a low seismicity (Wahlström and Grünthal 2001) and a lack of volcanic activity in addition to other advantageous properties (IAEA, 1981a).

The location of GAEC on the Accra Plains and the need for a disposal option for the stored radioactive waste materials generated in Ghana influenced the selection of the Precambrian geologic formation of the Accra Plain for this research work.

1.7.1. Location

The Accra Plains is located on the south-eastern part of Ghana. The area is roughly triangular in shape (Fig.1.2). It lies between latitude 5º 30' N and 6º 15' N of the equator, and latitude 0º 20' W and 0º 40' E of the Greenwich meridian. The Plains cover approximately 7000 km^2 (Kesse, 1985). It is bounded on the west and the northwest by the Akwapim Togo Mountains and in the north to the east by the Volta River and on the south by the Gulf of Guinea.

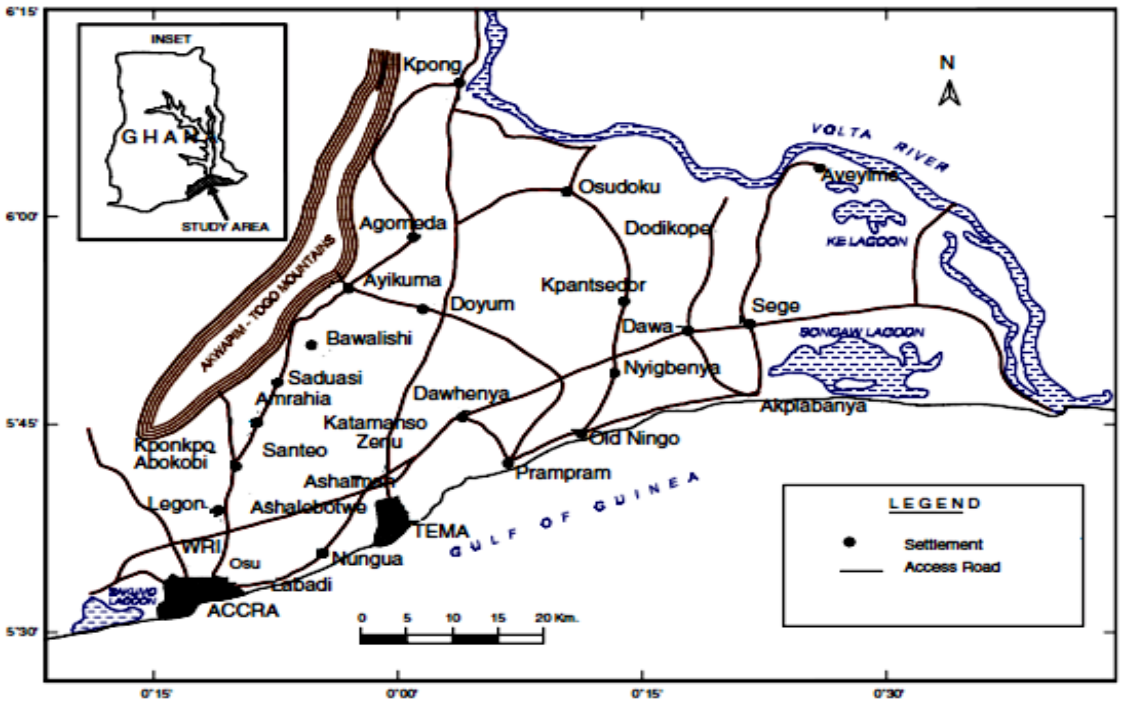

Figure. 1.2. The location map of the Accra Plains (Modified after Kortatsi, 2006)

1.7.2. Geomorphology

The Accra Plains is generally flat forming a monotonous low lying area with few isolated inselbergs and ridges such as the Shai, Krobo and Osudoku hills which rise above 100 m. The general elevation of the Plains is not more than 40 m. The Akwapim Togo Mountain made up of stratified rocks which dip to the south east, rises to a height of 365 meters above sea level and attains a width of approximately 3 to 6 km (Efa *et al*, 2006). Steeper slopes are rare and they only occur at the flanks of the University Hill at Legon and are made up of resistant rocks belonging to the Togo Series (Muff and Efa, 2006).

The Plains has no perennial river due to the uneven distribution of rainfall with the exception of the Volta River which forms the northern and eastern borders of the Plains. With low groundwater recharge to the streams, their intermittent flow and drying up during the long dry season reflect the rainfall regime of the area. The drainage pattern is dendritic and linked to the structural features of the Plains.

Streams in the north subbasin (Okwe and Danwhe) have their source from the Akwapim Togo Mountains, flow north eastwards and drain into the Volta River (Fig 1.3). Streams in the south (Mamahuma, Dechidaw and Onyasia) have their sources from the Akwapim Togo Mountains and the gradient of the streams towards the ocean (Gulf of Guinea) is very gentle. Along the coastline, several sandy platforms are associated with lagoon inlets and river deltas. These sandy platforms are flat, they consist of unconsolidated sands and their surface is less than 5 meters above sea level.

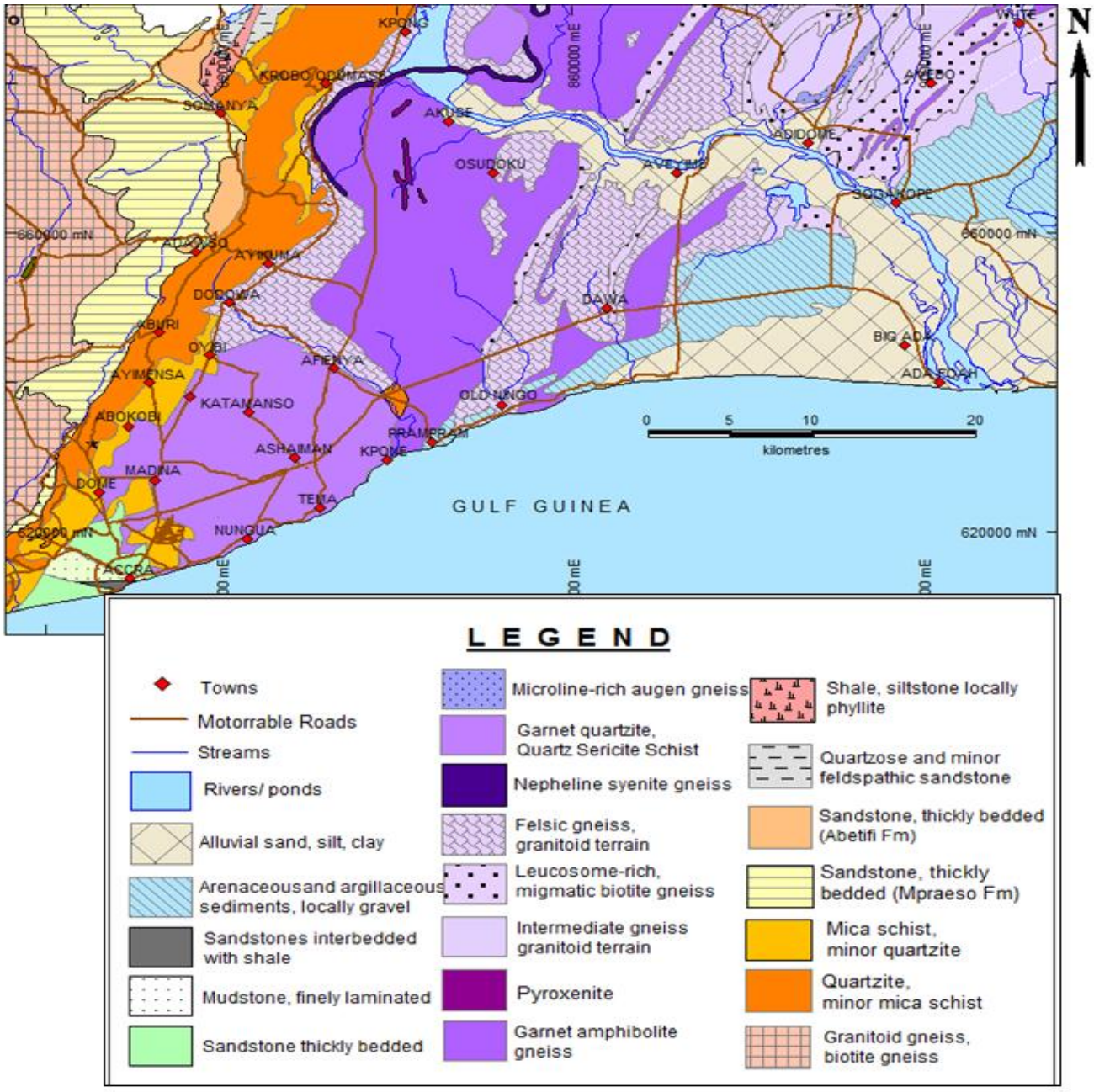

Figure 1.3 Geological Map of the Accra Plains

1.7.3. Geology

The main bedrock underlying the Accra Plains consists of the Dahomenyan Supergroup that covers about 75% of the area. Other geological formations in the Plains include the Togo

structural units, the Accraian Series, the Tertiary and Recent sediments. The geology of the Accra Plains has been described in detail by Junner and Bates (1945), Holm (1973) and Kesse (1985).

1.7.3.1. Dahomeyan Supergroup

The Dahomeyan Supergroup belongs to the Pan-African terrain, also called the Dahomeyides (Attoh, 1998). It covers the flat lying terrain to the east of the hill range made up of the Togo Structural Unit. It has been attributed a Middle - Late Precambrian age (Muff and Efa, 2006). It occurs as four alternate belts of felsic and mafic gneisses (Fig 1.3). All the four belts trend in a south-southwest to north-northeast direction from the coastal Plains of Accra and enter the Republic of Togo.

The mafic groups of rocks, which are generally well exposed on the inselbergs are very uniform, coarse-grained and usually of well foliated garnet hornblende gneiss and granulites with minor layers of hornblende and biotitic schist and pyroxene gneiss at the base. In the lower areas, exposures are scattered (usually on low ridges) and the rocks are covered by a varying thickness of overburden. This overburden, the result of the rocks decomposition, consists of black or dark grey calcareous clay and silt which usually contains white or grey and nodular carbonate concretions (Crooks *et al,* 2003). When wet, this clay is plastic but when dry exhibits numerous shrinkage cracks.

In general, rocks of the felsic gneiss group are composed of quartz, feldspar, epidote and mica, although some amphibolites occur locally. Hornblende and garnet, in addition to quartz, feldspar epidote and mica are the principal minerals of the rocks of the composite groups (Holm, 1973).

Rock-types included in the felsic gneiss group are muscovite-biotite gneiss, biotite gneiss, muscovite gneiss, augen gneiss, quartzo- feldspathic gneiss and minor local amphibolites. Making up the composite groups are interbedded layers of biotite gneiss, biotite- hornblende gneiss, hornblende gneiss, epidote amphibolite, mica schist and minor mica-bearing quartzites. Garnet is an important constituent in some of the epidote amphibolites and mica schists. Rocks of the felsic gneiss and composite groups do not form good outcrops on the savannah and wide distances occur between outcrops (Crooks *et al*, 2003).

Studies by Akiti *et al*, (1972) and Attoh *et al*., (1997), showed the alkaline rocks in the Kpong areas, where the suture zone of the Dahomeyide orogen is exposed, referred to as the Kpong complex, to consist of carbonatite and nepheline syenite rocks. They occur as deformed layers in tectonic contact with garnet granulites (Attoh *et al*, 2007). Carbonatitites are intrusive carbonate-mineral rich igneous rocks, many of which contain distinctive abundances of apatite, magnetite, barite and fluorite that may contain economic or anomalous concentrations of rare earth elements. They are sources of certain metals and commodities including Cu, V, vermiculite and also potential sources of thorium and uranium (Nude, 2006).

Mineralogy studies carried out by Nude (2006) on the Kpong complex rocks showed that the rocks had calcite and biotite. The detailed mineralogical, geochemical, and isotopic data on the rocks of the Kpong complex have been described by Nude (2006).

1.7.3.2. Togo Structural Units

The Togo Unit is Upper Proterozoic in age (Muff and Efa, 2006). It makes up approximately 15 % of the Accra Plains. The rocks have been subjected to a low- to intermediate grade type of metamorphism. The Unit forms the greater part of the Akwapim Togo Mountains trending from Kpong in the south-western direction of the Volta River and continues southwards as far as western Accra. This unit consists of quartzites, schists, phyllite and phyllonite. Phyllonites make up a large part of this unit. Phyllonites are phyllitic rocks of mylonitic origin and they belong to the group of rocks called fault rocks (Muff and Efa, 2006). The Phyllonites underlie large parts of the eastern part of the Akwapim Range. They occur at the areas of thrust contact between the Togo Structural Unit and Dahomeyan Supergroup (e.g. northeast of the GAEC). Fragments of phyllonites are often found in the top of shallow elevations where red soil formed over mica schists of the Dahomeyan Supergroup. The fragments are relics of phyllonite layers which now have been eroded. The occurrence of phyllonite and fragments of phyllonites in soil over Dahomeyan indicates that much of the Dahomeyan terrane was formerly overlain by the Togo Structural unit.

The rock types of the Togo Structural unit include quartz-schist types. This rock type encompasses mainly sericitic quartz-schist and chlorite-schist and contains layers of quartzite, phyllite or chlorite schist. The sequence is well bedded and strongly jointed. The quartzite rock type comprises mainly quartzite and the amount of quartz-schist and phyllite is very variable.

1.7.3.3. Accraian Series

The Accraian Series underlie much of the Accra Metropolitan Area and extend to the north as far as Achimota. It covers approximately 3 % of the Accra Plains. The Accraian Series are thought to possess a Devonian age. Field investigation carried out by Harris (1970) confirmed the distribution of the Accraian Series which comprise three distinct formations. These are:

1. Upper Sandstone-Shale formation: It consists of thin-bedded, fine-grained sandstones which contain interbeddings of shales;
2. Middle Shale Formation: it is a fossil-rich argillitic unit which may reach a thickness of over 100 m;
3. Lower Sandstone Formation: it is mainly made up of sandstones with minor amounts of grits and pebbly beds.

Rocks of the Accraian Series have been deposited on an unconformity which exposed rocks of the Dahomeyan Supergroup and Togo Structural Unit. The engineering and hydrogeological properties of the three formations and their overlying weathering products are very variable. *In situ* overburden of the Middle Shale Formation and Upper Sandstone Shale Formation contain swelling clays which are problematic for shallow foundations. The bedrock is often overlain by superficial clays and sands with pebbles. They may be *in situ* formations (regolith) or sand/silt washing (slope wash). These superficial deposits may attain a depth of 10 meters, while depths ranging from 1 to 6 m are most common (Muff and Efa, 2006).

1.7.4. Structural Features

There are no major faults in the Dahomeyan gneiss as a whole. The felsic gneiss however shows strong recumbent folding, associated with numerous over-thrusts (Darko *et al*, 1995). Locally,

small folds and flexures are present, but their relationship with the major folds has not been established. Two common dips of foliation are identified – low angle dips of 15^{o} to 35^{o} and high angle dips of 60^{o} to 80^{o} towards the east and southeast.

The contact between the Togo and Dahomeyan is a fault zone, often referred to as the Akwapim fault. There is evidence of an over thrust relationship, the Togo being thrust over the Dahomeyan from the southeast. The contact is generally a fairly flat surface showing evidence of effects of intense differential pressure at considerable depth (Muff and Efa, 2006).

In the Togo rocks of the Akwapim Togo Mountains, two tectonic phases have been observed. First, there is the widespread development of axial planes striking mainly northeast-southwest of varying dips of 20^{o} to 70^{o}, all in the southeast. Secondly, the local development of upright folds of bedding and slaty cleavage on north, northwest-south, southeast (NNW-SSE) axial planes. These two tectonic phases exerted a strong influence on the morphology of the region producing the northeast-southwest topographic feature in prominient Akwapim Togo mountain (Junner and Bates 1945)

1.7.5. Climate

The Accra Plains lies in the coastal savannah zone. It has equatorial climate characterised by two rainfall seasons of unequal intensities. The period May to July represents the main rainy season with torrential rainfall. The peak occurs in June with a mean monthly rainfall of over 200 mm. A minor rainy season occurs in September and October with a mean monthly rainfall of about 66 mm. Average annual rainfall is about 800 mm. The rainfall is usually intense and short, and

gives rise to local flooding where drainage channels are obstructed, or imperviousness of the urban soil causes sheet floods which cannot be handled by the natural river system. The geographical positions and relief features of the Plains are some of the factors that attribute to the low rainfall regime within the Accra Plains. A dry season occurs from November to April during which period the mean monthly rainfall is about 30 mm per month (Darko *et al*, 1995). The variation in temperature throughout the year is minimal. Mean monthly temperatures range from 24.7º C in August to 32º C in March, with an annual average of about 26.8º C. The seasonal uniformity of the temperature could be partly due to the modifying influence of the sea breeze. Due to the closeness of the area to the equator, the daylight hours are practically uniform during the year. Relative humidity is generally high, varying from 65 % in the mid afternoon to 95 % at night.

The predominant wind direction ranges from west, southwest (WSW) to west, northwest (WNW) direction with a speed ranging 8-16 km/hr. Strong winds associated with thunderstorms often cause damage to property by removing roofing material. Along the Akwapim Togo Mountains, the wind velocity increases and this gives rise to slightly cooler temperatures along the foothills.

1.7.6. Vegetation

The development of vegetation is closely related to the climatic condition in the area, the soil types and the economic activities of the inhabitants of the area. The vegetation in the Plains is the typically Savannah-type. Grassland and clusters of shrub occupy the Western and Eastern Lowlands. Large trees are only occasionally present, and Baobab trees are sometimes found in the Eastern Lowlands. Dense shrub land or thicket covers most of the Akwapim Togo Mountain

and the land immediately adjoining the foothills e.g. Teiman, Ashongman, Dodowa and Ayikuma. Also scattered or at intervals along the main streams valleys on the Plains are thick mangroves trees and scrubs. In the northern part of the Plains between Doryumu, Agomeda, Somanya and Akuse where the rainfall pattern is very much appreciably higher and much better distributed and more uniform, there is a gradual change in the savannah type of vegetation in which there are more trees. Fen palms (Borassusaethiopum), Dum palm (Hyphaenethebaica) and Shea-butter trees (Butyrospemumparkii) are perhaps, the most characteristic of the trees.

Along the coast, wetlands and dune vegetations are found. Dense grass, palms and coconut trees prevail. Urban agriculture is practiced in several periurban and urban areas, and irrigated urban vegetable production is the most important type. Urban agriculture plays a very important role in supplying food to the metropolitan population, but as the agricultural plots are situated along heavily polluted urban streams and drainage channels, the vegetable farming is not without health hazards. Land use pressure due to expanding metropolitan areas may in the future reduce the space used for agricultural purposes in the urban and periurban areas. The vegetation supports farming and livestock breeding (mainly cattle) which constitutes the main occupants of the inhabitants.

1.7.7. Hydrogeological properties of rock formations

The crystalline basement rocks dominate the hydrogeological setting of the Accra Plains with aquifer regimes occurring under water table, semi-confined and confined conditions. The generally impervious nature of the weathered zone and the massive crystalline structure of the rocks limit the yields that can be obtained from hand-dug wells or boreholes.

The Dahomenyan formation is massive with few fractures. The porosity and permeability of the rocks are very low (0.1-3%). The main water bearing zones are that of porous fractured media. Boreholes drilled to depths ranging from 12 m to 104 m encountered aquifer regimes at a mean depth of 31.6 m within a range of 4.6 m to 77.0 m (Darko *et al*, 1995). The mean thickness of the aquifer was 3.2 m and varied from 0.2. to 12.5 m. The borehole yield was found to be 1.9 m^3/h (Darko, 2011). The mean transmissivity value was 1.8 m^2/day. The magnitude of the hydraulic conductivity (K) in the fractured media is 0.2 m/day and the storage coefficient of the order 10^{-5}. The specific capacity determined from transmissivity estimate ranged from 0.5 to 21.1 $m^3/day/m$ with an average value of 5.0 $m^3/day/m$. The mean potential yield of the Dahomenyan aquifer was estimated to be 5.9 m^3/day (Darko *et al*, 1995). The potential of the Dahomeyan formation as a source of drinking water is poor. However, several boreholes of moderate to good yield are located in the Adenta and Oyarifa areas along the northern border closer to the Akwapim Togo Mountain. Even though the produced water is brackish or saline, it is suitable for alternative uses such as washing.

Rocks of the Togo Formation are characterized by many fractures and joints, with an average density of 80 joints per cubic metre. The Togo quartzite and quartzitic sandstones weather into fine sands and fragements that is appreciably permeable. In areas where they are highly fractured, particularly along the tectonic contact zone between the Dahomenyan and Togo formation where the rocks are transversely fractured, fissure permeability is further enhanced.

Boreholes yields are highly variable, owing to jointed and fractured layers of highly folded quartzite that build up a fracture flow aquifer. Boreholes drilled to depths ranging from 26.2 m to

91.8 m with a mean depth of 56.2 m encountered water bearing bodies at a mean depth of 27.3 m. The water bearing zone ranged from 6.0 m to 59.0 m. The aquifer thickness varies from 0.3 m to 14.9 m with a mean value of 3.3 m. The yield is also highly variable and ranges from 0.3 to 20.5 m^3/hr. The mean transmissivity determined for the confined aquifer is 11.5 m^2/day with storage coefficient of 10^{-3}. The specific coefficient ranges from 1.5 to 127.8 m^3/day/m and has a mean value of 31.1 m^3/day/m. The mean potential yield was estimated at 174.1 m^3/day the highest in the Accra Plain (Darko, 2011).

Recharge is high where the overburden is made up of sand and rock fragments (arenaceous) materials, which generally are highly permeable. The Togo Formation thus has a moderate to good potential for groundwater and can be regarded as the most important groundwater aquifer in the Plain. Where weathering is sufficiently deep and water quality is adequate, this formation has as a moderate groundwater potential, which is at least suitable to sustain boreholes equipped with hand pumps. Groundwater is often encountered at shallow depths in this flat terrain so that access by hand dug wells are also possible.

Rocks of the Accraian Formation which consist dominantly of sandstones and to a lesser degree of interbeddings of shale could be good aquifers on account of their hydraulic properties. However, because of dense human settlement and lack of protective mechanism in place, vulnerability to pollution is very high. It is also very likely that groundwater in the Accraian formation is saline because of the proximity to the coast.

The groundwater potential decreases as you move from the Akwapim Togo Mountain to the coast. Fresh water, defined here as having an EC of less than 1500 µS/cm, is only encountered within and along the foot of the Akwapim Togo Mountain and in the northwestern corner of the Plains, which is underlain by granitoids. In general salt content increases with proximity to the coast and with decreasing elevation. This indicates the impact of underground salt water intrusion, possibly combined with the effect of sea spray.

1.7.8. Groundwater flow pattern

Based on chemical trends (concentration of chloride and sulphate) and supported by topographic features of the Plains, it has been asserted that the overall groundwater flow direction was from the foothill of the Akwapim Togo mountain, flow south-southeastwards into the Plain and towards the coast. This assertion was further corroborated by isotopic dating of groundwater samples obtained from boreholes in the Plains. The water was found to get older when moving towards the central part of the Plains (Akiti, 1980). However the results could not establish the continuity or otherwise of the aquifer as there were contradiction in C^{13} contents and isotopic composition of O^{18} .

Chapter Two

Literature Review

2.1. The Geological Disposal Concept

Geological disposal is the emplacement of solid radioactive waste in a disposal facility located underground in a stable geological formation so as to provide long term containment of the waste and isolation of the waste from the accessible biosphere (IAEA, 2011). Disposal means that there is no intention to retrieve the waste materials, although such a possibility is not ruled out. Geological repository is the facility for radioactive waste disposal located underground (usually a few tens to several hundred metres below the surface) in a stable host rock to provide long term isolation of radionuclides from the accessible environment (biosphere) (IAEA, 2003). The depth chosen for disposal in a particular facility depends on a number of factors including, but not limited to, climatic and groundwater conditions, rock stability, host rock composition and the nature and hazard of the waste (IAEA, 2011).

The repository system is represented by three main components (Fig. 2.1):

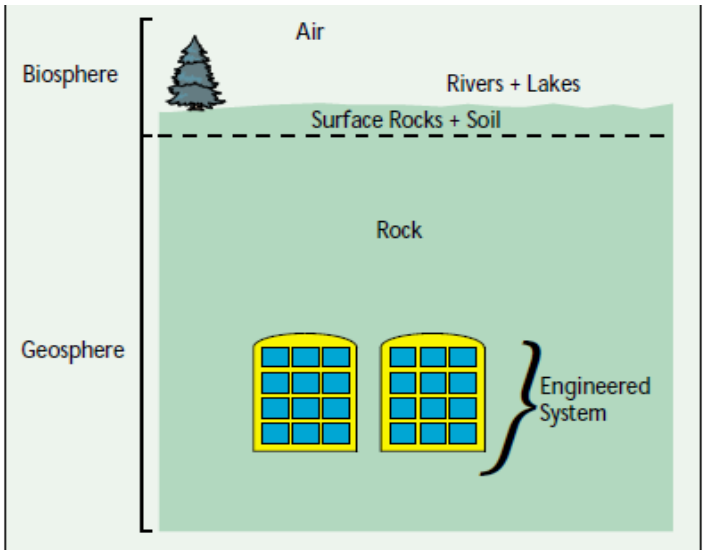

Figure 2.1.Three main components of a repository system (Nirex, 2000).

- the engineered system, comprises of the disposal vaults and their contents, which includes the waste materials, waste packaging, backfill and structural materials.
- the geosphere comprises of the rocks in which the repository has been constructed and those that surround them, extending to the surface;
- the biosphere: the environment accessible to humans. This includes the soil and surface rocks, surface water bodies, oceans and the atmosphere. The relevant boundaries of the biosphere may extend for several tens of kilometers.

The long term safety of the repository can be assured by ensuring that the period of isolation and containment of the radionuclides below the surface environment is sufficient to allow for decay of the radionuclides to low levels and also prevent their release to the surface environment in amounts that could cause harm to life and the environment. As a result the multiple barrier concept has been adopted to meet the requirements of containment and isolation in the short term followed by dilution and dispersion over extended time periods.

2.1.1. The Multiple Barrier Concept

The multiple barrier concept is based on the nesting of one barrier inside the other, so that the individual characteristics of all the barriers act together to ensure adequate isolation (Chapman and McKinley, 1987). The multiple barrier concept consists of three main barriers (Fig.2.2). They are the physical, chemical and natural barriers.

The physical barrier consists of the engineered barrier constructed by encapsulating the waste in cement within a steel or concrete container for LLW and ILW and canister for HLW. The combination of the encapsulation matrix and waste material constitute the waste form while the

waste form and container together constitute the waste package. The role of the waste form is to incorporate the waste material into a concrete matrix which is resistant to leaching by groundwater, thereby restricting release of the radionuclides. The physical barrier is therefore designed to physically contain the radionuclides for long period for them to decay and also delay the mobilization of the radionuclides into the geosphere.

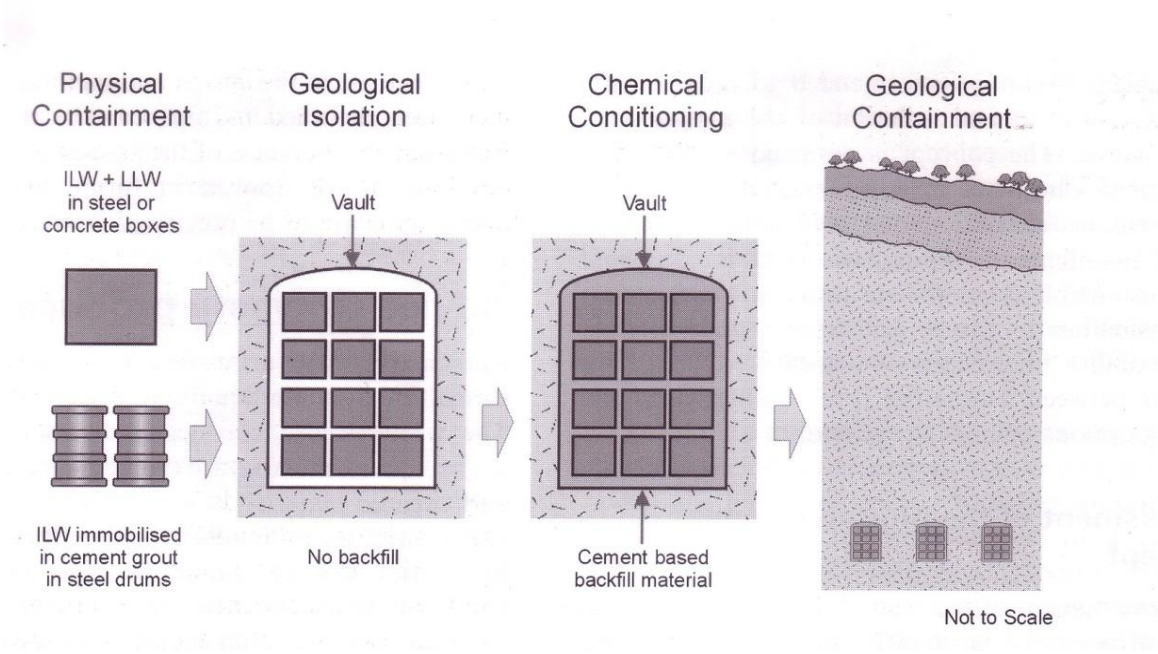

Figure. 2.2. Schematic representation of the multiple barrier concept (Nirex, 2000).

The chemical barrier is the second barrier constructed by providing the repository with a geochemical environment which impairs corrosion or deterioration of the waste packages and inhibits the movement of radionuclides. The waste packages for LLW and ILW are surrounded with a cement-based backfill, which creates uniform, alkaline chemical conditions. For many radionuclides, the alkaline conditions, which are expected to persist for over a million years, will significantly reduce the concentrations of radionuclides dissolved in the groundwater within and

around the repository. Cement has a high capacity for sorbing radionuclides, thus reducing the migration of radionuclides away from the repository.

The geological barrier which is also called the natural barrier is made of the rocks that surround the repository and other geological formations that lie between them and the biosphere.The geological barrier is the ultimate barrier to prevent, delay and attenuate radionuclides released from the repository to the biosphere.

The characteristics of the physical and chemical barriers also referred to as the near-field environment are within the control of man. The properties of the barriers can be varied to suit the waste type and disposal environment. This control is observed in the development of a variety of waste forms and waste packages. However the principal control over the performance of the geological barrier is limited to site selection and characterization, so a thorough understanding of the properties of the selected geological formation is essential for repository evaluation.

Siting is a fundamentally important activity in the geological disposal of radioactive waste. A promising site should display evidence of favourable natural containment and isolation characteristics for the waste types under consideration and should provide indications that all necessary engineered barriers can prevent or retard the movement of radionuclides from the disposal system to the accessible environment (IAEA, 2011). This evidence needs to be tested in subsequent detailed site investigation, characterization and associated safety assessment modelling.

Site characterization is an activity undertaken in order to understand the natural features, events and processes at a site (at the present time, in the past and potentially in the future) and to describe adequately their spatial and temporal extent and variability.

2.1.2. The Geological Barrier

Of prime importance in the selection of a suitable geological component for a multiple barrier system is the hydrogeochemical characteristics of the host rock and of a surrounding geological environment (IAEA, 1999). The engineered components of the repository are designed to be compatible with the geochemical conditions in the host rock. This is particularly important for ensuring that the engineered structures perform as expected for long period of time.

The geochemical conditions and processes in the host rock serve as a barrier by providing an environment that slows or prevents the degradation of engineered barriers and limits the rate of mobilization and transport of radionuclides when they are released from the repository. The rock should display significant radionuclide retardation properties and high thermal capacity to accommodate the increased thermal loading which will be induced by the emplacement of the waste package (Hagros, 2006).

Although no ideal rock type exists which displays all the required characteristics, a number of rock types have been proposed as potential repository host materials, The main rock types include evaporites (bedded and dome deposits), sediments (clays and shales), volcanic rocks (including basalts and tuffs) and crystalline rocks (igneous intrusive and high-grade metamorphic rocks).

2.1.2.1. Evaporite

An evaporite is any sediment formed by evaporation of water with resulting precipitation and/or crystallization of compounds previously in solution (Sumerling and Smith, 1998). The most commonly occurring evaporite is halite (common rock salt) formed from cyclic evaporation of ancient seas, but the term also includes other minerals such as anhydrite (calcium sulphate), often found as interbeds within salt deposits and sometimes as thicker deposits. Evaporites occur as extensive lateral formations (bedded salts) and also as salt domes or pillows. The most important salt deposits, which provide an adequate thicknessfor potential use in waste disposal, are of marine origin (IAEA, 1999).

Rock salt was the first geological medium to be suggested for the disposal of high level radioactive waste (IAEA 1999). They have many advantages from hydrogeological view point which includes high plasticity which increases with temperature and pressures and allows for self-sealing of fractures. They have good thermal conductivity so that they can accommodate the increased heat loading of the waste package. They also have negligible free water content and effectively zero permeability and high stability in the groundwater environment.

Some disadvantages in the use of salt are, saline solutions (brine) tend to promote metal corrosion, salt is itself a resource and may include commercial quantities of potash and gypsum. Bedded salt is often found in association with hydrocarbon resources at greater depth. Salt deposits are being investigation as a potential host rock for geological disposal of radioactive waste in Germany (at Gorleden), and the Netherlands and more limited studies are being undertaken in Denmark (Sumerling and Smith, 1998). The United States Department of Energy

was granted certification to dispose of defence related transuranic wastes (TRU) in bedded salt at the Waste Isolation Pilot Plant (WIPP) site in New Mexico (Sumerling and Smith, 1998).

2.1.2.2. Argillaceous Sediments

Argillaceous sediment is a broad term used to describe any sediment with significant clay content. This includes silts, muds and clays deposited in both fresh and marine environments. Because of burial under the weight of overlying sediments over geological timescales, these materials become indurated, i.e. water is squeezed out with accompanying mineralogical changes to form siltstone, mudstone and claystone. If distinct laminations are present so that the rock may be fissile they are termed shale (Sumerling and Smith, 1998).

Clays are generally more plastic than shales and both display low hydraulic permeability and general reducing groundwater environment. The favourable hydrological properties are essentially: very low hydraulic conductivity, high sorption capacity for dissolved cations, effective filtration capacity for colloids and large molecules, low solubility of the clay constituents, and in the case of plastic clays a self-healing property which tends to restorethe previous condition after a disturbance. The high chemical buffering capacity maintains reducing conditions and a near neutral pH of pore fluids thus inhibiting corrosion and minimizing solubility of actinoid species. The remarkably low hydraulic conductivity and high sorption capacity are relatedto the clay mineral content of the argillaceous formation.

Prolonged temperatures above 100 ^{o}C may change the clay properties and induce excessive pore pressure (Sumerling and Smith, 1998). This in addition to relatively low thermal conductivity

implies relatively low density of emplacement of heat generating waste. The difficulties experienced in mining these rocks have led to only limited development mainly in Belgium, France, Japan, Spain and Switzerland and in the past in Canada, Italy, the UK and the USA (Sumerling and Smith, 1998).

2.1.2.3. Tuffs

Tuff is a rock formed of volcanic ash and lava residues and may be quite variable in its characteristics. Tuffs are the result of silicic and andesitic volcanism and thus indicate that the region was tectonically active at the time of their deposition (IAEA, 1999). Because the hot ash flows are deposited while hot, glass shards may be welded to varying degrees, depending on their location within the individual flow unit, or the time interval that elapsed between ash flows. Compression of the ash by overlying material may squeeze trapped gases into pockets or cavities. Contraction of the ash while cooling produces a joint system that may be partially or completely filled by minerals that have crystallized from the vapour phase.

Individual tuff layers may be rich in minerals (zeolites and clays) that have a large capacity to sorb most radionuclides. Tuff formations possess high matrix porosity compared with crystalline rocks, enhancing matrix diffusion of radionuclides migrating along fracture pathways. Tuff formations located within the unsaturated zone in arid regions have effective permeabilities in existing moisture states that are orders of magnitude less than their intrinsic permeabilities, so that water fluxes are very low (IAEA, 1999). For tuff, repositories sited in the unsaturated zone, the greater capillary attraction for water associated with generally smaller pores of the rock matrix tends to draw water from the fractures, making fractures generally non-transmissive to water except in areas of locally high saturation. Investigations into usage of tuff as a host

geological formation has been limited to site specific studies, mainly in the USA where tuff has been selected as the candidate repository rock.

2.1.2.4. Crystalline rocks

Crystalline rocks are formed at high temperature and pressure either by cooling from a molten state or by the deformation and recrystallization of pre-existing rocks. They occur as individual igneous intrusions (plutons or massifs) or as extensive igneous or metamorphic terrains whose formation and emplacement occurred during various phases of orogeny. They are strong and brittle and commonly show evidence of at least one period of brittle deformation. As most crystalline rocks are formed at high temperature, they are thermally stable and display good heat conductivity. Crystalline rocks display slow rates of change in the geological environment. They also have typically low porosity and permeability, high structural strength and are easily mined. Although the rock matrix has low porosity and poor permeability, fractures and faults can have high porosity and high transmissivity. However some studies have shown that where major fracture zones have been avoided during site characterization, groundwater penetration is limited to localized flow cells and is therefore easily predictable (Chapman and McKinley 1987).

There is a variety of crystalline (i.e. igneous or metamorphic) rocks that have been proposed to host nuclear waste repositories. These include granites, granodiorites, gneisses, and gabbro. However Precambrian crystalline rocks are regarded as a favourable host rock for the long-term disposal of radioactive wastes. Countries where the disposal of radioactive waste has been decided to be carried out in Precambrian crystalline bedrock include Sweden, Finland and Canada (Milnes 2002, Hagros, 2006).

In stable Precambrian bedrock, the movement of groundwater is basically the only natural process through which the radioactive materials can migrate in the bedrock (Hagros, 2006). The properties of Precambrian bedrock that is relevant for the disposal of high-level nuclear wastes have been extensively discussed by Niini *et al*. (1982).

2.1.3. Expected evolution of the radioactive waste repository

During repository excavation and operations, oxidizing conditions would develop in the adjacent rock, either by the movement of air into the rock or by dissolution of air in groundwater at the interface (McMurry *et al*, 2003). In addition, the presence of open rooms at depth would result in the temporary drawdown of the water table in the immediate vicinity of the repository, causing oxidizing meteoric waters to move downwards through the fractured rock mass.

Following closure of a repository, the groundwater regime will be progressively re-established and the whole system will resaturate. Thus the hydrogeochemical environment around the disposal system begins to stabilize (Fig.2.3). Any remaining oxygen in trapped air will react with the rock and engineered barrier system (EBS) materials (IAEA, 2003). Microbes may play an important role in consuming the trapped oxygen. The main determinants of the performance of the near field of disposal environments will, however, be the content, movement and composition of groundwater in the rock immediately surrounding the EBS (IAEA, 2003).

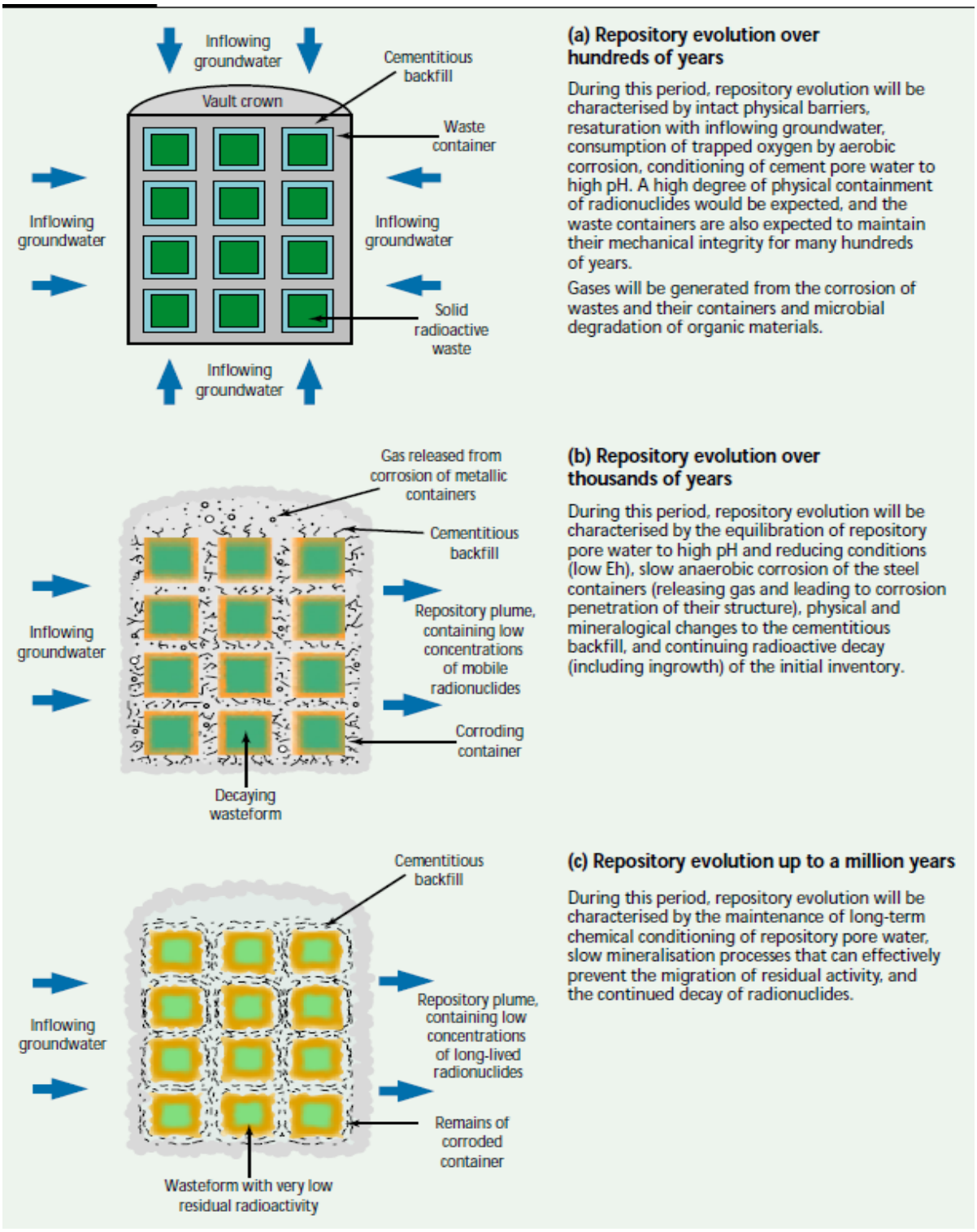

Figure 2.3.Summary of the expected evolution of the repository (schematic) (Nirex, 2000).

The warm porewater will come into contact with the waste package and overpacks upon saturation of the repository. This will initiate the process of corrosion which is controlled by the rate of groundwater flow or corroding species diffusing from the host rock through the backfill to the waste container surface. The rate of removal of soluble or gaseous corrosion products and the build-up of reaction layers also affect the rate of corrosion (McMurry *et al*, 2003). With time, waste package failure occurs as corrosion eats through the overpack and the container, enhanced by localized pitting corrosion. The waste package failure may also occur as a result of mechanical weakening of the package.

Redox conditions in the repository have great influence on the solubility of some radionuclides and will be buffered by the container material and its corrosion products and can also be affected by radiolysis of the porewaters (Gascoyne, 1997). Owing to radiolysis, conditions around the waste are considered to be oxidizing with a possible abrupt change to reducing conditions (redox front) caused by buffering either by the iron overpack (Fe/FeO) or iron oxides (e.g. magnetite) present in the backfill or host rock.

The redox condition will move out into the rock very slowly as the iron buffering capacity is progressively exhausted. During this period radionuclides will have diffused out to the rock at very low concentration controlled either by their solubilities or by their slow release from the waste matrix and the redox sensitive elements may precipitate at the redox front, to be picked up and moved along in a typical roll-front. Others may be co-precipitate or may be free to migrate in the mobile groundwater either in solution or on colloids

The diffusion of porewater components or the mixing of fluids at the repository-geosphere interface is likely to result in the precipitation of secondary phases such as calcite and gypsum at the interface or in nearby fractures in the geosphere (McMurry 1995). A broader effect would be due to heat from the repository, which would raise the temperature of water in the geosphere (McMurry 1995). This would result in a slightly greater dissolution rate for feldspars, which are generally the most abundant minerals in plutonic rocks, and for other minerals (McMurry 1995). Later, as the water cools, precipitation of secondary phases such as amorphous silica and calcite would be promoted. The extent and significance of the precipitation would depend on site specific characteristics such as the distribution and dimensions of the fractures (McMurry 1995).

2.1.4 Hydrogeochemical Studies on Crystalline Rocks

Much of the hydrogeochemical research on crystalline rock aquifers has been motivated by the need to find a safe disposal option for radioactive waste. The Stripa Project was one such research project that brought together international group of geochemical and isotopic specialists to develop and evaluate geochemical concepts and techniques suitable for the assessment of crystalline bedrock in Central Sweden as an ultimate barrier to the movement of radioactive and toxic materials from nuclear fuel wastes (Nordstrom *et al* 1989(a)). The study led to hydrogeochemistry becoming a very major component in the safety assessment process of a radioactive waste repository.

Geological, geochemical and hydrological investigation in the Canadian Shield was another research project. The aim was to characterize the rock and the chemical composition of the groundwaters in the different rock types (granite, gabbro, and gneiss) in order to gain a better

understanding of their suitability as a long-term barrier to radionuclide migration (Gascoyne, 2004).

The Finnish crystalline bedrock is also being studied for the final disposal of spent nuclear fuel. According to studies carried out by Pitkänen *et al* (2004), the bedrock is Precambrian in age and consists of schists and gneisses deformed and metamorphosed during the Svecofennian orogeny 1900-1800 Ma ago. Characterisation of the Olkiluoto site revealed that the host rock for a radioactive waste repository should have the following properties; a geochemical environment free of oxygen, representing reducing conditions, a nearly neutral pH and low sulphide concentrations; not to high groundwater salinity level (TDS< 100 g/L) (Posiva, 2000).

In Switzerland, the following chemical properties of the groundwater were considered to favour good performance of the engineered barriers of a repository: a near-neutral pH, reducing groundwater and a low to moderate salinity (Nagra, 1994). Andersson *et al* (2000) also suggested that the groundwater chemistry at a repository level should not contain dissolved oxygen. This suggestion was supported by crystalline rock groundwater studies carried out in Sweden, Finland and Canada (Laaksoharju *et al*., 1998 and Laaksoharju *et al*., 1993). Dissolved oxygen in the groundwater, will lead to pit corrosion of the waste package. Absence of dissolved oxygen is therefore essential in fulfilling the fundamental safety function of an intact waste package. The absence of oxygen is indicated by a negative Eh, occurrence of Fe(II), or occurrence of sulphide.

TDS influences the buffer (bentonite) stability and sorption of radionuclides. The swelling capacity of the buffer decreases with very high TDS. The swelling capacity of bentonite with

density of 2,000 kg/m^3 decreases more than half its capacity at TDS concentrations higher than 100 g/L (Karnland, 1997). High salinities also reduce the sorption capacity in the rock for many radionuclides (Carbol and Engkvist, 1997). In addition, Andersson *et al.* (2000) mention as a preference that undisturbed groundwater at repository level should have a pH in the range of 6–10, a low concentration of organic compounds ([DOC] < 20 mg/L), a low colloid concentration (lower than 0.5 mg/l), low ammonium concentrations, some content of calcium and magnesium ([Ca^{2+}] + [Mg^{2+}] > 4 mg/L) and low concentrations of radon and radium. The Swedish Nuclear Fuel and Waste Management Co (SKB), Stockholm demonstrated that the total concentration of divalent cations should exceed 1 mM (i.e. 40 mg/L) and that NaCl concentrations of 35 g/L and 100 g/L form upper limits for maintaining the backfill and buffer properties, respectively (SKB 2004, SKB 2005).

Suitable ground water chemistry will assist in maintaining the integrity of the engineered multi-barrier system to at least 10 000 years into the future.The expected concentration ranges for groundwater constituents at repository level for the Swedish sites are shown in Table 2.1.

The results of the studies carried out in the above mentioned countries indicate that an understanding of the hydrogeochemical groundwater conditions and evolution of the groundwater are essential in evaluating the long-term safety of a radioactive waste repository. The hydrogeochemical studies were mainly focused on disposal in fully saturated conditions in crystalline rock in ancient shield areas. They tried to understand the flow and composition of groundwaters in the rock to depths of 1000 m. It is not only the chemistry and hydrodynamics of the groundwater at repository depths that are important, but also the variation in groundwater

chemistry at progressively shallower depths along the discharging groundwater flow paths. Therefore, characterising a site for the disposal of radioactive waste must include detailed studies of groundwaters sampled from the surface together with the near-surface and sub-surface bedrock environments.

Table 2.1The concentration intervals expected for groundwaters at repository level for the Swedish sites (SKB, 1999).

Component	At repository closure	After 1000 years
pH	6 to 9	7 to 10
Eh (mV)	0 to –400	–250 ± 100
Major components (mg/L):		
Na^+	10 to 3000	50 to 2000
K^+	1 to 20	0 to 10
Ca^{2+}	1 to 3000	10 to 2000
Mg^{2+}	1 to 200	1 to 100
HCO_3^-	10 to 1000	10 to 40
Cl^-	20 to 10000	100 to 5000
SO_4^{2-}	0.1 to 600	0.1 to 400
HS^-	0.01 to 10	< 1
TOC	0 to 30	< 2

2.2. The Relationship between Rock Composition and Groundwater Chemistry

The radioactive waste repository can be regarded as a system where the rock's different mineral component, fracture filling products as well as the disposal system constitute a solid stationary phase whilst the groundwater constitute the liquid mobile phase. The rock may consist of quartz, feldspars (potassium feldspar and plagioclase), mica minerals (biotite and muscovite) and amphiboles (hornblende). In addition there may be small quantities of accessory minerals such as, chlorite, magnetite, calcite, dolomite, fluorite, apatite, anhydrite and different clay minerals.

The groundwater constitutes a medium that actively participates in the chemical processes between the components in the repository and the rock. Groundwater chemistry is largely a function of the mineral composition of the aquifer through which it flows (Hiscock, 2005). Reactions may occur between different components in the groundwater, between groundwater and fracture minerals, and between groundwater and rock matrix. Groundwater chemistry provides information on the chemical nature of the groundwater for characterisation of the local hydrogeochemical conditions. The groundwater flow will transport reactive groundwater components into the repository and reaction products out of the near-field of the repository mainly in fractures, either in solution or as particulates, but diffusion into microfissures in the bedrock would also be expected. The flowing groundwater also leads to a mixing of different groundwater types from different areas in the geosphere.

2.3. Process that Control Groundwater Chemistry

Chemical signatures of groundwater, in terms of concentrations and isotopic ratios, can be used to understand groundwater processes. Groundwater contains a variety of chemical constituents at different concentrations. The greater part of the soluble constituents in groundwater comes from soluble minerals in soils and rocks (Waterwatch, 2005). A much smaller part has its origin in the atmosphere and surface water bodies. 95% of the ions in groundwaters are represented by the few major ionic species: the positively charged cations sodium (Na^+), potassium (K^+), calcium (Ca^{2+}) and magnesium (Mg^{2+}), and the negatively charged anions chloride (Cl^-), sulfate (SO_4^{2-}), bicarbonate (HCO_3^-) and nitrate (NO_3^-). These ionic species when added together account for most of the salinity that is commonly referred to as total mineralisation or Total Dissolved Solids

(TDS). They contain signatures of the whole history of the groundwater and its reactions with the surrounding mineral assemblages over the course of time (Hiscock, 2005).

Most groundwater originates as rain. Once the groundwater has infiltrated the rock it begins to take on some geochemical properties derived from the rock mass which complicate its interpretation but, it also retains some chemical and isotopic signature of its earlier and independent history (Hiscock, 2005). By the time water reaches the water table, it has acquired the chemical signature of the geologic materials it is flowing through. The evolutionary sequence is controlled by the availability of mineral and their solubility (Fig.2.4).

The concentration of dissolved and undersaturated ions in groundwater is generally considered proportional to the length of the flow path and residence time of the groundwater (Locsey, 2004). Chebotarev (1955) deduced that groundwater tends to evolve chemically towards the composition of seawater. Thus as water moves along the flow path the dominating anionic species follows the pattern in equation 2.1

$$HCO_3^- \rightarrow HCO_3^- + SO_4^{2-} \rightarrow SO_4^{2-} + HCO_3^- \rightarrow SO_4^{2-} + Cl^- \rightarrow Cl^- + SO_4^{2-} \rightarrow Cl^- \qquad (2.1)$$

The flow of groundwater in crystalline bedrock is dependent on existing fractures system. It may occur in single fractures or in complex networks of fractures. Fractures represent brittle deformation in response to stress (McMurry *et al*, 2003). The Stripa project showed that groundwater flowpaths in crystalline bedrocks are usually restricted to small channels along minor paths of the fractures or along shear line of two fractures (KBS-3, 1983). In old fractures

which have been exposed to groundwater three main categories of minerals could be found besides the major mineral components (Allard, 1982).

1. Weathering and alteration products originating from the host rocks
2. Precipitates and crystallization products from supersaturated aqueous solution
3. Metamorphic products

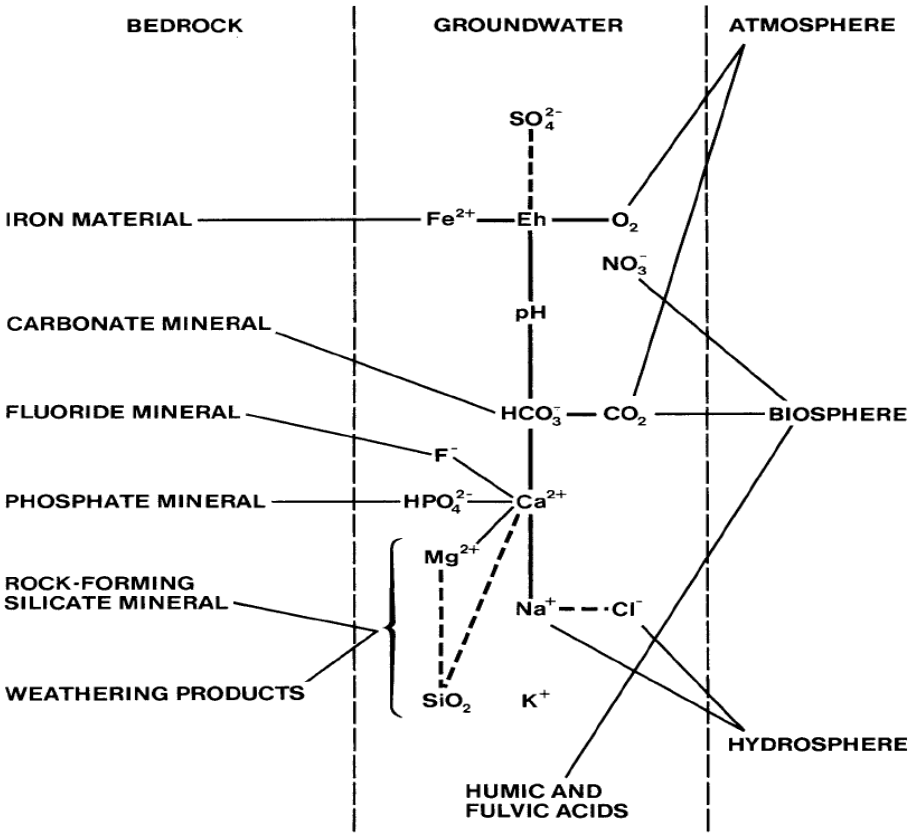

Figure 2.4.Relationship between mineral composition of rock, species in groundwater and the atmosphere and biosphere (KBS-3, 1983).

The fracture mineralogy is not necessarily the same as the mineralogy of the bulk rock. However, the physical and chemical environment in the fractures depends on the mineralogy of the rock and groundwater composition in the rock (Torstenfelt *et al*, 1982).

The natural processes that influence the composition of groundwater include the production of carbon dioxide and mineral dissolution and weathering, oxidation and reduction reactions, ion-exchange and sorption and evaporation. Decay of organic matter is also an important process with respect to production of carbon dioxide.

2.3.1. Carbon Dioxide in Water

The chemical evolution of groundwater begins when rainwater infiltrates the soil. Carbon dioxide present in the atmosphere dissolves in the rainwater and forms aqueous CO_2 according to Henry's law

$$m_{CO_2} = k_H P_{CO_2} = 10^{-1.5} P_{CO_2} \quad (2.2)$$

where m_{CO_2} is the molality of CO_2 in the solution. The dissolved CO_2 associates with the water molecules to form weak carbonic acid, H_2CO_3 (eqn2.3).

$$CO_{2(aq)} + H_2O \rightarrow H_2CO_3 \quad (2.3)$$

Carbonic acid tends to dissociate into hydrogen, bicarbonate and carbonate ions (Garcia *et al* 2001) in a two-step equation.

$$H_2CO_3 \rightarrow H^+ + HCO_3^- \quad (2.4)$$

$$K_1 = 10^{-6.3}$$

$$HCO_3^- \rightarrow H^+ + CO_3^{2-} \quad (2.5)$$

$$K_2 = 10^{-10.3}$$

Based on the present day atmospheric CO_2 pressure of $10^{-3.5}$atm, unpolluted rain water is slightly acidic with a pH value of 5.6 (Appelo and Postma, 2005). The distribution of CO_2 species in water as a function of pH is described by Appelo and Postma (2005). At different pH values, different species of CO_2 are dominant according to the dissociation constants, *K*, noted above.

Carbonic acid is dominant at pH < 6.3, CO_3^{2-} becomes dominant at pH > 10.3 and at intermediate pH values HCO_3^- is the major CO_2 species in water (Appelo and Postma, 2005).

The decay of organic matter, an oxidation reaction that may occur in soil and also within aquifers where fossil organic matter may be present, and the respiration of plant roots also produce CO_2 (Appelo and Postma, 2005; Freeze and Cherry 1979).

$$CH_2O + O_2 \rightarrow H_2O + CO_2\ (g) \qquad (2.6)$$

The waters that enter igneous rocks from the soil zone have CO_2 content 10 to 100 times higher than that expected from equilibrium with the earth's atmosphere the pressure of CO_2 in soils is commonly $10^{-1.5}$ to $10^{-2.5}$atm (Appelo and Postma, 2005). Temperature increases CO_2 production in soil (Drake, 1983).

2.3.2. Mineral Dissolution and Weathering

Dissolution is one of the most generally effective processes in groundwater chemistry and could be considered as the first step in the chemical evolution of groundwater. The degree of dissolution depends on the solubility of the minerals, the antecedent concentration of the water, and the pressure and temperature of the locality (Toth, 1999). Dissolution can be either congruent (simple dissolution of the entire solid) or incongruent (partial dissolution or complete dissolution with immediate reprecipitation of some components to form secondary, and commonly hydrous minerals), sometimes with secondary minerals inheriting structural and chemical constituents of the primary mineral (Harley and Gilkes, 2000).

Dissolution rate of minerals increases exponentially with increasing temperature as described by Arrhenius equation

$$k = k' e^{-Ea/(RT)} \quad (2.7)$$

The $e^{-Ea/RT}$ term corresponds to the temperature effect. *Ea* is the activation energy which depends on pH and mineralogy of the geologic formation (Lasaga *et al*., 1994), R is the gas constant, and T is the temperature in Kelvin. *k* is the dissolution rate constant and *k'* is the temperature-independent pre-exponential factor. This relation indicates an increase in the weathering rate with increasing temperature. By measuring rates of silicate weathering in granitic catchments, White and Blum (1995) showed that weathering of Ca- and Mg silicates increased with increased temperature at constant precipitation. Warmer climate zones may have increased precipitation, thereby increasing silicate dissolution (Berner, 1995).

Decomposition of rock materials involves a set of geochemical processes known collectively as weathering. In a thermodynamic sense, weathering systems are open, irreversible and incongruent (Locsey *et al*, 2012). Weathering reactions are irreversible because they take place primarily as a result of disequilibria between the rocks and their current physico-chemical conditions and incongruent because the dissolved ions are removed by flowing water, while the remaining solid phases differ from the initial solid phases.

Chemical weathering is one of the fundamental processes in nature and is caused mainly by water-rock (mineral) interaction. It is defined as the release of elements due to chemical dissolution and transformation of specific minerals in the soil matrix and the bedrock, and the changes in the alkalinity or acidity in the soil solution connected to this process (Holmqvist,

2001). Chemical weathering is dominant in warm and humid climates (Larson, 1984) and considered to be a significant natural process that controls the composition of groundwater.

The distribution of primary silicate minerals during weathering was recognized by Goldich (1938) who showed that the susceptibility of silicate minerals to weathering could be related to their position in Bowen's reaction series (Fig.2.5). Thus, olivine and anorthite, the first formed minerals in the discontinuous and continuous reaction series, respectively, are the most susceptible to weathering. In both series, minerals that crystallize at successively lower temperatures are more stable to weathering, with quartz, muscovite and K-feldspar being particularly resistant. Eggleton *et al*. (1987) note that although plagioclase begins to alter earlier than pyroxene, pyroxene weathers quicker than plagioclase. This variation relates to the differential between conditions at magmatic crystallization and at the Earth's surface during weathering, as well as to overall mineral structure and chemistry.

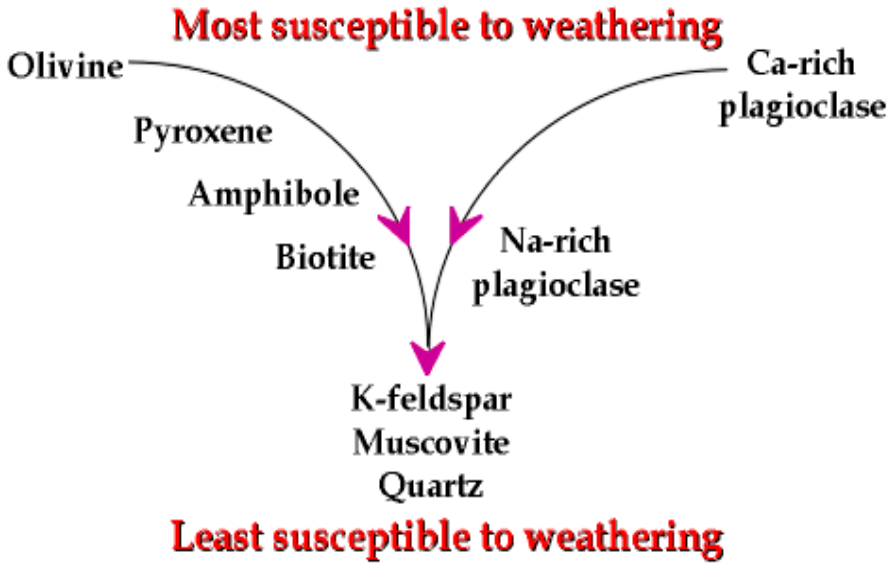

Figure 2.5. The Goldich weathering sequence based on observation of the sequence of their disappearance (Goldich 1938).

A general silicate weathering reaction with carbonic acid can be written as:

(Na, K, Mg, Ca) silicate + H_2CO_3 = H_4SiO_4 + HCO_3 + Na+ K+ Mg + Ca + solid products (2.8)

The elements released into solution during water-rock interaction behave in two different ways (Beaucaire *et al*, 2008). The concentration of elements such as Na, K, Al, Si, Ca and Mg are generally fixed by saturation with respect to available minerals. They are called controlled elements. The precipitation depends on the global composition of the solution, pH, and temperature. The activity of each controlled element M_i is involved in a mass action law equation:

$$K_i\,(T^oC) = \frac{M_i^{n+}}{(H^+)}\gamma \qquad (2.9)$$

corresponding to an equilibrium of this kind

K-feldspar + ½ H_2O + H^+ =K^+ + ½kaolinite + 2 quartz (2.10)

The concentration of mobile ions such as Cl^- and SO_4^{2-} can increase in solution without being controlled by secondary mineral phase solubility. Their concentration is externally fixed and only involved in the charge balance relationship, as follows:

$$\sum_i \frac{n_i(H^+)1^{n_i}K_i}{\gamma_i} - (A^-) = 0 \qquad (2.11)$$

The phase rule implies that the concentration of each controlled element is constrained by saturation with a mineral phase, H^+ being associated with the aqueous phase. It is considered that Si is controlled by quartz, Al^{3+} by kaolinite, Ca^{2+} by calcite, Mg^{2+} by dolomite (or chlorite), Na^+ by albite and K^+ by K-feldspar. Chloride and sulphate are externally fixed as sulphate is not constrained by the solubility of a mineral such as gypsum.

In silicate weathering reactions, sodium is mainly derived from Na-feldspars such as albite ($NaAlSi_3O_8$) or any member of the plagioclase solid solution series between albite and anorthite (Appelo and Postma, 2005). Clay minerals may also release exchangeable sodium (Locsey, 2004). Calcium is released from weathering of plagioclase and hornblende and pyroxenes. The sodium and calcium liberated participate in ion exchange reactions, seldom in identical positions, due to their similar ionic radii (0.99Å for Ca^{2+}, 0.95Å for Na^{+})(KBS-3, 1983). As a result the Na^{+} and Ca^{2+} concentrations are often related to each other as well as to some extent to pH.

Magnesium is liberated through weathering of biotite and amphiboles whilst potassium is released to solution by the dissolution of K-feldspar. They also participate in ion exchange equilibria, but not in direct exchange with sodium or calcium, due to their different ionic radii (0.65Å for Mg^{2+} and 1.33Å for K^{+}). K is removed from weathering solutions to a greater extent than Na both in secondary clay mineral formation and in mineral-solution exchanges (adsorption) (KBS-3, 1983). The rate of K removal by these processes is controlled by the chemistry of ambient solutions and the physical and chemical properties of available surfaces (Kronberg *et al*, 1987).

The hydrological conditions in combination with the rate of mineral weathering determine the nature of the weathering product. Kaolinite is the common weathering product of plagioclase and other primary minerals (Ceryan *et al,* 2008). Illite is a common weathering product of granitic rocks and smectites are abundant secondary products after weathering of mafic minerals and basic rocks (Ceryan *et al,* 2008). The weathering reactions for some aluminosilicate primary minerals are presented in Equations 2.12 – 2.16.

$$3NaAlSi_3O_8 + Mg^{2+} + 4H_2O \rightarrow 2Na_{0.5}Al_{1.5}Mg_{0.5}Si_4O_{10}(OH)_2 + 2Na^+ + H_4SiO_4 \quad (2.12)$$

Albite *montmorillonite*

$$3NaAlSi_3O_8 + 2H^+ + 9H_2O \rightarrow Al_2Si_2O_5(OH)_4 + 2Na^+ + 4H_4SiO_4 \quad (2.13)$$

Albite *Kaolinite*

$$3NaAlSi_3O_8 + H^+ + 7H_2O \rightarrow Al(OH)_3 + Na^+ + 3H_4SiO_4 \quad (2.14)$$

Albite *gibbsite*

$$Ca(Al_2Si_2)O_8 + 2H^+ + H_2O \rightarrow Al_2Si_2O_5(OH)_4 + Ca^{2+} \quad (2.15)$$

Anorthite *Kaolinite*

$$(Mg_{0.7}CaAl_{0.3})(Al_{0.3}Si_{1.7})O_6 + 3.4H^+ + 1.1H_2O \rightarrow 0.3Al_2Si_2O_5(OH)_4 + Ca^{2+} + 0.7Mg^{2+} + 1.1H_4SiO_4 \quad (2.16)$$

Augite *Kaolinite*

Many of the intermediate or end products in the weathering sequences have higher ion exchange capacity than the starting material. Cs and Sr are sorbed on weathering products (clay) to a concentration that is about 2000 times higher than in the groundwater with which the clay is in contact (KBS-3, 1983). Increase in pH leads to enhanced cation exchange capacity (CEC). Thus unaltered feldspars usually exhibit a CEC below 10 meq/kg at pH 8, while kaolinite could have a CEC up to 20-30 and montmorillonite up to 700 – 800 meq/kg (KBS-3, 1983).

2.3.3. Thermodynamic Controls on Groundwater Chemistry

The equilibrium state of groundwater with respect to a mineral phase can be determined by calculating the Saturation Index (SI) using analytical data (Stumm and Morgan, 1981). The SI is defined as the logarithm of the ratio of Ion Activity Product (IAP) to the mineral equilibrium constant at a given temperature and is given as:

$$SI = \log(IAP/Ksp), \quad (2.17)$$

where IAP denotes the ion activity product of the solution, and Ksp denotes the solubility product of the solid phase. The SI reflects the direction of the reaction. A negative SI indicates that the solution is undersaturated and that dissolution is expected, whilst a positive SI indicates that the solution is supersaturated and that precipitation should occur. Because of inherent uncertainties in the calculation of SI, a range of values near zero, such as SI = 0 ± 0.5 are considered to be within equilibrium (Deutsch, 1997). The calculation of ion activities and saturation states can be undertaken using computer based hydrochemical models such as PHREEQC (Parkhurst and Appelo, 1999).

One of the drawbacks of the saturation state approach, particularly with respect to silicate minerals noted by Appelo and Postma (2005) is that the aluminum concentration in groundwater is often below the detection limit. Mineral stability diagrams (Fig 2.6) may be used to display such data, and are based on the assumption that all the aluminum is preserved in the weathering product. The cation/proton activity ratio is a useful measure of the evolution of a water body towards equilibrium in a particular geological environment since progressive water-rock interaction involves simultaneous increase in aqueous cation concentration from the mineral and decrease in hydrogen ion concentration (Locsey, 2004). The lines on stability diagrams represent the alternation of one mineral to another, based on thermodynamic data. The stability diagrams thus can be used to predict which minerals will react with natural waters, to provide information about the nature of the reaction products and to predict the directions these reactions take.

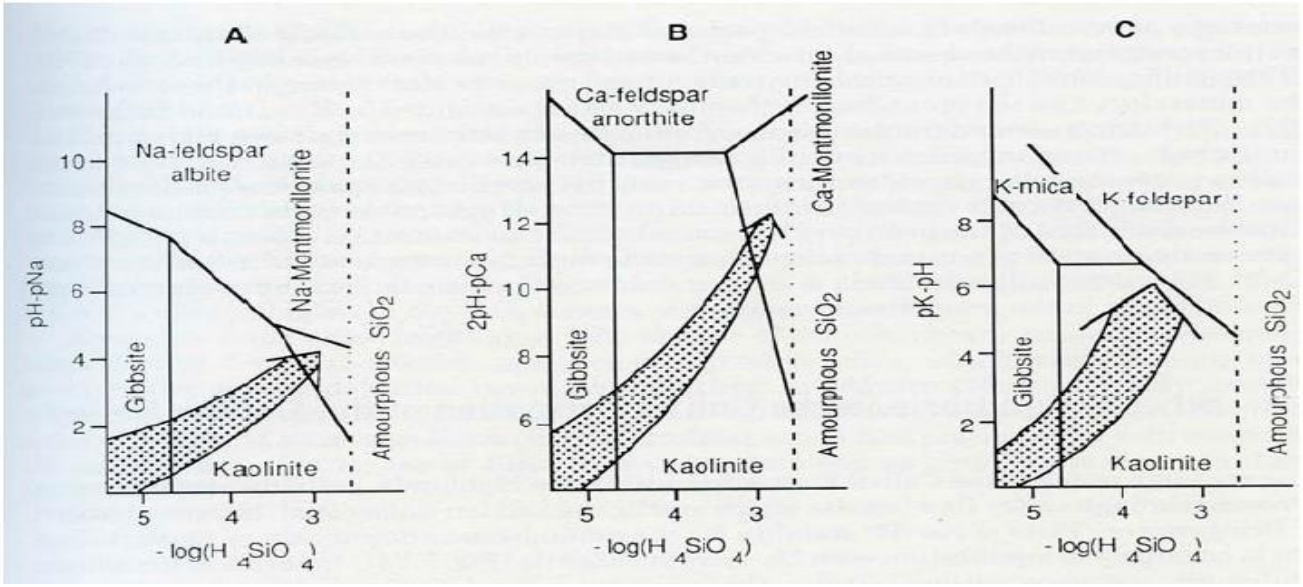

Figure 2.6.Predominance diagrams illustrating the stability relationships between gibbsite, kaolinite, montmorillonite and feldspars. Arrows indicate hypothetical paths taken during the weathering process (after Stumm and Morgan, 1981).

2.4. Salinity

There were many possible sources of salinity that has been broadly categorized as originating internally (rock-derived) or externally (infiltrating fluids from a distant location and time) (Nordstrom *et al,* 1989b). Recent or ancient marine sources, recent or ancient meteoric sources, residual metamorphic/magmatic fluids (fluid inclusions) and hydrothermal fluids (Nordstrom *et al*,1985) are factors that influence the origin, evolution, reactive processes and flow characteristics of groundwaters in crystalline rocks. Any combination of these may occur and they may be modified in composition by interaction with the local rock mass.

Water/mineral interaction processes that may constitute local salinity sources within the bedrock include:

• Hydrolysis of silicate minerals

• Release of salts from the rupture of fluid inclusions

• Radiolytic decomposition of groundwater

Investigations carried out by Pitkanen *et al* (1994) suggested that at shallow depths of bedrock, increase in groundwater salinity seems to be controlled by the interaction of the groundwater with the bedrock, whereas at deeper depths such an influence is only minor.

2.5. Radiolysis

An important factor in evaluating the chemistry of the near field of a repository is the perturbation caused by the radioactive waste. Water radiolysis may occur in the near field environment due to interaction between the gamma-rays produced by the waste and the groundwater (Yonezawa *et al*, 1996). The products of the groundwater radiolysis will accelerate the weathering of the rocks and minerals surrounding the repository. Two mechanisms have been proposed to explain the interaction features observed: direct reaction of mineral surfaces with the radiolysis products, and the effect of valence change of ions in the solution during irradiation.

Radiolysis of the groundwater produces equivalent amount of oxidative (principally oxygen gas and H_2O_2) and reducing species mainly hydrogen gas, represented by equation 2.18 as:

$$H_2O \rightarrow H_2O^* \rightarrow H_2, H_2O, H_2O_2, OH, O_2, H^+, e^- , \text{etc} \qquad (2.18)$$

These reactions occur within a very short time (about 10 sec) after the passage of the ionizing particle through the system. Hydrogen is fairly unreactive and will be transported away by diffusion and convection. Hydrogen peroxide is a strong oxidizing agent and will oxidize any ferrous iron it encounters into ferric iron (Yonezawa *et al*, 1996). The result is a transformation of a reducing environment into an oxidizing one. Thus the rock surrounding the waste package

or repository will act as a buffer consuming the oxidants in the water and will itself be oxidized progressively. A redox front will move very slowly into the rock carrying dissolved radionuclide behind it and precipitating it at the front.

In such an oxidizing environment, some elements of concern to radioactive waste, particularly, the actinide elements and technetium are likely to be more soluble and less readily adsorbed than in a reducing one. The effect of radiolysis thus would render certain waste elements more mobile than they might have been in the ambient reducing environment of the host rock. These mobile elements would move through the oxidized rocks until they encounter a reducing environment i.e. rocks in which the available ferrous iron has not been oxidized by radiolysis. These mobile species would then form aureoles around the radioactive materials along an oxidation – reduction front defined by the valence state of iron. Studies carried out by Jantzen and Bibler (1985) suggests that radiolysis may not cause the groundwaters to become oxidizing in a crystalline repository when abundant Fe^{2+} species are present.

The rocks around the Oklo natural reactor in Oklo, have been exposed to higher levels of radiation than any known rock type on earth. Studies carried out by Curtis and Gancarz (1983) indicated that radiation effect resulted in a net reduction of iron in the reactor zone rocks. They considered that the reduction in iron was most likely due to the production of hydrogen ions by radiolysis of the groundwater during nuclear criticality. The addition of hydrogen, as the reduction mechanism, rather than the removal of oxygen, was favoured because the oxygen fugacity was considered much too low to facilitate oxygen removal.

2.6. Environmental Stable Isotope

Potential sites for the disposal of radioactive wastes imply very low-permeability rocks. Aquifers as such are not present, but weak and isolated groundwater circulation may occur, giving rise to low total flow. These groundwaters may have various origins. They can be inherited from ancient marine transgressions, produced by sediment compaction or pressure dehydration of hydrated salts or can be old waters of meteoric origin corresponding to conditions of recharge and circulation which are no longer prevailing. The limitations in use of classical and conventional tools for studies of low permeability rocks represent basic reason for extensive use of environmental isotopes.

Environmental isotopes are commonly categorized into two general groups: stable isotopes and unstable (radioactive) isotopes. Stable isotopes are not involved in radioactive decay. Most stable isotopes do not react chemically in the subsurface environment and are of particular use in determining the source of groundwater. Unstable (radioactive) isotopes are involved in radioactive decay and they are of particular use in determining the age of water.

Stable isotopes of hydrogen and oxygen are very suitable tools for hydrogeological investigations because they are part of the water molecules and follow their behaviour through hydrological cycles. The determination of ^{18}O and ^{2}H concentrations in groundwaters of the Stripa granite permitted the recognition of different groundwater regimes and emphasized the lack of interconnectivity in several parallel or subparallel fracture systems (Moser *et al*, 1989). Environmental isotope analyses of groundwater were used to determine the chemical evolution of fresh and saline groundwaters in the crystalline rocks of the Canadian Shield (Frape *et al*,

1984). The results suggested that many of the saline groundwaters do not represent different stages along a geochemical evolutionary path during which increasing amounts of TDS are imparted to the groundwaters through rock-water interactions, but, in fact represent mixtures of local fresh waters with brine fluids. Environmental isotope hydrology studies in Ghana have been attributed to Akiti (1977, 1980). Akiti (1980) applied environmental isotopes such as ^{2}H, ^{18}O, ^{3}H (tritium) and ^{14}C to study groundwater in the foothills ofthe Accra Plains.

2.6.1. ^{18}O and ^{2}H – Stable isotopes of groundwater

Hydrogen and oxygen each have naturally occurring stable isotopes. Stable hydrogen exists as hydrogen, ^{1}H, and deuterium, D or ^{2}H. Oxygen exists as three stable isotopes, ^{16}O, ^{17}O, and ^{18}O. A water molecule may be composed of any combination of these stable isotopes plus tritium, ^{3}H, which is a short half-life (about 12.5 years) radioactive hydrogen isotope. The variations in natural abundance of oxygen and hydrogen isotopes in water samples are measured as deviations from an international standard, which is a composite sample of water from several oceans called SMOW (Standard Mean Ocean Water). SMOW is composed of 99.726 percent $H_2{}^{16}O$, 0.200 percent $H_2{}^{I8}O$, 0.042 percent $H_2{}^{17}O$, and 0.031 percent $HD^{16}O$. All the other possible isotope combinations compose the remaining 0.001 percent (Craig, 1961). Of these, stable hydrogen ($\delta^{2}H$) and oxygen isotope (primarily $\delta^{18}O$) ratios in water are ideal conservative tracers of water sources. Stable isotope ratios of water are conservative in aquifers at low temperature, but water can be isotopically fractionated on the surface at less than 100% humidity (Gat, 1970). Because the vapor pressure and diffusivity of $H_2{}^{16}O$ is greater than that of $H_2{}^{18}O$, the residual liquid is characterized by a higher $H_2{}^{18}O$ content after evaporation and rain from clouds is enriched in $H_2{}^{18}O$, preferentially depleting air masses in $H_2{}^{18}O$ as they move across continents. Protium (^{1}H)

and deuterium (^{2}H) can also fractionate, but to a greater extent due to larger relative mass difference. ^{2}H is also enriched in precipitation falling from clouds, which caused air masses to become preferentially depleted in ^{2}H as they become colder and lose their moisture. Additionally, evaporation preferentially enriches surface water in ^{18}O relative to ^{2}H. These processes create a seasonal cycle in surface water. As a result, $^{18}O/^{16}O$ and $^{2}H/^{1}H$ ratios can be used to identify the source and timing of groundwater flow (Maloszewski *et al*., 1990; Krabbenhoft *et al*., 1990, Fritz, 1981).

The usefulness of environmental isotopes as isotopic tools relies on the fact that mass (energy) differences cause slight variations in the geochemical and physical behavior. Reaction rates and equilibrium constants differ for isotopic compounds which result in isotope fractionation effects. Spatial and temporal variations in stable isotope ratios of hydrogen ($^{2}H/^{1}H$) and oxygen ($^{18}O/^{16}O$) in atmospheric water vapour and precipitation are caused by equilibrium and kinetic isotopic fractionation mechanisms associated with evaporation and condensation processes during global circulation of water vapour (Fontes, 1980). Fractionation of the isotopic species of water is denoted by the symbol;

$$\alpha = \frac{R_{vapour}}{R_{liquid}} \qquad (2.19)$$

Fractionation of oxygen and hydrogen from a reservoir of water produces values of $\delta^{2}H$ and $\delta^{18}O$ that follow the Rayleigh Law,

$$\delta f = \delta O - \varepsilon^{*} \cdot \log f, \qquad (2.20)$$

where ε^{*} is the equilibrium fractionation factor, f is the fraction of water remaining in the system ($0 < f < 1$), and δO and δf are the isotopic signatures of the water before and after fractionation, respectively. In precipitation formed in equilibrium with atmospheric water vapour at a certain

temperature and disconnected from the moisture source, the degree of Rayleigh distillation during the cloud rainout depends largely upon: source and event latitude, altitude of condensation, and the amount and duration of precipitation events (Kendell and Coplen 2001; Clark and Fritz, 1997; Yurtsever and Gat 1981). The ^{18}O and D concentrations in precipitation are temperature dependent and their mean annual concentrations are directly related to the mean annual temperature (Dansgaard, 1964).

2.6.2. Global Meteoric Water Line

Worldwide analyses of precipitation have established that a relation exists between δD and $\delta^{18}O$. When δD is plotted against $\delta^{18}O$, almost all analyses of precipitation cluster about a line known as the Global Meteoric Water Line (GMWL) defined by Craig, 1961, as

$$\delta D = 8\ \delta^{18}O + 10\ ‰) \qquad (2.21)$$

While the slope of 8 is usually consistent for meteoric waters, the intercept may vary significantly, depending on "local" precipitation conditions. The GMWL is a convenient reference line for understanding and tracing local groundwater origins and movements. Deviations from the GMWL are found on a seasonal basis in many arid and semi-arid regions, mainly asa result of partial evaporation of raindrops in a relatively dry atmosphere below the cloud base.

2.6.3. Deuterium Excess

A crucial parameter for the discussion of the origin of a given water is the deuterium (d) excess (Dansgaard, 1964), which is defined as

$$d\ (\text{per mil}) = \delta^{2}H - 8\ \delta^{18}O. \qquad (2.22)$$

It is the δ^2H intercept value of a line of slope 8 fitted through a dataset, and typically has values close to +10‰ for rain samples. The slope of 8 is used because it is the slope of the GMWL and results from the fact that the global average water vapour forms from an average humidity of about 85% over the oceans.

The d-excess parameter has been shown to be a diagnostic tool for measuring the contribution of evaporated moisture to the downwind atmosphere because evaporation of recharging water generally causes a decrease in the d-excess. (Gat *et al*., 1994). This is as a result of the greater kinetic isotope fractionation of oxygen isotopes than for hydrogen isotopes due to the relative diffusion rates of different water isotopologues (Clark and Fritz, 1997). Therefore the d-excess values of groundwater may indicate the effect of evaporation before and during recharge (Deshpande *et al*., 2003).

Merlivat and Jouzel (1979) showed that the d-excess in air masses (and hence precipitation) depends on the relative humidity of the air masses at their oceanic origin, the ocean surface temperature, and kinetic isotope effects during evaporation. Because of the link to humidity, d-excess values are sensitive to evaporative processes. High d-excess values (10‰) generally indicate that more evaporated moisture has been added to the atmosphere (Gat and Matsui, 1991), commonly interpreted as resulting from cooler and dryer air masses (Merlivat and Jouzel, 1979). Deuterium excess values lower than 10‰ may be indicative of secondary evaporation processes, suggesting evaporation from a source more humid than the global ocean average. The deuterium excess offers a possibility for characterizing the interaction of different air masses and their temporal evolution

2.6.4. Effects of Meteoric Processes on the Isotopic Composition of Water

Meteoric processes modify the stable isotopic composition of water, and consequently the recharge waters in a particular environment will have a characteristic isotopic signature, often allowing the separation of waters from different environments (Clark and Fritz, 1997). The first process which may modify the stable isotope content of groundwater is evaporation. As water evaporates from the ocean, moves through the atmosphere, and condenses to form precipitation, the percentage of each isotopic species (molecule) changes due to fractionation (Fig.2.7).

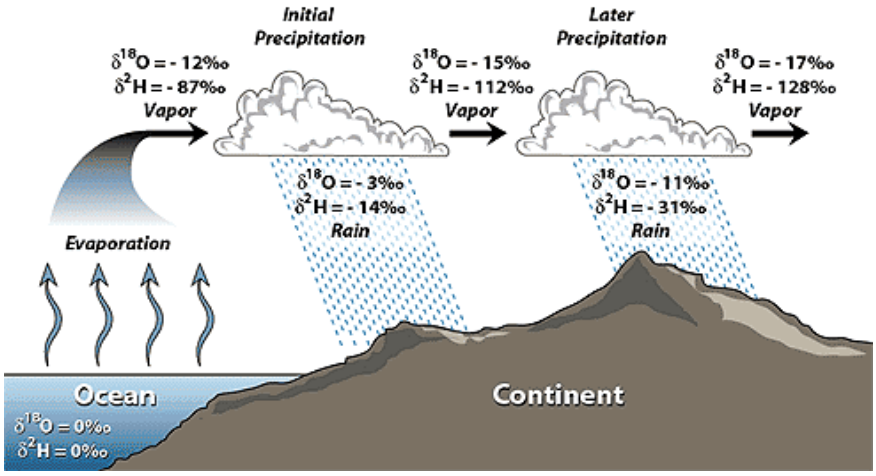

Figure 2.7. Rainout effect on ^{2}H and ^{18}O values (Coplen *et al*, 2000)

Isotopically light water molecules evaporate more efficiently than heavy ones. As a result, the vapour is enriched in light water molecules, reflected in relatively negatively δD and $\delta^{18}O$. In contrast, the residual water phase becomes relatively enriched in the heavy isotopes, reflected in more positive δD and $\delta^{18}O$ values. Evaporation, because it results in irreversible kinetic effects, tends to bring about deviation from the GMWL.

Isotopic fractionation during evaporation causes fractionation during cloud formation. The vapour in the clouds has a lighter isotopic composition than the ocean that supplied the water.

Upon condensation from the cloud, during rain formation, the heavy water molecules condense more efficiently, leaving the cloud residual vapour depleted of deuterium and ^{18}O. The result of this differential evaporation, condensation, or freezing is that, isotopic composition of precipitation differs from that of the water body from which it originated. The precipitation gets lighter as the rain continues, a phenomenon known as rainout effect.

As water moves into the ground, it begins to record information on the history of its recharge source and properties, mainly from rainfall as well as isotopic ratios in the water molecule. For most groundwater in the "normal" temperature range, there are no modifications of their ^{2}H and ^{18}O content due to interactions between the aqueous phase and solid minerals (geochemical behaviour). However a variety of processes such as the following may cause changes in the isotopic composition of the water (Gat, 1981; IAEA, 1981(b); Fontes, 1980).

(1) recharge to the aquifer from areas of a differing altitude and latitude;

(2) recharge from a body of surface water that has been partially evaporated;

(3) recharge that occurred at an earlier time when local or worldwide climate was different;

(4) mixing with other sources of water, such as brines or magmatic water; and

(5) interaction with aquifer materials.

These factors have a definite, predictable effect on a $\delta^{2}H$-$\delta^{18}O$ plot (Fig.2.8) which can be used to estimate recharge areas, mixing fractions between aquifers and between surface water and groundwater, as well as to provide a window into past changes in recharge or climatic condition during the recharge processes (Salem *et al.* 2004).

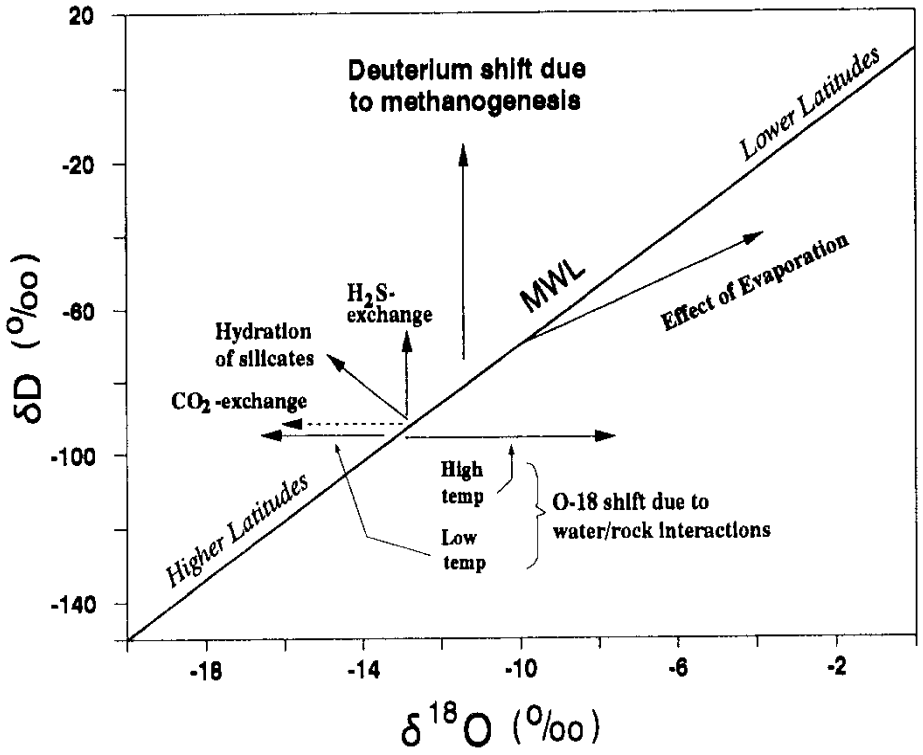

Figure 2.8 Summary diagram of how hydrologic processes affect oxygen and hydrogen isotopic composition of water (IAEA, 1983)

Despite the strong evaporation in arid regions, it is possible to have present day recharged waters with isotope contents close to the mean composition of precipitation. This has been observed in Central Africa (Mathieu and Bariac, 1996) where soil profiles show the typical evaporative isotope enrichments, yet little to no enrichment is observed in the groundwater. This has been attributed to macropores and preferential flow channels in the unsaturated zone, permitting the fast movement of water to the water table with very limited mixing with the enriched water found in the upper parts of the profile. What is significant here is tracing the stable isotope signal of rainfall in groundwater in order to demonstrate present day recharge.

When the mixing of meteoric water with recent or connate marine water is the primary cause of salinity, then variations in the salinity of the aquifer are expected as a result of variations in the degree of mixing. The ^{18}O vs either ^{2}H or chloride values of the groundwater should be positively correlated and plot on a mixing line between the composition of seawater and that of the least saline ground water (Sami, 1992).

If salinity is primarily due to the concentration of dissolved salts by evaporation, then the ^{18}O-^{2}H relationship will have a low slope reflecting kinetic fractionation. In addition, a plot of chloride mass per solution against either isotope will be positively correlated, as increased evaporation would result in isotopic enrichment as well as an increased chloride concentration (Payne 1988). Lateral mixing of waters may obscure the chloride vs isotope relationship resulting in a poor correlation when waters with different chemical and isotopic content signatures exist concurrently.

If salinity is due to the leaching of evaporitic salts by rapid percolation through preferential pathways, then the groundwater should retain an ^{18}O-^{2}H relationship similar to that of the regional rainfall. As leaching process does not affect the isotopic composition of water (Payne, 1988), there would be no correlation between isotope and chloride.

2.7. Naturally Occurring Radionuclide

Disposal of radioactive wastes in a geological repository will add a concentrated source of radioactivity to the natural radioactivity dispersed in the geologic formation. According to the United Nations Scientific Committee on Effects of Atomic Radiation (UNSCEAR) 2000 report, natural sources of radiation are the largest contributors (87%) to the external dose of the world

population. Natural sources of radiation are the concentration of naturally occurring radionuclides that represent ambient conditions present in the environment that are in no way influenced by human activity (Egidi, 1998). The world average of annual effective dose from natural background radiation is 2.4 mSv (UNSCEAR, 2000). The most common terrestrial radionuclides and the biggest contributors to total background radiation are ^{238}U, ^{232}Th daughter products and ^{40}K (Langmuir and Herman, 1980; Langmuir, 1978). The intensity of the terrestrial natural radioactivity varies by an order of magnitude for different regions due to geological factors (Langmuir, 1978).

The actinides with their daughter products (Th, Pa, U, Np, Pu, Am, Cm) which will be present in the disposed waste materials will dominate the hazard due to their long half-lives. Because of the very long half-lives of these radionuclides, the safety of the disposal must be assured for tens of thousands of years into the future. Since the actinide elements do not occur naturally in appreciable quantities, their behavior in a repository environment cannot be predicted from evidence of their movement in groundwater in the geologic past (Krauskopf, 1986). A useful means of reducing the uncertainty is to observe the behavior of naturally occurring elements with similar properties.

The naturally occurring uranium (^{238}U) and thorium (^{232}Th) are thus of particular interest in radioactive waste disposal since they represent useful analogues of the actinides (Smellie *et al*., 1986) and show different solubility characteristics (Langmuir and Herman, 1980). They decay to stable isotopes of Pb through a series of intermediate daughters consisting of elements with

diverse chemical properties and a wide range of decay mean lives (Fig. 2.9). Their high geochemical mobility allows them to be easily mobilized into the environment (Faanhof, 1999).

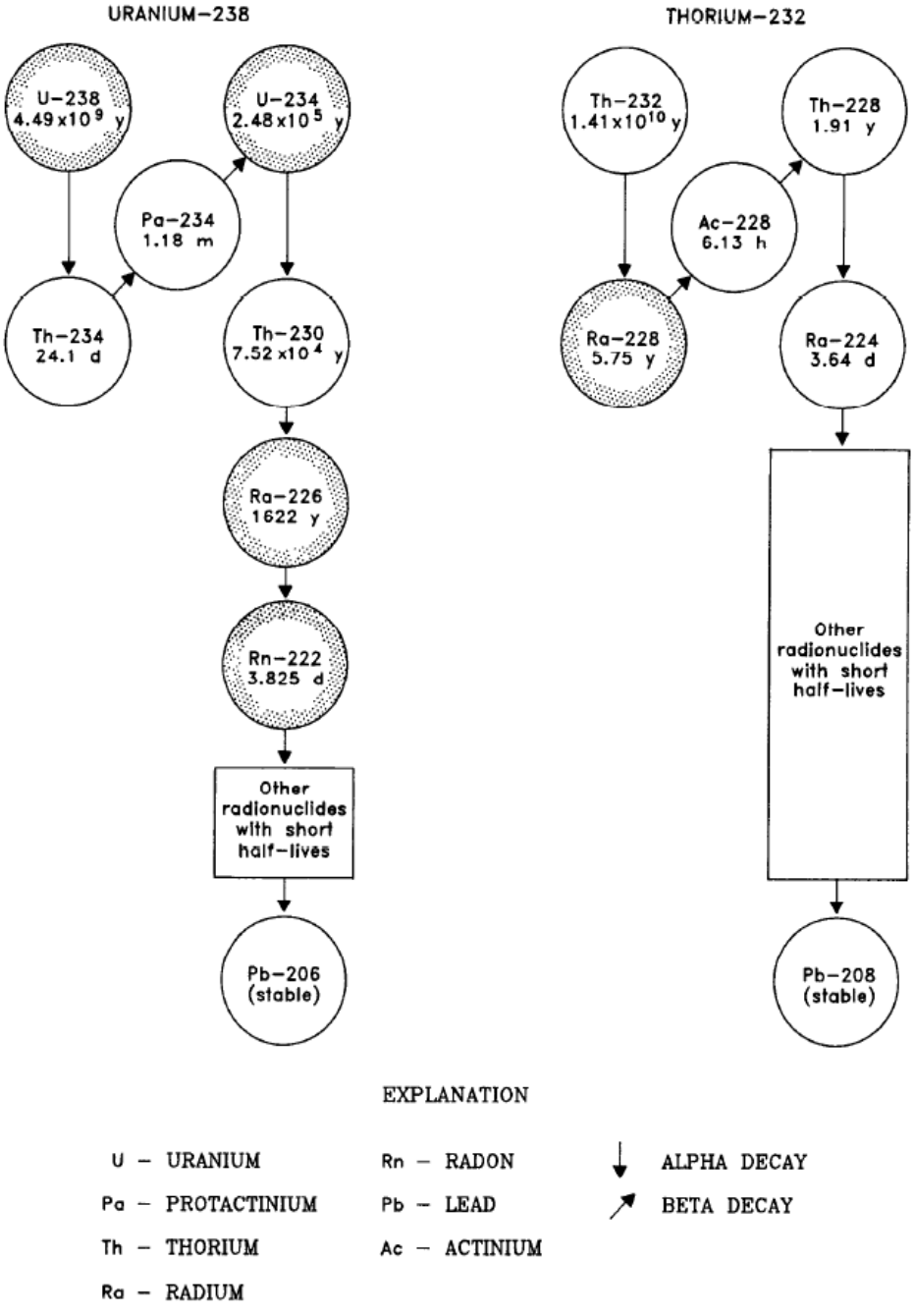

Figure. 2.9. Simplified schematic representation of the ^{238}U and ^{232}Th decay series (Ivanovich and Harmon, 1982).

2.7.1. Isotopes of Uranium, Thorium and Potassium

Naturally occurring uranium (U) consists of three isotopes, of which two, ^{238}U (99.2739%, half-life 4.5 x 10^9 years), and ^{235}U (0.7025%, half-life 7.3 x 10^8 years), are primordial and initiate two of the three naturally occurring radioactive decay series. The third isotope ^{234}U (0.0057%, half-life 2.48 x 10^5 years), being a member of the ^{238}U decay series, is radiogenic. The ^{238}U and ^{234}U belong to one family called the uranium series (4n+2), while the ^{235}U isotope belongs to another series called the actinium series (4n+3)(Table 2.2). Although by weight the overwhelming fractions of natural uranium is the ^{238}U isotope, because of the higher specific activity of ^{234}U, the radioactivity in freshly separated natural uranium is about equally divided between ^{238}U and ^{234}U (Kathren, 1998). These two isotopes contribute about 98% of the total activity from freshly separated uranium. ^{234}U is a decay product of the ^{238}U series. In a sealed rock mass with no water–rock interactions, all intermediate radionuclides will attain radioactive equilibrium (equal levels of radioactivity) with one another within a maximum of 1 to 2 Ma, based on the half-life of the longest-lived intermediate, ^{234}U (depending on analytical capabilities, up to 5 half-life periods are required before the $^{234}U/^{238}U$ activity ratio attains radioactive equilibrium) (Ivanovich and Harmon, 1982).

Table.2.2 Naturally occurring radioactivity decay series (Suksi, 2001)

Name of series	Type	Primordial nucleus Nucleus	Half-life (y)	Longest-lived daughter Nucleus	Half-life (y)	Final nucleus (stable)
Thorium	4n*	^{232}Th	$1.39 \cdot 10^{10}$	^{228}Ra	5.7	^{208}Pb
Neptunium**	4n + 1	^{237}Np	$2.20 \cdot 10^{6}$	^{233}U	$1.59 \cdot 10^{5}$	^{209}Pb
Uranium	4n + 2	^{238}U	$4.49 \cdot 10^{9}$	^{234}U	$2.48 \cdot 10^{5}$	^{206}Pb
Actinium	4n + 3	^{235}U	$7.13 \cdot 10^{8}$	^{231}Pa	$3.3 \cdot 10^{4}$	^{207}Pb

* n is an integer

** the neptunium series, characterised by the geologically short half-life of ^{237}Np, does not occur in nature

Uranium occurs naturally at trace levels (<1–10 ppm) in the major rock-forming minerals (quartz, feldspars, micas) in volcanic and plutonic rocks and is concentrated (10–1000 ppm) in accessory minerals such as zircon, sphene and apatite (Gascoyne *et al*, 2002). The average uranium concentration in most crustal rocks is about 2.7ppm or 3.7Bq/kg (UNSCEAR 2000). Uranium has two relatively stable oxidation states, 4^+ (uranous) and 6^+ (uranyl), in essentially all geologic environments. The tetravalent state is the normal ionic condition within rocks while the hexavalent state is the normal form in oxidising conditions and in many secondary U minerals (Langmuir, 1978). Uranyl is more soluble than the uranous (NRC, 1999) and transported generally in oxidising water and ground water as uranyl ion (UO_2^{2+}) or as uranyl fluoride, phosphate, or carbonate complexes. The greater solubility of U^{6+} as the uranyl ion (UO_2^{2+}) is due to its ability to form stable soluble complexes with various organic and inorganic ligands. The occurrence and distribution of uranyl species in surface and subsurface environments is controlled by the redox conditions, pH and the CO_2 partial pressure (Giblin *et al.*, 1981). In oxidising and acidic waters, UO_2^{2+} and uranyl fluoride complexes dominate whereas the carbonate and phosphate complexes dominate in near-neutral to alkaline oxidising conditions.

Only two long-lived isotopes of thorium occur in nature (Langmuir and Herman, 1980). The major one is Th^{232}, which is the parent nuclide of a long decay series terminating with Pb^{2O8}. The half-life of Th^{232} is $1.39x10^{10}$ years, which is considerably longer than that of either U^{238} or U^{235}. The other natural isotope of thorium, Th^{230}, is generally present in minerals which contain uranium. Thorium-230 is the decay product of U^{234}, an intermediate in the decay of U^{238}. Its half-life is 80,000 years. The decay product of ^{232}Th, ^{208}Tl is measured by gamma-ray spectrometry because it is directly related to thorium radioactivity.

Thorium is widely found in crustal rocks, being more abundant in acidic materials than alkaline ones. By weight the average thorium content of the continental upper crust and soils is about 9-10 ppm, about four-fold greater than that of uranium (Kathren, 1998). However, thorium has a much lower specific activity than uranium and the radioactivity concentration of the two elements is about the same. Thorium exhibits only the (IV) oxidation state and, like uranium (IV), its oxide is extremely insoluble and forms strong bonds with a variety of anions. The principal mode of transport for thorium is in insoluble resistate materials as it is too insoluble to be carried in solution. Thorium forms a large number of salts such as the sulfate, chloride, etc. which are soluble in acid solutions. Slightly basic solutions however, hydrolyse the thorium ion to an oxide or hydroxide precipitate. The solubility is commonly given in terms of the solubility product of $Th(OH)_4$ which is approximately 10^{-42}.

Both thorium and uranium decay series include isotopes of radium (Ra). The isotope ^{226}Ra is particularly important. It decays by alpha emission to^{222}Rn (radon). ^{222}Rn has a half-life of 3.82 days and is chemical inert gas. The geologic behavior of radium is strongly influenced by its ability to form, and be co-precipitated with, insoluble sulfates and carbonates. It also forms a number of complex ions (Ivanovich and Harmon, 1982). Insoluble radium carbonates can be mobilized by the introduction of sufficient carbon dioxide to form the more soluble bicarbonate. The principal hazards posed by U and Th are their chemical toxicity and the radiological hazards posed by some of their decay products, especially those that are alpha particle emitters (^{226}Ra and ^{222}Rn) which become a concern if they are inhaled or ingested (Ivanovich and Harmon, 1982).

Potassium (K) is a major constituent of many rock forming minerals and is enriched in acidic igneous rocks relative to basic ones. Potassium-40 (^{40}K) is a secondary isotope of K. It is radioactive and has a half-life of 1.28 x 10^9yr and isotopic abundance of 0.0118% which gives specific activity of 31.4Bq/g of natural potassium (Kathren, 1998). ^{40}K decays to stable ^{40}Ar (11.2%) by electron capture and by positron emission resulting in the release of gamma photons with maximum energy of 1.46 MeV. ^{40}K also undergoes decay to stable ^{40}Ca (89%), emitting a 1.314 Mev beta particle in the process. Potassium is highly soluble in surface waters under a wide range of pH and Eh conditions however sorption by clay minerals limits its mobility. Its concentrations range from about 0.1% for limestone to more than 4% for some granite. For crustal rock, the mean ^{40}K activity is 0.62Bq/g with basalt averaging about half the concentration. Granites with low calcium have concentrations exceeding 1.85Bq/g. Potassium is a major element in the composition of K-feldspars (orthoclase, microcline), present in all granitic rocks, and biotite and muscovite, present in most of the granitic rocks, as main rock-forming minerals. The K_2O content of K-feldspars varies from 11 to 15% while in biotite and muscovite it varies from 8 to 10% and from 10 to 11%, respectively. Overall, in the geologic environment uranium is the most mobile of the three elements and thorium is the least (Langmuir and Herman, 1980).

2.7.2. Radioactive Series Disequilibrium

The uranium and thorium radionuclides in the decay series are more or less in radiological equilibrium. Equilibrium is attained in a radioactive series when all the daughter products decay at the same rate that they are produced from the parent isotope (Langmuir and Herman, 1980). Thus, at equilibrium each of the daughter products would be present in a constant proportion to

its parent isotope. Under the equilibrium conditions the radiation from these radionuclides are virtually trapped underground and exposures only occur in the state of disequilibrium between the radionuclides.

Radioactive disequilibrium develops because the decay series elements have diverse chemical properties and half-lives. The time needed to restore radioactive equilibrium after disruption of the initial state of equilibrium and the rate at which the restoration occurs are determined by the half-lives of the respective nuclides (cf. Table 2.2). This disequilibrium is as a result of differences in properties of the radionuclides in the series, due to geochemical migration processes and differences in their half-lifes (Cember, 1996). The disequilibria owe their origin largely to adsorption and desorption processes, except for those involving long-lived Th (^{230}Th and ^{232}Th), U (^{238}U and ^{234}U) and Ra (^{226}Ra) isotopes, whose distributions are affected by dissolution and precipitation as well (Sato and Endo, 2001). Adsorption of Ra and Th by aquifer solids takes place on time scales of a few tenths of a minute to several minutes. The desorption are several days for Ra and several years for Th. These time constants lead to estimates of the *in-situ* retardation factors (i.e., the ratio of flow rates of fluid to those of dissolved radionuclides) of the order of $.10^6$ for Th, 10^4 for ^{226}Ra, and 10^3 for ^{238}U (Luo, *et al*., 2000).

A pronounced disequilibrium is easily produced between the U and Th isotopes because pH and Eh control U behaviour (Langmuir, 1978) and Th is practically insoluble in a wide range of natural conditions (Langmuir and Herman, 1980). In groundwater−rock systems such changes are generally brought about through groundwater recharge and when oxic groundwaters are introduced in anoxic conditions. Taken together, as a result of disequilibration processes the

liquid phase has an excess of soluble radionuclides, and surfaces of the solid phase have a deficiency of them.

2.7.3. Geochemistry of Uranium and Thorium

The chemical and geochemical similarities between thorium and uranium can be related fundamentally to similarities in their outer electronic configurations that led to their classification as actinides (Adams *et al*, 1959). Both uranium and thorium exist in the +4 oxidation states in most geologic environment. They have big cation radii, small electronegativities and ionization potentials (U^{4+}: 9.7 nm, 1.4, 6.08 eV respectively; Th^{4+}: 11.4 nm, 1.0, 6.95 eV respectively). Therefore, their ions are similar to K^+, Na^+ and Rare Earth Elements (REE) in these aspects (Liu 1984), and are prone to form compounds with weak chemical bonds and migrate easily. Consequently, uranium and thorium are usually enriched in rocks that are also rich in K^+, Na^+ and REE ions (Krass and Nobayev, 1980).

In aqueous solutions, the chemistry of U and Th is highly dependent on their ability to form complexes with other ions in solution. In non-complexing acid media, they generally exist as M^{n+}. At higher oxidation states (e.g., U^{6+}), the cations will react with water, hydrolysis:

$$M^{n+} + xH_2O \rightarrow MOx^{(n-2x)+} + 2xH^+ \qquad (2.23)$$

U^{6+} in the aqueous solutions is thus present as the uranyl ion $(UO_2)^{2+}$. As pH increases, the form of these ions evolves to $M(OH)^{(n.1)+}$ or $MO_xOH^{(n.2x.1)+}$ (Bourdon *et al*., 2003). In a non-complexing media, the limitation to solubility is generally the hydroxide form (e.g., $Th(OH)_4$ or

$UO_2(OH)_2$). The mobility of U and Th is largely controlled by their ability to form complexes both with inorganic (F^-, Cl^-, PO_4^{3-}, CO_3^{2-}) and organic ligands. For inorganic ligands, the strongest affinity is obtained with those ligands with the highest charge.

The migration of uranium and thorium depends on the presence and amount of oxygen or oxidative volatiles or H_2O, or their ions (Hu and Chen, 1992). The major factors controlling the distribution of thorium and uranium in rocks are:

1. The tendency of thorium and uranium to fractionate because of oxidation of the uranium to the soluble uranyl ion.
2. The precipitation of uranium out of solution in reducing environments, carbonates, etc.
3. The selective adsorption of thorium in clays and its retention in heavy resistate minerals

Many studies have demonstrated that thorium and uranium in intrusive rocks are concentrated in accessory minerals such as zircon, apatite and sphene, either as separate grains or as inclusions in the major minerals (Adams *et al*, 1959). Though accessory minerals apparently contain much of the thorium and uranium, some of the thorium and uranium is contained in major constituents such as quartz and the feldspars. The thorium and uranium contents of quartz, feldspars and ferromagnesian minerals may be attributed to one or more of the following

1. Entrapment in lattice imperfections
2. Entrapment in liquid inclusion
3. Deposition along fractures
4. Adsorption on crystal surfaces

According to Whitfield *et al,* (1959) and Rogers and Ragland (1961), the concentration of both uranium and thorium generally increases in granitic rocks during differentiation with the increase in thorium being fairly regular and that of uranium being rather erratic. They proposed a slight increase in the Th/U ratio with petrogenic evolution. They suggested that variations in the Th/U ratio and in the abundance of both elements are dependent not only on the general composition of the rock in which they are measured but also on secondary processes such as oxidation and leaching of uranium or deuteric formation of thorium rich allanite. The relatively immobile thorium becomes concentrated in residual materials such as soil and weathered rocks. Such processes may cause wide fluctuation in the abundance of radioactive elements from place to place in some igneous bodies.

Chapter Three

Methodology

3.1. Petrography and Mineralogical Investigation

3.1.1. Sampling and Sample Preparation

Fifteen (15) geological samples consisting of rock chippings, clay and soil were collected from six (6) different locations and depths for petrography and mineralogical analyses (Fig. 3.1). Six (6) of the rock chippings samples (BF12-72) were collected from a borehole drilled to a depth of 74 m at the Ghana Atomic Energy Commission (GAEC) premises at Kwabenya. The samples were collected at 12 m interval from a depth of 12m to 72m. One (1) sample of rock chippings (ASH1) was collected from a site at Adjei-Kojo, a suburb of Ashiaman at depth of about 5m. One (1) clay mineral sample (S3) was collected from a borehole drilled near the Afua Sunderland Children's Park in Accra at depth of about 17.5 m. Three (3) samples of rock chippings (RD1A, RD2C, and RD3B) were collected from a borehole drilled to a depth of 15.5m within the Ghacem Factory premises in Tema. Three (3) rock outcrops (KD 1-3) were also collected from three different points around the foothills of the Krobo Mountain whilst one (1) clay sample (CK1) was collected at Okwenya near Kpong.

The rock chippings were washed after which all the samples (both rock chippings and soil) were air dried in trays for 5 days. The soil samples were then oven dried at a temperature of 110 ^{o}C for between 3-4 hours until the samples were well dried with a constant weight (IAEA, 1989).

3.1.2. Analytical Method

The mineralogical analyses of the samples were carried out at the Institute of Environmental Geology and Geoengineering (IGAG) in Rome, Italy, by employing X-ray diffraction (XRD), Scanning Electron Microscopy (SEM) and Electron probe microanalysis (EPMA) techniques.

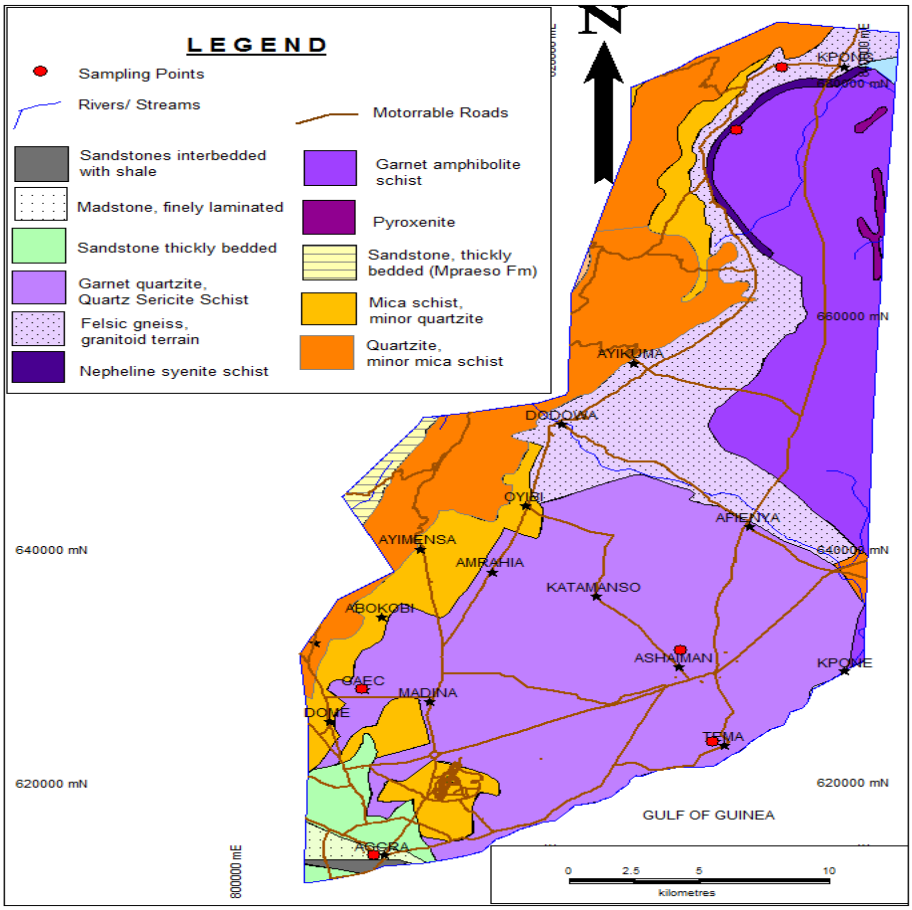

Figure 3.1. Geological map of study area showing sampling locations for mineralogical investigation.

3.1.2.1. X-Ray Diffraction Analysis

The X-ray diffraction analysis (XRD) was used for determining the bulk mineralogy, thus identification of the different minerals phases in the samples. The dried samples were thoroughly and finely ground with a mortar and pestle to avoid fractionation of the minerals. About 0.5g of each pulverized sample was used for the analysis. The powdered sample was placed on the bulk powder holder assuring a flat upper surface. The bulk powder holder was then placed in a fully automated Bruker AXS D8 diffractometer, operating in reflection mode, equipped with a Peltiercooled Si(Li) solid state energy dispersive SOL-X detector in θ-θ geometry. The sample was scanned from an angle of 0 to 70 degrees 2θ (two theta) at a scanning rate of 0.02º with a counting time of 3s in each step. A copper K alpha radiation

(copper source) was used to produce the spectrum. The generator's voltage and current values were set at 40 kV and 40 mA respectively.

3.1.2.2. Scanning Electron Microscope (SEM)

The chemistry of the minerals was performed on polished thin sections of the samples. The sample grains were dispersed on a clean surface and a sticky carbon mounting disc stub was pressed down the grains. The excess grains were trapped away. The grains on the disc stub were carbon coated. The SEM spectra were collected using an accelerating voltage of 15kV and point-beam 1-5 µm in size operative conditions. The operating conditions (magnification, chamber pressure, spot diameter, voltage, detector type, sample distance from detector) are reported on the sample photographs as shown in figure 3.2.

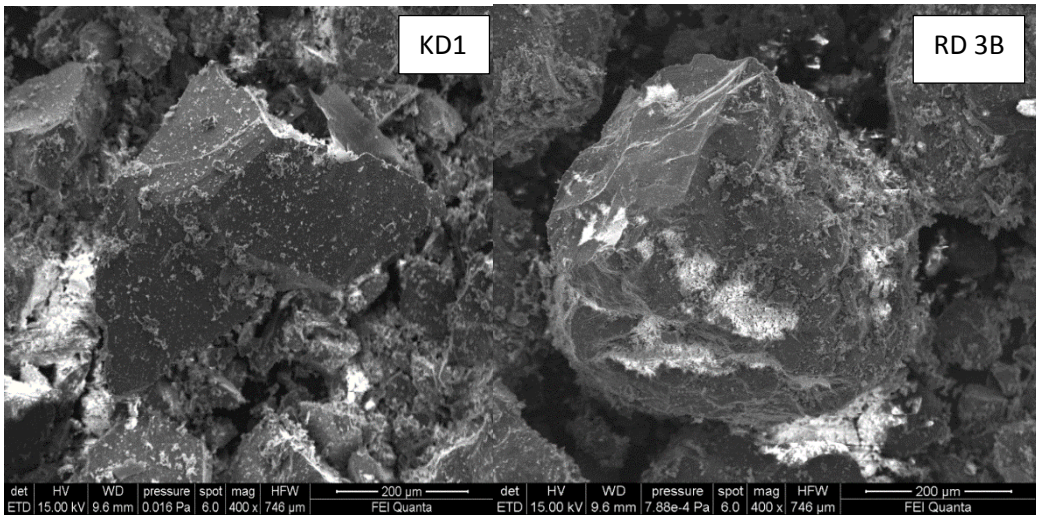

Figure 3.2 SEM photography's of KD1 and RD3B samples indicating operating conditions

3.1.2.3. Electron Probe Microanalysis

Electron probe microanalysis (EPMA) was used to determine the major and minor element in the samples. Quantitative microanalyses were performed using a CAMECA SX 50 electron microprobe, equipped with five spectometers (EMPA-WDS, Electro Probe X-Ray Microanalyzer and BSE-back-scattered electron) device for images acquisition. Before

probing, polished thin sections of the samples were prepared. The grains were placed in a circular one inch mould and impregnated with epoxy resin without creating air bubbles. The excess grains were removed and the resin block was ground to ensure that the top and base of resin blocks were parallel. The samples were then finely polished yielding a flat surface of uniform smoothness so that surface imperfections do not interfere with electron-sample interactions. Using a Vacuum Evaporator the samples were coated with a thin layer of carbon of about 20nm thickness. The analyses were performed in point beam mode (focused or 5 µm in size) at an accelerating voltage of 15 kV and an electron current of 15 nA operative conditions. Natural and synthetic (wollastonite: SiKα and CaKα, rutile: TiKα, corundum: AlKα, magnetite: FeKα, manganese: MnKα, periclase: MgKα, orthoclase: KKα, jadeite: NaKα, F-phlogopite: FKα, and silvite: ClKα) mineral standards were employed for calibration and also to check the precision and accuracy of the instrument. Microprobe data was reported as weight percent for each chemical group: SiO_2, TiO_2, Na_2O, Cr_2O_3, FeO, Al_2O_3, CaO, MgO, and MnO.

3.2. Hydrochemical Investigation

3.2.1. Sampling and Sample Preparation

One hundred and four (104) groundwater samples were collected from existing boreholes at thirty three (33) locations in the Accra Plains (figure 3.3). The depth of the boreholes ranged from 40 to 90 m. The boreholes were purged prior to sampling to remove any stagnant water within the borehole, allowing a representative groundwater sample from the aquifer to be collected. The physical parameters (temperature, pH, electrical conductivity and total dissolved solids (TDS)) of the pumped groundwater were measured using portable field kits during purging to indicate the presence of natural groundwater suitable for sampling and analysis. The probes of the portable kits used for measurement of the physical parameters

were calibrated in the laboratory on the day of sampling. The groundwater samples were collected after stabilization of the field parameters into acid washed 250 ml screw-cap polyethylene bottles and filtered through a 0.45µm pore size filters. Samples for cation determination were preserved by acidification with concentrated analytical grade nitric acid (1 vol.% HNO_3). The sample bottles were tightly capped to protect the samples from atmospheric CO_2 and transported to the laboratory in an ice chest maintained at a temperature of 4 ^oC. The samples were stored in a refrigerator until analyses.

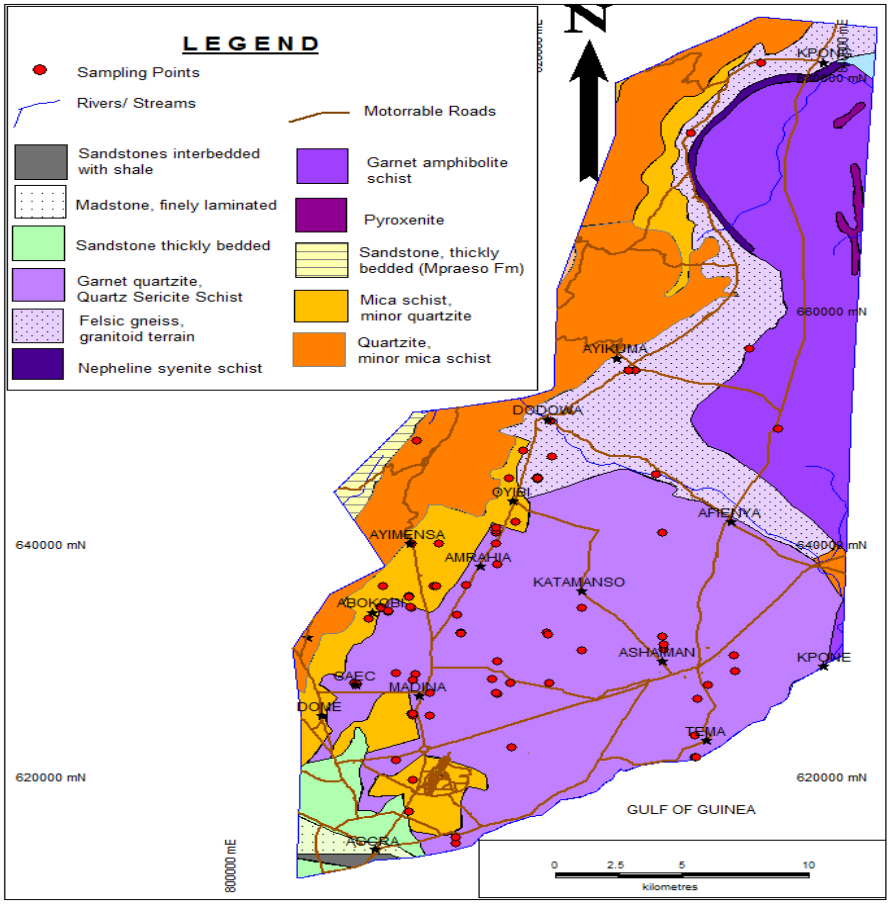

Figure 3.3. Groundwater sampling locations

3.2.2. Analytical Method

The major cations (Ca^{2+},Mg^{2+}, Na^+ and K^+) were analysed using inductively coupled plasma atomic emission spectrometer (ICP-AES). The major anions (Cl^-, SO_4^{2-}, NO_3^-), were analysed

by ion chromatography. The HCO_3, anion was determined by titration with 0.1 N HCl. The quality control process included the use of blanks, duplicates and analytical grade chemicals. Prior to data analysis the ionic balance of each sample was assessed for data reliability using the ionic balance equation

$$\text{Ionic Balance} = \frac{(\text{Sum of cations} - \text{Sum of anions})}{(\text{Sum of cations} + \text{Sum of anions})} \text{ X } 100 \qquad (3.1)$$

Ionic balance error (IBE) was computed on the basis of ions expressed in milliequivalents per liter for analytical precision for the measurements of cations and anions. The value of IBE was observed to be within a limit of ±5% (Domenico and Schwartz, 1990).

The Statistical Package for Social Sciences, (SPSS) software was used to carry out multivariate statistical analyses. 13 hydrogeochemical variables (temperature, pH, TDS, electrical conductivity, Ca, Mg, Na, K, HCO_3, Cl, SO_4, NO_3, SiO_2) were used in the multivariate statistical analyses. It is assumed that most of the variability related to groundwater composition can be described with these variables. The variables were log-transformed to reduce the influence of extreme values or outliers so that they may closely correspond to normally distributed data. The data were then standardized to their corresponding standard z-scores (Eq 3.2) in order to achieve the objectives of normal distribution and homogeneity.

$$Z = \frac{x - \mu}{s} \qquad (3.2)$$

Where x is the data, μ, s are respectively the mean and standard deviation of the datasets.

The transformed (log-transformed and standardized) data were used for Hierarchical Cluster Analysis (HCA) and Principal Component Analysis (PCA).

Q-mode hierarchical cluster analysis (HCA) was applied to the standard z-scores of the data to examine the interrelationship among the variables. Squared Euclidean distances were used to classify the parameters into initial clusters, whilst the Ward's agglomeration method was used to link the resulting initial clusters. The HCA method provided a graphical result, which showed the classification of the groundwater into distinct groups on the basis of their hydrogeochemical characteristics (dendrogram).

R-mode factor analysis was applied to the standard z-scores of the data to distinguish the contributions of natural processes and anthropogenic inputs to the chemical composition of the groundwater. In the factor analysis, 'principal components' was selected as the solution method, whilst the Varimax rotation was used to maximize the differences among selected factors in order to facilitate interpretation of the results of the analysis.

The raw data were used for the graphical analyses (binary diagram) to display the hydrochemical data. The Piper and Chadha diagrams were used to display the hydrochemical facies. Aquachem software version 4.0 (Waterloo Hydrogeologic Inc) incorporated with the hydrogeochemical modelling program PHREEQC was used to calculate the aqueous speciation and thermodynamic equilibrium conditions of the groundwater with respect to the main minerals phases present in the aquifer. The result of the speciation was used to construct mineral stability diagrams with thermodynamic boundary conditions taken from Tardy (1971). The stability diagrams were used for the interpretation of thermodynamic controls on the geological formation to explain the phase transitions occurring in the study area.

3. 3. Stable Isotope Investigation

3.3.1. Sampling and Sample Preparation

Fifty seven (57) groundwater samples for stable isotope analyses were collected from existing boreholes (Fig. 3.3). Applying a similar sampling method used for the hydrochemical studies, the boreholes were purged prior to sampling to remove any stagnant water within the borehole, allowing a representative groundwater sample from the aquifer to be collected. The physical parameters (temperature, pH, electrical conductivity and total dissolved solids (TDS)) of the pumped groundwater were measured during purging to indicate the presence of natural groundwater suitable for sampling and analysis. The probes of the portable kits used for measurement of the physical parameters were calibrated in the laboratory on the day of sampling. The samples were collected after stabilization of the field parameters into 100 ml pre conditioned high density polyethylene screw-cap bottles and sealed tightly to prevent evaporation. In the laboratory the samples were transferred into clean dry 50 ml glass vials and sealed with bromobutyl synthetic rubber stopper and further protected by aluminum cap using hand held crimping tool to prevent evaporation that can alter the $^{18}O/^{16}O$ and $^{2}H/^{1}H$ ratios. The samples were analyzed for stable isotopes concentrations (^{18}O, ^{2}H) at the isotope laboratory of the Institute of Environmental Geology and Geoengineering (IGAG), Rome.

3.3.2. Analytical Method

Oxygen isotopic ratios were determined using a modified version of Epstein and Mayeda (1953) technique (Krishnamurthy, 1984). 2ml of the groundwater sample was equilibrated with a fixed amount (28 ml at 86 mm Hg) of purified tank CO_2 in a glass bottle (8 ml) at 25 ^{o}C ±1 ^{o}C in a shaking equilibration bath for a period of 24 h. The CO_2 gas were then extracted and cryogenically purified in a vacuum line. The isotopic ratios were determined using a gas

source mass-spectrometer with analytical reproducibility (determined by repeated analyses of the laboratory standard) of 0.2‰.

Deuterium was analysed on hydrogen obtained by reduction of the groundwater on zinc (Coleman *et al*. 1982). Samples were first injected onto a stainless steel filter in an evacuated, heated inlet, which vapourized the sample and removed solutes. Water vapour was frozen onto the zinc in a glass breakseal cooled with liquid nitrogen, then reduced to hydrogen gas at 500 ^{o}C for analyses using a gas-source mass-spectrometer.

The isotopic values obtained were reported in the usual standard delta units (in parts per million relative to Vienna Standard Mean Ocean Water (VSMOW)), with the δ being defined by the following the relationship

$$\delta(‰) = \frac{R_{Sample} - R_{VSMOW}}{R_{VSMOW}} \times 1000 \qquad (3.3)$$

where R_{sample} is the mass ratio of the stable isotope and R_{VSMOW} is the value for the Vienna Standard Mean Ocean Water. The $\delta^{18}O$ and δD have an overall precision of 0.2 and 2‰, respectively.

3.4 Naturally Occurring Radionuclide Investigation

3.4.1. Sampling and Sample preparation

Thirty six (36) geological samples consisting of rock chippings, outcrops and soil were collected from six (6) different locations in the Accra Plains (Fig 3.1). Twenty two (22) samples of rock chippings (BF 9-72) were collected from a borehole drilled at the Ghana Atomic Energy Commission (GAEC) premises at Atomic-Kwabenya. The samples were collected at 3m interval from a depth of 9 m to 72 m. Two (2) samples of rock chippings (ASH 1-2) were collected at Adjei-Kojo a suburb of Ashiaman at depths of 3 and 5 m

respectively. Three (3) clay mineral samples (S1, S3 and S4) were also collected from a borehole drilled near the Afua Sunderland Children's Park in Accra at depths ranging from 5 to 20 m. In Tema, five (5) samples of rock chippings (RD1B, RD2C, RD3B, RD3C and RD4B) were collected from two (2) boreholes drilled to depths of 15.5 m at different points within the Ghacem Factory premises. Three (3) rock samples (outcrops) were also collected from different points around the foothill of the Krobo Mountain (KD) whilst a clay mineral sample (CK) was also collected from a farm at Okwenya near Kpong.

The rocks samples were crushed using a jaw crusher. After which all the samples were air dried in trays for 5 days and then oven dried at a temperature of 110 ^{o}C for between 3-4 hours until the samples were well dried with a constant weight (IAEA, 1989). The samples were then grinded into a fine powder using a ball mill grinder and sieved through a 250µcm pore size mesh into a previously cleaned plastic bags. 70 g of each sample was transferred into an airtight cylindrical PVC container with a volume of 250 cm^3. The containers were covered and sealed with a paper tape to prevent the escape of the gaseous radionuclides in the sample. The samples were stored for 30 days before analysis were carried out on each sample. This allowed the in-growth of uranium and thorium decay products and prevented the escape of radiogenic gases ^{222}Rn and ^{220}Rn as well as allowed secular equilibrium to be reached between the long-lived parent radionuclide and their short-lived daughters.

3.4.2. Analytical Method

The concentrations of the radionuclides in the sample were determined by employing a high resolution hyper pure germanium (HPGe) detector with a relative efficiency of 30% relative to a 3" x 3" NaI (Tl) scintillator. The energy resolution (FWHM) of the detector was 2 keV at 1.332 MeV of a ^{60}Co source. The detector was placed in a lead shield to reduce the

background radiation originating from the building materials and surroundings cosmic rays. Advanced Multi-Channel analyzer (MCA) emulation software (MAESTRO) was used for data acquisition, storage, display and online analysis of the acquired gamma-spectra. Each sample was put into the shielded HPGe detector and measured for an accumulating time of about 16 h. Prior to measurement of the samples, the environmental gamma background radiation in the laboratory was determined with an empty cylindrical container of the same geometry as the sample containers, under identical measurement conditions. The measured background activity was subtracted from the measured activity of each sample.

The activity concentration of ^{40}K was measured directly by its own gamma ray of 1461 keV. As ^{238}U and ^{232}Th are not directly gamma emitters, their activity concentrations were measured through gamma rays of their decay products. Decay products taken for ^{238}U were ^{214}Pb: 295 and 352 keV and ^{214}Bi: 609, 1120 and 1764 keV and ^{226}Ra:186 keV whereas for ^{232}Th were ^{228}Ac: 338, 463, 911 and 968 keV, ^{212}Bi: 727 keV, ^{212}Pb: 238 keV and ^{234}Pa: 1001 keV gamma ray by assuming the decay series to be in equilibrium. The 661.66 keV gamma transition was used for the determination ^{137}Cs concentration.

3.4.2.1. Energy Calibration of the Gamma Ray Detector

One of the essential requirements in nuclear spectroscopy measurement is the ability to identify the photo peaks present in a spectrum produced by the detector system (IAEA, 1989). This is achieved by carrying out energy calibration of the detection system.

The calibration was carried out by counting standard radionuclides of known activities with well-defined energies within the energy range of interest from 60 keV to 2000 keV. The calibration standard was counted long enough to produce well defined photo peaks. The

channel number that corresponds to the centroid of each full energy event on the MCA was recorded and plotted to obtain a linear curve with second order polynomial. The linear curve obtained from the data points is an indication that the system is operating properly (IAEA, 1989).

3.4.3. Calculation of Activity Concentration

Calculation of count rates for each detected photopeak and radiological concentrations (activity per mass unit) of detected radionuclides depend on the establishment of a secular equilibrium in the samples. Since secular equilibrium was reached between ^{232}Th and ^{238}U and their decay products, the ^{232}Th concentration was determined from the average concentrations of ^{208}Tl and ^{228}Ac in the samples. The ^{238}U concentrations were determined from the average concentrations of the ^{226}Ra, ^{214}Pb and ^{214} Bi decay products. A true measurement of ^{226}Ra, ^{40}K and ^{137}Cs concentrations were made. The specific activity in Bq/kg was calculated using the equation 3.4

$$\mathbf{A_{Ei}} = \frac{\mathbf{N_{Ei}}}{\boldsymbol{\varepsilon_E} . \mathbf{t} . \boldsymbol{\gamma_d} . \mathbf{M_s}} \qquad (3.4)$$

where N_{Ei} is the net peak area of a peak at energy E, ε_E the detection efficiency at energy *E*, *t* the counting live-time, γ_d the gamma ray yield per disintegration of the specific nuclide for a transition at energy R and M_s the mass if the measured sample in kilogram (kg). Radiological concentrations of ^{232}Th, ^{238}U, ^{226}Ra and ^{40}K were converted into total elemental concentrations of thorium, uranium, radium and potassium respectively according to the expression in equation 3.5

$$\mathbf{F_E} = \frac{\mathbf{M_E C}}{\boldsymbol{\lambda_E N_A f_{A,E}}} \frac{\mathbf{1}}{\boldsymbol{n}} \sum_{\boldsymbol{i=1}}^{\boldsymbol{n}} \boldsymbol{A_i} \qquad (3.5)$$

where F_E is the fraction of element E in the sample, M_E is the atomic mass (kg mol^{-1}), λ_E is the decay constant (s^{-1}) of the parent isotope, N_A is Avogadro's number(6.023 x 10^{23} atoms

mol^{-1}), $f_{A,E}$ is the fractional atomic abundance of ^{232}Th, ^{238}U, ^{226}Ra or ^{40}K in nature, C is a constant that converts the ratio of the element's mass to soil mass into a percentage or ppm and A_i is the radiological concentration of ^{40}K(n=1) or that of selected daughter radionuclides in the decay series of ^{232}Th and ^{238}U(n=2).

The total uncertainty (σ_{tot}) of the calculated activity values is composed of the counting statistical (σ_{st}) and weighted systematic errors ($\sigma_{sys,i}$) calculated by the following formula

$$\boldsymbol{\sigma_{tot} = \sqrt{\sigma_{st}^2 + \frac{1}{3}\sum_i \sigma_{sys,i}^2}} \quad (3.6)$$

The systematic uncertainties considered include, the uncertainty of the source activity (3%), the uncertainty in the efficiency fitting function (1-10%) and uncertainties in the nuclide master library used. The total uncertainty in the calculated activity concentration for the rock and soil samples was below 5%.

3.4.4. Calculation of Radiological Effects

The contribution of naturally occurring radionuclides to the absorbed dose rate in air depends on the concentrations of the radionuclides (^{238}U, ^{232}Th and ^{40}K) in the rock and soil. There is a relationship between terrestrial gamma radiation and radionuclide concentrations. If a radionuclide activity is known then its exposure dose rate in air at 1 m above the ground can be calculated using the formula proposed by UNSCEAR (2000):

$$\boldsymbol{\check{D} = \sum_x A_x \text{ x } C_x} \quad (3.7)$$

where A_x (Bq/kg) is the activities of the radionuclides and C_x (nGy/h per Bq/kg) their corresponding dose conversion factors. The dose conversion factors reported by UNSECAR (2000) was used assuming that contribution from other naturally occurring radionuclides were insignificant. Hence the absorbed dose rate was calculated using equation 3.8

$$\mathbf{D(nGy/h) = 0.462C_u + 0.604C_{Th} + 0.0417C_K} \quad (3.8)$$

where C_u, C_{Th} and C_K are the activity concentrations of U, Th and K respectively.

The annual effective dose equivalent (AEDE) was calculated from the absorbed gamma dose rate using the conversion coefficient from absorbed dose in air to the effective dose (0.7Sv/Gy) and the outdoor occupancy factor (0.2) (UNSCEAR, 2000). Thus the AEDE was calculated from the formula

$$\mathbf{\dot{E}\ (mSv/yr) = \dot{D}(nGy/h) \times 8760\ h.yr^{-1} \times 0.7 \times (10^3 mSv/10^9)\ nGy \times 0.2} \quad (3.9)$$

$$\mathbf{= \dot{D} \times 1.23 \times 10^{-3}\ (mSv/yr)} \quad (3.10)$$

The gamma-ray radiation hazards due to the specified radionuclides were assessed by two different indices (radium-equivalent activity and external radiation hazard). The indices were defined by Beretka and Mathew (1985). 98.5% of the radiological effects of the uranium series are produced by radium and its daughter products. The radium equivalent activity (Ra_{eq}) is defined by the estimate that 1Bq/kg of ^{226}Ra, 0.7Bq/kg of ^{232}Th and 13 Bq/kg of ^{40}K produce the same gamma ray dose and mathematically represented by equation **3.11**

$$\mathbf{Ra_{eq}(Bq/kg) = A_{Ra} + 1.43A_{Th} + 0.077A_K} \quad (3.11)$$

where A_{Ra}, A_{Th} and A_K are the activity concentrations of ^{226}Ra, ^{232}Th and ^{40}K respectively.

The external hazard index (H_{ex}) was used to measure the external hazard due to the emitted gamma radiation. It was calculated using the equation 3.12

$$\mathbf{H_{ex} = C_{Ra}/370 + C_{Th}/259 + C_K/4810 \leq 1} \quad (3.12)$$

Chapter Four

Petrography and mineralogy of the rocks of Accra Plains

4.1 Results

A summary of the mineral phases identified in the samples are shown in Table 4.1.

Table 4.1. Mineral phases identified in the geological samples

Sample ID	Location		EPMA	SEM	XRD
	Long (X)	Lat(Y)			
ASH 1	-0.04462	5.67689	K-feldspar (orthoclase), Na-feldspar (Oligolase),Feldspar (microcline), amphibole, mica (Biotite), epidote, magnetite, sphene	Orthoclase, Na-feldspar, quartz, Biotite, epidote, zircon	Albite, orthoclase, biotite, quartz, magnetite, epidote,
CK	0.04347	6.09331	(Na-Ca) feldspar (andesine), amphibole (gedritic),pyroxene, quartz, mica, rutile, ilmenite, titaniferous magnetite	(Na-Ca) feldspar, Na-feldspar, quartz, garnet, amphibole, montmorillonite	albite, clinochlore, montmorillonite, pargasitic hornblende, rutile, quartz
S 3	-0.20009	5.55678	K-feldspar (orthoclase), quartz, zeolite, mica(muscovite), illite, kaolinite, Fe-chlorite	Illite, quartz, kaolinite, many grains with composition Al, Si, K, (± Fe)	Orthoclase, Quartz, muscovite, illite, kaolinite
KD 1	0.04885	6.08733	(Na-Ca) feldspar (andesine), K-feldspar (orthoclase), amphibole (hornblende, gedrite, kaersutite), clinopyroxene, magnetite, ilmenite, garnet	(Na-Ca) Feldspar, Amphibole (hornblende, kaersutite), garnet	Albite, andesine, , hornblende, augite
KD 2	0.04860	6.08693	(Na-Ca) feldspar (andesine), pyroxene (augite), amphibole (hornblende), quartz, titaniferous magnetite, titanite	(Na-Ca) feldspar, amphibole (hornblende), mica (Biotite), quartz, titaniferous magnetite, vermiculate	Albite, Anorthite, hornblende, quartz,
KD 3	0.04925	6.09018	(Na-Ca) feldspar (andesine), ilmenite, amphibole (hornblende)	(Na-Ca) feldspar, amphibole (hornblende), ilmenite, titaniferous magnetite	Andesine, hornblende, biotite, ilmenite, pyroxene

RD 1A	0.00766	5.63702	K-feldspar (orthoclase), Na-Ca feldspar (oligoclase), amphibole (hornblende), mica, sphene, magnetite,	Na-feldspar (albite), K-feldspar (orthoclase), mica, quartz, amphibole, apatite, chlorite	Albite, orthoclase, phlogopite, hornblende, quartz, clinochlore
RD 2C			Plagioclase (andesine, oligoclase), K-feldspar (orthoclase), Amphibole (hornblende, gedrite), spinel, rutile	Na-Ca feldspar, montmorillonite, amphibole, quartz	Albite, chlorite, hornblende, quartz, montmorillonite
RD 3B			Na-Ca feldspar (oligoclase), K-feldspar (orthoclase) amphibole (hornblende, Al-tschermakite), pyroxene (augite), titaniferous magnetite	Feldspar, augite, quartz, epidote, amphibole ((hornblende, actinolite), titaniferous magnetite,	Orthoclase, albite, nepheline, diopside, phlogopite, quartz
BF 12	-0.21638	5.674042	Na-feldspar (albite), K-feldspar (orthoclase), epidote, mica(phlogopite, biotite), spinel	Na-feldspar, mica (phlogopite), quartz, sphene, epidote	Albite, phlogopite, quartz, clinochlore,
BF 24			Na-feldspar (albite), K-feldspar (microcline), K-Na feldspar (sanidine), amphibole (actinolite), epidote, quartz, mica (phlogopite), carbonate, sphene	Na-feldspar, mica (phlogopite), quartz, calcite, epidote, apatite, sphene	Albite, phlogopite, clinochlore magnesian-calcite, quartz,
BF 36			Na-feldspar (albite), Na-K feldspar (anorthoclase), amphibole (edenite, alumino-ferrotschermakite), mica (biotite), sphene, carbonate	Na-feldspar, mica, quartz, epidote, calcite, chlorite, ilmenite, apatite	Albite, quartz, clinochlore, calcite magnesian, biotite,
BF 48			Na-feldspar (albite), K-feldspar (orthoclase), sanidine mica (muscovite), carbonate	K-feldspar, Ca-feldspar (labradorite), mica (phlogopite), chlorite, quartz, sphene, calcite	Albite, orthoclase, quartz, muscovite, clinochlore
BF 57			Albite, orthoclase, sanidine, anorthoclase, pyroxene (Fe-augite), mica (muscovite), ilmenite, titanite, chlorite, rutile, magnetite, carbonate	Orthoclase, albite, quartz, mica (muscovite), zircon, sphene, iron oxide	Albite, muscovite magnesian, chlorite, calcite, quartz, polyhalite, ilmenite
BF 72			albite, orthoclase, microcline, sanidine, mica (muscovite), chlorite, ilmenite, magnetite, spinel and quartz	K-feldspar, Na-feldspar, Na-Ca feldspar, Quartz, dolomite	Albite, orthoclase, muscovite, quartz, clinochlore,

4.2. X-Ray Diffraction Analyses

The results of the X-Ray Diffraction (XRD) analyses of the Krobo Mountain (KD) rock samples are summarized in Table 4.2 and the spectrum of one of the samples (KD 1) is shown in Figure 4.1. Hornblende, plagioclase feldspar, alkali feldspar, and quartz, are the primary minerals in the KD samples with hornblende being the most abundant mineral (35.7 to 55.5%). This agrees with the observation made by Holm (1973) that hornblende is abundant in the mafic gneiss along the northwestern margin of the Accra Plains.

Table 4.2 Results of XRD quantitative analyses of mineral phases in the KD samples expressed in %)

Sample ID	Albite	Andesine	Anorthite	Pyroxene	Hornblende	Quartz	Biotite	Ilmenite
KD 1(%)	22.1	39.6	-	2.6	35.7	-	-	-
KD 2(%)	24.1	-	25.5	-	41.1	9.3	-	-
KD 3 (%)	-	17.1	-	11.8	55.3	-	13.2	2.7

The Tema (RD) samples had plagioclase feldspar (albite), K-feldspar (orthoclase), hornblende and quartz as the dominant mineral phases. The samples have a relatively high amount of hornblende. The hornblende which ranged from 10.6 to 30.1 % decreased in quantity with depth (Table 4.3). The RD 2C samples which were collected at 16 m deep had the highest amount of the albite mineral. The quartz content also increases with depth from 5.5 to 15.5 %. The RD 3B sample has high content of diopside, a mafic mineral.

The BF samples collected from GAEC premises at Kwabenya have plagioclase feldspar (albite), quartz and mica as primary minerals with chlorite, ilmenite and calcite occurring as secondary minerals (Table 4.4). Phlogopite decreases in amount (84.1 to 21.9%) with depth whilst muscovite remains relatively constant with depth.

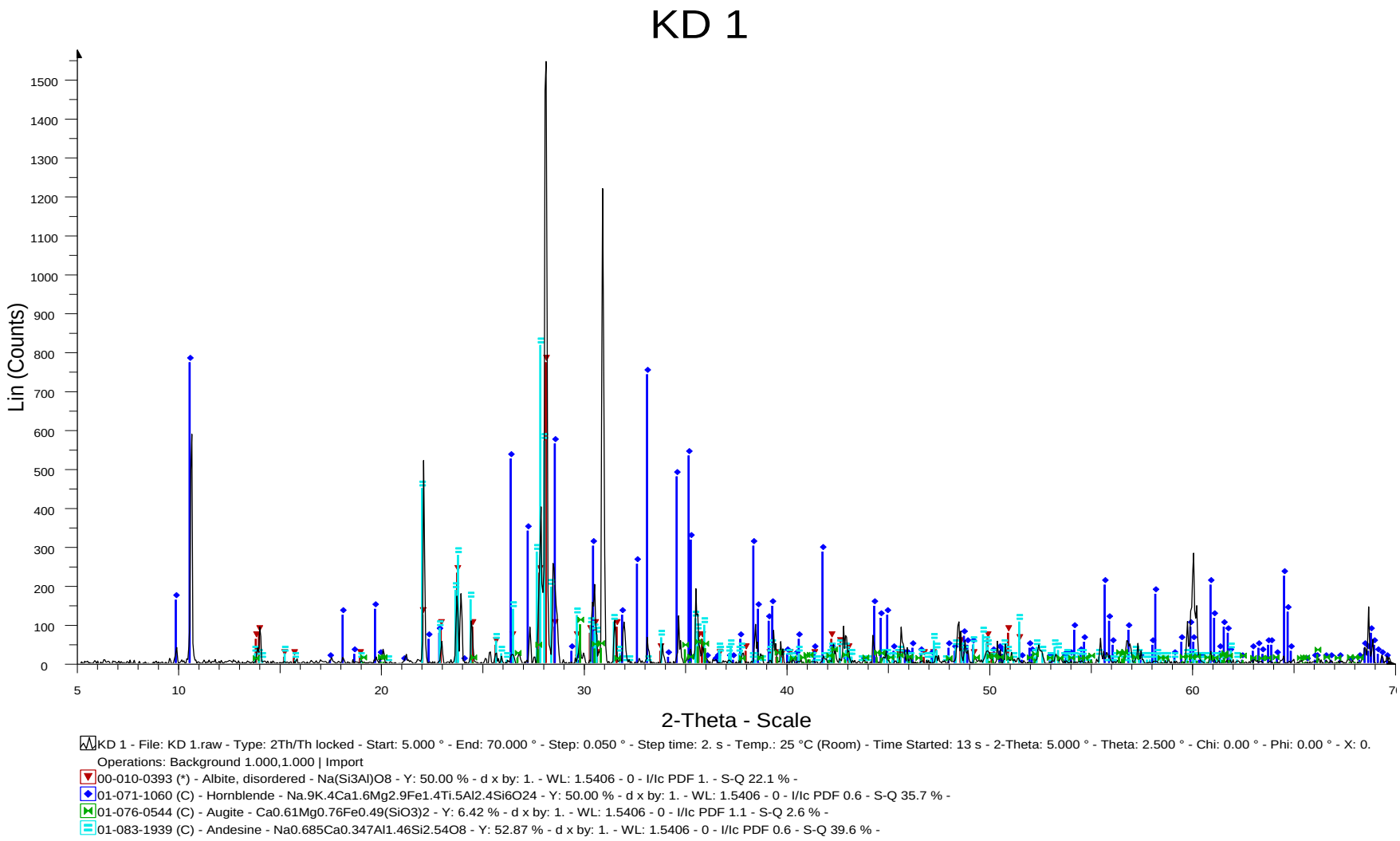

Figure 4.1 XRD spectrum of the sample KD 1

Table 4.3: XRD quantitative analyses of mineral phases in the RD samples (expressed in %)

Mineral Phase	RD 1A (4.50m) %	RD 2C (16m) %	RD 3B (10.5m) %
Albite	8.9	52.8	17.2
Orthoclase	18.6	-	17.2
Hornblende	30.1	10.6	-
Phlogopite	12.1	-	29.1
Clinochlore	24.9	-	-
Montmorillonite	-	6.2	-
Diopside	-	-	14.2
Nepheline	-	-	17.2
Chlorite	-	15	-
Quartz	5.5	15.5	5.8

Table 4.4: XRD quantitative analyses of mineral phases in the BF samples (expressed in %)

Mineral Phase	BF 12	BF 24	BF 36	BF 48	BF 57	BF 72
Albite	10.1	15.2	44.3	17.1	28.6	18.5
Orthoclase	-	-	-	26.4	-	9.3
Amphibole	-		9.7	-	-	-
Phlogopite	84.1	50.5	21.9	-	-	-
Muscovite	-	-	-	42.8	43.6	44.2
Chlorite*	1.9	21.5	11.2	3.2	7.4	18.7
Quartz	3.9	4.5	13.0	10.5	5.6	9.3
Calcite	-	0.2	-	-	6.2	-
Polyhalite	-	-	-	-	4.3	-
Ilmenite	-	-	-	-	4.2	-

*Chlorite + clinochlore

The mineral contents of the remaining samples (ASH, CK and S) are shown in Table 4.5. The clay mineral (CK) sample has high montmorillonite content. The high montmorillonite content may be as a result of weathering of the primary minerals in the mafic gneiss around the Krobo Mountains. The illite content in the shale sample (S3) was 56 % .

Table 4.5:XRD quantitative analyses of mineral phases in the ASH, CK and S samples (expressed in %)

Mineral Phase	ASH 1	CK	S 3
Albite	26.1	18.7	-
Orthoclase	20.1	-	2.5
Hornblende	-	16.5	-
Biotite	20.0	-	-
Muscovite	-	-	12.4
Clinochlore	-	17.8	-
Epidote	9.7	-	-
Magnetite	0.4	-	-
Montmorillonite	-	29.8	-
rutile	-	3.4	-
quartz	23.6	13.7	14.6
Illite	-	-	56.0
Kaolinite	-	-	14.4

4.3. Mineral chemistry

4.3.1. Feldspars

The KD samples collected along the foothills of the Krobo Mountains were composed mainly of andesine with an average mineral composition of An_{33} $Ab_{65}Or_2$ (Table 4.6). Their albite content varied from 56 to 69 mole %, whilst their anorthite composition varied from 28 to 38 mole% (Fig. 4.2(a)). The orthoclase composition varied from 0.9 to 3 mole%. The clay sample (CK) collected from Okwenya, about 2 km from the foothill of the Krobo Mountains was also composed mainly of andesine (Table 4.7). Their albite content varied from 63 to 70 mole %, whilst their anorthite composition varied from 30 to 34 mole% (Fig 4.2(b)). The orthoclase composition was approximately 3 mole%. The andesine mineral for both the CK and KD samples showed similar variation in their SiO_2 and CaO contents which ranged from 58.72 to 63.28 wt% and 5.55 to 8.52 wt% respectively. Their Al_2O_3 contents were between 23.74 to 25.98 wt%. Thus the feldspar mineral composition of the clay sample was similar to the feldspar mineral composition identified in the KD samples.

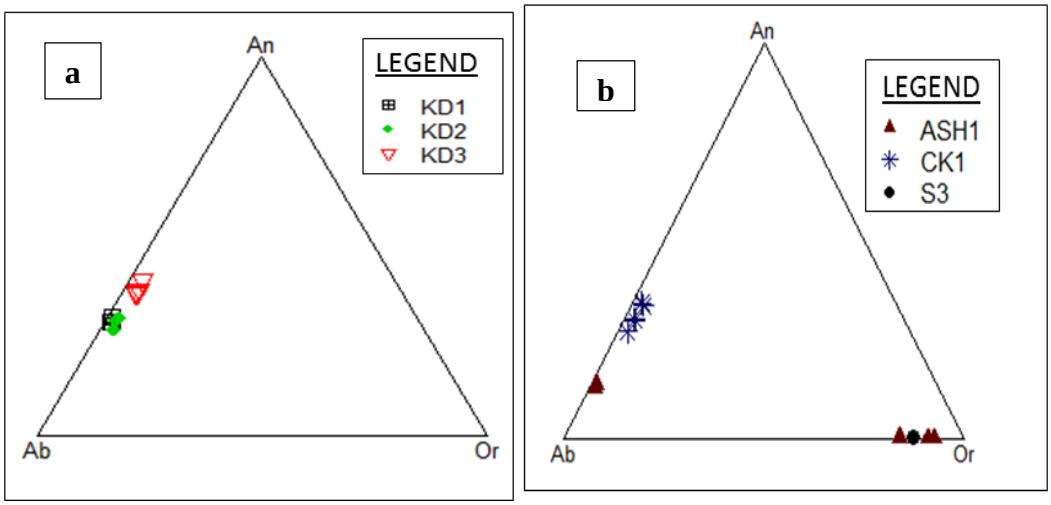

Figure 4.2 An-Ab-Or diagrams of feldspars in (a) the KD and (b) ASH1, CK1 and S3samples

The ASH sample which was collected from a rock formation made of quartzo-feldspathic gneiss was mainly composed of the quartz, alkali feldspars, orthoclase, microcline and the plagioclase feldspar, oligoclase. The K-feldspar had an average chemical composition of Or_{89} Ab_{11} An_0 (Table 4.7). The K_2O content varied from 13.24 to 15.11 wt%. The plagioclase feldspar-oligoclase had a chemical composition of Ab_{86} $An_{13}Or_1$. Its average Na_2O content was 10.14 wt%. The orthoclase mineral identified in the shale (S3) had a chemical composition of 87 mole % Or and 12.7 mole% Ab.

The RD samples consist of the plagioclase feldspars, andesine and oligoclase as well as alkali feldspar (orthoclase). The orthoclase had an average Or chemical compositions of about 95 mole%, and an Ab composition of 5 mole% (Table 4.8). The andesine mineral identified was made up of 61 mole % Ab, 36 mole% An and 3 mole % Or. The oligoclase was made up of 72 mole% Ab, 27 mole% An and 1 mole% Or (Fig.4.3(a)). The RD samples have SiO_2 content which ranged from 60.23 to 65.83 wt% and Al_2O_3 content between 17.80 and 24.97 wt%.

The BF samples which were collected from a geological formation consisting of quartz schists were composed mainly of quartz, albite and the alkali feldspars-microcline, orthoclase, sanidine and anorthoclase. Most of the albite in the samples were pure with chemical composition of 98 mole% Ab (Table 4.9 (a-b)). The orthoclase and microcline in the samples were also pure with about 98 mole % Or (Fig 4.3(b and c)). The mineral phase, sanidine had its Ab chemical composition ranging from 26 mole% to 70 mole %, whilst the Or varied from 29 mole% to 73 mole %. The feldspars minerals are susceptible to the action of hydrothermal solution, the more sodic varieties being more stable than those richer in anorthite component.

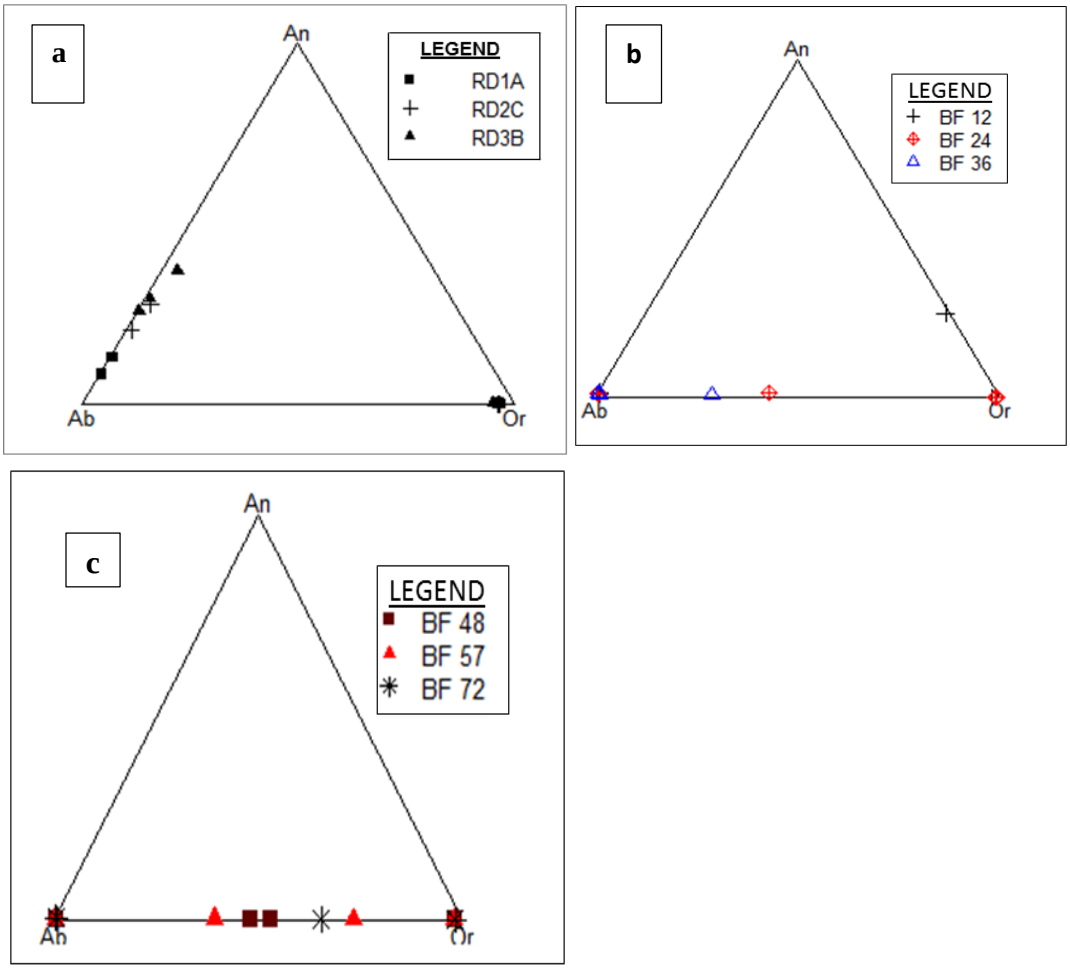

Figure 4.3 An-Ab-Or diagrams of feldspars in (a) RD and (b & c) BF rock samples

Table 4.6: Electron Microprobe analyses of feldspars in the KD samples

	KD 1			KD 2				KD 3			
	Andesine	Andesine	Andesite	Andesine	Andesine	Andesine	Andesine	Andesine	Andesine	Andesine	Andesine
SiO_2	61.894	61.783	61.435	61.877	61.885	61.332	59.219	59.910	59.586	58.721	58.848
TiO_2	0.004	0.000	0.030	0.037	0.007	0.000	0.026	0.000	0.000	0.000	0.000
Al_2O_3	24.179	24.642	24.030	24.437	24.134	24.663	23.741	25.307	25.556	25.985	25.976
Cr_2O_3	0.015	0.000	0.000	0.015	0.000	0.021	0.009	0.000	0.000	0.024	0.013
MgO	0.000	0.000	0.008	0.007	0.000	0.019	0.000	0.001	0.000	0.002	0.014
CaO	6.225	6.544	6.284	6.425	5.788	6.526	6.311	7.860	7.858	8.517	8.157
MnO	0.021	0.033	0.088	0.000	0.048	0.000	0.015	0.000	0.000	0.000	0.000
FeO	0.090	0.079	0.081	0.214	0.165	0.108	0.209	0.018	0.095	0.060	0.120
Na_2O	7.964	7.871	7.914	7.882	7.884	7.748	7.790	6.852	6.829	6.483	6.817
K_2O	0.232	0.163	0.256	0.414	0.490	0.448	0.404	0.574	0.508	0.491	0.544
Total	100.624	101.115	100.126	101.308	100.401	100.865	97.724	100.522	100.432	100.283	100.489
Cations					**Based on 24 Oxygens**						
Si	8.198	8.149	8.186	8.159	8.216	8.124	8.111	7.988	7.954	7.865	7.870
Ti	0.000	0.000	0.003	0.004	0.001	0.000	0.003	0.000	0.000	0.000	0.000
Al^{iv}	0.000	0.000	0.000	0.000	0.000	0.000	0.000	0.012	0.047	0.134	0.130
Al^{vi}	3.775	3.830	3.774	3.798	3.776	3.850	3.833	3.965	3.974	3.968	3.964
Cr	0.002	0.000	0.000	0.002	0.000	0.002	0.001	0.000	0.000	0.003	0.001
Mg	0.000	0.000	0.002	0.001	0.000	0.004	0.000	0.000	0.000	0.000	0.003
Ca	0.884	0.925	0.897	0.908	0.823	0.926	0.926	1.123	1.124	1.222	1.169
Mn	0.002	0.004	0.010	0.000	0.005	0.000	0.002	0.000	0.000	0.000	0.000
Fe^{3+}	0.000	0.000	0.000	0.000	0.000	0.000	0.000	0.000	0.000	0.000	0.000
Fe^{2+}	0.010	0.009	0.009	0.024	0.018	0.012	0.024	0.002	0.011	0.007	0.013
Na	2.045	2.013	2.045	2.015	2.029	1.990	2.069	1.771	1.767	1.683	1.768
K	0.039	0.027	0.043	0.070	0.083	0.076	0.071	0.098	0.087	0.084	0.093
An	29.766	31.189	30.052	30.333	28.045	30.958	30.212	37.530	37.741	40.881	38.584
Ab	68.913	67.886	68.490	67.340	69.128	66.512	67.485	59.206	59.354	56.312	58.352
Or	1.321	0.925	1.458	2.327	2.827	2.530	2.303	3.263	2.905	2.806	3.064

Table 4.7: Electron Microprobe analyses of feldspars in the CK, ASH and S samples

	CK 1					ASH 1					S 3
	Andesine	Andesine	Andesine	Andesine	Andesine	orthoclase	orhoclase	mircocline	Oligoclase	Oligoclase	orthoclase
SiO_2	61.221	59.464	62.304	63.277	60.587	64.191	64.614	65.052	64.498	65.759	65.860
TiO_2	0.009	0.016	0.000	0.000	0.000	0.000	0.000	0.009	0.026	0.014	0.016
Al_2O_3	24.658	24.911	23.495	24.189	25.185	17.303	17.622	18.109	20.171	20.983	18.587
Cr_2O_3	0.010	0.015	0.000	0.032	0.011	0.000	0.007	0.000	0.000	0.000	0.000
MgO	0.015	0.016	0.008	0.007	0.000	0.000	0.000	0.000	0.019	0.006	0.019
CaO	6.260	7.137	6.212	5.551	7.059	0.000	0.000	0.012	2.746	2.915	0.012
MnO	0.021	0.000	0.039	0.015	0.000	0.003	0.000	0.003	0.027	0.000	0.027
FeO	0.172	0.143	0.114	0.084	0.147	0.071	0.000	0.025	0.115	0.073	0.157
Na_2O	7.776	7.338	7.760	8.026	7.366	0.977	0.808	1.675	10.169	10.113	1.418
K_2O	0.459	0.421	0.504	0.443	0.542	15.039	15.106	13.239	0.245	0.231	14.802
Total	100.601	99.461	100.436	101.624	100.897	97.584	98.157	98.124	98.016	100.094	100.898
Cations					**Based on 24 oxygen**						
Si	8.128	8.009	8.191	8.278	8.039	9.085	9.079	9.065	8.706	8.682	9.001
Ti	0.001	0.002	0.000	0.000	0.000	0.000	0.000	0.001	0.003	0.001	0.002
Al^{iv}	0.000	0.000	0.000	0.000	0.000	0.000	0.000	0.000	0.000	0.000	0.000
Al^{vi}	3.858	3.954	3.795	3.729	3.938	2.886	2.918	2.974	3.209	3.265	2.994
Cr	0.001	0.002	0.000	0.003	0.001	0.000	0.001	0.000	0.000	0.000	0.000
Mg	0.003	0.003	0.001	0.001	0.000	0.000	0.000	0.000	0.004	0.001	0.004
Ca	0.890	1.030	0.875	0.778	1.003	0.000	0.000	0.002	0.397	0.412	0.002
Mn	0.002	0.000	0.004	0.002	0.000	0.000	0.000	0.000	0.003	0.000	0.003
Fe^{3+}	0.002	0.004	0.000	0.000	0.002	0.000	0.000	0.000	0.000	0.000	0.000
Fe^{2+}	0.017	0.012	0.012	0.009	0.014	0.008	0.000	0.003	0.013	0.008	0.018
Na	2.001	1.916	1.978	2.036	1.895	0.268	0.220	0.453	2.661	2.589	0.376
K	0.078	0.072	0.085	0.074	0.092	2.715	2.708	2.354	0.042	0.039	2.581
An	29.983	34.120	29.787	26.943	33.560	0.000	0.000	0.064	12.808	13.564	0.059
Ab	67.399	63.483	67.336	70.496	63.372	8.986	7.518	16.117	85.831	85.156	12.702
Or	2.618	2.396	2.878	2.560	3.068	91.014	92.482	83.819	1.361	1.280	87.239

Table 4.8: Electron Microprobe analyses of feldspars in the RD samples

	RD 1A				RD 2C				RD 3B			
	orthoclase	orthoclase	Albite	Albite	Andesine	Andesine	sanidine	sanidine	Andesine	Oligoclase	Oligoclase	orthoclase
SiO_2	64.324	63.989	65.832	68.33	63.544	61.516	64.746	63.444	60.228	62.757	62.594	62.609
TiO_2	0.000	0.002	0.009	0.019	0.003	0.000	0.009	0.000	0.005	0.004	0.009	0.012
Al_2O_3	18.183	18.016	21.229	19.919	22.393	23.368	17.881	18.011	24.975	23.053	24.497	17.802
Cr_2O_3	0.000	0.000	0.000	0.000	0.000	0.000	0.000	0.000	0.028	0.023	0.000	0.000
MgO	0.000	0.000	0.006	0.035	0.000	0.000	0.000	0.007	0.010	0.000	0.000	0.006
CaO	0.000	0.028	2.718	1.682	4.480	5.805	0.000	0.006	7.680	5.828	6.078	0.046
MnO	0.000	0.000	0.051	0.012	0.003	0.006	0.057	0.000	0.012	0.000	0.000	0.003
FeO	0.133	0.142	0.09	0.060	0.144	0.193	0.125	0.105	0.042	0.031	0.220	0.020
Na_2O	0.314	0.375	9.945	10.361	9.421	8.115	0.409	0.346	6.832	9.212	8.040	0.460
K_2O	15.647	15.573	0.095	0.056	0.187	0.350	15.831	15.733	0.613	0.027	0.198	14.370
Total	98.601	98.125	99.975	100.474	100.175	99.353	99.058	97.652	100.425	100.935	101.636	95.328
Cations					**Based on 24 Oxygens**							
Si	9.018	9.019	8.684	8.918	8.432	8.256	9.047	8.999	8.038	8.278	8.203	9.030
Ti	0.000	0.000	0.001	0.002	0.000	0.000	0.001	0.000	0.001	0.000	0.001	0.001
Al^{iv}	0.000	0.000	0.000	0.000	0.000	0.000	0.000	0.000	0.000	0.000	0.000	0.000
Al^{vi}	3.004	2.993	3.300	3.064	3.502	3.696	2.945	3.011	3.928	3.584	3.784	3.026
Cr	0.000	0.000	0.000	0.000	0.000	0.000	0.000	0.000	0.003	0.002	0.000	0.000
Mg	0.000	0.000	0.001	0.007	0.000	0.000	0.000	0.002	0.002	0.000	0.000	0.001
Ca	0.000	0.004	0.384	0.235	0.637	0.835	0.000	0.001	1.098	0.824	0.853	0.007
Mn	0.000	0.000	0.006	0.001	0.000	0.001	0.007	0.000	0.001	0.000	0.000	0.000
Fe^{3+}	0.000	0.000	0.000	0.000	0.000	0.000	0.000	0.000	0.000	0.000	0.003	0.000
Fe^{2+}	0.016	0.017	0.010	0.007	0.016	0.022	0.015	0.013	0.005	0.003	0.021	0.002
Na	0.085	0.102	2.543	2.622	2.424	2.112	0.111	0.095	1.768	2.356	2.043	0.129
K	2.798	2.800	0.016	0.009	0.032	0.060	2.822	2.847	0.104	0.005	0.033	2.644
An	0.000	0.145	13.050	8.206	20.597	27.766	0.000	0.031	36.971	25.867	29.133	0.256
Ab	2.960	3.525	86.407	91.469	78.380	70.241	3.778	3.233	59.516	73.990	69.737	4.628
Or	97.040	96.329	0.543	0.325	1.024	1.993	96.222	96.736	3.514	0.143	1.130	95.117

Table 4.9 a: Electron Microprobe analyses of feldspars in the BF samples

	BF 12				BF 24					BF 36		
	Albite	Albite	mircocline		Albite	Albite	mircocline	mircocline	sanidine	Albite	Albite	Sanidine
SiO_2	68.654	68.706	65.668	55.598	69.048	68.615	65.299	64.276	67.169	69.250	69.433	68.014
TiO_2	0.000	0.018	0.000	2.721	0.023	0.007	0.012	0.018	0.000	0.000	0.005	0.002
Al_2O_3	19.619	19.308	17.891	17.130	19.649	19.363	18.367	17.900	19.047	19.583	19.374	19.247
Cr_2O_3	0.000	0.000	0.000	0.057	0.012	0.015	0.036	0.000	0.028	0.029	0.000	0.012
MgO	0.026	0.000	0.002	0.608	0.009	0.014	0.000	0.002	0.000	0.014	0.017	0.013
CaO	0.141	0.298	0.001	4.874	0.184	0.266	0.002	0.000	0.271	0.177	0.200	0.096
MnO	0.033	0.046	0.030	0.024	0.000	0.030	0.063	0.006	0.045	0.003	0.036	0.027
FeO	0.112	0.149	0.104	2.563	0.143	0.114	0.097	0.130	0.207	0.117	0.108	0.211
Na_2O	11.549	11.615	0.224	0.121	11.199	11.169	0.107	0.130	6.303	11.458	11.455	8.440
K_2O	0.181	0.072	16.003	12.231	0.067	0.045	16.309	15.758	7.223	0.126	0.061	5.186
Total	100.315	100.212	99.923	95.927	100.334	99.638	100.292	98.220	100.293	100.757	100.689	101.248
Cations					**Based on 24 oxygens**							
Si	9.006	9.025	9.083	8.244	9.001	9.010	9.019	9.046	8.993	9.001	9.026	8.975
Ti	0.000	0.002	0.000	0.303	0.002	0.001	0.001	0.002	0.000	0.000	0.001	0.000
Al^{iv}	0.000	0.000	0.000	0.000	0.000	0.000	0.000	0.000	0.000	0.000	0.000	0.000
Al^{vi}	2.990	2.946	2.917	2.994	3.019	2.997	2.990	2.969	3.005	3.000	2.968	2.993
Cr	0.000	0.000	0.000	0.007	0.001	0.002	0.004	0.000	0.003	0.003	0.000	0.001
Mg	0.005	0.000	0.000	0.134	0.002	0.003	0.000	0.001	0.000	0.003	0.003	0.003
Ca	0.019	0.041	0.000	0.774	0.026	0.037	0.000	0.000	0.039	0.025	0.028	0.014
Mn	0.004	0.005	0.004	0.003	0.000	0.003	0.007	0.001	0.005	0.000	0.004	0.003
Fe^{3+}	0.001	0.002	0.001	0.000	0.000	0.000	0.000	0.001	0.000	0.000	0.000	0.000
Fe^{2+}	0.011	0.014	0.011	0.318	0.016	0.013	0.011	0.015	0.023	0.013	0.012	0.023
Na	2.895	2.916	0.060	0.035	2.831	2.844	0.029	0.035	1.636	2.887	2.887	2.159
K	0.030	0.012	2.824	2.314	0.011	0.008	2.874	2.829	1.234	0.021	0.010	0.873
An	0.663	1.392	0.005	24.796	0.896	1.296	0.010	0.011	1.336	0.840	0.952	0.446
Ab	98.323	98.207	2.083	1.114	98.715	98.443	0.987	1.238	56.250	98.447	98.702	70.893
Or	1.014	0.401	97.912	74.090	0.389	0.261	99.003	98.751	42.414	0.712	0.346	28.662

Table 4.9b: Electron Microprobe analyses of feldspars in the BF samples

	BF 48				BF 57				BF 72			
	Orthoclase	Albite	sanidine	sanidine	Orthoclase	Anorthoclase	Albite	Sanidine	Albite	Albite	orthoclase	Sanidine
SiO_2	65.707	69.215	66.890	66.728	65.440	67.358	69.138	66.169	68.942	69.723	64.468	66.540
TiO_2	0.002	0.047	0.000	0.000	0.033	0.047	0.000	0.035	0.000	0.000	0.000	0.000
Al_2O_3	18.182	19.335	18.684	18.813	17.861	19.015	18.938	17.92	19.246	19.035	17.843	18.629
Cr_2O_3	0.000	0.000	0.000	0.008	0.000	0.013	0.022	0.000	0.012	0.000	0.000	0.000
MgO	0.023	0.000	0.021	0.012	0.010	0.012	0.011	0.000	0.000	0.025	0.000	0.000
CaO	0.000	0.061	0.053	0.013	0.008	0.021	0.041	0.000	0.072	0.089	0.000	0.000
MnO	0.000	0.015	0.030	0.000	0.063	0.000	0.006	0.009	0.009	0.033	0.036	0.018
FeO	0.133	0.048	0.044	0.093	0.044	0.056	0.048	0.011	0.009	0.048	0.011	0.000
Na_2O	0.195	11.828	5.319	5.971	0.232	7.179	11.606	2.865	11.839	11.788	0.187	4.007
K_2O	15.955	0.129	9.079	8.465	16.132	7.083	0.070	12.01	0.092	0.074	16.142	11.551
Total	100.197	100.678	100.12	100.103	99.823	100.784	99.88	99.019	100.221	100.815	98.687	100.745
cations					**Based on 24 Oxygens**							
Si	9.058	9.011	9.024	8.996	9.071	8.982	9.058	9.099	9.014	9.056	9.048	9.008
Ti	0.000	0.005	0.000	0.000	0.003	0.005	0.000	0.004	0.000	0.000	0.000	0.000
Al^{iv}	0.000	0.000	0.000	0.000	0.000	0.000	0.000	0.000	0.000	0.000	0.000	0.000
Al^{vi}	2.954	2.967	2.971	2.989	2.918	2.988	2.924	2.904	2.966	2.914	2.951	2.972
Cr	0.000	0.000	0.000	0.001	0.000	0.001	0.002	0.000	0.001	0.000	0.000	0.000
Mg	0.005	0.000	0.004	0.002	0.002	0.002	0.002	0.000	0.000	0.005	0.000	0.000
Ca	0.000	0.009	0.008	0.002	0.001	0.003	0.006	0.000	0.010	0.012	0.000	0.000
Mn	0.000	0.002	0.003	0.000	0.007	0.000	0.001	0.001	0.001	0.004	0.004	0.002
Fe^{3+}	0.005	0.000	0.000	0.000	0.000	0.003	0.001	0.000	0.000	0.000	0.000	0.000
Fe^{2+}	0.011	0.005	0.005	0.011	0.005	0.003	0.004	0.001	0.001	0.005	0.001	0.000
Na	0.052	2.985	1.391	1.561	0.062	1.856	2.948	0.764	3.001	2.969	0.051	1.052
K	2.806	0.021	1.562	1.456	2.853	1.205	0.012	2.107	0.015	0.012	2.890	1.995
An	0.000	0.282	0.259	0.062	0.041	0.098	0.194	0.000	0.333	0.414	0.000	0.0000
Ab	1.824	99.007	46.979	51.706	2.138	60.577	99.411	26.608	99.160	99.176	1.730	34.521
Or	98.176	0.710	52.762	48.232	97.821	39.325	0.394	73.391	0.507	0.410	98.270	65.479

4.3.2. Amphiboles

The amphiboles were classified mostly as Ca-amphiboles according to the International Mineralogical Association 1997 recommendation for the nomenclature of amphiboles (Leake *et al*, 1997). The amphibole grains show a wide range of composition which include; aluminoferro-pargasite, pargasite, alumino-pargasite, edenite and actinolite (Fig.4.4).

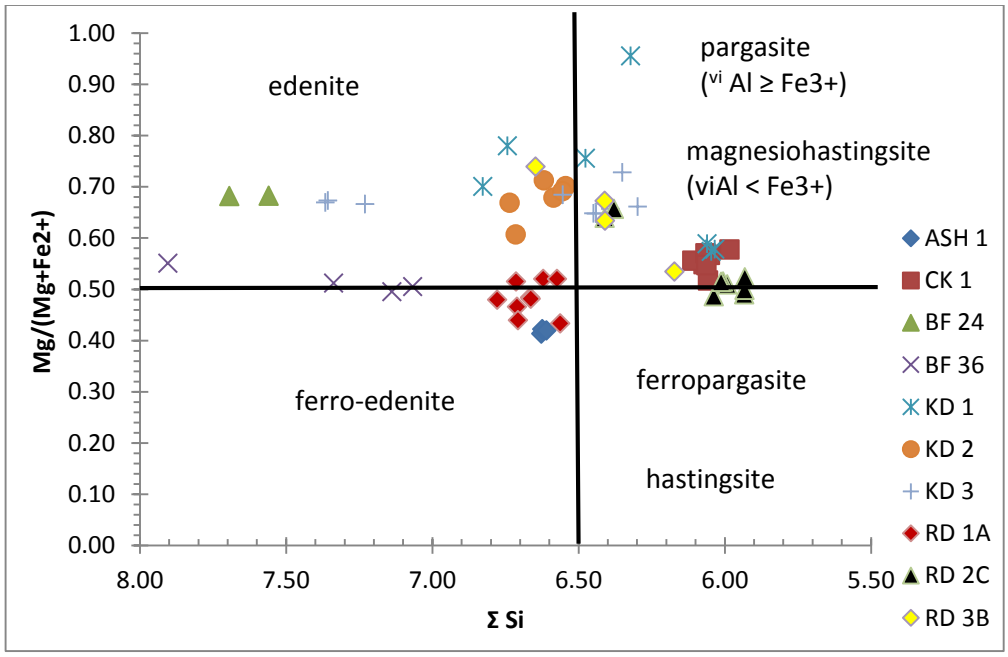

Figure 4.4. Ampibole classification plot in terms of Si [apfu] vrs Mg/(Mg+Fe^{2+}) by Leake *et al* (1997).

The amphiboles in the CK samples are rich in Al-Fe (Table 4.10) and thus belong to the pargasite suite (gedrite). Together with the RD 2C samples (Table 4.11), the CK samples can be classified as calcian gedrite because their Ca atom per formula unit (apfu) is greater than 0.50. (Leake *et al*, 1997). The ASH and RD 1A samples are Fe-Ca rich and belong to the ferro-edenite suite. They can be classified as potassian ferro-edenitic hornblende. The BF 24 samples are rich in Fe-Ca-Mg belong to the actinolite suite The KD2, KD3 (Table 4.12), RD 1A, RD 3B and ASH samples can be classified as potassian since their potassium atom per formula unit (apfu) is

greater than 0.25. They are also rich in Al, Fe and Ca. The contents of K and Na as well as Ti are very low in the CK and BF samples. The Al_2O_3 content of all the hornblende varieties are greater than 10 wt% expect the BF samples (Table 4.13) that had some of the hornblende varieties having lower Al_2O_3 content. Amphiboles were not identified in the BF samples below the depth of 36 m The Mg* = Mg/(Mg+Fe) ratios (atomic) range from 0.00 to 0.69 with the KD and BF samples having the higher values. The calculated average felsic index (F) for the amphibole mineral in the KD samples is: 17.074.

4.3.3. Mica

Two mica varieties (i.e. biotite and muscovite) were identified. The biotite was identified in the RD 1A, ASH (Table 4.14) and BF (12- 36) samples (Table 4.15a). The muscovite was identified in the S3 and BF (48-72) samples (Table 4.15b). Thus with increase in depth the mica variety changed from biotite to muscovite. The major elemental composition of the biotite was plotted on the conventional Al-Mg-Fe^{2+} diagram and shown in Figure 4.5. The diagram showed two types of biotites, an Al-Mg rich and relatively low Fe variety and another type in which Al-Mg is relatively low and Fe is higher (ASH 1, BF 36, BF 48). The average felsic index (F) calculated for the mica mineral in the BF samples was: 98.480 whilst the average for the RD, ASH and S samples was 98.221.This implies that the rocks are generally felsic and less mafic.

The alteration products from biotite include chlorite, muscovite, illite, kaolinite, calcite, epidote and rutile (Deer *et al*, 1992). Mineralizing solutions commonly leach iron and magnesium and substitute potassium, yielding secondary muscovite and sericite pseudomorphous after biotite. The alternation of biotite by weathering produces either montmorillonite or vermiculite. The

weathering of muscovite may proceed through illite and hydromuscovite to montmorillonite and eventually kaolinite by loss of potassium and increase of water and silica. Microprobe analyses of the muscovite indicate that they contain significant amounts of Fe and Mg,

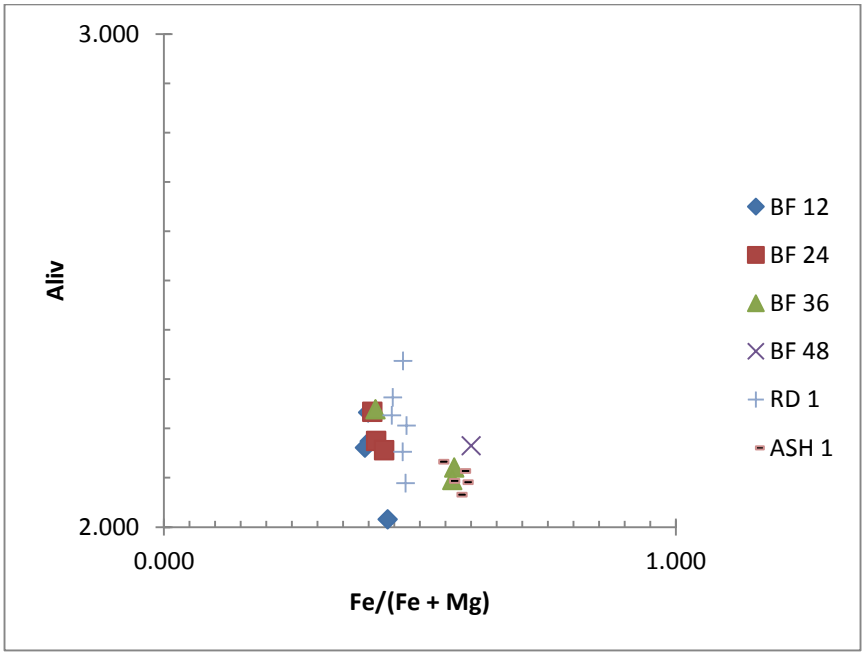

Figure 4.5. Composition of biotite on the Fe/(Fe+Mg) vrs Al^{iv} diagram

4.3.4. Pyroxene

Pyroxene was identified in all the KD (Table 4.16) and CK (Table 4.17) samples which are mafic gneiss collected around the Krobo Mountains. However pyroxene was identified in only one of the Tema (RD 3B) and GAEC (BF57) samples which were composed of quartzo-feldspathic gneiss and quartz schists respectively. The pyroxene mineral identified in the samples was augite with the composition $Ca(Mg,Fe,)Si_2O_6$ or $Ca(Fe,Mg)Si_2O_6$. Their Mg* varied from 63 to 75 with the KD 1 sample having the higher value and the BF sample having the lower value. Augites are essential constituents of basic igneous rocks. They occur in ultramafic rocks and in the ultrabasic nodules and megacyrsts in basic rocks (Deer *et al*, 1992).

Table 4.10: Electron Microprobe analyses of amphiboles in the CK and ASH samples.

	CK 1							ASH 1		
SiO_2	39.528	39.499	39.078	39.639	40.209	39.745	39.656	40.986	41.142	40.872
TiO_2	0.060	0.058	0.087	0.035	0.059	0.107	0.070	0.537	0.627	0.490
Al_2O_3	21.630	21.801	21.732	21.315	22.297	21.724	21.700	11.014	10.951	10.909
Cr_2O_3	0.000	0.000	0.266	0.046	0.000	0.000	0.000	0.004	0.023	0.034
MgO	9.286	8.479	10.214	9.119	9.518	9.69	9.835	7.113	7.169	7.101
CaO	7.480	7.261	7.646	7.143	6.926	6.896	6.595	11.238	11.005	11.056
MnO	0.393	0.622	0.435	0.585	0.580	0.413	0.421	0.472	0.515	0.495
FeO	21.751	22.808	20.703	22.475	21.394	21.761	22.633	22.131	22.226	22.417
Na_2O	0.004	0.000	0.000	0.023	0.012	0.008	0.004	1.867	1.941	1.934
K_2O	0.000	0.000	0.000	0.000	0.023	0.044	0.000	1.660	1.694	1.658
Total	100.132	100.528	100.161	100.38	101.018	100.388	100.914	97.022	97.293	96.966
CATIONS			Based on 24 Oxygens							
Si	5.867	5.874	5.767	5.889	5.908	5.879	5.839	6.629	6.624	6.610
Ti	0.007	0.006	0.010	0.004	0.007	0.012	0.008	0.065	0.076	0.060
Al^{iv}	2.133	2.126	2.233	2.111	2.092	2.121	2.161	1.371	1.376	1.390
Al^{vi}	1.652	1.694	1.546	1.621	1.769	1.667	1.605	0.728	0.703	0.689
Cr	0.000	0.000	0.031	0.005	0.000	0.000	0.000	0.001	0.003	0.004
Mg	2.055	1.880	2.247	2.02	2.085	2.137	2.159	1.714	1.721	1.712
Ca	1.190	1.157	1.209	1.137	1.090	1.093	1.040	1.947	1.898	1.916
Mn	0.049	0.078	0.054	0.074	0.072	0.052	0.053	0.065	0.070	0.068
Fe^{3+}	1.162	1.115	1.332	1.167	0.997	1.115	1.234	0.560	0.637	0.666
Fe^{2+}	1.538	1.722	1.223	1.626	1.631	1.577	1.553	2.432	2.350	2.366
Na	0.001	0.000	0.000	0.007	0.003	0.002	0.001	0.585	0.606	0.606
K	0.000	0.000	0.000	0.000	0.004	0.008	0.000	0.342	0.348	0.342
Mg*	0.432	0.399	0.468	0.420	0.442	0.443	0.437	0.364	0.366	0.361
Felsic index	0.053	0.000	0.000	0.321	0.503	0.748	0.061	23.888	24.829	24.522

Table.4.11: Electron Microprobe analyses of amphiboles in the RD samples

	RD 1A					RD 2C				RD 3B		
SiO_2	42.540	37.29	42.156	42.492	42.175	41.736	39.294	39.485	39.034	43.893	41.498	41.669
TiO_2	0.463	0.058	0.680	0.676	0.729	1.687	0.048	0.050	0.017	1.570	1.689	1.937
Al_2O_3	10.143	21.908	10.617	11.206	10.747	15.231	21.544	21.876	21.769	12.659	13.867	14.180
Cr_2O_3	0.044	0.047	0.052	0.06	0.029	0.071	0.014	0.031	0.008	0.056	0.088	0.000
MgO	8.933	0.000	8.324	9.304	8.678	11.083	8.899	9.246	9.134	13.142	10.881	11.804
CaO	11.505	23.226	11.622	11.689	11.544	11.036	8.181	8.129	7.598	11.473	11.669	11.789
MnO	0.421	0.15	0.456	0.364	0.407	0.109	0.522	0.54	0.819	0.107	0.333	0.311
FeO	20.795	14.024	20.561	19.307	19.468	13.298	21.744	21.319	22.103	11.772	14.504	12.523
Na_2O	1.665	0.013	1.642	1.827	1.717	2.968	0.003	0.018	0.008	2.222	1.514	1.517
K_2O	1.329	0.001	1.694	1.733	1.567	0.484	0.000	0.000	0.000	0.656	1.912	2.008
Total	97.838	96.717	97.804	98.658	97.061	97.703	100.249	100.694	100.49	97.55	97.955	97.738
Cations							**Based on 24 Oxygens**					
Si	6.715	5.958	6.711	6.658	6.733	6.379	5.836	5.824	5.783	6.648	6.410	6.411
Ti	0.055	0.007	0.081	0.080	0.088	0.194	0.005	0.006	0.002	0.179	0.196	0.224
Al^{iv}	1.285	2.042	1.289	1.342	1.267	1.621	2.164	2.176	2.217	1.352	1.590	1.589
Al^{vi}	0.602	2.084	0.703	0.727	0.755	1.123	1.607	1.628	1.584	0.908	0.935	0.982
Cr	0.005	0.006	0.007	0.007	0.004	0.009	0.002	0.004	0.001	0.007	0.011	0.000
Mg	2.102	0.000	1.975	2.037	2.065	2.525	1.970	2.033	2.017	2.967	2.506	2.707
Ca	1.946	3.976	1.982	1.962	1.974	1.807	1.320	1.285	1.206	1.862	1.931	1.943
Mn	0.056	0.020	0.061	0.048	0.055	0.014	0.066	0.067	0.103	0.014	0.044	0.041
Fe^{3+}	0.770	0.000	0.471	0.492	0.404	0.382	1.970	1.224	1.321	0.447	0.428	0.295
Fe^{2+}	1.975	1.874	2.267	2.037	2.195	1.318	1.320	1.406	1.418	1.044	1.446	1.316
Na	0.510	0.004	0.507	0.555	0.531	0.880	0.001	0.005	0.002	0.653	0.453	0.452
K	0.268	0.000	0.344	0.346	0.319	0.094	0.000	0.000	0.000	0.127	0.377	0.394
Mg*	0.434	0.000	0.419	0.446	0.443	0.598	0.375	0.436	0.424	0.666	0.572	0.627
Felsic index	20.650	0.060	22.302	23.346	22.147	23.827	0.037	0.221	0.105	20.054	22.696	23.018

Table 4.12: Electron Microprobe analyses of amphiboles in the KD samples

	KD 1				KD 2				KD 3			
SiO_2	42.500	44.673	40.014	43.925	42.983	43.555	43.689	42.606	41.725	41.757	42.282	50.168
TiO_2	1.781	1.716	0.074	0.172	1.553	1.810	1.989	1.650	1.820	1.738	1.037	0.177
Al_2O_3	13.496	12.248	21.668	16.238	13.066	11.680	13.191	12.783	13.900	14.033	14.199	6.839
Cr_2O_3	0.086	0.023	0.036	0.035	0.025	0.100	0.005	0.083	0.023	0.059	0.000	0.000
MgO	12.904	13.587	9.587	11.385	11.946	12.218	10.861	12.105	11.415	12.083	11.038	10.919
CaO	11.784	11.956	7.163	11.256	11.476	11.637	11.993	11.300	11.716	11.611	11.835	21.218
MnO	0.068	0.000	0.775	0.721	0.225	0.242	0.254	0.136	0.286	0.324	0.188	0.276
FeO	10.127	10.465	18.733	14.126	13.115	12.95	12.538	13.366	13.165	13.253	14.506	9.455
Na_2O	2.345	2.214	0.017	0.602	1.882	1.651	1.602	1.825	1.564	1.433	1.277	1.299
K_2O	0.849	0.668	0.018	0.000	1.330	1.267	1.806	1.406	1.961	1.784	1.994	0.013
Total	95.94	97.55	98.085	98.46	97.601	97.11	97.928	97.26	97.575	98.075	98.356	100.364
Cations	Based on 24 Oxygens				Based on 24 Oxygens							
Si	6.583	6.777	6.027	6.434	6.586	6.713	6.715	6.544	6.449	6.363	6.478	7.473
Ti	0.208	0.196	0.008	0.019	0.179	0.210	0.230	0.191	0.212	0.199	0.121	0.020
Al^{iv}	1.417	1.223	1.973	1.566	1.414	1.287	1.285	1.456	1.551	1.637	1.522	0.527
Al^{vi}	1.047	0.966	1.873	1.237	0.945	0.855	1.105	0.858	0.981	0.883	1.042	0.674
Cr	0.011	0.003	0.004	0.004	0.003	0.012	0.001	0.010	0.003	0.007	0.000	0.000
Mg	2.980	3.073	2.153	2.486	2.729	2.807	2.489	2.772	2.630	2.745	2.521	2.425
Ca	1.956	1.943	1.156	1.766	1.884	1.922	1.975	1.860	1.940	1.896	1.943	3.386
Mn	0.009	0.000	0.099	0.089	0.029	0.032	0.033	0.018	0.037	0.042	0.024	0.035
Fe^{3+}	0.031	0.065	0.767	1.454	0.391	0.304	0.000	0.538	0.277	0.656	0.457	0.000
Fe^{2+}	1.281	1.262	1.593	0.277	1.289	1.366	1.612	1.179	1.425	1.033	1.402	1.178
Na	0.704	0.651	0.005	0.171	0.559	0.493	0.477	0.544	0.469	0.423	0.379	0.375
K	0.168	0.129	0.003	0.000	0.260	0.249	0.354	0.276	0.387	0.347	0.39	0.002
Mg*	0.694	0.698	0.477	0.590	0.619	0.627	0.607	0.618	0.607	0.619	0.576	0.673
Felsic index	21.325	19.423	0.486	5.077	21.868	20.048	22.128	22.235	23.128	21.695	21.654	5.823

Table 4.13: Electron Microprobe analyses of amphiboles in the BF samples.

	BF 24		BF 36								
SiO_2	50.843	49.346	45.068	47.102	45.464	38.001	38.06	37.968	53.461	50.062	38.192
TiO_2	0.137	0.903	0.214	0.194	0.232	0.028	0.067	0.041	1.284	0.281	0.007
Al_2O_3	5.355	4.313	9.394	7.711	8.989	23.88	22.291	22.576	1.721	2.146	20.326
Cr_2O_3	0.030	0.013	0.000	0.000	0.000	0.018	0.027	0.004	0.011	0.014	0.131
MgO	12.352	11.797	8.772	9.464	8.726	0.000	0.000	0.000	13.778	11.693	0.777
CaO	11.691	10.871	11.076	11.21	10.967	23.557	23.449	23.215	13.389	12.039	22.746
MnO	0.532	0.421	0.426	0.445	0.301	0.223	0.154	0.124	0.266	0.443	0.148
FeO	14.343	16.729	20.043	19.433	20.208	10.626	12.263	12.408	13.945	18.65	13.117
Na_2O	0.859	1.100	1.714	1.584	1.705	0.005	0.012	0.000	0.233	0.729	0.025
K_2O	0.187	0.418	0.403	0.358	0.467	0.021	0.029	0.024	0.072	0.244	0.017
Total	96.329	95.911	97.110	97.501	97.059	96.359	96.352	96.360	98.160	96.301	95.486
Cations					**Based on 24 Oxygens**						
Si	7.825	7.69	7.067	7.338	7.138	5.976	6.041	6.023	8.072	7.877	6.146
Ti	0.016	0.106	0.025	0.023	0.027	0.003	0.008	0.005	0.146	0.033	0.001
Al^{iv}	0.175	0.31	0.933	0.662	0.862	2.024	1.959	1.977	0.000	0.123	1.854
Al^{vi}	0.796	0.482	0.804	0.754	0.802	2.402	2.211	2.244	0.306	0.275	2.001
Cr	0.004	0.002	0.000	0.000	0.000	0.002	0.003	0.001	0.001	0.002	0.017
Mg	2.834	2.74	2.051	2.198	2.042	0.000	0.000	0.000	3.101	2.741	0.186
Ca	1.928	1.815	1.861	1.871	1.845	3.969	3.988	3.946	2.166	2.03	3.922
Mn	0.069	0.056	0.057	0.059	0.04	0.030	0.021	0.017	0.034	0.059	0.020
Fe^{3+}	0.069	0.44	0.624	0.440	0.572	0.000	0.000	0.000	0.000	0.319	0.000
Fe^{2+}	1.782	1.74	2.005	2.092	2.081	1.398	1.628	1.646	1.761	2.135	1.765
Na	0.256	0.332	0.521	0.478	0.519	0.002	0.004	0.000	0.068	0.222	0.008
K	0.037	0.083	0.081	0.071	0.094	0.004	0.006	0.005	0.014	0.049	0.003
Mg*	0.605	0.557	0.438	0.465	0.435	0.000	0.000	0.000	0.638	0.528	0.095
Felsic index	8.212	12.253	16.046	14.766	16.531	0.110	0.175	0.103	2.227	7.478	0.184

Table. 4.14: Electron Microprobe analyses of mica in the RD, ASH and S samples

	RD 1						ASH 1					S 3
SiO_2	38.298	37.775	38.316	38.99	38.455	38.476	38.691	38.850	38.214	38.735	38.574	45.973
TiO_2	2.842	2.709	2.750	2.195	2.791	2.196	2.005	2.724	2.745	2.867	2.661	0.520
Al_2O_3	14.033	16.215	14.49	13.683	14.389	14.248	14.171	14.656	13.894	13.551	14.051	27.460
Cr_2O_3	0.016	0.039	0.054	0.005	0.022	0.102	0.015	0.000	0.006	0.036	0.000	0.019
MgO	12.68	11.526	11.635	11.683	12.469	11.706	9.084	8.600	8.911	9.750	10.157	1.427
CaO	0.052	0.083	0.038	0.445	0.130	0.336	0.092	0.198	0.247	0.138	0.143	0.059
MnO	0.235	0.314	0.261	0.273	0.267	0.269	0.395	0.401	0.352	0.326	0.254	0.000
FeO	18.099	17.983	18.68	18.585	17.935	18.205	21.732	21.587	21.914	21.98	21.053	11.682
Na_2O	0.083	0.089	0.084	0.142	0.101	0.067	0.120	0.131	0.221	0.051	0.083	0.344
K_2O	9.224	9.075	9.090	9.167	8.798	9.412	8.967	8.419	8.346	8.102	8.565	8.093
Total	95.562	95.808	95.398	95.168	95.357	95.017	95.272	95.566	94.85	95.536	95.541	95.577
CATIONS						**Based on 24 Oxygens**						
Si	5.773	5.663	5.794	5.911	5.737	5.847	5.934	5.909	5.886	5.906	5.867	6.372
Ti	0.322	0.305	0.313	0.313	0.333	0.251	0.231	0.312	0.318	0.329	0.304	0.054
Al^{iv}	2.227	2.337	2.206	2.089	2.263	2.153	2.066	2.091	2.114	2.094	2.133	1.628
Al^{vi}	0.267	0.529	0.376	0.356	0.365	0.399	0.496	0.537	0.408	0.341	0.386	2.858
Cr	0.000	0.000	0.000	0.000	0.000	0.000	0.000	0.000	0.000	0.000	0.000	0.000
Mg	2.849	2.576	2.623	2.640	2.773	2.652	2.077	1.950	2.046	2.216	2.303	0.295
Ca	0.008	0.013	0.006	0.072	0.021	0.055	0.015	0.032	0.041	0.023	0.024	0.009
Mn	0.030	0.040	0.035	0.035	0.034	0.035	0.051	0.052	0.046	0.042	0.033	0.000
Fe^{3+}	0.181	0.179	0.187	0.187	0.177	0.183	0.221	0.217	0.224	0.222	0.212	1.193
Fe^{2+}	2.101	2.076	2.175	2.169	2.061	2.131	2.567	2.529	2.599	2.581	2.466	0.161
Na	0.024	0.026	0.025	0.042	0.029	0.020	0.036	0.039	0.066	0.015	0.024	0.092
K	1.774	1.735	1.753	1.773	1.674	1.824	1.754	1.633	1.640	1.576	1.662	1.431
Mg*	0.555	0.533	0.526	0.528	0.553	0.534	0.427	0.415	0.420	0.442	0.462	0.179
Fe*	0.445	0.467	0.474	0.472	0.447	0.466	0.573	0.585	0.580	0.558	0.538	0.821
ΣAl	2.494	2.866	2.582	2.445	2.628	2.552	2.562	2.628	2.522	2.435	2.519	4.486
Felsic index	99.444	99.102	99.587	95.438	98.560	96.577	98.998	97.737	97.198	98.336	98.373	99.306

Table. 4.15 a: Electron Microprobe analyses of mica in the BF samples

	BF 12				BF 24			BF 36		
SiO_2	38.221	39.126	39.138	40.676	38.912	38.873	38.052	38.572	38.660	38.300
TiO_2	1.095	1.093	1.180	1.053	1.019	0.975	1.114	0.651	1.385	1.143
Al_2O_3	16.044	16.197	16.159	17.162	15.045	15.576	15.242	15.966	14.618	13.833
Cr_2O_3	0.000	0.031	0.056	0.001	0.027	0.000	0.037	0.000	0.000	0.007
MgO	13.36	13.329	13.056	11.290	13.633	12.736	13.619	13.670	9.766	9.695
CaO	0.118	0.265	0.408	0.469	0.072	0.191	0.235	0.000	0.156	0.168
MnO	0.279	0.255	0.135	0.25	0.149	0.21	0.176	0.272	0.410	0.312
FeO	15.777	15.958	15.033	15.607	17.171	17.137	16.67	17.245	22.810	22.276
Na_2O	0.054	0.095	0.063	0.054	0.029	0.015	0.066	0.050	0.031	0.089
K_2O	9.135	8.470	9.708	8.802	9.568	9.208	9.022	9.186	8.204	9.926
Total	94.083	94.819	94.936	95.364	95.625	94.921	94.233	95.612	96.04	95.749
CATIONS	**Based on 24 Oxygens**				**Based on 24 Oxygens**			**Based on 24 Oxygens**		
Si	5.767	5.825	5.839	5.984	5.825	5.844	5.766	5.761	5.879	5.904
Ti	0.124	1.222	0.132	0.117	0.115	0.110	0.127	0.073	0.180	0.133
Al^{iv}	2.233	2.174	2.161	2.016	2.175	2.156	2.234	2.239	2.121	2.096
Al^{vi}	0.620	0.669	0.681	0.960	0.479	0.604	0.488	0.572	0.500	0.417
Cr	0.000	0.000	0.000	0.000	0.000	0.000	0.000	0.000	0.000	0.000
Mg	3.005	2.959	2.904	2.476	3.042	2.854	3.076	3.044	2.214	2.228
Ca	0.019	0.042	0.063	0.074	0.012	0.031	0.038	0.000	0.025	0.028
Mn	0.036	0.032	0.017	0.031	0.019	0.027	0.023	0.034	0.053	0.041
Fe^{3+}	0.157	0.157	0.148	0.152	0.170	0.171	0.167	0.171	0.230	0.227
Fe^{2+}	1.834	1.830	1.728	1.768	1.980	1.984	1.945	1.973	2.671	2.645
Na	0.016	0.027	0.018	0.015	0.008	0.004	0.019	0.014	0.009	0.027
K	1.758	1.609	1.847	1.652	1.827	1.766	1.744	1.756	1.591	1.952
Mg*	0.601	0.598	0.608	0.563	0.586	0.570	0.593	0.587	0.433	0.437
Fe*	0.399	0.402	0.392	0.437	0.414	0.430	0.407	0.413	0.567	0.563
Σ Al	2.853	2.843	2.842	2.976	2.654	2.760	2.722	2.811	2.621	2.513
Felsic index	98.732	96.999	95.992	94.971	99.255	97.971	97.479	100.000	98.141	98.350

Table 4.15b: Electron Microprobe analyses of mica in the BF samples

		BF 48				BF 57			BF 72	
	Muscovite	Muscovite	Muscovite	Muscovite	biotite	Muscovite	Muscovite	Muscovite	Muscovite	Muscovite
SiO_2	48.538	48.259	47.964	48.503	38.213	48.650	49.362	47.926	48.476	48.986
TiO_2	1.046	0.610	0.671	0.412	2.363	0.195	0.474	0.818	0.428	0.424
Al_2O_3	27.087	27.104	27.705	27.556	15.391	25.838	25.187	25.909	25.650	24.768
Cr_2O_3	0.069	0.017	0.011	0.029	0.022	0.000	0.000	0.037	0.010	0.000
MgO	1.807	2.156	2.292	2.191	8.129	1.859	1.997	1.898	1.902	1.865
CaO	0.195	0.000	0.025	0.064	0.199	0.004	0.114	0.066	0.115	0.099
MnO	0.015	0.000	0.000	0.063	0.275	0.056	0.059	0.000	0.042	0.039
FeO	6.209	5.716	5.663	6.759	21.758	8.403	8.285	8.169	8.954	8.092
Na_2O	0.138	0.139	0.157	0.146	0.026	0.109	0.093	0.148	0.138	0.141
K_2O	11.339	11.642	10.868	10.360	9.566	10.558	10.214	10.555	10.091	10.663
Total	96.443	95.643	95.356	96.083	95.942	95.672	95.785	95.526	95.806	95.077
CATIONS		**Based on 24 Oxygens**				**Based on 24 Oxygens**				
Si	6.591	6.598	6.547	6.581	5.835	6.691	6.760	6.611	6.666	6.777
Ti	0.107	0.063	0.069	0.042	0.271	0.020	0.049	0.085	0.044	0.044
Al^{iv}	1.749	1.402	1.453	1.419	2.165	1.309	1.240	1.389	1.334	1.223
Al^{vi}	2.926	2.966	3.004	2.989	0.605	2.879	2.825	2.823	2.823	2.816
Cr	0.000	0.000	0.000	0.000	0.000	0.000	0.000	0.000	0.000	0.000
Mg	0.366	0.439	0.466	0.443	1.850	0.381	0.408	0.390	0.390	0.385
Ca	0.028	0.000	0.004	0.009	0.033	0.001	0.017	0.010	0.017	0.015
Mn	0.002	0.000	0.000	0.007	0.036	0.007	0.007	0.000	0.005	0.005
Fe^{3+}	0.664	0.631	0.627	0.660	0.352	0.852	0.836	0.830	0.908	0.825
Fe^{2+}	0.041	0.023	0.019	0.087	2.427	0.115	0.113	0.112	0.122	0.111
Na	0.036	0.037	0.042	0.038	0.008	0.029	0.025	0.040	0.037	0.038
K	1.964	2.030	1.892	1.793	1.863	1.852	1.784	1.856	1.770	1.882
Mg*	0.342	0.402	0.419	0.372	0.400	0.283	0.301	0.293	0.275	0.291
Fe*	0.658	0.598	0.581	0.634	0.600	0.717	0.699	0.707	0.725	0.709
ΣAl	4.675	4.368	4.457	4.408	2.770	4.188	4.065	4.212	4.157	4.039
Felsic Index	98.329	100.000	99.774	99.395	97.968	99.963	98.906	99.387	98.888	99.092

Table 4.16: Electron Microprobe analyses of pyroxenes in the KD samples

	KD 1			KD 2			KD 3		
SiO_2	51.481	51.106	52.383	51.494	51.161	51.453	50.299	49.837	49.451
TiO_2	0.447	0.516	0.273	0.205	0.326	0.269	0.114	0.391	0.290
Al_2O_3	6.048	7.218	4.620	4.562	6.286	5.752	6.543	7.236	7.129
Cr_2O_3	0.058	0.070	0.009	0.034	0.041	0.107	0.000	0.054	0.000
MgO	11.757	10.959	12.319	12.256	11.085	11.442	10.958	10.418	10.259
CaO	21.269	20.450	20.901	20.952	20.227	20.232	21.209	20.346	20.873
MnO	0.018	0.036	0.093	0.355	0.397	0.251	0.416	0.318	0.469
FeO	7.239	7.581	7.205	8.492	9.342	9.078	9.295	9.725	9.546
Na_2O	1.732	1.978	1.571	1.451	1.778	1.675	1.530	1.727	1.373
K_2O	0.004	0.000	0.000	0.021	0.007	0.000	0.033	0.000	0.000
Total	100.053	99.914	99.374	99.822	100.65	100.259	100.397	100.052	99.39
Cations				**Based on 24 Oxygens**					
Si	7.605	7.554	7.773	7.679	7.577	7.634	7.497	7.451	7.450
Ti	0.05	0.057	0.030	0.023	0.036	0.030	0.013	0.044	0.033
Al^{iv}	0.395	0.446	0.227	0.321	0.423	0.366	0.503	0.549	0.550
Al^{vi}	0.658	0.812	0.581	0.481	0.674	0.640	0.646	0.726	0.716
Cr	0.007	0.008	0.001	0.004	0.005	0.013	0.000	0.006	0.000
Mg	2.589	2.415	2.725	2.725	2.447	2.531	2.435	2.322	2.304
Ca	3.366	3.239	3.323	3.347	3.210	3.216	3.387	3.259	3.369
Mn	0.002	0.005	0.012	0.045	0.050	0.032	0.053	0.040	0.060
Fe^{3+}	0.004	0.001	0.000	0.004	0.005	0.000	0.002	0.002	0.000
Fe^{2+}	0.89	0.936	0.894	1.055	1.152	1.126	1.157	1.214	1.203
Na	0.496	0.567	0.452	0.419	0.510	0.482	0.442	0.501	0.401
K	0.001	0.000	0.000	0.004	0.001	0.000	0.006	0.000	0.000
Total	16.063	16.039	16.018	16.107	16.090	16.070	16.141	16.114	16.086
Ortho and Calcic CPX				%	%	%	%	%	%
Wo	49.145	49.140	47.866	46.942	47.103	46.792	48.521	47.949	48.999
En	37.799	36.641	39.254	38.207	35.917	36.820	34.881	34.162	33.509
Fs	13.056	14.219	12.879	14.851	16.981	16.388	16.598	17.889	17.491
Mg*	74.332	71.946	75.053	71.167	66.968	68.609	66.767	64.897	64.592
	Augite	Augite	Augite	Augite	Augite	Augite	Augite	Augite	Augite

Table 4.17: Electron Microprobe analyses of pyroxenes in the RD, CK and BF samples

	RD 3			CK 1		BF 57	
SiO_2	50.495	49.657	50.274	51.222	50.452	53.781	51.08
TiO_2	0.269	0.438	0.215	0.357	0.360	0.290	0.755
Al_2O_3	7.569	7.436	6.995	5.793	5.847	2.200	4.400
Cr_2O_3	0.000	0.106	0.026	0.033	0.060	0.007	0.005
MgO	10.443	10.881	10.678	11.885	12.053	14.669	13.994
CaO	20.298	20.873	21.260	20.604	20.613	12.469	11.864
MnO	0.322	0.319	0.391	0.072	0.188	0.377	0.353
FeO	9.343	9.337	9.670	8.417	8.600	14.146	14.84
Na_2O	1.754	1.567	1.382	2.014	1.935	0.365	0.746
K_2O	0.000	0.000	0.019	0.017	0.032	0.138	0.291
Total	100.493	100.614	100.91	100.414	100.14	98.442	98.328
Cations				Based on 24 Oxygens			
Si	7.486	7.383	7.460	7.559	7.490	8.082	7.746
Ti	0.030	0.049	0.024	0.039	0.040	0.033	0.086
Al^{iv}	0.514	0.617	0.540	0.000	0.000	0.000	0.340
Al^{vi}	0.809	0.686	0.683	1.007	1.023	0.390	0.446
Cr	0.000	0.012	0.003	0.004	0.007	0.001	0.001
Mg	2.308	2.412	2.362	2.615	2.668	3.286	3.163
Ca	3.224	3.325	3.380	3.258	3.279	2.007	1.928
Mn	0.040	0.040	0.049	0.009	0.024	0.048	0.045
Fe^{3+}	0.004	0.000	0.005	0.156	0.151	0.000	0.002
Fe^{2+}	1.154	1.161	1.195	0.883	0.917	1.778	1.880
Na	0.504	0.452	0.398	0.576	0.556	0.106	0.219
K	0.000	0.000	0.004	0.003	0.006	0.026	0.056
Total	16.073	16.137	16.103	16.109	16.161	15.757	15.912
Ortho and Calcic CPX				%			
Wo	48.222	48.205	48.689	47.137	47.772	28.390	27.651
En	34.519	34.964	34.025	37.832	38.865	46.470	45.379
Fs	17.259	16.831	17.286	15.030	13.363	25.140	26.971
Mg*	66.590	67.506	66.311	71.565	71.413	64.889	62.696

4.3.5. Chlorite

Chlorite mineral phase was identified in the BF samples at depth ranging from 48 – 72 m and also in the **S** sample which was sampled at a depth of 17.5 m (Table 4.18). The chlorites had Al_2O_3 contents ranging from 10.44 to 19.47 wt% and SiO_2 contents between 24.48 – 30.46 wt.%. The Cr_2O_3 contents of the chlorites range from 0.00 – 0.12wt.%.

Chlorite is a common product of the hydrothermal alteration of pyroxenes, amphiboles and biotite in igneous rocks. The composition of the chlorite is often related to that of the original igneous mineral, so that more iron-rich chlorites are commonly found as replacement of the iron-rich ferromagnesian minerals (Deer *et al*, 1992).

4.3.6. Ilmenite

Ilmenite is a weakly crystalline magnetic titanium-iron oxide mineral ($FeTiO_3$). The formula of ilmenite may be more fully expressed as $(Fe,Mg,Mn)TiO_3$. It is a common accessory mineral in many igneous and metamorphic rocks (Deer *et al*, 1992). Ilmenite minerals were identified in the KD1, KD 3, RD 3, BF 57, BF 72 and the CK samples (Table 4 19). The ilmenites had TiO_2 contents ranging from 16.72 – 70.11 wt% with the FeO contents ranging from 21.77 – 74.37 wt%. The SiO_2 contents ranged from 0.00 – 0.25 wt%.

4.3.7. Epidote

Epidote forms a group of related minerals, with the mineral epidote being the most prominent member of the group. It is a calcium aluminum iron sorosilicate mineral,

$Ca_2Al_2(Fe^{3+};Al)(SiO_4)$ $(Si_2O_7)O(OH)$. Epidote was identified in three samples (BF 12, BF 24 and ASH 1). The epidote had Al_2O_3 contents between 21.07 – 24.38 % and SiO_2 contents ranging from 36.52 – 38.39 wt% (Table 4.20). The CaO contents of the ranged from 21.44 – 23.60 wt.%.

Epidote is a common filling material in the fractures, and is generally associated with white mica. It is an abundant rock-forming mineral, but one of secondary origin. It is also a product of hydrothermal alteration of various minerals (feldspars, micas, pyroxenes, amphiboles, garnets, and others) composing igneous rocks.

4.3.8. Carbonate

Carbonates minerals in which the essential structural unit is the $(CO_3)^{2-}$ ion were identified only in the BF samples. The carbonate minerals identified were calcite and dolomite (Table 4.21). With increase in depth the Mg content of the minerals increased, with decrease in the Ca content, thus the mineral phase changes from calcite to dolomite with depth. The CaO content of the calcite ranged from 57.52 to 60.47 wt% (22.93 – 23.37 apfu) whilst the MgO content varied from 0.18 to 0.59 wt%. The dolomite had an average CaO content of 30.35wt % with an average MgO content of 16.77wt %. The carbonatite rocks of the Kpong complex analysed by Nude (2006) had CaO contents ranging from 13.78 to 27.07 wt%.

Table 4.18 Electron Microprobe analyses of chlorite in the BF samples

	BF 48		BF 57		BF 72				S 3
SiO_2	28.043	27.451	26.419	26.255	26.299	24.503	30.462	24.464	24.483
TiO_2	0.154	0.243	0.057	0.363	0.068	0.019	0.129	0.000	0.325
Al_2O_3	19.472	18.29	16.028	17.235	16.059	15.391	18.458	15.370	10.435
Cr_2O_3	0.049	0.116	0.000	0.068	0.000	0.011	0.000	0.004	0.003
MgO	18.973	17.813	9.875	8.358	9.850	8.665	8.369	9.332	0.591
CaO	0.098	0.075	0.062	0.03	0.046	0.062	0.108	0.115	0.171
MnO	0.085	0.143	0.310	0.454	0.315	0.356	0.379	0.311	0.000
FeO	16.242	17.313	34.976	36.425	33.696	32.475	31.588	32.744	42.192
Na_2O	0.015	0.013	0.038	0.025	0.000	0.051	0.014	0.030	0.106
K_2O	0.473	0.538	0.033	0.076	0.000	0.009	0.641	0.024	2.043
Total	83.604	81.995	87.798	89.289	86.333	81.542	90.148	82.394	80.349
Cations			Based on 24 Oxygens		Based on 24 Oxygens				
Si	5.054	5.094	5.047	4.961	5.079	5.037	5.476	4.983	5.561
Ti	0.021	0.034	0.008	0.052	0.010	0.003	0.017	0.000	0.056
Al^{iv}	3.202	3.210	3.237	3.326	3.212	3.252	2.898	3.295	2.793
Al^{vi}	0.934	0.790	0.372	0.512	0.443	0.477	1.013	0.395	0.000
Cr	0.007	0.017	0.000	0.010	0.000	0.002	0.000	0.001	0.001
Mg	5.098	4.928	2.813	2.354	2.836	2.655	2.243	2.833	0.200
Ca	0.019	0.015	0.013	0.006	0.010	0.014	0.021	0.025	0.042
Mn	0.013	0.022	0.050	0.073	0.051	0.062	0.058	0.054	0.000
Fe^{3+}	2.324	2.599	2.846	2.920	2.905	2.888	3.304	2.817	0.588
Fe^{2+}	0.124	0.088	2.742	2.836	2.537	2.695	1.445	2.760	7.427
Na	0.005	0.005	0.014	0.009	0.000	0.021	0.005	0.012	0.047
K	0.109	0.127	0.008	0.018	0.000	0.002	0.147	0.006	0.592
Total	16.910	16.929	17.150	17.077	17.083	17.108	16.627	17.181	17.307

Table 4.19 Microprobe analyses of Ilmenite in representative samples

	KD 1		KD 3			RD 3			BF 57		BF 72	CK 1
SiO_2	0.067	0.079	0.000	0.005	0.000	0.008	0.038	0.247	0.030	0.247	0.047	0.034
TiO_2	51.174	48.975	25.437	18.858	16.717	17.018	19.449	45.059	64.754	70.113	62.514	40.614
Al_2O_3	0.000	0.000	0.136	0.265	0.335	0.296	0.186	0.095	0.000	0.013	0.000	0.057
Cr_2O_3	0.083	0.039	0.127	0.104	0.126	0.111	0.127	0.055	0.000	0.035	0.000	0.081
MgO	0.184	0.238	0.05	0.075	0.135	0.124	0.033	0.497	0.000	0.033	0.013	0.023
CaO	0.000	0.046	0.049	0.032	0.033	0.045	0.065	0.089	0.022	0.566	0.051	0.042
MnO	0.000	0.019	0.113	0.137	0.157	0.026	0.183	0.084	0.075	0.339	0.100	0.114
FeO	38.392	41.217	66.903	71.885	74.371	70.184	68.075	44.218	28.066	21.767	31.553	38.040
Na_2O	0.044	0.045	0.019	0.009	0.009	0.000	0.000	0.019	0.024	0.041	0.002	0.019
K_2O	0.000	0.029	0.000	0.000	0.000	0.002	0.000	0.014	0.042	0.016	0.003	0.000
Total	89.944	90.687	92.834	91.37	91.883	87.814	88.156	90.377	93.013	93.17	94.283	79.024
Cations						**Based on 24 Oxygens**						
Si	0.015	0.017	0.000	0.001	0.000	0.002	0.011	0.056	0.006	0.047	0.009	0.009
Ti	8.425	8.123	4.841	3.809	3.411	3.604	4.034	7.642	9.654	10.107	9.350	7.852
Al^{iv}	0.000	0.000	0.000	0.000	0.000	0.000	0.000	0.000	0.000	0.003	0.000	0.000
Al^{vi}	0.000	0.000	0.040	0.084	0.107	0.098	0.061	0.025	0.000	0.000	0.000	0.017
Cr	0.014	0.007	0.025	0.022	0.027	0.025	0.028	0.010	0.000	0.005	0.000	0.016
Mg	0.060	0.078	0.019	0.030	0.054	0.052	0.014	0.167	0.000	0.010	0.004	0.009
Ca	0.000	0.011	0.013	0.009	0.010	0.014	0.019	0.022	0.005	0.116	0.011	0.012
Mn	0.000	0.004	0.024	0.031	0.036	0.006	0.043	0.016	0.013	0.055	0.017	0.025
Fe^{3+}	0.000	0.000	0.037	0.026	0.027	0.031	0.032	0.057	0.000	0.000	0.000	0.034
Fe^{2+}	7.029	7.602	14.122	16.121	16.847	16.499	15.671	8.283	4.653	3.489	5.248	8.144
Na	0.019	0.019	0.009	0.005	0.005	0.000	0.000	0.008	0.009	0.015	0.001	0.010
K	0.000	0.008	0.000	0.000	0.000	0.001	0.000	0.004	0.011	0.004	0.001	0.000
Total	15.562	15.869	19.130	20.138	20.524	20.332	19.913	16.290	14.351	13.851	14.641	16.128

Table 4.20 Microprobe analyses of epidote in representative samples

	BF 12				BF 24				ASH 1			
SiO_2	38.360	37.612	38.059	38.284	38.395	38.287	38.454	38.443	37.262	36.518	36.905	37.542
TiO_2	0.103	0.063	0.054	0.064	0.138	0.164	0.074	0.073	0.041	0.110	0.077	0.103
Al_2O_3	24.259	23.377	23.978	23.848	23.528	22.930	24.234	24.38	21.830	21.079	22.156	22.203
Cr_2O_3	0.120	0.022	0.062	0.090	0.089	0.009	0.052	0.051	0.027	0.084	0.023	0.077
MgO	0.018	0.025	0.013	0.018	0.023	0.025	0.022	0.043	0.047	0.107	0.069	0.029
CaO	23.301	23.194	23.567	23.242	23.309	22.828	23.601	23.378	22.408	21.437	21.88	22.369
MnO	0.205	0.188	0.259	0.273	0.323	0.267	0.208	0.285	0.194	0.253	0.174	0.256
FeO	9.248	9.012	9.607	9.885	10.757	11.607	10.408	10.012	12.809	12.239	11.985	12.920
Na_2O	0.008	0.014	0.051	0.019	0.004	0.021	0.000	0.000	0.000	0.003	0.000	0.000
K_2O	0.000	0.005	0.051	0.020	0.011	0.021	0.003	0.022	0.030	0.010	0.003	0.035
Total	95.622	93.512	95.701	95.743	96.577	96.159	97.056	96.687	94.648	91.84	93.272	95.534
Cations					**Based on 24 Oxygens**							
Si	6.025	6.047	5.999	6.029	6.023	6.052	5.988	5.995	6.035	6.080	6.032	6.201
Ti	0.012	0.008	0.006	0.008	0.016	0.020	0.009	0.009	0.005	0.014	0.009	0.012
Al^{iv}	1.975	1.953	2.001	1.971	1.977	1.948	2.012	2.005	1.965	1.920	1.968	1.979
Al^{vi}	2.515	2.477	2.453	2.456	2.373	2.324	2.436	2.476	2.202	2.216	2.300	2.218
Cr	0.015	0.003	0.008	0.011	0.011	0.001	0.006	0.006	0.003	0.011	0.003	0.010
Mg	0.004	0.006	0.003	0.004	0.005	0.006	0.005	0.010	0.011	0.027	0.017	0.007
Ca	3.921	3.995	3.980	3.922	3.918	3.866	3.938	3.906	3.888	3.824	3.831	3.844
Mn	0.027	0.026	0.035	0.036	0.043	0.036	0.027	0.038	0.027	0.036	0.024	0.035
Fe^{3+}	0.002	0.000	0.012	0.004	0.006	0.004	0.000	0.003	0.008	0.000	0.003	0.008
Fe^{2+}	1.213	1.212	1.254	1.298	1.405	1.530	1.355	1.303	1.727	1.704	1.635	1.725
Na	0.002	0.004	0.015	0.006	0.001	0.006	0.000	0.000	0.000	0.001	0.000	0.000
K	0.000	0.001	0.010	0.004	0.002	0.004	0.001	0.004	0.006	0.002	0.001	0.007
Total	15.711	15.732	15.776	15.749	15.780	15.797	15.777	15.755	15.877	15.835	15.823	16.046

Table 4.21: Microprobe analyses of carbonate in BF samples

	BF 24		BF 36		BF 48	BF 57	
SiO_2	0.018	0.035	0.132	0.059	0.054	9.962	2.895
TiO_2	0.049	0.016	0.018	0.016	0.024	11.698	1.446
Al_2O_3	0.000	0.000	0.008	0.018	0.002	0.742	0.115
Cr_2O_3	0.065	0.037	0.064	0.000	0.000	0.000	0.000
MgO	0.586	0.358	0.180	0.267	0.287	13.504	20.042
CaO	57.519	61.242	61.161	62.467	61.474	29.892	30.808
MnO	1.188	1.18	0.977	1.329	0.922	0.952	1.278
FeO	0.942	0.632	0.661	0.788	0.481	1.199	1.325
Na_2O	0.004	0.016	0.000	0.000	0.001	0.028	0.034
K_2O	0.022	0.000	0.014	0.016	0.019	0.001	0.013
Total	60.393	63.516	63.215	64.96	63.264	67.978	57.956
Cations			**Based on 24 oxygen**				
Si	0.007	0.012	0.047	0.020	0.019	2.576	0.948
Ti	0.014	0.004	0.005	0.004	0.006	2.274	0.356
Al^{iv}	0.000	0.000	0.003	0.007	0.001	0.226	0.044
Al^{vi}	0.000	0.000	0.000	0.000	0.000	0.000	0.000
Cr	0.019	0.010	0.018	0.000	0.000	0.000	0.000
Mg	0.325	0.189	0.095	0.138	0.152	5.205	9.784
Ca	22.931	23.217	23.275	23.180	23.372	8.281	10.810
Mn	0.375	0.354	0.294	0.390	0.277	0.208	0.354
Fe^{3+}	0.009	0.000	0.002	0.003	0.000	0.000	0.000
Fe^{2+}	0.284	0.187	0.195	0.225	0.143	0.259	0.363
Na	0.003	0.011	0.000	0.000	0.001	0.014	0.022
K	0.011	0.000	0.006	0.007	0.009	0.000	0.006
Total	23.978	23.984	23.940	23.974	23.980	19.043	22.687
	Calcite	Calcite	Calcite	Calcite	Calcite	Dolomite	Dolomite

4.3.9. Other Minerals

Rutile, magnetite, titaniferous magnetite and sphene (Appendix I tables A1.1-5) were other minerals identified in some of the geological samples. The mineral rutile was identified in RD2C, BF57, BF72 and the CK samples. Some of the rutile minerals were very pure. The TiO_2 contents ranged from 92 –99.88 wt%, the FeO content ranged from 0.07 – 1.98 wt%, MgO varied from 0.00 – 0.025 wt%, and Cr_2O_3 <0.21 wt% corresponding to Cr 0.004–0.027 apfu (table 4.12). Low Cr contents in the rutiles might be an indicator for high pressure conditions (Zack *et al*., 2002). In most amphibolites, rutiles are mantled by sphene and/or ilmenite.

Magnetite was identified in the KD 1, KD 2, RD 1A. BF57, BF 72 and ASH1 samples. The FeO contents of the magnetite ranged from 86 to 99wt% whilst the MgO content varied from 0.01 to 1.90 wt%. Titaniferous magnetite was identified in KD 2, RD3 and CK 1 samples. Their TiO content varied from 20 to 36 wt% with their FeO content varying from 62 to 79 wt%.The clay minerals illite and kaolinite were also identified in the shale (S3) samples. The SiO_2 content of the illites ranged from 45.70 to 50.68 wt %, the Al_2O_3 content varied from 22.50 to 24.67 wt % whilst the FeO varied from 2.37 to 5.16 wt %. The kaolinite had an average SiO_2 content of 47.23 wt%, Al_2O_3 content of 38.28 wt% and low FeO content of 0.45wt%.

4.4. Discussion

The mineral chemistry and X-ray diffraction analyses of the rock and soil samples indicate that the mineralogy of the rocks of the Accra Plain consist of a mixture of the four major rock-forming mineral groups; quartz, feldspars, micas and ferromagnesian minerals. Quartz, sodic plagioclase feldspar, K-feldspar, Ca-amphibole and biotite are the primary minerals, with

chlorites, epidote, magnetite, and carbonates occurring as secondary minerals. The shale sample also contain clay minerals-illite, and kaolinite. Montmorillonite clay mineral was identified in the CK sample.

Incongruent dissolution of the abundant plagioclase and ferromagesian (hornblende) minerals in the rocks of the Accra Plains will increase the major ion content of the groundwater especially along the groundwater flow path. Calcium and sodium which show the greatest relative mobility during weathering of granitic rocks due to their high concentration in plagioclase feldspar and mafic minerals (hornblende) and their high solubility in natural waters (Nesbitt *et al*., 1980) will increase the ionic content of the groundwater. The albite minerals will liberate sodium ions to solution. The feldspars and ferromagnesian minerals will be altered to montmorillonite and or kaolinite. Feldspars are readily altered to kaolinite by CO_2-rich, low-pH recharge.

$$2\ Na(AlSi_3)O_8 + 2H^+ + 9H_2O \rightarrow Al_2Si_2O_5(OH)_4 + 4H_4SiO_4 + 2Na^+ \quad (4.1)$$

Albite *kaolinite*

$$3NaAlSi_3O_8 + Mg^{2+} + 4H_2O \rightarrow 2Na_{0.5}Al_{1.5}Mg_{0.5}Si_4O_{10}(OH)_2 + 2Na^+ + H_4SiO_4 \quad (4.2)$$

Albite *montmorillonite*

The crystal structure of pyroxene and amphibole minerals allows substitution of a wide and diverse range of elements. These minerals are also quite susceptible to weathering (Allen and Hajek, 1989, Eggleton, 1986), making them important sources of Fe, Mg, and trace elements in rock formation.

$$(Mg_{0.7}CaAl_{0.3})(Al_{0.3}Si_{1.7})O_6 + 3.4H^+ + 1.1H_2O \rightarrow .3Al_2Si_2O_5(OH)_4 + Ca^{2+} + 0.7Mg^{2+} +$$

(augite) $1.1H_4SiO_4$ (4.3)

Table 4.22: The mean lifetime in years of 1mm crystals of various minerals calculated from laboratory dissolution studies at 25 °C and pH 5 (Lasaga *et al*, 1994)

Mineral	Log rate (mol/m²/s)	Mol. vol. (cm³/mol)	Lifetime (y)
Quartz	−13.39	22.688	34,000,000
Kaolinite	−13.28	99.52	6,000,000
Muscovite	−13.07	140.71	2,600,000
Epidote	−12.61	139.2	923,000
Microcline	−12.50	108.741	921,000
Prehnite	−12.41	140.33	579,000
Albite	−12.26	100.07	575,00
Sanidine	−12.00	109.008	291,000
Gibbsite	−11.45	31.956	276,000
Enstatite	−10.00	31.276	10,100
Diopside	−10.15	66.09	6,800
Forsterite	−9.5	43.79	2,300
Nepheline	−8.55	55.16	211
Anorthite	−8.55	100.79	112
Wollastonite	−8.00	39.93	79

According to Appelo and Postma (2005), clay minerals that originate from silicate weathering remain fairly stable during erosion and transport, and are deposited as coatings on sand grains, often closely intermingled with iron oxide. Thus the kaolinite and montmorillonite minerals which will be produced as a result of weathering of the rocks of Accra Plains, made up of mainly albite and K-feldspars, will be more resistant to weathering and will remain stable for a long period of time. The mean lifetime in years of 1mm crystals of various minerals calculated from laboratory dissolution studies at 25 °C and pH 5 are shown in Table 4.22 (Lasaga *et al*, 1994).

Kaolinite has a lifetime dissolution rate of 6,000,000 years whiles muscovite which occurs with depth in the rock formation has a lifetime dissolution rate of 2,600,000 years. The long time stability of these minerals together with their ion exchange properties which can retard the migration of long-lived radionuclides makes them a useful backfill and or buffer material for a radioactive waste repository. The rock formation in the Plains will be able to maintain the integrity of the engineered barriers of the disposal system for a long time making it a suitable host material for radioactive waste.

A fundamental safety requirement is that reducing conditions should prevail in the chemical evolution of the groundwater system because the mobility of leaking radionuclides is often sensitive to oxidation-reduction reactions. A necessary condition is the absence of dissolved oxygen, because any evidence of its presence would indicate oxidizing conditions. According to Iwatsuki and Yoshida (1999), the redox conditions of the groundwater tend to reflect the minerals present in the host rock, even when chemical equilibrium has not been attained between all the solid mineral phases and all the dissolved species present in the groundwater. The presence of reducing agents that react quickly with oxygen, such as Fe(II) and sulphide, is sufficient to indicate reducing conditions. According to Bullen *et al*. (1996, 1997), in the presence of dissolved oxygen, iron-rich mafic minerals readily produce iron (i.e. Fe^{3+}) oxyhydroxides and silica as a result of chemical weathering in moderate Eh conditions according to the equation below:

$$2KFe_3AlSi_3O_{10}(OH)_2 + 2H^+ + 3.5O_2 + 8H_2O = 6Fe(OH)_3 + Al_2Si_2O_5(OH)_4 + 2K^+ + 6SiO_2 \quad (4.4)$$

The iron rich minerals, biotite, magnetite, titaniferous magnetite and spinel which are present in the rock formation in the Plains although in small quantities may readily release iron for redox reactions in accordance with Eqn 4.4 creating a reducing environment. Dissolved irons affect the pH values of groundwater, in the sense that the aqueous iron may occur as iron hydroxide complexes and thus contribute to buffering the pH values at a relatively low level (around 7.5).

Reducing environment required for a radioactive waste repository will be created by interaction between the groundwater and the mafic gneiss in the Plains which contains iron rich minerals, such as magnetite, biotite, chlorite, and amphiboles. These hydrogeochemical conditions make the Krobo Mountain and Okwenya areas a probable repository candidate sites.

However, studies from Oklo suggest that there will be mineralogical changes in the geological formation as a result of radiation damage (Curtis, 1985). The changes will be a consequence of convective circulation of fluid that transports elements in and out of the rocks. There will also be changes in the electrochemical conditions in the rocks. These changes can be attributed to oxidizing and reducing species produced by radiolysis of the groundwater. According to Arrhenius equation, weathering rate increases with temperature. The warm groundwater that will be produced due heat from the radioactive waste will also increase the dissolution rate. Thus the effect of radiolysis on the geological formation in the Accra Plains must be studied

4.5. Conclusion

The primary minerals in the Accra Plains are predominantly feldspars, amphiboles, mica, quartz with minor pyroxenes and other secondary minerals which include chlorite, epidote, magnetite, rutile and sphene. The secondary minerals present were illite, kaolinite, montmorillonite and carbonates. The weathering of these minerals will influence the ion composition of the groundwater chemistry especially, the feldspar and ferromagnesian minerals due to their abundance in the geological formation and reactivity.

The clay minerals, kaolinite and montmorillonite minerals, that may originate from silicate weathering will remain fairly stable for a long period of time. The long time stability of these minerals together with their ion exchange properties which can retard the migration of long-lived radionuclides makes them a useful backfill and or buffer material for a radioactive waste repository.

A fundamental safety requirement is that reducing conditions should prevail in the chemical evolution of the groundwater system. A necessary condition is the absence of dissolved oxygen, because any evidence of its presence would indicate oxidizing conditions. The mafic gneiss in the Plains contains iron rich minerals, such as magnetite, biotite, chlorite, and amphiboles. The immobility of the irons released from weathering of these redox-sensitive minerals as a result of the low solubility of the iron hydroxide and hydrated oxide which forms quickly will create a reducing condition in the aquifer. Thus the mafic gneiss in the geological formation in the Plains will create a reducing environment required for a repository.

Chapter Five

Groundwater Geochemistry in the Accra Plains

5.1. Results and Discussion

5.1.1. Major Ion Chemistry

Groundwater chemistry was characterized by analyses of the major ions and physical parameters of the groundwater and their interpretation to understand the hydrogeochemical processes controlling the groundwater composition. The detailed analytical data for each sample is presented in Table 5.1 whilst the summarized descriptive statistics is presented in Table 5.2. The pH values of groundwater samples ranged from 5.6 to 8.5 indicating that the groundwater ranges from slightly acidic to alkaline condition. The acidic pH values were found along the foothills of the Akwapim Togo Mountains.

The total dissolved solids (TDS) concentration ranged from 50 to 8748 mg/L indicating a variation from fresh to brackish groundwaters. The groundwater can be described as brackish as about 56% of the groundwater samples analysed had TDS values greater than 1,000mg/L (Freeze and Cherry, 1979). TDS concentrations were relatively low along the foot of the Akwapim Togo Mountains (Fig.5.1). This area is probably the recharge area for groundwaters within the Plains and the groundwaters have short residence time within the rocks which are mainly quartzites with little minerals to be dissolved (Kortatsi, 2006). The high brackish waters occurring in the central and coastal areas of the Plains suggests that the waters have had enough contact time with the rock minerals and might be saturated with respect to both calcite and dolomite. The values of EC range from 129 to 13700 µS/cm with mean of 3130 µS/cm. The large variations in EC maybe attributed to geochemical reactions.

Table: 5.1. Chemical analyses of groundwater samples from boreholes in the Accra Plains

BH ID	Location	T °C	pH	TDS (mg/L)	Ele. Con. (µS/cm)	Ca (mg/L)	Mg (mg/L)	Na (mg/L)	K (mg/L)	HCO_3 (mg/L)	Cl (mg/L)	SO_4 (mg/L)	NO_3 (mg/L)	SiO_2 (mg/L)
AB1	Abokobi	28.80	6.40	248.00	595.00	30.50	21.50	58.50	12.30	102.50	111.50	42.50	1.95	14.10
AB1Res	Abokobi	29.20	6.30	249.00	601.00	32.50	21.20	58.80	12.00	99.70	115.25	45.90	2.48	13.50
AB2S	Abokobi	29.90	6.50	276.00	670.00	31.70	26.00	65.40	12.50	86.80	147.90	49.70	1.93	13.37
AB 3R	Abokobi	29.00	6.40	241.00	564.00	26.00	21.90	60.70	11.00	81.00	144.00	42.70	2.30	14.10
PWC 2	Abokobi	30.30	6.20	827.00	2020.00	30.70	29.34	298.39	9.80	117.10	436.65	99.50	4.53	15.38
PWC 2R	Abokobi	29.90	6.10	830.00	2025.00	27.80	21.90	306.00	18.50	119.50	441.48	92.04	8.53	20.11
PWC F	Abokobi	29.50	6.80	1262.00	2650.00	22.70	21.30	285.41	18.75	112.20	458.45	62.00	4.80	8.90
PWC K	Abokobi	32.10	6.50	1510.00	2370.00	29.10	26.00	278.50	14.00	114.00	468.70	64.80	2.80	18.80
KP 1	Kponkpo	28.40	6.80	190.00	297.00	16.10	10.00	36.80	2.00	45.40	67.40	16.70	1.50	8.30
DA 2K	Danfa	28.10	6.30	195.00	250.00	8.00	10.00	21.00	7.00	38.00	44.00	15.00	1.00	3.00
DA 1	Danfa	30.00	6.10	848.00	1330.00	50.00	62.00	161.00	12.00	187.50	337.70	54.20	2.10	10.00
DA 1K	Danfa	27.80	6.80	847.00	1320.00	57.00	68.30	153.00	16.00	189.70	362.00	51.20	1.70	15.00
SAD A	Saduase	26.80	7.10	552.00	680.00	51.02	29.27	61.86	6.30	274.59	116.43	24.76	2.53	26.60
SAD K	Saduase	28.80	7.10	540.00	842.00	52.30	28.60	61.00	4.00	275.00	103.00	25.00	1.00	38.00
AYM F	Ayimensa	29.40	6.80	356.00	568.00	15.80	11.60	68.00	8.30	49.02	113.10	24.00	1.30	15.00

AYM K	Ayimensa	29.80	6.40	338.00	528.00	23.50	18.80	72.00	6.00	60.00	147.80	29.00	1.00	14.00
AYM 72	Ayimensa	29.50	6.70	365.00	570.00	32.50	24.80	70.00	12.00	77.50	148.00	49.50	2.80	12.00
AYR 82	Ayimensa	30.00	6.75	408.00	638.00	20.00	17.50	90.00	10.50	64.10	168.00	24.80	1.75	24.00
OY1	Oyarifa	26.40	6.70	1517.00	2900.00	104.00	64.90	198.60	19.00	227.20	493.80	138.70	4.35	14.97
OY K	Oyarifa	28.40	6.80	1320.00	2060.00	122.82	81.60	198.15	21.00	226.00	517.98	145.00	3.55	10.00
OY 163	Oyarifa	30.00	6.80	1410.00	2200.00	94.50	77.70	197.35	21.70	240.00	532.00	130.00	5.80	8.00
OY F	Oyarifa	31.50	6.70	1784.00	3420.00	93.00	77.40	198.78	19.00	272.80	519.30	113.50	4.10	15.00
AHD 1	Adenta	25.50	6.98	235.00	350.00	47.60	28.70	141.00	6.90	172.56	271.89	81.82	1.20	13.50
AHD 2	Adenta	26.60	6.32	50.00	129.00	19.26	10.90	54.60	2.40	52.19	93.80	19.10	0.67	5.20
ADH 3	Adenta	26.80	8.11	1470.00	2337.00	113.50	57.74	285.13	13.98	318.50	493.88	102.70	2.80	24.80
BF 1	GAEC	26.80	7.70	1671.00	3760.00	144.30	85.90	395.00	70.00	395.01	746.08	130.30	1.50	35.10
BF2	GAEC	26.00	7.50	438.00	684.00	32.40	17.50	87.90	10.80	92.66	149.95	41.10	2.05	11.40
BF3	GAEC	26.60	7.70	379.00	592.00	31.50	17.80	74.50	12.50	83.15	139.98	39.10	1.50	11.50
VV1	Oyibi	30.50	6.50	242.00	600.00	21.80	14.90	67.70	12.80	87.90	99.64	38.60	1.00	58.60
VV2	Oyibi	31.00	6.20	243.00	601.00	25.60	16.20	76.80	11.50	92.70	119.63	36.84	1.00	55.60
VV3	Oyibi	29.70	5.60	226.00	550.00	23.20	14.30	79.10	8.50	88.59	121.96	32.90	1.80	54.76
ASB 1	Ash Botwe	26.50	7.42	233.00	488.00	26.00	15.95	91.10	1.45	75.59	143.99	47.85	1.40	8.50
ASB 1D	Ash Botwe	26.50	7.20	156.00	244.00	10.00	6.35	36.40	2.40	28.00	55.00	24.00	1.00	3.00

ASB 11D	Ash Botwe	30.00	7.00	3074.00	4800.00	252.00	165.00	665.00	27.00	277.00	1430.00	300.00	4.10	5.80
ASB 12D	Ash Botwe	27.20	6.95	3861.00	6030.00	280.00	240.00	760.00	32.00	345.00	1850.00	354.00	1.90	9.80
OG 56	Ogbojo	30.00	6.90	1167.00	1820.00	130.00	170.00	475.00	25.00	265.00	1045.00	279.00	4.20	40.00
OG 59	Ogbojo	30.00	7.30	1330.00	2080.00	140.00	167.50	532.00	45.00	241.00	1192.00	248.00	5.00	40.00
AR A	Armahia	28.80	7.30	875.00	1260.00	48.98	37.68	164.42	32.40	445.45	178.93	12.86	7.20	48.00
AR1	Armahia	29.80	7.40	539.00	1318.00	41.80	36.10	173.30	14.90	169.20	272.00	75.20	1.12	44.28
AR2	Armahia	30.50	6.90	259.00	640.00	30.09	21.70	118.00	16.20	56.10	172.00	113.80	10.10	66.74
AR K	Armhia	29.00	7.30	711.00	1110.00	45.00	38.00	138.00	18.00	145.00	282.00	64.50	2.80	48.00
AR 35	Armahia	28.40	6.90	740.00	1160.00	56.40	39.60	103.00	10.60	168.45	194.60	78.20	1.20	12.00
AR F	Armahia	29.00	6.80	422.00	1190.00	53.40	35.12	114.80	10.00	172.80	198.87	69.80	1.32	24.00
AP37	Armahia	28.00	6.70	660.00	1030.00	60.50	43.00	89.50	16.30	143.00	232.00	59.80	3.00	11.30
PRE 1	Legon	24.00	7.70	1489.00	3240.00	135.60	97.90	402.00	28.70	170.63	877.46	141.37	16.40	25.62
PRE 2	Legon	24.40	7.50	1204.00	2640.00	123.70	96.30	334.00	24.90	142.30	789.73	93.33	16.50	46.11
PRE K	Legon	27.50	7.10	1260.00	1970.00	129.00	91.00	181.00	17.00	195.00	528.00	121.00	16.70	17.00
PRE F	Legon	30.20	7.40	1490.00	2800.00	116.70	87.00	218.00	19.00	201.00	543.90	138.00	19.00	24.00
UG K	Legon	26.70	5.60	288.00	450.00	23.04	18.12	67.00	7.10	44.23	143.46	21.00	1.00	3.00
UG 93	Legon	30.00	7.70	4270.00	6680.00	295.53	192.76	965.00	38.00	350.00	1915.00	420.00	8.30	40.00
UG 109	Legon	30.00	8.50	1360.00	2160.00	142.00	94.00	210.00	18.00	217.00	585.00	120.00	15.00	20.00

DO 94D	Dodowa	30.00	7.70	2970.00	4640.00	228.00	193.00	442.00	25.00	275.00	1384.00	315.00	1.20	84.00
DO 139	Dodowa	30.00	7.20	2410.00	3270.00	175.00	153.00	437.00	27.00	210.00	1118.00	171.00	2.10	67.00
DO 151	Dodowa	30.00	7.80	2397.00	3750.00	168.00	154.00	398.75	28.00	225.00	1195.00	180.00	1.50	52.00
DO K	Dodowa	30.00	7.80	3715.00	5810.00	285.00	213.00	670.00	35.00	290.00	1650.00	360.00	2.50	64.00
AYK A	Ayikumah	28.00	7.20	920.00	2400.00	65.30	75.44	185.12	7.60	595.00	284.10	69.53	3.27	40.00
AYK 20	Ayikumah	28.50	7.10	1885.00	2900.00	62.00	82.00	185.56	15.60	497.00	265.00	90.00	2.80	22.00
KA 3	Katamanso	30.00	7.30	5500.00	8590.00	416.00	349.80	954.70	48.00	310.60	2985.00	373.90	4.20	15.10
KA 68	Katamanso	30.50	7.50	2970.00	4400.00	232.65	165.85	659.30	21.20	360.02	1448.21	248.10	2.50	36.80
KA 69	Katamanso	29.80	7.00	3882.00	6070.00	285.00	186.00	885.00	31.00	312.00	1824.00	355.00	2.80	12.00
KA 70	Katamanso	30.00	7.50	4103.00	6410.00	300.00	213.00	865.00	38.00	360.00	1910.00	375.00	2.40	24.00
BA 40	Bawaleshie	28.40	7.40	600.00	1445.00	72.00	53.96	220.00	32.00	190.37	263.00	296.95	1.80	28.00
BA 42	Bawaleshie	28.70	7.10	1420.00	2200.00	154.29	96.59	244.19	12.00	298.99	487.50	294.76	1.60	53.60
MAA	Malejor	28.50	7.25	2895.00	4200.00	71.24	128.41	717.00	21.20	435.08	1269.29	347.14	3.78	28.00
DZ 47	Dzorwulu	30.00	7.40	2160.00	3380.00	85.15	121.72	511.56	24.36	224.36	967.95	238.90	3.20	13.00
FRA K	Fafraha	28.60	6.90	1753.00	2740.00	93.00	71.00	179.95	19.00	170.98	458.95	95.00	2.50	11.34
SH 80A	Shai Hills	29.00	7.45	1546.00	2590.00	146.53	109.15	404.65	10.80	274.45	755.45	238.10	12.50	93.60
AGT 1	Afienya	29.20	7.00	696.00	1681.00	51.34	37.76	115.75	12.01	56.08	299.93	48.67	5.34	35.34
AGT AF	Afienya	29.00	7.40	2190.00	3420.00	183.63	140.93	430.82	25.00	222.00	1140.79	125.00	4.60	14.12

TFS K	La	29.00	7.60	7516.00	11710.00	246.53	324.36	1892.23	53.12	35.62	3876.14	249.00	13.00	85.00
TFS 176	La	28.00	7.50	8748.00	13700.00	134.00	482.00	1845.00	52.20	97.60	4830.00	83.00	11.40	21.00
TFS 177	La	27.30	7.30	6250.00	9770.00	254.48	564.87	1520.38	50.04	157.38	3854.67	355.00	9.20	18.04
KDE 55	Kordiabe	30.00	7.40	1107.00	1730.00	52.00	64.00	227.50	18.00	114.00	446.00	118.00	8.20	40.00
SMA 63	Somanya	30.00	8.30	581.00	908.00	35.50	34.40	90.50	21.00	96.80	186.00	73.00	4.50	12.00
KPG 53	Kpong	30.00	7.30	1640.00	2560.00	121.00	93.21	198.86	14.00	511.70	318.95	190.50	3.78	40.00
KPG 54	Kpong	27.00	7.30	1400.00	2300.00	102.40	85.12	181.40	12.00	452.77	257.83	183.33	3.80	38.00
KPE 67	Kpone	30.00	7.60	592.00	925.00	61.06	21.50	89.23	25.46	71.40	280.10	51.00	1.70	4.00
KPE 66	Kpone	30.00	7.80	369.00	577.00	26.50	14.89	86.45	18.05	43.96	179.87	27.60	1.00	8.00
LQP	Madina	25.30	6.00	1102.00	2450.00	69.94	42.70	272.10	14.30	236.58	459.79	63.36	1.75	24.50
WAS	Madina	25.30	6.10	937.00	2090.00	64.90	47.80	243.50	18.48	276.70	481.90	77.20	2.53	32.50
AA	Madina	26.00	6.49	110.20	242.00	26.76	21.10	113.00	9.70	141.45	194.95	44.24	1.20	13.50
ALA	Madina	25.60	6.72	1027.00	2300.00	81.80	52.60	151.00	26.00	125.10	397.38	60.60	3.50	21.40
TTL 170K	Tema	30.00	7.40	2550.00	3980.00	195.25	102.57	573.85	24.58	192.58	1302.39	73.10	4.20	23.00
TTL 175K	Tema	30.40	7.50	2210.00	3450.00	185.43	95.84	448.68	36.12	168.23	1080.00	112.51	6.20	26.40
VAL 74	Tema	30.00	7.40	2060.00	3220.00	208.68	78.60	401.49	28.00	44.32	1035.00	126.00	1.10	22.40
VAL 158	Tema	30.00	6.70	3370.00	5270.00	362.60	126.00	486.50	32.40	340.57	1650.25	114.70	7.10	11.78
VAL 75	Tema	30.00	7.40	4320.00	6760.00	310.50	159.20	956.40	38.00	298.00	2354.00	257.00	8.20	32.80

TE 174K	Tema	29.40	7.50	2890.00	4520.00	198.03	68.02	685.21	42.55	79.00	1463.00	21.00	1.23	5.50
TE K	Tema	28.90	7.00	2141.00	3350.00	178.26	86.41	381.21	26.80	315.25	1020.72	78.10	1.75	5.10
WRI 13	CSRI	30.00	7.40	1633.00	2550.00	72.00	121.00	143.00	33.00	439.70	449.00	44.30	3.80	46.50
WRI 19	CSRI	26.00	7.60	1437.00	2400.00	68.00	158.00	182.00	22.00	440.00	518.00	47.00	1.90	20.00
WRI 30	CSRI	29.80	7.55	1114.00	1460.00	42.45	124.39	115.12	32.00	427.00	351.00	20.00	1.80	42.00
SAN 1R	Santeo	30.50	7.00	4230.00	6610.00	360.00	253.00	850.00	32.00	347.00	2180.00	264.00	5.10	15.00
SAN 15	Santeo	30.00	7.10	4000.00	6250.00	279.00	177.40	879.90	32.00	348.00	1770.00	372.00	4.20	11.40
SAN 2R	Santeo	30.40	7.10	4280.00	6690.00	345.00	231.00	898.00	35.00	310.00	2020.00	350.00	9.00	21.00
SAN 14	Santeo	30.40	7.00	3965.00	6200.00	335.00	263.00	750.00	35.00	360.00	1998.80	250.00	11.20	14.11
SAN 117	Santeo	30.00	7.00	4440.00	6940.00	395.00	274.00	866.50	63.00	360.00	2135.00	392.50	5.30	24.00
ASH 77	Ashiaman	29.60	7.20	3843.00	5800.00	371.43	245.61	704.19	20.00	360.02	1875.00	261.91	6.90	14.60
ASH 166	Ashiaman	30.00	7.80	7327.00	11500.00	495.00	380.00	1420.00	55.00	445.00	3285.00	510.00	16.60	32.00
ASH K	Ashiaman	29.70	7.30	5980.00	9370.00	395.52	261.32	1474.24	48.17	370.08	3048.21	363.00	10.00	24.00
ASH CCF	Ashiaman	29.70	6.90	8220.00	12800.00	573.90	365.40	1702.50	58.00	562.00	4232.40	586.00	31.00	32.00
AF 1	Michel Camp	28.70	7.20	4895.00	7650.00	312.46	216.78	739.80	36.80	273.48	1912.00	137.00	13.50	34.00
AF 2	Michel Camp	30.00	7.40	2732.00	4270.00	195.26	134.60	650.12	25.00	265.00	1285.03	245.00	10.60	21.00

Table 5.2: Descriptive Statistical of geochemical data

	Minimum	Maximum	Mean	Std. Deviation
Temp ^{o}C	24.00	32.10	28.89	1.61
pH	5.60	8.50	7.08	0.53
TDS	50.00	8748.00	1920.00	1893.44
EC (µS/cm)	129.00	13700.00	3130.00	2902.98
Ca	8.00	573.90	133.00	122.92
Mg	6.35	564.87	107.00	105.23
Na	21.00	1892.23	394.00	409.75
K	1.45	70.00	22.81	14.14
HCO_3	28.00	595.00	221.00	134.12
Cl	44.00	4830.00	900.00	993.42
SO4	12.86	586.00	145.00	127.57
NO_3	0.67	31.00	4.84	4.99
SiO_2	3.00	95.45	26.59	19.87

(All in mg/L)

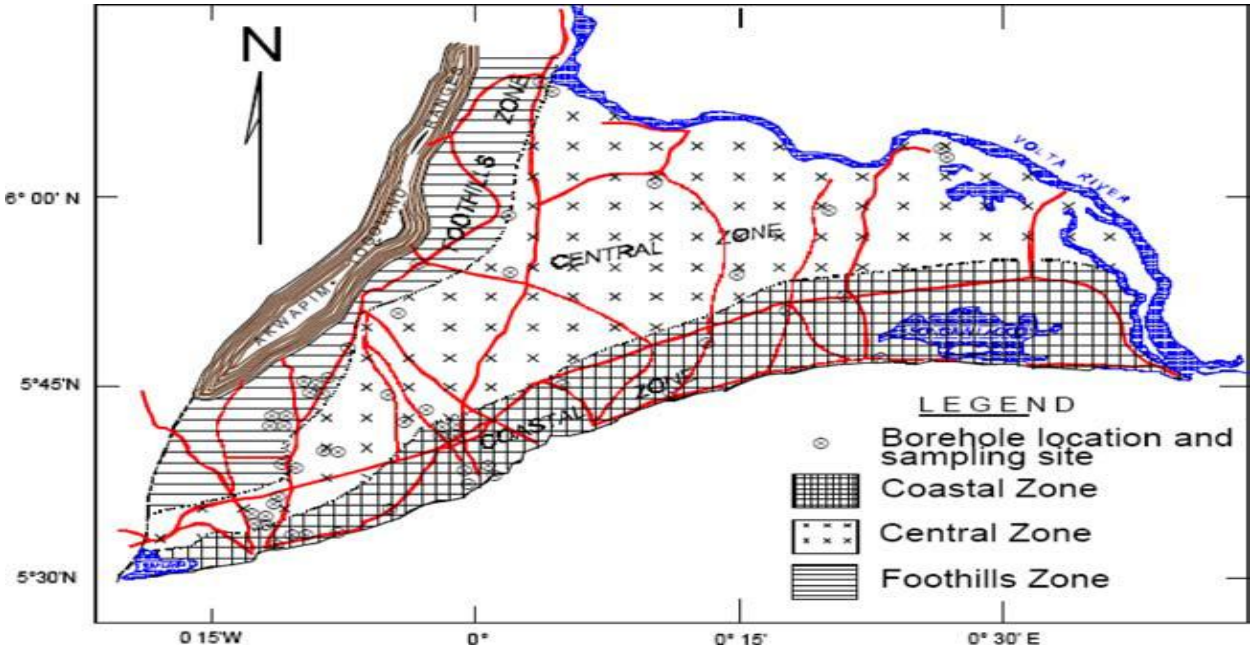

Figure 5.1. Groundwater zones according to spatial distribution of TDS mg L^{-1} (Kortatsi, 2006).

The relative abundance of anions in the groundwater is in the order Cl^- >HCO_3^->SO_4^{2-}> NO_3^- with the chloride concentration constituting about 76% of the total concentration of anions and ranged from 1.24 to 136.06 meq/L (44 to 4830 mg/L). The relative abundance of the cations is in the order Na^+>Ca^{2+}>Mg^{2+} > K^+ with Na^+ ion constituting about 50% of the total cation concentration. The high Na^+ concentration maybe due to the weathering of the sodium feldsdpar minerals (albite). The K^+ concentration are low, despite the substantial mineral sources of K^+ in the aquifer. The low levels of K^+ ions can be attributed to its resistance to weathering and its tendency to participate in the formation of secondary minerals (Zhu *et al* 2006).

The Finnish Radiation and Nuclear Safety Authority states that exceptionally adverse groundwater characteristics, such as the lack of reducing capacity and high concentrations of substances which might substantially impair the performance of the barriers, indicate the unsuitability of a disposal site (STUK, 2001).

The pH of the groundwater primarily influences corrosion of the waste containers and degradation of the barriers as well as sorption and solubilities of radionuclides. The pH of the groundwaters in the study area ranged from 5.6 to 8.5 with the groundwaters at the Valley View University situated at Oyibi having pH values less than recommended pH values (6-10). This indicates the unsuitable of the Valley View University site for a radioactive waste repository.

The stability of the buffer and backfill of the repository are influenced by the concentrations of major cations (Na^+, Ca^{2+} and Mg^{2+}) in the groundwater. In order for the buffer and backfill to be chemically stable and not be dispersed to a colloidal suspension, it is recommended that the concentration of divalent ions (Ca^{2+} and Mg^{2+}) exceeds 4 mg/L (Laaksoharju et al., 1995).

Analyses of the groundwaters in Accra Plains show that, the concentrations of the divalent ions ranged from 16.00 –939 mg/L with the divalent ions together constituting 48% of the total cations in the groundwater (Fig. 5.2(a)). Thus the groundwaters in the Plains will provide a stable chemical environment for a backfill and buffer materials of a radioactive waste repository.

TDS concentration of the groundwater influences the stability of the backfill materials and sorption of radionuclides. Very high TDS decreases the backfill swelling capacity. High salinities also reduce the sorption capacity in the rock of many radionuclides. It recommended that the measured TDS at repository environment must be lower than 100 g/L. The measured TDS values ranging from 50.0 to 8748 mg/L will provide a favourable environment for a backfill material for a radioactive waste repository (Fig 5.2(b)).

5.1.2. Statistical Analyses

Statistical relationship among the dissolved constituent in the groundwater was investigated to understand the interrelationships among variables and to quantify their contributions and other impacts on the chemical composition of groundwater. In this study, Pearson's correlation matrix was used to find relationships between the 13 (temperature, pH, TDS, electrical conductivity, Ca, Mg, Na, K, HCO_3, Cl, SO_4, NO_3, SiO_2) variables. The resultant matrix showed weak correlation of pH with all the other variables (Table 5.3). It likewise revealed a strong correlation of TDS with EC, Ca, Mg, Na, K, Cl and SO_4 and moderate correlation with NO_3. Strong correlation exist among the major elements Na, Ca, Mg, and Cl (r >7) identifying these elements as the major contributors to the groundwater chemistry in the Plains. These elements are likely to be combined together or derived from the same source.

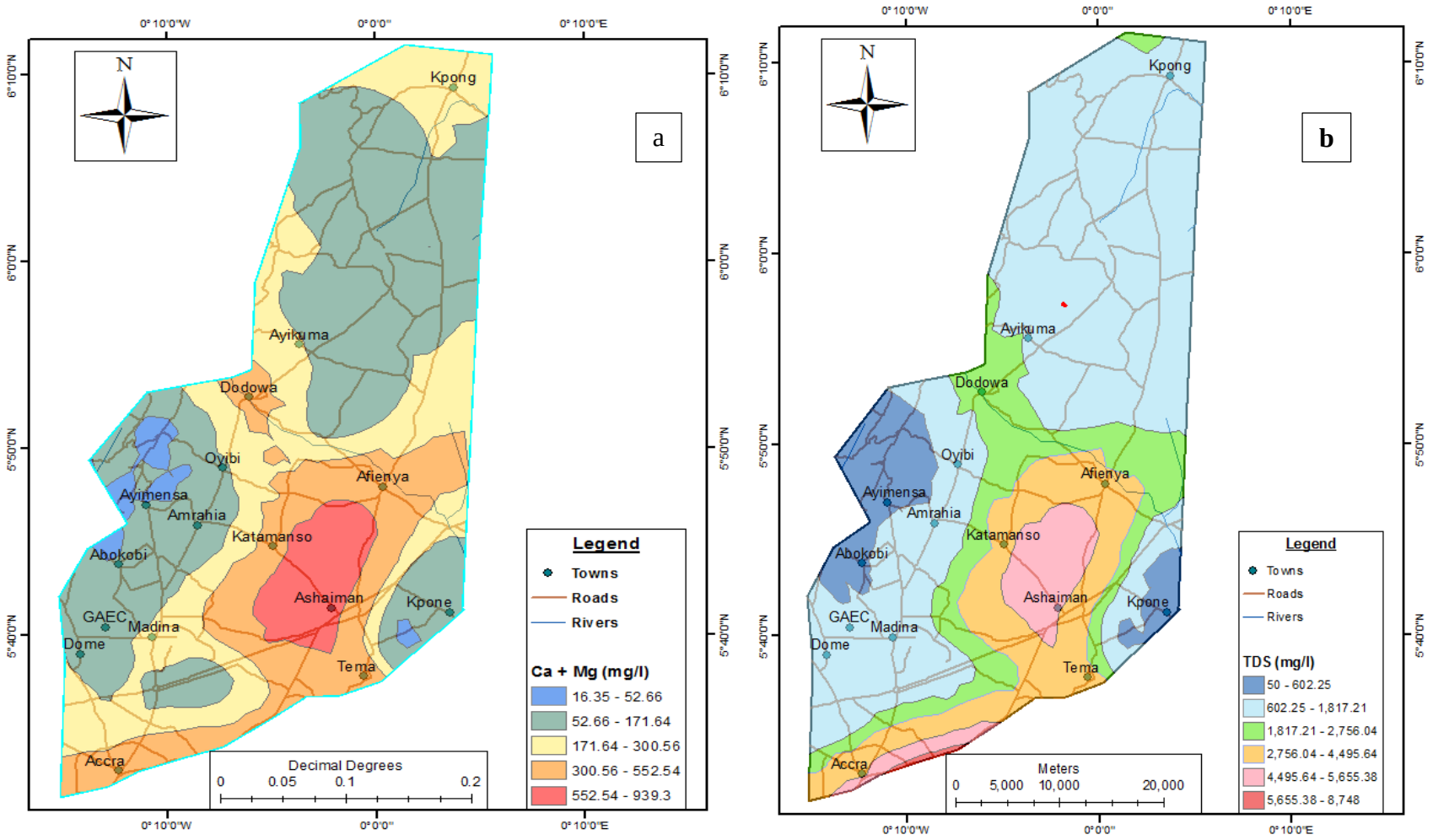

Figure 5.2 Areal distribution maps of (a) Ca + Mg ion concentration and (b) TDS in the groundwaters in the study area

Table 5.3. Pearson correlation matrix

	Temp	pH	TDS	EC	Ca	Mg	Na	K	HCO_3	Cl	SO_4	NO_3	SiO_2
Temp	1												
pH	.043	1											
TDS	.223*	.327**	1										
EC	.197*	.315**	.996**	1									
Ca	.269**	.317**	.864**	.857**	1								
Mg	.159	.339**	.930**	.924**	.802**	1							
Na	.191	.299**	.970**	.970**	.809**	.909**	1						
K	.197*	.406**	.800**	.811**	.749**	.773**	.794**	1					
HCO_3	.079	.289**	.437**	.438**	.542**	.442**	.350**	.414**	1				
Cl	.193	.299**	.981**	.978**	.837**	.944**	.983**	.802**	.343**	1			
SO_4	.266**	.308**	.758**	.753**	.839**	.756**	.759**	.650**	.549**	.737**	1		
NO_3	.048	.257**	.544**	.563**	.515**	.491**	.539**	.442**	.248*	.541**	.445**	1	
SiO_2	.171	.226*	.131	.136	.094	.155	.150	.160	.199*	.121	.210*	.184	1

*. Correlation is significant at the 0.05 level (2-tailed).

**. Correlation is significant at the 0.01 level (2-tailed).

The Principal Component Analysis (PCA) identified three factors influencing the groundwater chemistry. The three factors cumulatively account for 83.65% of the total variance. Table 5.4 presents the loading of each variable under each of the three factors. Loadings of Table 5.4 are shown graphically in Figure 5.3. The first factor (PC1), which accounts for about 68.94% of the variance, has positive loadings for TDS, EC, Ca^{2+}, Mg^{2+}, Na^{+}, K^{+}, HCO_3^{-} Cl^{-}, $NO_3^{-}$and $SO^2_4^{-}$. The bicarbonate ion (HCO_3^{-}) was dropped after a series of trials indicated that it loaded highly in more than one factor. The parameters associated with factor 1 connote salinity enhancement arising from mineral dissolution. The high positive loading for NO_3 can be attributed to the small scale farming activities that occur all year through using both surface and groundwater. Animal

manure (compost) and chemical fertilizers are being used extensively to increase crop yield. Some of these chemicals infiltrate through recharging waters into the aquifers.

Table 5.4: Principal component loadings of geochemical variables

Rotated Component Matrix			
	PC 1	PC 2	PC 3
pH	0.261	0.129	**0.949**
TDS	**0.941**	0.121	0.205
EC	**0.945**	0.167	0.159
Ca	**0.914**	0.161	0.199
Mg	**0.914**	0.243	0.194
Na	**0.944**	0.123	0.142
K	**0.799**	0.161	0.21
HCO_3	**0.593**	**0.515**	0.005
Cl	**0.962**	0.077	0.163
SO_4	**0.833**	0.231	0.105
NO_3	**0.623**	0.22	0.133
SiO_2	0.113	**0.938**	0.135

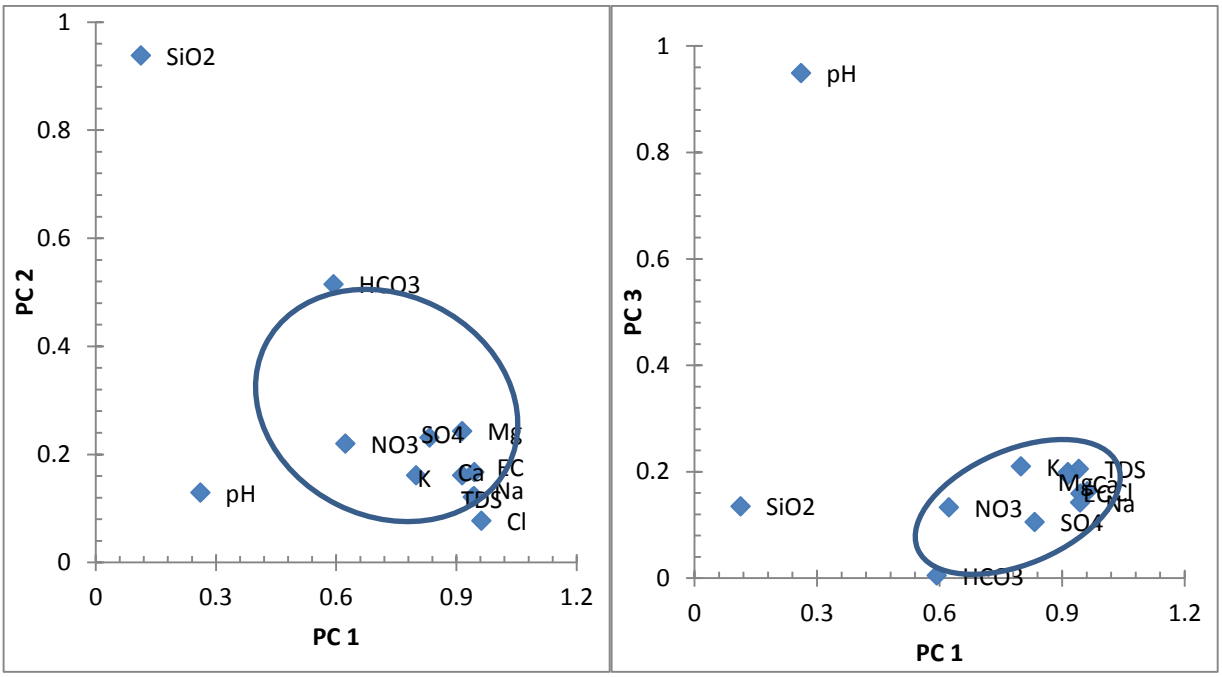

Figure 5.3. Principal component loadings in binary plot presentations

The second factor (PC2) accounts for 8.27% of the variance and has positive loading for SiO_2 and HCO_3. The positive loading for SiO_2 could be due to dissolution of the rock mineral feldspars. The relatively high positive loading for bicarbonate could be the result of reaction of CO_2 in the soil with alkali-feldspars. The third factor (PC3) accounts for 6.40% of the variance and has a positive loading for pH. The PCA suggests that weathering of the silicate minerals have influence on the hydrogeochemical conditions in the Plains. The weathering is caused by the alternate wet and dry conditions that characterize the semi-arid climate of the Accra Plains.

The relationships among the sampling sites were obtained through Q-mode hierarchical cluster analysis (HCA). The HCA provided a graphical result, the dendogram, which showed the classification of the groundwater into three distinct groups on the basis of their hydrogeochemical characteristics (Figure 5.4).

Group 1 is mainly made up of groundwater samples collected from borehole located along the foothills of the Akwapim Togo Mountain. It accounted for about 26.42% of the total groundwater samples. The group is divided into 3 subgroups (SG 1A, 1B, 1C). The groundwater is relatively fresh with a mean TDS value of 311 mg/L and EC value of 544 µS/cm. The average concentration of Ca was 1.41 meq/L with Mg ion having a mean concentration of 1.56 meq/L. The mean Na ion concentration was 3.11meq/L. Chloride the dominant anion had a mean concentration of 3.91meq/L. The low degree of mineralization of these waters suggests that the contact time with rock and soil may have been short.

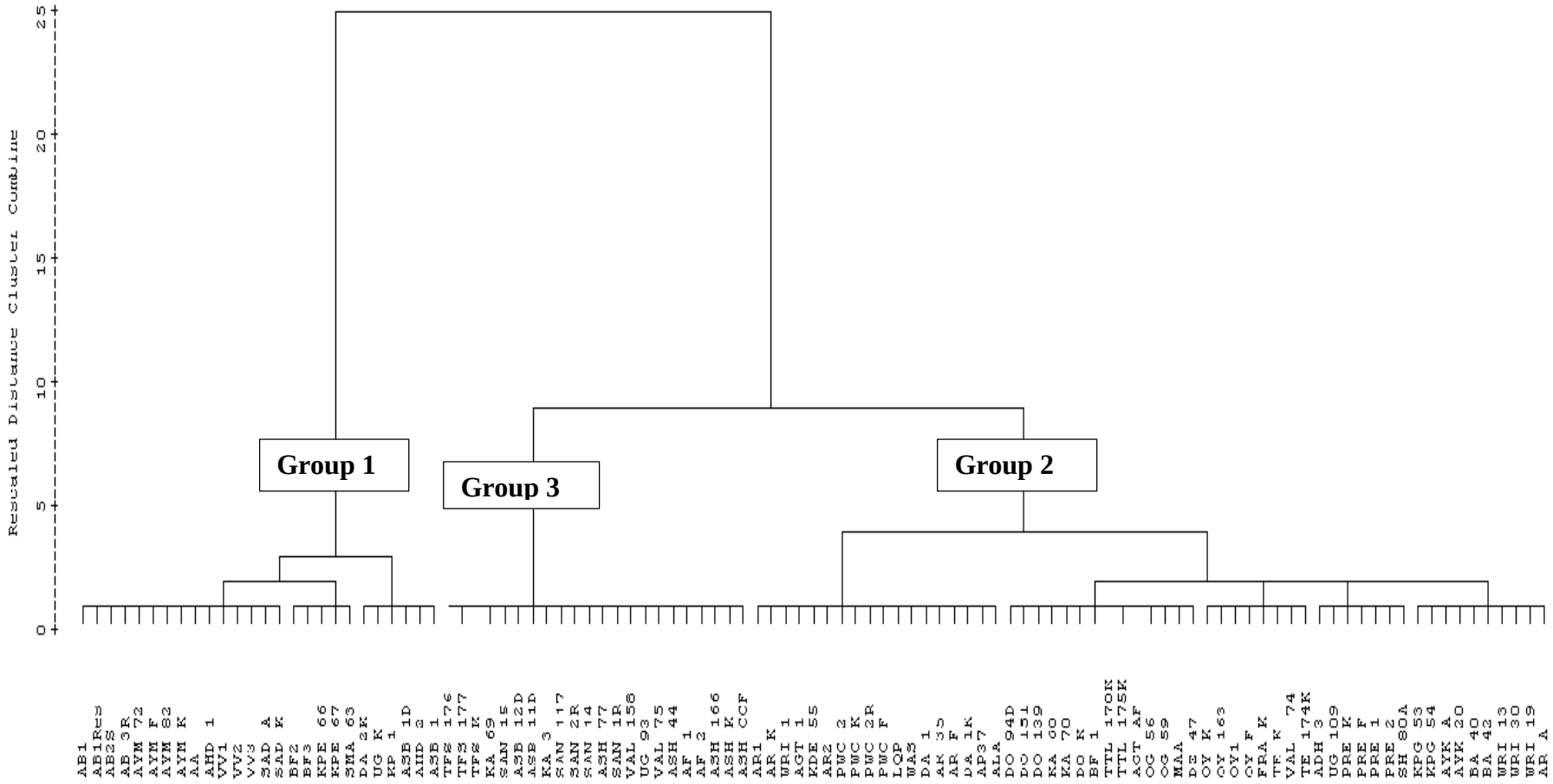

Figure 5.4. Dendrogram of Q-mode HCA of the groundwater samples from the Accra Plains

Group 2 is divided into 5 subgroup (SG 2A, 2B, 2C, 2D, 2E) and constiute about 54 % of the groundwater. The mean TDS is 1532 mg/L with a mean EC value of 2587 µS/cm. Sodium and chloride are the dominate species in the group. The Ca ions had an average concentration of 5.23 meq/L with Mg ion having a mean concentration of 7.23 meq/L. The mean Na ion concentration was 13 meq/L whilst chloride ion had a mean concentration of 18.61 meq/L.

Group 3 (G3) had no subgroups and account for 19.58% of the groundwater. The mean TDS is 4985 mg/L with a mean EC value of 7783 µS/cm. The Ca ions had a mean concentration of 16.1 meq/L with Mg ion having a mean concentration of 21.84 meq/L. The mean Na ion concentration was 44.77 meq/L whilst chloride ion had a mean concentration of 70.17 meq/L. The groundwaters in this group have high ion concentrations compared to the other groups suggesting a longer contact time with rock and soil. As dissolution of aluminosilicate minerals is a slow process, the increase in TDS and EC from group 1 to group 3 (groundwater flowpath) may be interpreted as the consequence of the long residence time or contact time between the ground water and the rocks.

5.1.3. Hydrogeochemical Processes

5.1.3.1. Hydrochemical Facies

The Piper (Fig.5.5) and Chadha (Fig.5.6) diagrams, plotting the proportions in milliequivalents per litre (meq/L) of the major cations and anions showed the main hydrogeochemical features of the Plains. The plots suggest that Na, Mg and Ca and Cl dominate the aquifer. However the groundwater can be distinguished and grouped into three water types by their position on the

Piper and Chadha plots. The three groundwater types conform to the three different groups of groundwater obtained from the HCA.

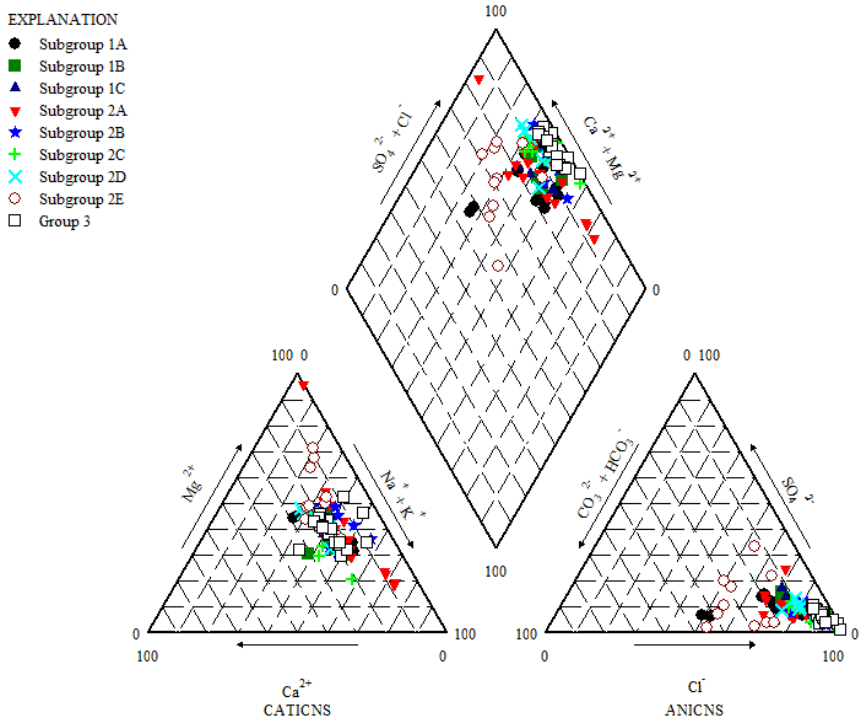

Figure 5.5: Piper trilinear diagram showing hydrochemical facies

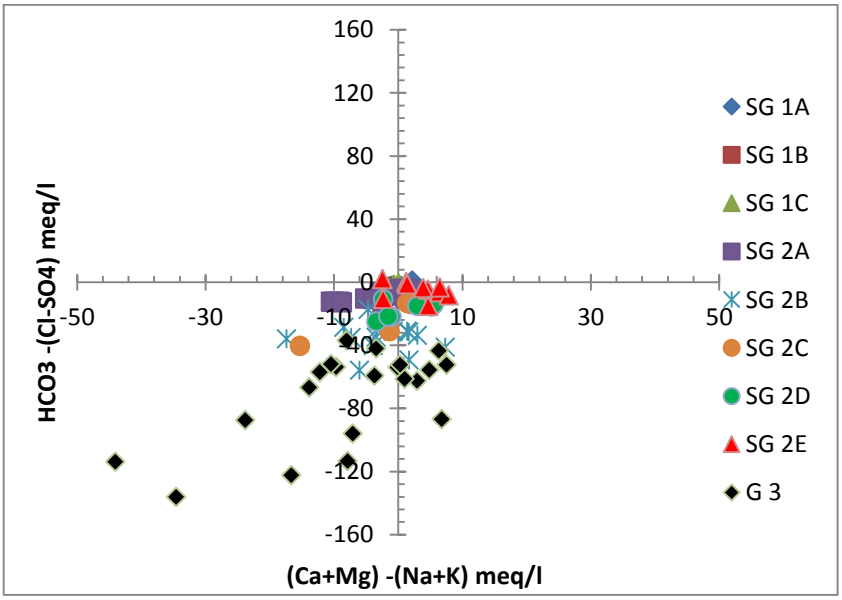

Figure 5.6: Chadha diagram for geochemical classification of the groundwater

Groundwater type 1 is mainly composed of Na-Mg-Ca-Cl-HCO_3. This type of groundwater is found along the foothill of the Akwapim-Togo Mountain where the Dahomeyides and Togo series of rocks underlying the area contain ferromagnesian silicates (hornblende, pyroxenes and biotite). The groundwaters in the area are generally fresh (TDS < 1000mg/L) and are characterised by low Cl, as well as low pH (5.6 - 6.3) values, except for the groundwaters sampled at Presbyterian Women Centre (PWC, Abokobi), Ayikumah (AYK) and Kpong. They had TDS values greater than 1000 mg/L. The groundwater type at PWC was of the Na-Cl type. The samples from PWC come from quartzites and the borehole is far from the coast. It is therefore doubtful that sea water intrusion could have transversed the gneiss of the Plains. The water facies at Ayikumah and Kpong could be attributed to the presence of marbles in the gneiss at Agomeda (3 km from Ayikumah) and the carbonatites rocks at Kpong (Akiti 1980).

Groundwater type 2 is composed mainly of Na-Mg-Ca-Cl and found in most parts of the central area of the Plain. The water is slightly or moderately brackish as the TDS values range from 1107 to 4495 mg/L. This water type generally characterizes mixed water (Akiti, 1980).

Groundwater type 3 found along the coastal zone of the Plain is composed mainly of Na-Ca-Cl with the TDS values ranging from 1760 to 8747 mg/L. The groundwater is basic, having pH values between 7.4- 8.5. The groundwater type is attributed to preferential leaching of high soluble surface or near surface soil NaCl salts, which are completely dissolved during resolution (Akiti, 1980). Subsequent evaporative concentration may also cause the less soluble salts to precipitate out of solution resulting in the percolating water becoming enriched with NaCl (Drever and Smith, 1978).

5.1.3.2. Gibbs Plots

The Gibbs plot (Gibbs 1970) was used to assess the mechanism controlling the groundwater chemistry and the functional sources of dissolved ions by plotting the ratios of the major cations and anions separately as functions of TDS (Fig. 5.7 (a-b)). The Gibbs diagram shows most of the groundwater samples plotting in the rock dominance field whilst a few plot in the evaporation field. The data points suggest that chemical weathering of the rock forming minerals and to a marginally extent evaporation are the main processes that control the groundwater chemistry. The rock of the Accra Plains consists of mainly of alumino-silicate minerals and weathering of the alumino-silicate minerals particularly plagioclase (albite), hornblende, micas and pyroxenes will increase the concentration of Na^+, Ca^{2+}, Mg^{2+}, K^+ and HCO_3^- in the groundwater.

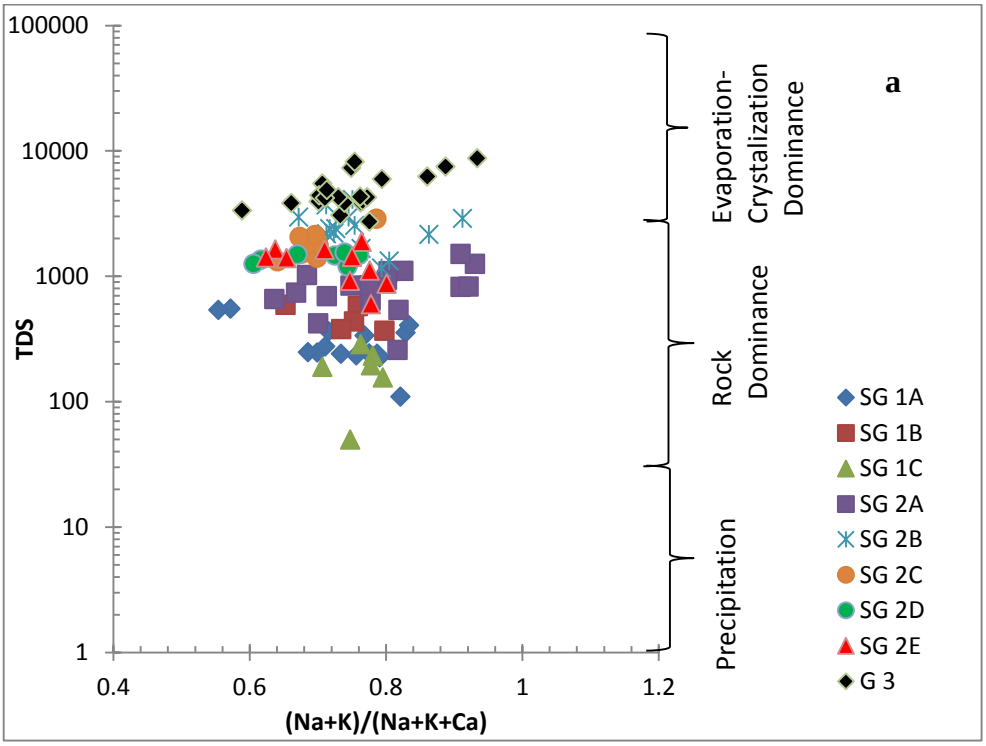

Figure 5. 7(a). Gibbs plots to explain groundwater chemistry and geochemical process in the Accra Plains

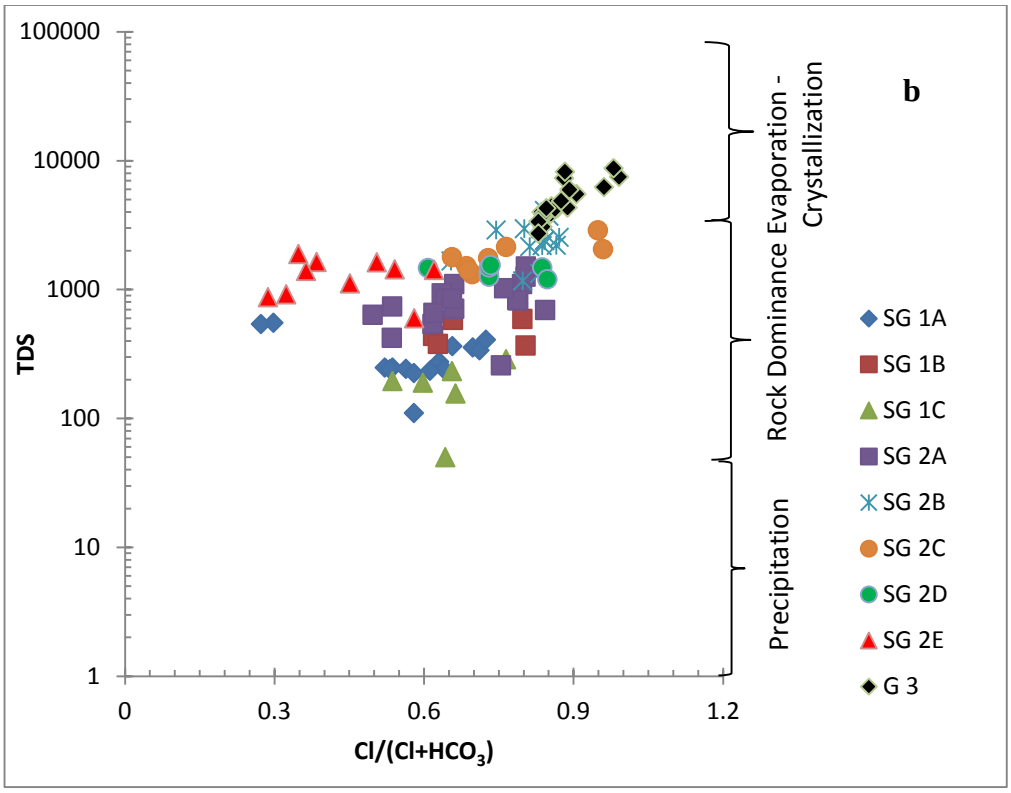

Figure 5. 7(b). Gibbs plots to explain groundwater chemistry and geochemical process in the Accra Plains

Evaporation will greatly increase the concentration of the ions formed by chemical weathering leading to higher salinity (TDS). This suggests that weathering of the rock forming minerals by the groundwater is one of the major geochemical processes controlling the ion chemistry of the groundwater.

5.1.3.3. Ionic Ratios

The ionic ratios of the groundwater samples were compared to determine whether any subsequent evolution of the groundwater chemistry has occurred. Chloride acts in a conservative manner in most hydrogeochemical processes not participating in geochemical reactions and remaining in the system. Sodium is frequently conserved in hydrochemical processes in which it

is strongly associated with chloride. Therefore Na/Cl is often used to identify the origin of groundwater and source of the groundwater chemical constituents.

The positive correlation sodium showed as a function of increasing Cl (Fig 5.8) suggests a common hydrogeochemical source for these ions. Mixing is proposed to be the controlling process of the Na concentration due to the linear behaviour of the different water types. At low concentrations, the groundwaters plot along the 1:1 trend line suggesting the release of sodium due to incongruent weathering of silicate minerals. However with increasing ion concentration the ions deviate or plot below the equiline. The decline in Na/Cl ratio with increasing salinity may be due to enrichment of Ca and Mg and depletion of Na. Thus indicating the occurrence of reverse cation exchange in these locations. Increasing Ca^{2+} with decreasing Na^{+} may correspond to a prolong contact time with aquifer matrix (clay).

The semi-log plot of the same data set (Fig.5.9.) indicates two distinct slopes, a steep slope at low concentrations and a lower slope at high concentrations. The Na/Cl ratio for the steep slope is approximately unity (1), greater than the sea water ratio of 0.55 (Nordstrom *et al* 1989(c)). The shallow slope has a ratio of 0.4. Groundwater along the foothill of the Akwapim Togo Mountains had the high ratios (Group 1). The high ratio is typical of river waters, rainwaters, fresh groundwater and groundwater dominated by halite dissolution. The low ratio tends to occur when other cations, Ca and/or Mg become comparable to or greater than Na in concentration (Nordstrom *et al* 1989 (c)). The bimodal slope suggests a transition from water in the weathered zone at shallow depths and in permeable rocks to water possessing a saline component, enriched in Ca and/Mg and associated with impermeable rocks. Those samples with Na^{+}/Cl^{-} ratio value

higher than 1 also show a deficit in Ca^{2+} + Mg^{2+}. This is consistent with a Ca^{2+}–Na^{+} cation exchange process which leads to a softening of the water (Hidalgo and Cruz-Sanjulian 2001).

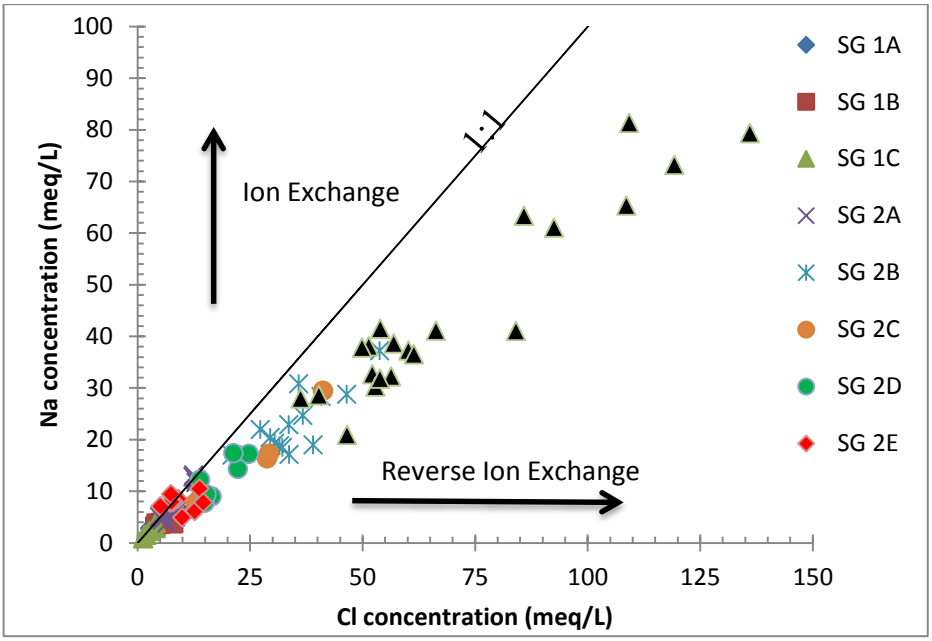

Figure 5.8. Relationship between Na and Cl ion concentration

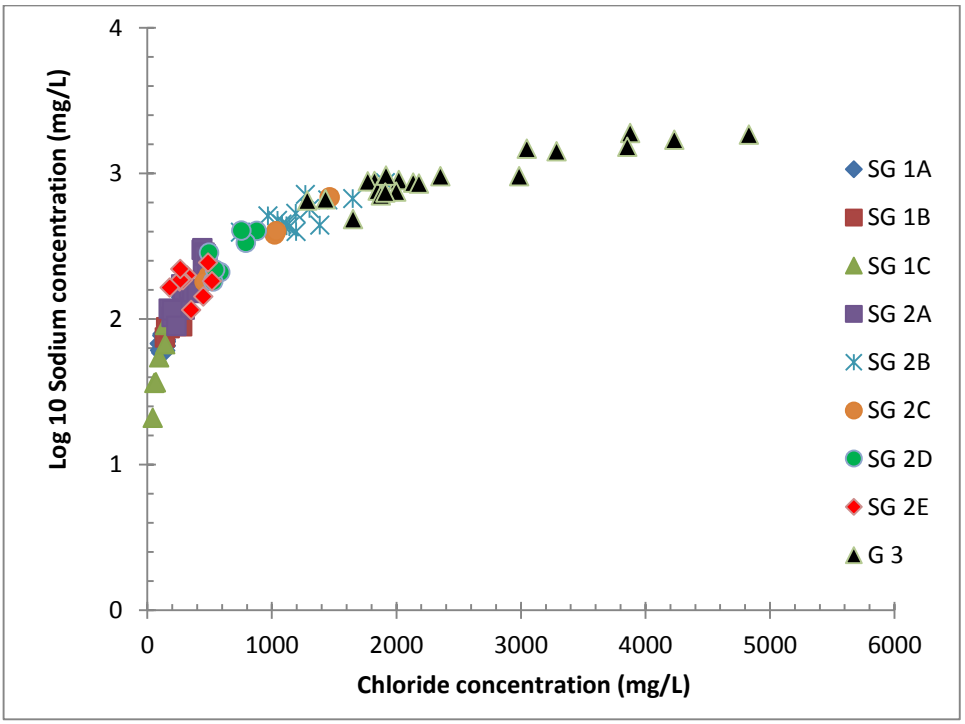

Figure 5.9: Semi-log plot of Na^{+} and Cl^{-} concentration

The Na^+/Cl^- ratio which ranges from 0.45 to 1.40 generally decreases with salinity. Ratios in excess of 1.0 at low salinities imply that meteoric NaCl is not the only source of Na^+ (Nkotagu, 1996(a)). Plagioclase (albite) weathering may be occurring in the bedrock releasing Na^+, HCO_3^- and kaolinite according to the weathering reaction below

$$2NaAlSi_3O_8 + 2H_2CO_3 = Al_2Si_2O_5(OH)_4 + 2Na^+ + 2HCO_3 + 4H_2SiO_2 \qquad (5.1)$$

Calcium and magnesium together constitute 48% of the total cations in the groundwater. The pyroxene, amphiboles and feldspars which are common minerals in the mafic gneisses will contribute Ca^{2+} and Mg^{2+} to the groundwater chemistry, as these minerals are easily weathered during rainfall infiltration and groundwater movement.

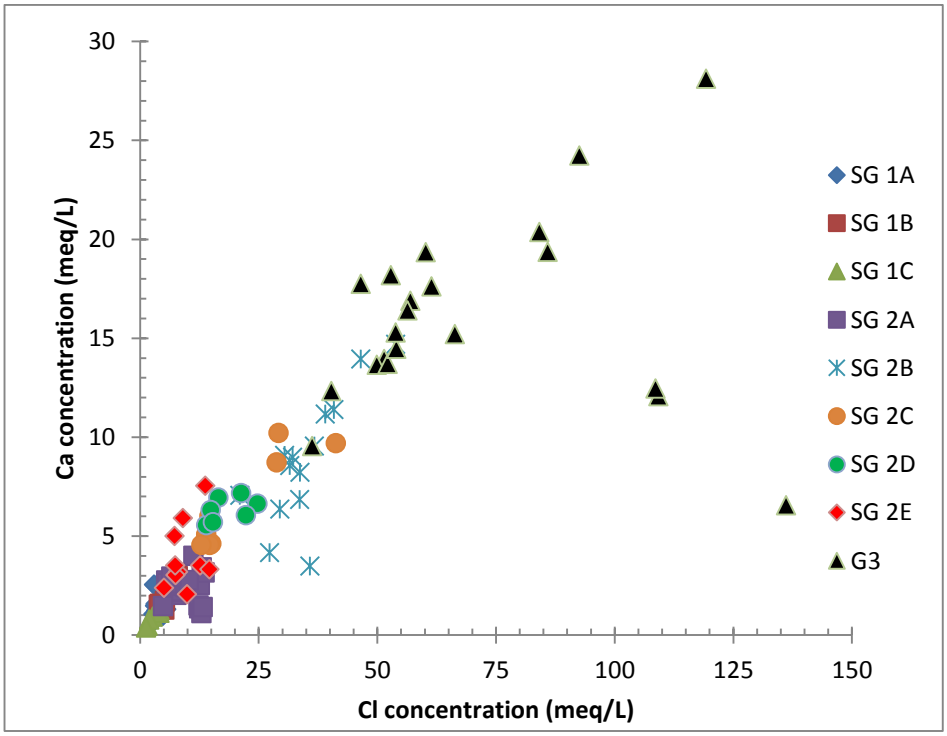

Figure 5.10. Plot of calcium as a function of chloride

The linear growth of Ca as function of Cl (Fig 5.10) suggests that mixing mainly controls Ca concentration and these elements have a common source in brackish groundwaters. Calcium is assumed to dissolve from fracture calcite, but may be released from rock minerals as well.

Cation exchange is an important process in an aquifer which has been exposed to sequential meteoric water intrusions (Nordstrom, 1986). In cation exchange the divalent ions are more strongly bonded to a solid surface such that the divalent ions tend to replace monovalent ions. The monovalent ions have a small energy of adsorption and therefore more likely to remain in solution. As a result of a large energy of adsorption, divalent ions are more abundant as an exchangeable cations. The energy absorption sequence is $Ca^{2+} > Mg^{2+} > K^{+} > Na^{+}$. Thus, Ca^{2+} is typically more abundant as an exchangeable cation than Mg^{2+}, K^{+} or Na^{+}. Cation exchange probably retards Ca and Mg enrichment in the groundwater, particularly as Cl increases and Na is released into the groundwater (Pitkänen *et al*, 2004).

The Mg^{2+}/Ca^{2+} ratio varies from 0.57 to 4.90 over a wide range of salinity with few ratios having values less than 1 (Fig.5.11). The increase of the ratio with salinity can be attributed to increased cation exchange of Na^{+} with bound Ca^{2+} and Mg^{2+} as salinity increases. In addition, Ca^{2+} is more electropositive than Mg^{2+} due its lager hydrated size thus keeping the ratio at less than 1. The ratio of Mg^{2+}/Ca^{2+} greater than 1 indicates dissolution of amphiboles which results in the addition of more Mg^{2+} ions than Ca^{2+} ions. High Mg^{2+}/Ca^{2+} also give an indication of the great age of the groundwater (Akiti, 1980).

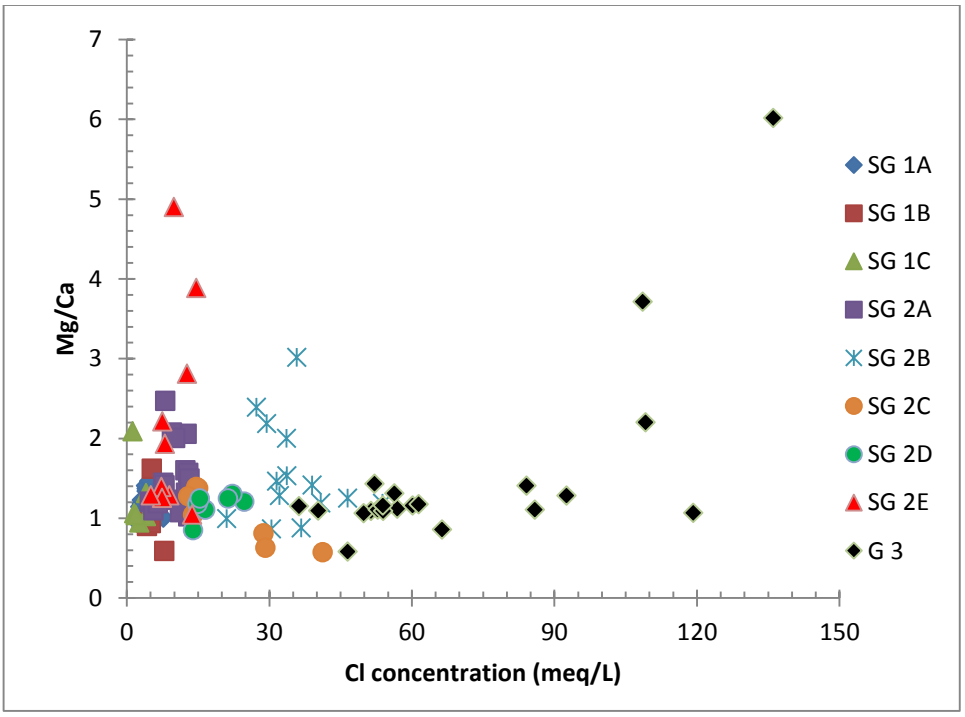

Figure 5. 11 Relationship between Mg/Ca and Cl

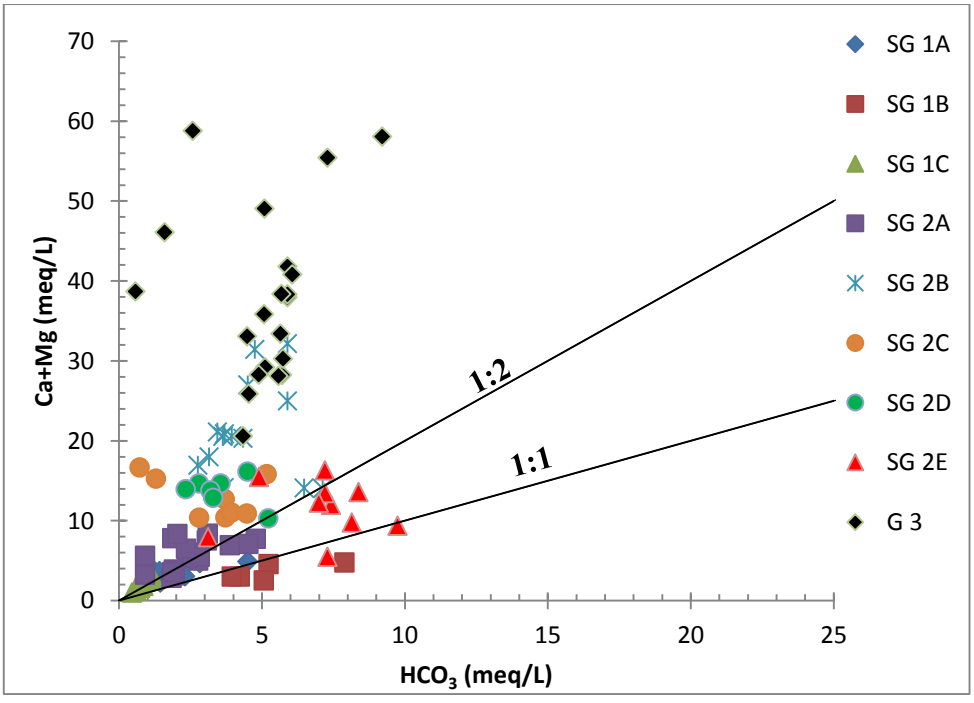

Figure 5. 12. Scatter diagram of Ca + Mg vrs HCO_3

In the scatter diagram of Ca + Mg vrs HCO_3 (Fig.5.12) most of the samples plot away from the equiline to the 2:1 line indicating predominance of alkali earth by silicate weathering over bicarbonate. Few samples plot in the bicarbonate zone due to the reaction of the feldspar minerals with carbonic acid in the presence of water which releases HCO_3 (Elango *et al*, 2003).

The $(Mg^{2+} + Ca^{2+})/HCO_3^-$ ratio varies between 0.75 and 11.8. The ratio increases with salinity indicating that Ca^{2+} and Mg^{2+} are being added to the groundwater at a greater rate than HCO_3. The high $(Mg^{2+} + Ca^{2+})/HCO_3^-$ ratios cannot be attributed to HCO_3 depletion under the existing slightly alkaline geoenvironmental conditions (Nkotagu, 1996(a)). Since HCO_3 does not form carbonic acid (H_2CO_3), (Appelo and Postma, 2005), the excess Ca and Mg might have been contributed to the groundwater from other sources such as reverse ion exchange process (Rajmohan and Elango, 2004). The calcium and magnesium in aquifer material exchanged with sodium in the water as explained by the equation below

$$2Na^+ + Ca\ (Mg)\ clay \leftrightarrow Na - clay + Ca^{2+}\ (Mg^{2+}) \qquad (5.2)$$

Due to the presence of marbles at Agomeda, the carbonatite rocks at Kpong and carbonate rocks identified at GAEC (Kwabenya), carbonate weathering could also contribute calcium and magnesium ion to the groundwater. To determine the dominant sources (carbonate or silicate weathering) of the major ions, Ca+Mg was plotted against Na+K. Most of the samples plotted along the 1:1 trendline (Ca+Mg=Na+K) (Fig.5.13). However few of the samples especially from group 3 samples plotted above the 1:1 trendline indicating that although carbonate and silicate weathering contribute ions to the groundwater, silicate weathering dominate the weathering process. Drever (1997) demonstrated that a ratio of $Mg^{2+}/(Mg^{2+} + Ca^{2+})$ in crystalline

environment greater than 0.5 indicates silicate weathering. In this study 72.6% of the samples had ratios exceeding 0.5 suggesting that incongruent dissolution of the silicate minerals significantly contribute Mg^{2+} and Ca^{2+} to the groundwater.

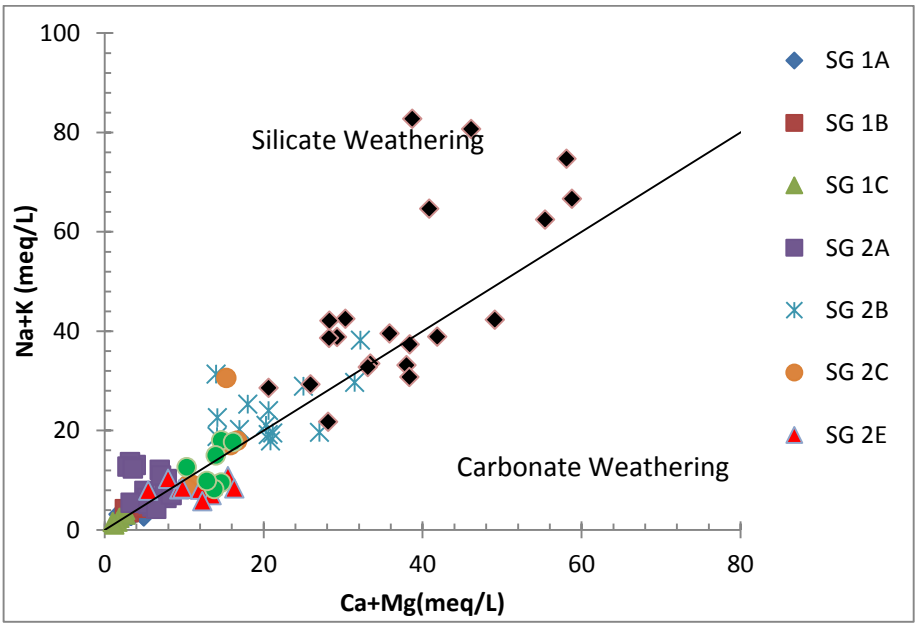

Figure.5.13 Relationship between Ca+Mg and Na+K

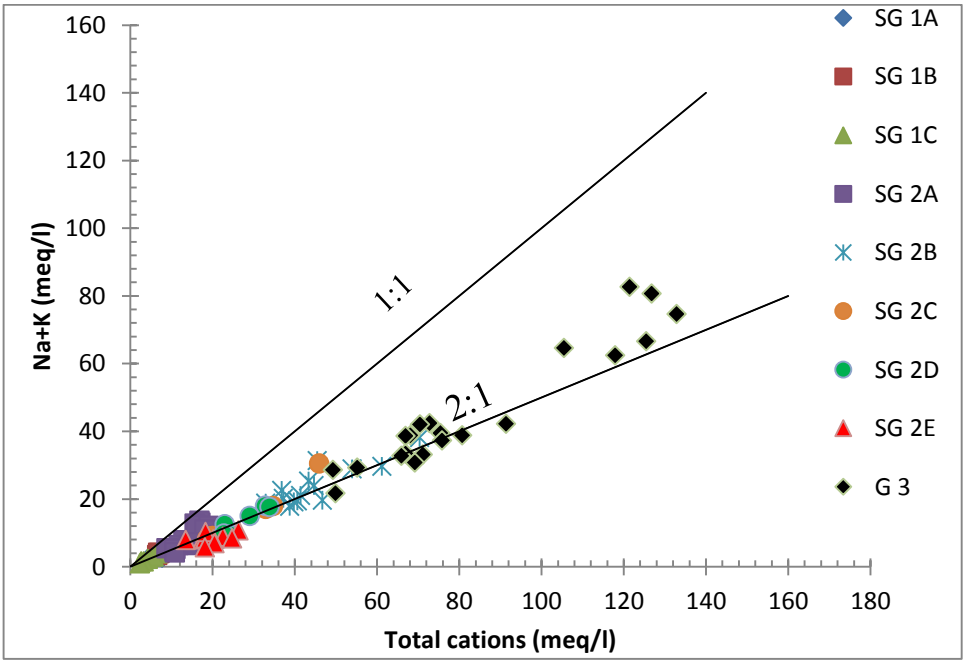

Figure 5.14. Scatter diagram of Na + K vrs TZ^{+}

The ratio (Na + K)/ total cation (TZ^+) is an index used to assess the contribution of cations by silicate weathering. The scatter diagram of Na + K vrs TZ^+ (Fig.5.14) concentration indicates that majority of the samples plot below the equiline but along the Na+ K=0.5TZ^+ line indicating contribution of cation from silicate weathering according to Datta and Tyagi (1996). This indicates weathering processes of both alkali and alkali earth from feldspar, soda feldspar (albite) and potash feldspar, which are common in the gneiss in the Accra Plains. This suggests the involvement of silicate weathering in the geochemical processes which contributes mainly sodium and potassium ions to the groundwater.

From the Gibbs plot another dominant process determining the groundwater composition is evaporation. The dry climatic condition in the Accra Plains is expected to influence the groundwater chemistry. The evaporation process would cause an increase in concentrations of all the species in the groundwater. If the evaporation process is dominant, assuming that no mineral species are precipitated, the Na/Cl ratio would be constant with increasing electrical conductivity (EC) (Jankowski and Acworth 1997).

The scatter plot of EC vs Na/Cl (Fig.5.15) showed that the Na/Cl ratio decreases slightly with increase in EC indicating removal of Na ions by ion exchange. However, the Na/Cl ratio remains constant with increasing EC for Group 3 groundwater samples. Thus, evaporation has influence on the groundwater in the coastal areas of the Plains.

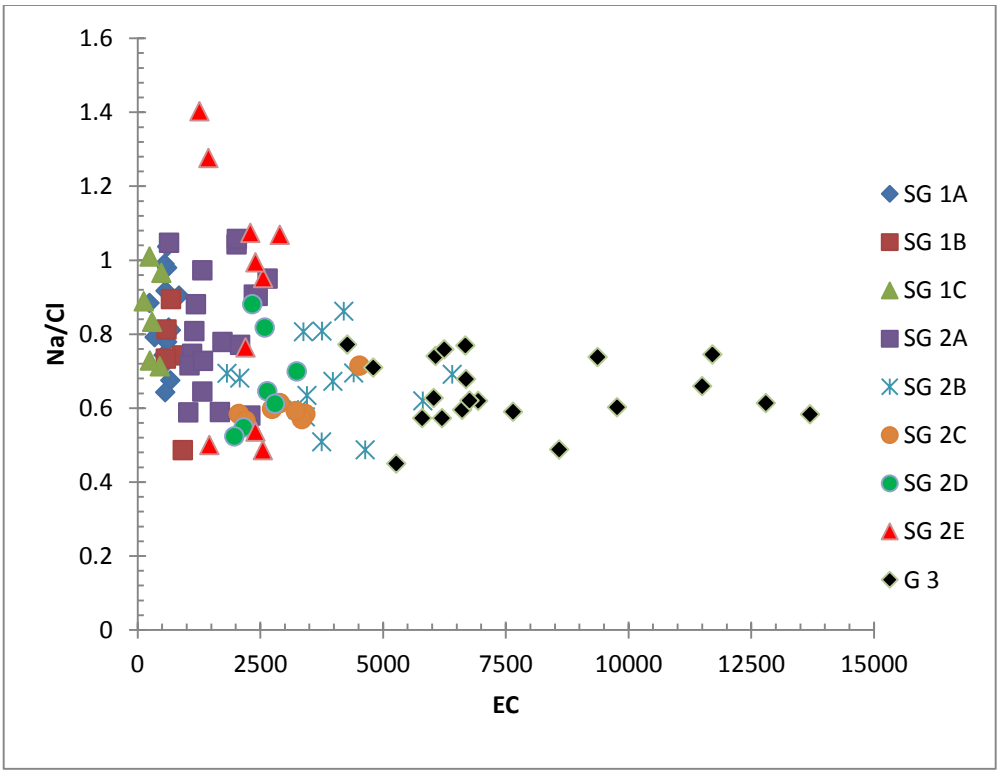

Figure 5.15: EC vs Na/Cl scatter diagram

5.1.3.4. Ion exchange

Ion exchange is one of the important processes responsible for concentration of ions in the groundwater. The existence of abundant Na^+ may promote cation exchange. This can be confirmed by the two Indices of Base Exchange (IBE) namely the Chloro Alkaline Indices (CAI 1 and CAI 2) suggested by Schoeller (1977).

$$CAI\ 1 = Cl - \frac{(Na+K)}{Cl} \qquad (5.3)$$

$$\text{CAI } 2 = Cl - \frac{(Na+K)}{SO_4} + HCO_3 + CO_3 + NO_3 \qquad (5.4)$$

(all values expressed in meq/L)

When there is exchange between Na and /or K in groundwater with Mg and/or Ca in the aquifer material both indices are positive, indicating reverse ion exchange. If the exchange takes place between Ca and/or Mg in groundwater with Na and/or K in the aquifer material, the indices will be negative, indicating ion exchange. The CAI 1 and CAI 2 values obtained in this study were positive except for a few of the samples in group 1 which had negative CAI 2 values. This suggests that reverse ion exchange is a dominant process in the groundwater. Ca^{2+} and Mg^{2+} exchange Na^{+} sorbed on the exchangeable sites on the aquifer minerals, resulting in the decrease of Ca^{2+} and Mg^{2+} and increase of Na^{+} in groundwaters by reverse ion exchange.

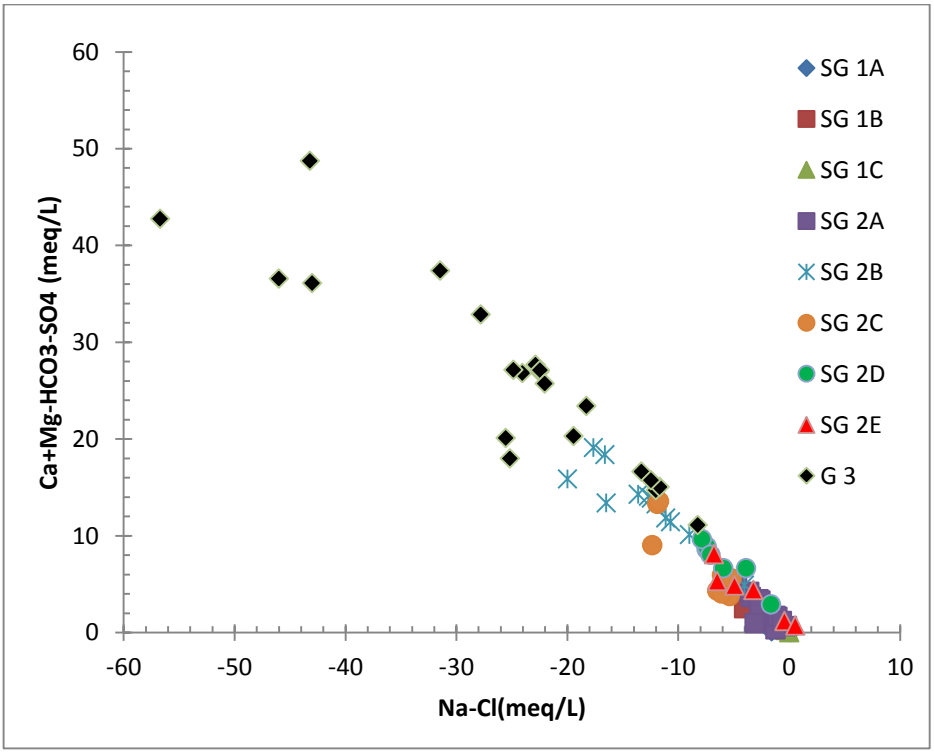

Figure 5. 16: scattered plot of Na-Cl versus Ca+Mg-HCO_3-SO_4

The dominance of reverse ion exchange in the study area was further demonstrated by the Na-Cl and Ca+Mg-HCO_3-SO_4 scatter plot (Fig. 5.16). According to Fisher and Mullican (1997) if

reverse ion exchange is a geochemical process controlling the composition of groundwater, the relationship between Na-Cl and Ca+Mg-HCO_3-SO_4 should be linear with a gradient of -1. The scattered plot of Na-Cl versus Ca+Mg-HCO_3-SO_4 shows that the points give a straight line (R^2=0.94) with a slope of -0.95. This confirms that Ca, Mg and Na concentration are interrelated through reverse ion exchange.

5.1.4. Thermodynamic Control

The computed aqueous speciation was used to define the possible chemical reactions in the aquifer system and to assess the state of equilibrium between the groundwater and minerals. The Saturation Indices (SI) describes quantitatively the deviation of the groundwater from equilibrium with respect to dissolved minerals. SI is defined as

$$SI = \log\frac{IAP}{K_{sp}} \qquad (5.5)$$

where *IAP* is the Ion Activity Product of the mineral-water reaction and K_{sp} the thermodynamic equilibrium constant for the mineral at the measured temperature. A negative SI indicates that the solution is undersaturated and that dissolution is expected, whilst a positive SI indicates that the solution is supersaturated and that precipitation should occur. The K_{sp} values are needed for constructing activity diagrams (Pitkanen *et al*, 2001). The diagrams give important information on potentially stable silicate phases after incongruent weathering of primary silicate minerals in groundwater solutions.

Calcite is one of the most common fracture minerals and studies have shown its importance in buffering and controlling the pH of groundwater. About 47% of the groundwater samples were oversaturated with respect to calcite and dolomite (Fig. 5.17). This consists mainly of group 3 groundwater samples and some of group 2 samples giving an indication of the long residence time of the groundwater. Calcite and dolomite saturation and supersaturation, observed with decreasing HCO_3 concentration could be the result of any of the following processes:(1) Calcite precipitation, (2) Incongruent dissolution of primary silicate minerals with clay mineral formation (thus maintaining constant aqueous SiO_2 concentrations) (3) Cation exchange of Ca^{2+} and Mg^{2+} from solution for Na^+ and H^+ from clay mineral surfaces

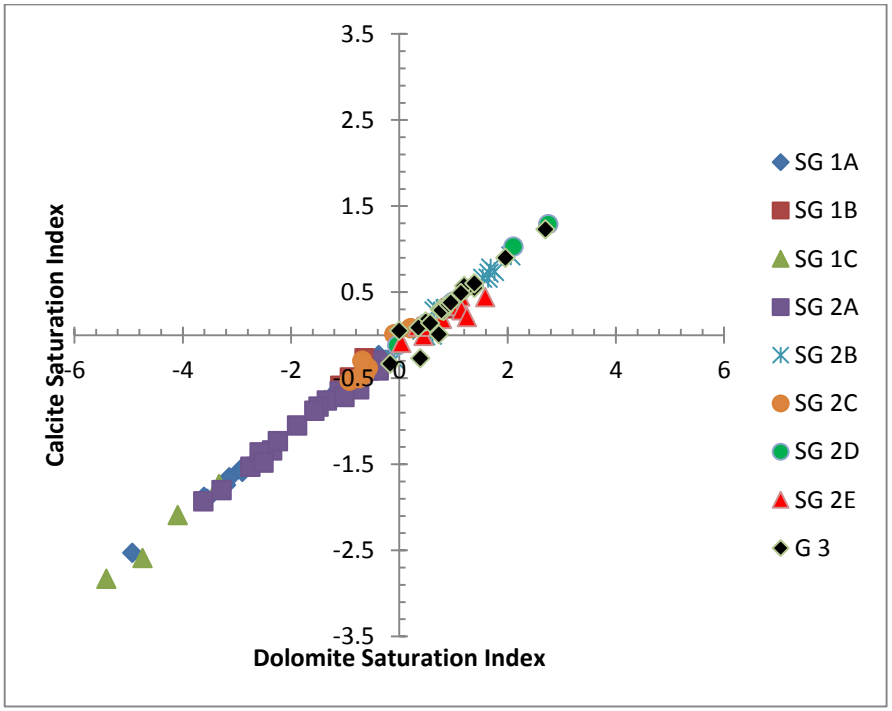

Figure 5.17. Relationship between calcite and dolomite saturation indices

About 30% of the groundwater samples located along the foothill of the Akwapim Togo Mountains (Group 1) were undersaturated with respect to quartz but all the groundwater samples were undersaturated with respect to amorphous silica (Table 5.5). Although quartz is an

abundant constituent of the geologic formation, its slow reactivity does not produce significant variations in the water chemistry (Lasaga, 1984) suggesting that the main sources of silica were either amorphous silica or the breakdown of aluminosilicates (Dongarra *et al*, 2009).

Table 5.5: Saturation Indices with respect to different minerals

Group 1 SG 1A	Location	Calcite	Dolomite	Gypsum	Anhydrite	Quartz	SiO(a)
AB1	Abokobi	-1.514	-2.790	-2.302	-2.505	0.297	-0.948
AB1Res	Abokobi	-1.595	-2.982	-2.246	-2.447	0.272	-0.970
AB2S	Abokobi	-1.467	-2.620	-2.247	-2.441	0.258	-0.980
AB 3R	Abokobi	-1.682	-3.047	-2.367	-2.570	0.294	-0.949
AYM F	Ayimensa	-1.676	-3.091	-2.762	-2.963	0.314	-0.926
AYM K	Ayimensa	-1.833	-3.364	-2.560	-2.759	0.279	-0.959
AYM 72	Ayimensa	-1.309	-2.340	-2.232	-2.432	0.216	-1.023
AYR 82	Ayimensa	-1.576	-2.809	-2.701	-2.899	0.510	-0.727
AA	Madina	-1.403	-2.550	-2.372	-2.588	0.319	-0.944
AHD 1	Adenta	-0.629	-1.124	-1.934	-2.152	0.326	-0.939
VV1	Oyibi	-1.588	-2.936	-2.453	-2.649	0.891	-0.343
VV2	Oyibi	-1.796	-3.381	-2.422	-2.615	0.861	-0.369
VV3	Oyibi	-2.551	-4.624	-3.178	-3.385	-0.366	-1.615
SAD A	Saduase	-0.222	-0.314	-2.377	-2.590	0.601	-0.656
SAD K	Saduase	-0.182	-0.234	-2.363	-2.567	0.727	-0.518
SG 1B							
SMA 63	Somanya	0.367	1.122	-2.085	-2.283	0.193	-1.043
BF2	GAEC	-0.480	-0.869	-2.295	-2.511	0.243	-1.019
BF3	GAEC	-0.327	-0.536	-2.320	-2.534	0.236	-1.022
KPE 67	Kpone	-0.202	-0.455	-2.004	-2.202	-0.270	-1.507
KPE 66	Kpone	-0.527	-0.903	-2.534	-2.732	0.028	-1.208

SG 1C							
ASB 1	Ashale Botwe	-0.732	-1.311	-2.310	-2.524	0.108	-1.151
ASB 1D	Ashale Botwe	-1.721	-3.265	-2.884	-3.098	-0.344	-1.603
AHD 2	Adenta	-2.071	-4.023	-2.761	-2.974	-0.105	-1.364
UG K	Legon	-2.805	-5.347	-2.692	-2.905	-0.345	-1.603
KP 1	Kponkpo	-1.688	-3.198	-2.688	-3.073	0.087	-1.160
DA 2K	Danfa	-2.551	-4.624	-3.178	-3.385	-0.366	-1.615
Group 2							
SG 2A							
AR1	Armahia	-0.224	-0.113	-2.049	-2.248	0.778	-0.460
AR K	Armhia	-0.354	-0.389	-2.221	-2.423	0.825	-0.418
WRI 1	CSRI	-0.557	-0.550	-2.225	-2.424	1.114	-0.124
AGT 1	Afienya	-0.998	-1.734	-2.129	-2.330	0.690	-0.552
KDE 55	Kordiabe	-0.345	-0.199	-1.854	-2.051	0.732	-0.505
AR2	Armahia	-0.983	-1.702	-2.233	-2.428	0.947	-0.286
PWC 2	Abokobi	-1.732	-3.082	-2.087	-2.283	0.315	-0.920
PWC 2R	Abokobi	-1.869	-3.442	-2.149	-2.347	0.437	-0.800
PWC K	Abokobi	-1.800	-3.591	-2.222	-2.478	0.769	-0.628
LQP	Madina	-1.355	-1.521	-1.981	-2.200	0.590	-0.677
WAS	Madina	-1.223	-2.225	-1.928	-2.146	0.712	-0.554
DA 1	Danfa	-1.409	-2.321	-2.169	-2.366	0.132	-1.105
AR 35	Armahia	-0.601	-0.971	-1.814	-2.099	0.233	-1.014
AR F	Armahia	-0.656	-1.102	-1.959	-2.162	0.525	-0.718
DA 1K	Danfa	-0.684	-0.907	-2.150	-2.358	0.329	-0.912
AP37	Armahia	-0.843	-1.453	-1.984	-2.192	0.213	-1.037
ALA	Madina	-0.818	-1.470	-1.912	-2.129	0.526	-0.739
SG 2B							
DO 94D	Dodowa	0.799	1.931	-1.111	-1.308	1.057	-0.179

DO 139	Dodowa	0.128	0.604	-1.415	-1.612	0.961	-0.276
DO 151	Dodowa	0.724	1.792	-1.403	-1.600	0.846	-0.390
D0 K	Dodowa	0.978	2.238	-1.016	-1.219	0.940	-0.297
KA 68	Katamanso	0.725	1.716	-1.208	-1.402	0.694	-0.539
KA 70	Katamanso	0.788	1.836	-1.004	-1.200	0.518	-0.718
BF 1	GAEC	0.803	1.755	-1.521	-1.733	0.722	-0.535
TTL 170K	Tema	0.344	0.819	-1.713	-1.910	0.496	-0.741
TTL 175K	Tema	0.381	0.888	-1.519	-1.714	0.549	0.686
AGT AF	Afienya	0.364	1.011	-1.518	-1.720	0.298	-0.945
OG 56	Ogbojo	-0.211	0.098	-1.340	-1.537	0.738	-0.499
OG 59	Ogbojo	0.171	0.825	-1.370	-1.568	0.737	-0.500
MAA	Malejor	0.048	0.739	-1.500	-1.701	0.604	-0.642
DZ 47	Dzorwulu	-0.022	0.562	-1.591	-1.789	0.247	-0.990
SG 2C							
OY1	Oyarifa	0.515	0.869	-1.527	-1.741	0.360	-0.900
OY K	Oyarifa	-0.331	-0.454	-1.475	-1.681	0.156	-1.091
OY 163	Oyarifa	-0.389	-0.460	-1.617	-1.814	0.036	-1.201
OY F	Oyarifa	-0.491	-0.646	-1.677	-1.867	0.287	-0.940
FRA K	Fafraha	-0.435	-0.605	-1.725	-1.930	0.207	-1.039
TE K	Tema	0.134	0.351	-1.670	-1.873	-0.142	-1.386
VAL 74	Tema	-0.239	-0.496	-1.399	-1.596	0.483	-0.754
TE 174K	Tema	0.066	0.076	-2.224	-2.423	-0.117	-1.358
SG 2D							
ADH 3	Adenta	1.047	2.175	-1.636	-1.848	0.563	-0.694
UG 109	Legon	1.336	2.904	-1.536	-1.734	0.407	-0.830
PRE 1	Legon	0.379	0.958	-1.506	-1.729	0.627	-0.649
PRE 2	Legon	0.093	0.423	-1.696	-1.918	0.877	-0.396
PRE K	Legon	-0.086	0.055	-1.540	-1.749	0.399	-0.854

PRE F	Legon	0.211	0.699	-1.531	-1.727	0.508	-0.727
SH 80A	Shai Hills	0.418	1.102	-1.286	-1.488	1.118	-0.125
SG 2E							
KPG 53	Kpong	0.511	1.312	-1.393	-1.591	0.734	-0.503
KPG 54	Kpong	0.384	1.059	-1.447	-1.658	0.763	-0.493
AYK A	Ayikumah	0.228	0.906	-2.014	-2.221	0.762	-0.487
AYK 20	Ayikumah	0.819	2.149	-1.933	-2.138	0.490	-0.756
BA 40	Bawaleshie	-0.043	0.166	-1.342	-1.547	0.600	-0.646
BA 42	Bawaleshie	0.145	0.472	-1.135	-1.338	0.881	-0.364
WRI 13	CSRI	0.351	1.337	-2.231	-2.429	0.798	-0.438
WRI 19	CSRI	0.448	1.632	-2.267	-2.483	0.489	-0.773
WRI 30	CSRI	0.276	1.426	-2.774	-2.973	0.756	-0.482
AR A	Armahia	0.148	0.579	-2.758	-2.962	0.828	-0.416
Group 3							
TFS K	La	-0.286	-0.044	-1.384	-1.584	1.089	-0.154
TFS 176	La	-0.229	0.503	-2.170	-2.379	0.500	-0.750
TFS 177	La	0.039	0.801	-1.284	-1.491	0.444	-0.810
KA 69	Katamanso	0.221	0.663	-1.025	-1.222	0.222	-1.016
SAN 15	Santeo	0.361	0.933	-1.009	-1.205	0.196	-1.041
ASB 11D	Ashale Botwe	0.153	0.529	-1.954	-1.292	0.099	-1.336
ASB 12D	Ashale Botwe	0.169	0.652	-1.048	-1.257	0.171	-1.083
KA 3	Katamanso	0.616	1.571	-0.981	-1.177	0.323	-0.914
SAN 2R	Santeo	0.389	1.018	-0.997	-1.191	0.457	-0.777
SAN 14	Santeo	0.350	1.011	-1.157	-1.351	0.284	-0.950
SAN 117	Santeo	0.390	1.003	-0.926	-1.122	0.522	-0.715
ASH 77	Ashiaman	0.602	1.446	-1.088	-1.280	0.290	-0.941
SAN 1R	Santeo	0.357	0.979	-1.113	-1.307	0.031	-0.923
VAL 158	Tema	0.115	0.183	-1.351	-1.548	0.209	-1.028

UG 93	Legon	0.957	2.137	-0.959	-1.155	0.739	-0.498
VAL 75	Tema	0.631	1.384	-1.134	-1.330	0.655	-0.581
ASH 166	Ashiaman	1.284	2.870	-0.833	-1.028	0.648	-0.589
ASH K	Ashiaman	0.603	1.558	-1.002	-1.199	0.529	-0.709
ASH CCF	Ashiaman	0.545	1.310	-0.744	-0.940	0.661	-0.577
AF 1	Michel Camp	0.403	1.048	-1.400	-1.602	0.689	-0.556
AF 2	Michel Camp	0.443	1.132	-1.242	-1.439	0.457	-0.779

Another approach to test the proposed hydrogeochemical evolution is the use of mineral stability diagrams (Drever, 1997). The diagrams give important information on potentially stable silicate phases after incongruent weathering of primary silicate minerals in groundwater solutions. Infiltrating water is corrosive and dissolves the aluminosilicate minerals to give argillaceous minerals of which the principal ones are: kaolinite, illite and montmorillonite.

The stability field diagrams of the Na_2O-SiO_2-Al_2O_3-H_2O, CaO-SiO_2-Al_2O_3-H_2O, MgO-SiO_2-Al_2O_3-H_2O and K_2O- SiO_2-Al_2O_3-H_2O, (Fig. 5.18 (a-d)) systems showed that most of the groundwaters plot essentially in the kaolinite stability field indicating that equilibrium with the kaolinite solid phase is one of the processes controlling groundwater chemistry. Kaolinite is a common weathering product of feldspar and other silicate (Rajmohan and Elango, 2004). However with increasing ionic content and TDS, the groundwaters tend to reach and follow the kaolinite-montmorillonite boundary and eventually to the montmorillonite stability field.

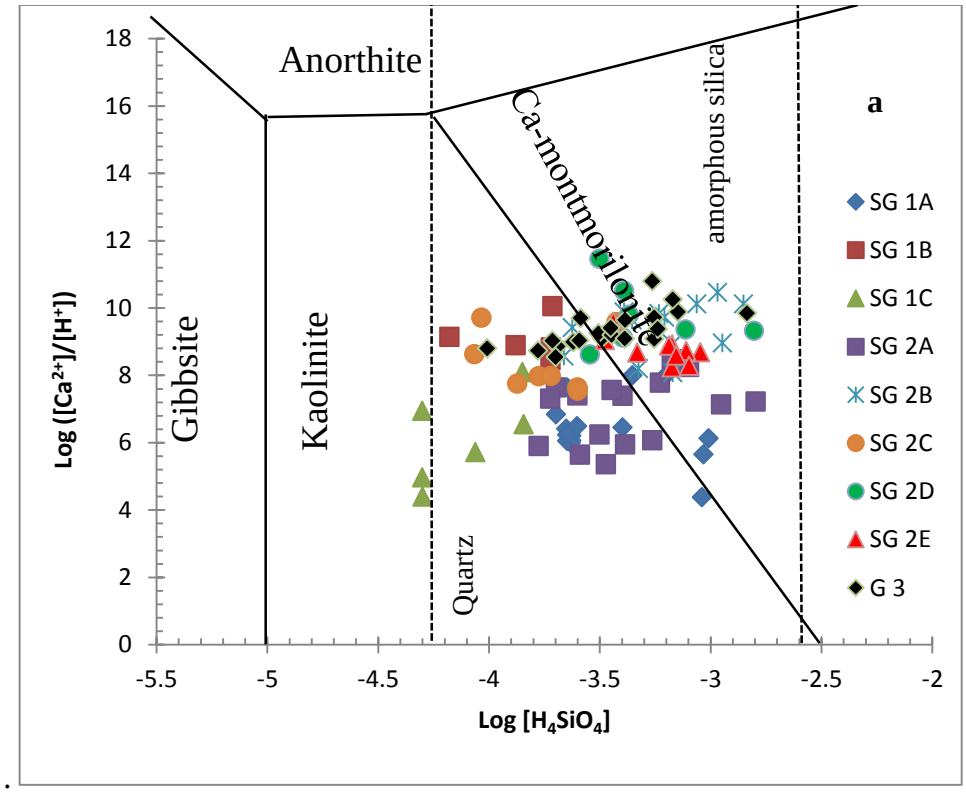

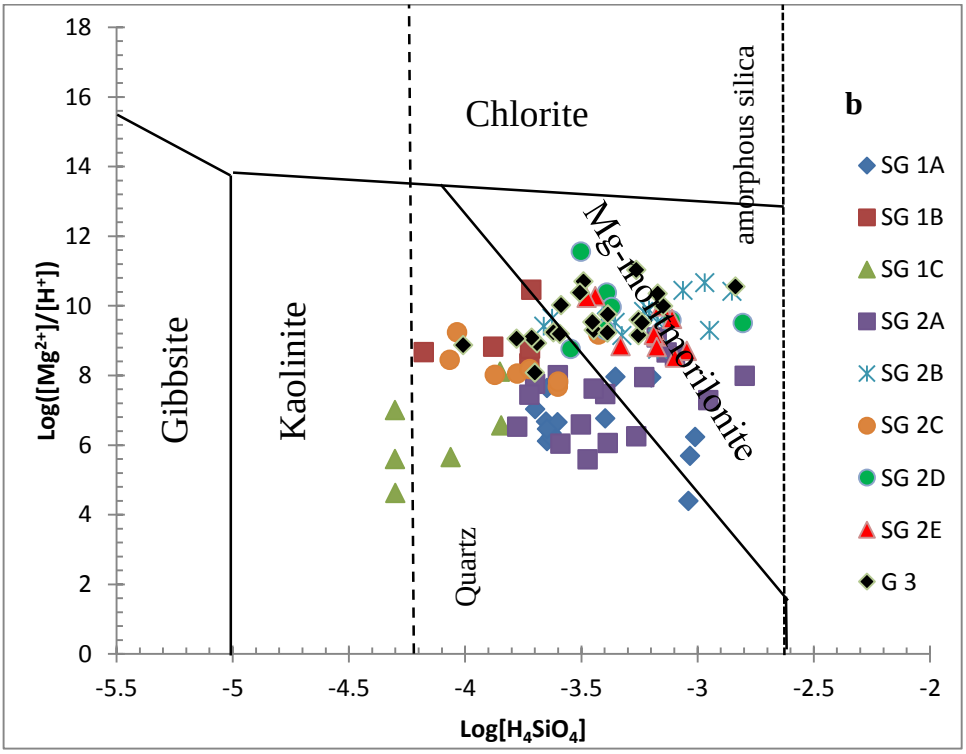

Figure 5 18(a-b): Mineral stability diagrams

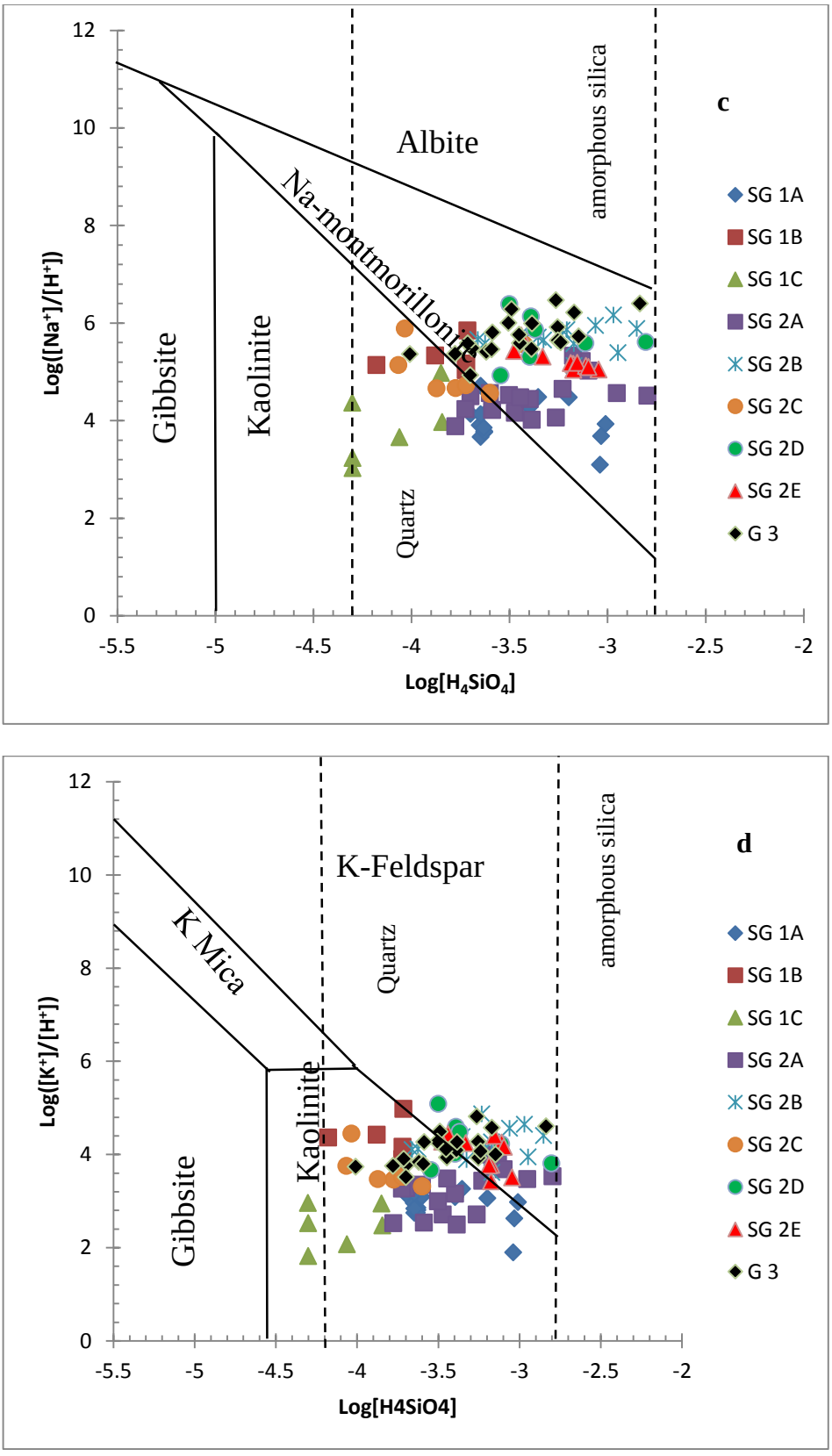

Figure 5 18 (c-d): Mineral stability diagrams

The Na_2O-SiO_2-Al_2O_3-H_2O stability diagram (Fig. 5.18c) had much of the data plotting within the Na-montmorillonite field. Na-montorillonite tends to be the stable solid phase in the central and coastal areas of the Plains because of the high concentration of Na^+ due to the precipitation of calcite, cation exchange and the higher ionic mobility of Na^+ with respect to Ca^{2+}. In terms of the silicate evolutionary sequence these waters are relatively mature. This apparent maturity may be due to the long residence time of the groundwater.

Both the Ca^{2+} and Mg^{2+} stability diagrams (Fig 15.18 a and b) indicate that the ground-waters are either in equilibrium with kaolinite or, at times, straddle the kaolinite-montmorillonite boundaries. The mineral composition of the rocks strongly influences the groundwater chemistry, as seen by the saturation indices for calcite and dolomite (Table 5.5). The incongruent dissolution of andesine produces kaolinite and Ca^{2+} ions (Freeze and Cherry, 1979); whilst biotite produces Mg^{2+} and K^+ ions. Silica is produced, while the pH rises as H^+ is consumed.

Weathering of primary silicate minerals to kaolinite or gibbsite occurs typically in tropical areas with intense rainfall and under well drained conditions (Appelo and Postma, 2005). However, montmorillonite is most favoured in drier climate where the rate of soil flushing is relatively slow. Thus the Accra Plains with a dry climate and a mean annual rainfall of 800 mm should have most of the groundwater samples plotting in the montmorillonite stability fields. Garrels (1967) demonstrated that initial reactions effected by solutions rich in CO_2 is the production of kaolinite followed by montmorillonite as CO_2 is consumed and the pH, silica and bicarbonate increase in the solution. This thus suggests that the groundwaters which plot in the kaolinite stability field are young or fresh and the groundwater is well drained.

5.2. Conclusion

The groundwater of the Accra Plains is dominated by sodium and chloride ions. The pH values of groundwater samples ranged from 5.6 to 8.5 indicating that the groundwater ranges from slightly acidic to alkaline condition. The pH of the groundwater at the Valley View University is lower than the recommended pH values for a repository environment, making the site unsuitable for a radioactive waste repository. Analyses of the groundwaters in Accra Plains show that, the concentrations of calcium and magnesium together constitute 48% of the total cations in the groundwater and will provide a stable chemical environment for a backfill and buffer materials.

The chemical composition of the groundwater is strongly influenced by the rock-water interaction, dissolution and deposition of the aluminosilicate rock minerals. Silicate weathering (plagioclase, micas, and hornblende) controls the major ion chemistry of calcium, magnesium and sodium and to a lesser extent carbonate dissolution reaction. The ion exchange and reverse ion exchange also controls the chemical composition of the groundwater especially along the coastal areas of the Plain.

The groundwater along the foothill of the Akwapim-Togo mountains are less mineralized than those from the gneiss. The hydrochemical facies evolves from Na-Mg-Ca-Cl-HCO_3 to Na-Ca-Cl following Cherebotarev groundwater flow sequence. Hydrolysis of plagioclase feldspars to liberate Na and Ca, coupled with Ca loss by calcite precipitation and/or ion exchange (for Na) on clay minerals in the flow paths, are the main chemical processes that cause this evolution. The Na-Ca-Cl groundwaters are oversaturated with respect to calcite and dolomite. The long residence time of the groundwater was indicated by saturation of the formation water with

respect to some of the solid phases of the rock. The presence of brackish groundwater, water with a high pH, and increasing TDS along the flowpath suggests a sluggish groundwater system. These geochemical conditions do not develop rapidly and suggest water ages in thousands of years. Meteoric salts that migrate from the ocean surface is a possible source of chloride in the groundwater.

The mineral stability relationship showed that the groundwater generally plots within the kaolinite stability field but evolves towards equilibrium with respect to montmorillonite with increasing cation concentration. This suggests that if one excludes earth-alkaline carbonates, the mineralogical pair kaolinite-montmorillonite would control most of the solution chemistry by direct precipitation. the chemistry of the groundwater favours the formation of kaolinite and montmorillonite. The long time stability of these minerals together with their ion exchange properties which can retard the migration of long-lived radionuclides makes them a useful backfill and or buffer material for a radioactive waste repository.

Chapter Six

Environmental Stable Isotope Studies of Groundwater in the Accra Plains

6.1. Results and Discussion

The $\delta^{18}O$ and $\delta^{2}H$ isotopic composition of the groundwater samples are shown in Table 6.1.

Table 6.1: Stable isotope analysis of groundwater samples from boreholes in the Accra Plains

BH ID	Location	Temp °C	pH	TDS (mg/l)	Ele. Con. (µS/cm)	Cl mg/L	O^{18} ‰	H^{2} ‰	d ‰
AB1	Abokobi	28.80	6.40	248.00	595.00	111.50	-3.56	-14.00	14.48
AB1Res	Abokobi	29.20	6.30	249.00	601.00	115.25	-3.50	-17.60	10.40
AB2S	Abokobi	29.90	6.50	276.00	670.00	147.90	-3.47	-12.00	15.76
AB 3R	Abokobi	29.00	6.40	241.00	564.00	144.00	-3.40	-15.00	12.20
PWC 2	Abokobi	30.30	6.20	827.00	2020.00	436.65	-3.22	-15.50	10.26
PWC 2R	Abokobi	29.90	6.10	830.00	2025.00	441.48	-3.79	-14.00	16.32
PWC F	Abokobi	29.50	6.80	1262.00	2650.00	458.45	-3.25	-15.30	10.70
PWC K	Abokobi	32.10	6.50	1510.00	2370.00	468.70	-3.36	-13.20	13.68
AYM K	Ayimensa	29.80	6.40	338.00	528.00	147.80	-3.55	-15.30	13.10
VV1	Oyibi	30.50	6.50	242.00	600.00	99.64	-4.53	-20.00	16.24
VV2	Oyibi	31.00	6.20	243.00	601.00	119.63	-3.94	-20.30	11.22
VV3	Oyibi	29.70	5.60	226.00	550.00	121.96	-4.07	-23.50	9.06
BF 1	GAEC	26.80	7.70	1671.00	3760.00	746.08	-2.96	-14.01	9.67
BF2	GAEC	26.00	7.50	438.00	684.00	149.95	-2.85	-11.89	10.91
BF3	GAEC	26.60	7.70	379.00	592.00	139.98	-2.67	-8.14	13.22
UG K	Legon	26.70	5.60	288.00	450.00	143.46	-3.39	-16.70	10.42
PRE 1	Legon	24.00	7.70	1489.00	3240.00	877.46	-2.98	-10.20	13.64
PRE 2	Legon	24.40	7.50	1204.00	2640.00	789.73	-3.16	-12.90	12.38
AA	Madina	26.00	6.49	110.20	242.00	194.95	-3.01	-13.20	10.88
LQP	Madina	25.30	6.00	1102.00	2450.00	459.79	-3.56	-16.03	12.45
WAS	Madina	25.30	6.10	937.00	2090.00	481.90	-3.57	-15.58	12.98
ALA	Madina	25.60	6.72	1027.00	2300.00	397.38	-2.42	-11.76	7.60
AHD 1	Adenta	25.50	6.98	235.00	350.00	271.89	-3.40	-13.80	13.40
AHD 2	Adenta	26.60	6.32	50.00	129.00	93.80	-2.65	-13.60	7.60
ADH 3	Adenta	26.80	8.11	1470.00	2337.00	493.88	-3.18	-15.65	9.79
SAD A	Saduase	26.80	7.10	552.00	680.00	116.43	-3.83	-17.60	13.04
AR A	Armahia	28.80	7.30	875.00	1260.00	178.93	-3.28	-15.00	11.24

AR1	Armahia	29.80	7.40	539.00	1318.00	272.00	-3.55	-14.70	13.70
AR2	Armahia	30.50	6.90	259.00	640.00	172.00	-3.63	-14.90	14.14
KPE 66	Kpone	30.00	7.80	369.00	577.00	179.87	-3.87	-17.80	13.16
ASB 1	Ash Botwe	26.50	7.42	233.00	488.00	143.99	-2.44	-13.60	5.92
DA 2K	Danfa	28.10	6.30	195.00	250.00	44.00	-3.30	-13.80	12.60
WRI 1	CSRI	29.80	6.80	639.00	1056.00	287.78	-2.89	-11.10	12.02
WRI 30	CSRI	29.80	7.55	1114.00	1460.00	351.00	-3.66	-15.90	13.38
AGT 1	Afienya	29.20	7.00	696.00	1681.00	299.93	-2.05	-8.40	8.00
DA 1K	Danfa	27.80	6.80	847.00	1320.00	337.70	-3.18	-14.20	11.24
KA 68	Katamanso	30.50	7.50	2970.00	4400.00	1448.21	-3.50	-15.50	12.50
MAA	Malejor	28.50	7.25	2895.00	4200.00	1269.29	-3.48	-16.90	10.94
OY1	Oyarifa	26.40	6.70	1517.00	2900.00	493.80	-2.74	-7.50	14.42
OY K	Oyarifa	28.40	6.80	1320.00	2060.00	517.98	-2.12	-8.90	8.06
FRA K	Fafraha	28.60	6.90	1753.00	2740.00	458.95	-3.88	-20.80	10.24
TE K	Tema	28.90	7.00	2141.00	3350.00	1020.72	-2.91	-14.30	8.98
TE 174K	Tema	29.40	7.50	2890.00	4520.00	1463.00	-2.09	-10.60	6.12
TTL170K	Tema	30.00	7.40	2550.00	3980.00	1302.39	-3.12	-17.30	7.66
TTL175K	Tema	30.40	7.50	2210.00	3450.00	1080.00	-2.22	-9.60	8.16
VAL 74	Tema	30.00	7.40	2060.00	3220.00	1035.00	-2.45	-12.60	7.00
VAL75	Tema	30.00	7.40	4320.00	6760.00	2354.00	-3.30	-12.25	14.15
SH 80A	Shai Hills	29.00	7.45	1546.00	2590.00	755.45	-3.56	-16.20	12.28
KPG 54	Kpong	27.00	7.30	1400.00	2300.00	257.83	-2.98	-14.40	9.44
AYK A	Ayikumah	28.00	7.20	920.00	2400.00	284.10	-3.38	-15.60	11.44
BA 40	Bawaleshie	28.40	7.40	600.00	1445.00	263.00	-1.72	-12.10	1.66
BA 42	Bawaleshie	28.70	7.10	1420.00	2200.00	487.50	-2.61	-10.90	9.98
TFS K	La	29.00	7.60	7516.00	11710.00	3876.14	-2.80	-12.90	9.50
ASH 44	Ashiaman	30.50	7.20	2780.00	4320.00		-3.83	-16.60	14.04
ASH 77	Ashiaman	29.60	7.20	3843.00	5800.00	1875.00	-3.80	-16.90	13.50
ASH K	Ashiaman	29.70	7.30	5980.00	9370.00	3048.21	-3.22	-16.10	9.66

The $\delta^{18}O$ isotope composition of the groundwater range from -4.53‰ vs V-SMOW at Valley View University (VV1) located at Oyibi to -1.72‰ vs V-SMOW at Bawaleshie. The mean $\delta^{18}O$ isotopic groundwater composition is -3.19‰ vs V-SMOW. The $\delta^{2}H$ isotope composition of the groundwater range from -23.5‰ vs V-SMOW at Valley View University (VV3) located at Oyibi to -7.5 ‰ vs V-SMOW at Oyarifa. The mean $\delta^{2}H$ isotopic groundwater composition is -14.36‰ vs V-SMOW. The groundwater samples collected along the foothill of the Akwapim Togo Mountain were relatively more negative than those from the central and coastal parts of the

Accra Plains. It may be due to the higher rain value observed along the foothill of the Akwapim Togo Mountain where the elevation is higher. Mountains are characterized by isotopically more depleted precipitation with increasing elevation due to the cooling of the air mass when it is forced to ascend (‘‘altitude effect’’).

The interpretation of these data in terms of both origin and recharge mechanisms of the groundwaters is generally based upon comparison of $\delta^{18}O$ and $\delta^{2}H$ data in groundwater and rainwater which is the dominant source of recharge for most continental hydrogeological systems. The oxygen-18 isotope composition of rainwaters in Accra (altitude 35m) analysed by Akiti (1980) varied from +0.12 to -8.42‰ vs SMOW with a mean of -3.20‰ vs SMOW. The oxygen-18 isotope composition of rainwaters in Aburi (altitude 365m) varied from +0.84 to -9.78‰ vs SMOW with a mean of -3.46‰ vs SMOW. Akiti (1980) established the local meteoric water line (LMWL) of the Ghana. He defined the LMWL by the equation,

$$\delta\,^{2}H‰ = 7.86\,\delta^{18}O + 13.6. \qquad (6.1)$$

The LMWL attributed to Akiti (1980) is identical to the LMWL obtained at Dodoma, Tanzania by Nkotagu(1996(b)) and defined by the equation

$$\delta\,^{2}H‰ = 7.9\,\delta^{18}O + 13.83, \qquad (6.2)$$

The deuterium excess intercept in the equation is higher than 10‰ and suggests a low relative humidity prevails in the air masses directly above the ocean surface in comparison with the

average relative humidity over the ocean surface at the time the vapours forming the analysed precipitations were formed (Nkotagu, 1996(b).

The deviation in the LMWL attributed to Akiti (1980) indicated that the rain particles underwent partial evaporation in the atmosphere. However the fact that the gradient is close to 8 explains enrichment due to partial evaporation in the atmosphere. This may be due to the high relative humidity during the rainy season

In the δ^2H–$\delta^{18}O$ plot (Fig. 6.1), obtained in this study, most of the samples collected along the foothill of the Akwapim Togo Mountain plot between the GMWL and the LMWL with the few remaining plotting along and above the LMWL. Some of the central and coastal samples also plot between the GMWL and LMWL lines. The rest of the central and coastal samples plot around the evaporation line. The concentration of plots between the GMWL and LMWL indicates: firstly, the common origin of the groundwaters, namely infiltrating modern precipitation; secondly, these groundwaters have not been subjected to surface or subsurface alteration of their isotopic composition and; thirdly, there have been no significant isotopic modifications by evaporation of the rain at the time of precipitation (Zhu *et al.* 2006). If a linear trend line is draw between the δ^2H and $\delta^{18}O$ values of the groundwater samples, the regression line obtained has the equation:

$$\delta^2H = 4.39\ \delta^{18}O - 0.34, \qquad (6.3)$$

with a correlation coefficient (r^2) of 0.62.

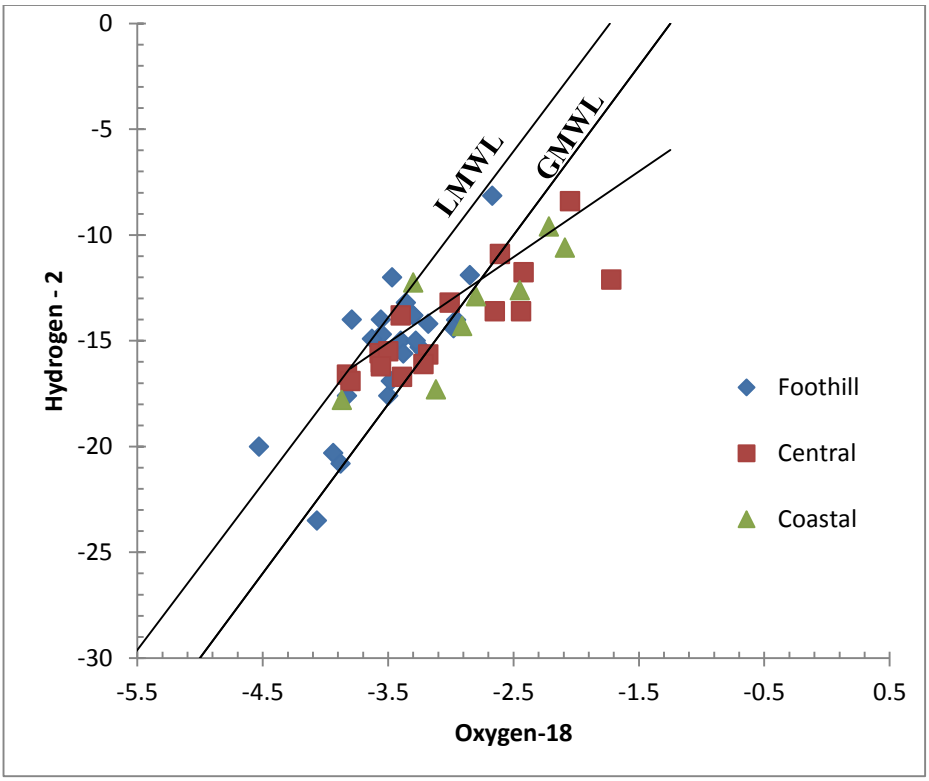

Figure 6.1: Relationship between ^{18}O and ^{2}H for groundwater in the Accra Plains

The slope of the δD vs $\delta^{18}O$ relationship is within the range of evaporated natural waters. Mainly depending on the humidity, the slope of an evaporating trend ranges from 3.5 to 6.0(Gat, 1981). According to Grassa *et al* (2006), the lower the humidity conditions, the lower the slope of the evaporation line. The low slope encountered in the Plains may be due to isotopic fractionations upon groundwater infiltration and its underground circulation. This is a result of the semi-arid climatic conditions characterizing the Accra Plains. The dry environmental conditions in the Accra Plains will result in secondary evaporation during rainfall. Friedman *et al* (1962) first showed that evaporation during rainfall would shift the water away from the GMWL. However the mean $\delta^{18}O$ value for the groundwater is similar to that of the rainfall value measured by Akiti (1980). This suggests that the local rainfall recharges the groundwater after minor evaporation, possibly during flash floods. Therefore, the slope of the equation might not indicate major

evaporation effects prior to infiltration, but the mixing of various rainfall events and/or surface runoff with variable stable isotopic contents. This also implies that the groundwater recharge takes place predominantly through macropores where further minor evaporation could occur (Nkotagu, 1996(b)).

Coplen *et al* (2000) and Scholl *et al* (1996) suggested that, variations in rainwater isotopic signatures may be due to rainout and altitudinal effects, where an approximate shift of – 0.2 ‰ per 100m were measured. The mean isotopic altitude recharge was found to be -0.13‰ vs SMOW per 100m (Akiti 1980).This value agrees with a value of -0.16 vs SMOW per 100 m obtained on the Cameroon Mountains (Gonfiantini *et al* 2001). The isotopic altitude of recharge is a variable quantity which depends on the nature of the rainfall and season (Fontes and Zuppi 1976).

Taking the enrichment of heavy isotopes in rain before infiltration studies carried out by Gat and Tzur (1967) together with the enrichment which can occur in shallow aquifers. It can be deduced that the aquifer in the Plains was recharged by vertical infiltration of meteoric waters. The isotopic values of shallow groundwater have a broader variation than deep groundwater and a narrower variation than precipitation. The broad variation of shallow groundwater indicates the presence of macropores and preferential flow. Macropores and preferential flow channels in the unsaturated zone permit the fast movement of mobile water to the water table with very limited mixing. In such cases, groundwater preserves an isotopic composition similar to that of precipitation.

The intercept of the evaporation line and the LMWL is the original isotopic composition of groundwater before evaporation. It is –3.85 and –16.35 ‰ for $\delta^{18}O$ and $\delta^{2}H$ respectively (fig. 6.1). The displacement of the evaporation line from the meteoric line is a reflection of the evaporative loss and can be used to calculate an average evaporative loss. The few groundwater samples that deviate considerable from the GWML and plot around the evaporation line indicate evaporative enrichment of ^{18}O and ^{2}H in the surface water before recharge or the rain water mixed with previous rainwater before infiltration to the groundwater. Evaporation can take place in the upper vadose zone before infiltration through the soil thus enriching groundwater in heavy isotopes mainly in areas characterized by an arid or semi-arid climate (Shivanna *et al* 2004; Leontiadis *et al*., 1996)

The calculate deuterium excess (d-excess) values for the groundwater samples (Table 6.1.) showed that all the groundwater samples that deviate from the GMWL had d-excess values less than 8-10‰ with Bawaleshie having a value of 1.66‰ suggesting evaporation from a source more humid than the global ocean average. The low 'd-excess' values (≤6) in major part of the study area suggest that there is significant evaporation of rainwater leaving the residual groundwater with lower values of 'd-excess'. The climate of the Accra Plains is influenced by the Atlantic Ocean where the relative humidity is high and more uniform. The d-excess above 10‰ were obtained for the groundwaters that plot between the GMWL and the LMWL with a mean value of 12.7‰. High d-excess in this area can be explained by addition of kinetically controlled reevaporated component from local surface waters to the oceanic vapour. One of the groundwaters sampled at Valley View University, Oyibi, had d-excess of 16.24‰. The groundwater samples from Abokobi also had d-excess of 14.48‰ and 15.76‰. Gonfiantini *et al.*

(2001) reported increase in deuterium excess in mountain areas. These areas are located near the Akwapim Togo Mountains. Dansgaard (1964) established that the mean 'd' value in Africa and Near East is about 15‰ with a considerable spread with the highest deviation being due to evaporation of raindrops.

It is known that subsurface stratigraphy and structures give rise to variations in hydraulic conductivity (Kendall and McDonnell, 1998). The differences in hydraulic conductivities can exist in an infinite variety and would have profound effect on groundwater flow. This is an important aspect to consider when characterizing a site for radioactive waste repository especially in the subsurface. A situation of this nature has been identified on the compound of the Valley View University on the Accra Plains.

Results in this study, showed that the chemistry of the groundwaters sampled on the compound of the Valley View University are different from those of the surrounding Plains. For example the TDS values were relatively low compared to others in the Plains. From the stable isotope measurement, it was found out that the groundwater have oxygen-18 values and deuterium which are more depleted than those that are occurring in the surrounding groundwaters. Mountains are characterized by isotopically more depleted precipitation with increasing elevation due to the cooling of the air mass when it is forced to ascend (''altitude effect''). This suggests that the groundwater at Valley View University are recharged at a high elevation, hence the depleted values. The Akwapim-Togo Mountains would be the source of these groundwaters. Taking the distance between the mountains and the University campus into consideration, in terms of hydrogeology, this would imply that there are preferential channels or routes through which

waters that are recharged on the Akwapim-Togo Mountains find their way to the university campus. This means that any waste disposal facility built in that area would be easy saturated with groundwater. It will lead to faster degradation of the disposal facility and any radionuclides released from the facility will find its way to the groundwater and hence to the surface water quicker than expected. This makes that area unsuitable for a waste repository

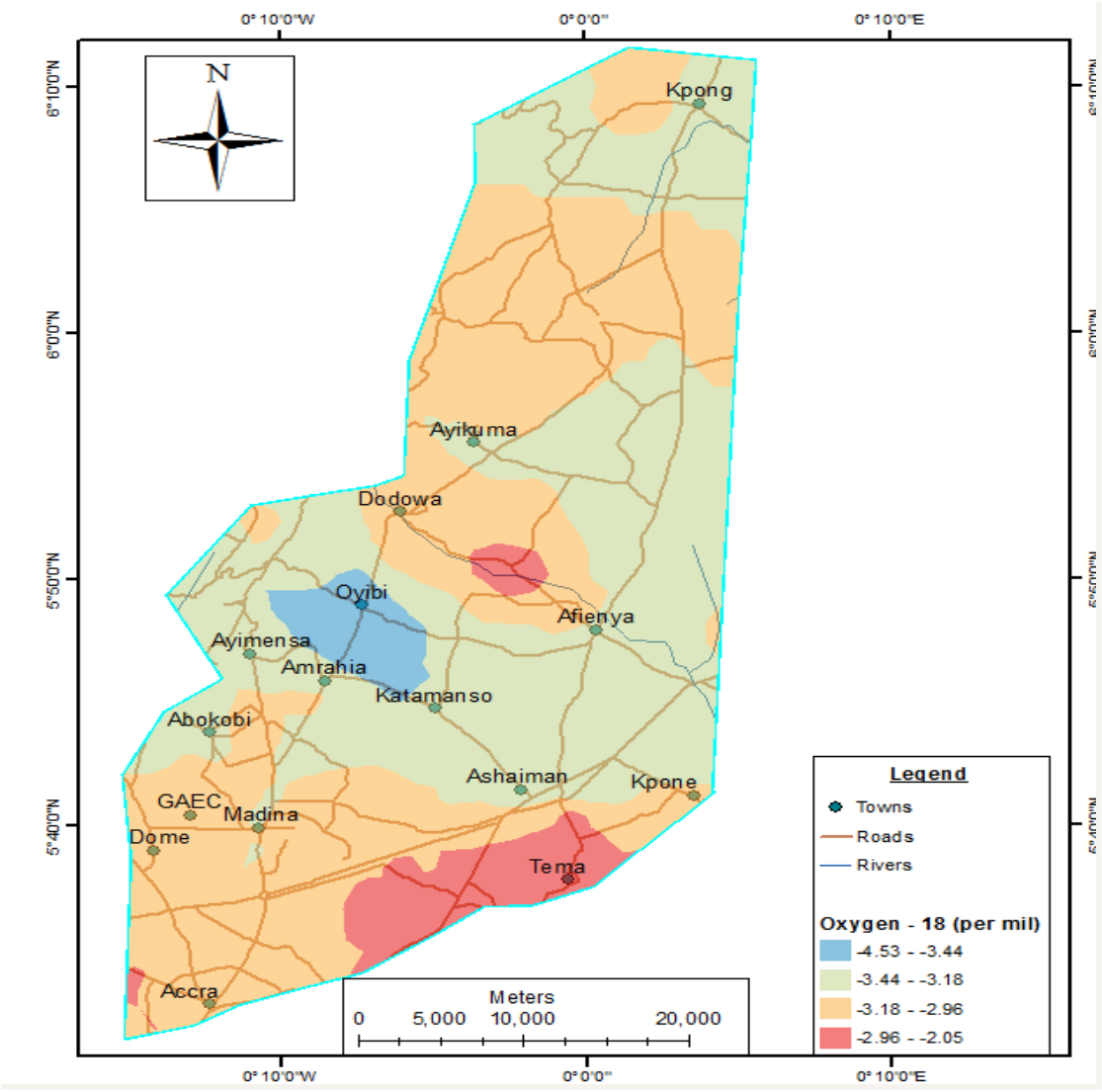

Figure 6.2: Spatial distribution of Oxygen-18 in the groundwaters in the study area

6.2. Conclusion

The stable environmental isotopes of hydrogen and oxygen of the groundwater in the Accra Plains indicate that most of the stable isotope composition of the 18O and D in the groundwater is meteoric water features. Thus meteoric water is the main recharge source to the groundwater system. The recharge takes place in fracture in the geologic formation but under the semi-arid conditions, the groundwaters undergo evaporation where the water can be lost from the unsaturated zone or from the water table. Thus the recharge of partially evaporated water, with an enriched isotopic signature takes place in some areas. The groundwater is also affected by the mixing of various rainfall events and/or surface runoff. In contrast recharge in other areas seems to take place rapidly, possibly via preferred pathways, preventing any significant evaporation.

The Valley View University located at Oyibi is not suitable site for a radioactive waste repository. Any radioactive waste repository built in that area would be easy saturated with groundwater due to the presence of preferential channels or routes through which waters that are recharged on the Akwapim-Togo Mountains easily find their way to the university campus. The pH conditions of the groundwater is also lower than the recommended pH values for a radioactive waste repository. It will result in faster degradation of the disposal facility which will result in the release of radionuclides into the groundwater before they decay to exemption levels. These radionuclides will be transported to the surface water faster than can be expected.

Chapter Seven

Geochemistry of Naturally Occurring Radionuclides

7.1. Results and Discussion

Results of the measured activity concentration of the radionuclides in the geological formation in the Accra Plains with their quoted errors as one-standard deviations based on the counting statistics are listed in Table 7.1. The descriptive statistics of the activity concentrations of all the samples and for only the GAEC (BF) samples are presented in tables 7.2 and 7.3 respectively. The reported world mean values for ^{238}U, ^{226}Ra, ^{232}Th and ^{40}K are 35, 32, 45 and 420 Bq/kg respectively (UNSCEAR, 2000).

The results obtained are also presented through respective histograms (Fig.7.1 (a – d)). Variations in the radionuclide concentrations in the samples from different sampling location were due to variations in the concentration of the elements in the geologic formation. The relative enrichment of the radionuclides is in the order K >Th> U > Ra. The high activity concentration of ^{40}K can be attributed to the abundance of K-feldspar minerals in the geological formation. The highest radionuclide concentrations were measured in the rock samples collected from GAEC (BF samples) premises which were composed mainly of felsic gneisses. The samples collected around the foothills of the Krobo Mountains (KD) composed of mafic gneiss had the lowest radionuclide concentrations. According to Roger and Adams (1969) uranium and thorium are generally enriched in the youngest, most felsic and potassic members of comagmatic suites of igneous rocks.

Table 7.1.Activity concentration of U^{238},Th^{232}, K^{40} and Cs^{137} in the Accra Plains

Sample ID	U-238 ppm ±1σ	Th-232 ppm ±1σ	Ra-226 ppm ±1σ	K % ±1σ	U-238 Bq/Kg	Th-232 Bq/k	Ra-226 Bq/kg	K-40 Bq/kg	Cs-137 Bq/kg
ASH1	5.73 ± 0.41	77.32 ± 0.65	4.93 ± 0.13	5.27 ± 0.08	70.61	314.69	60.84	1628.40	0.86
ASH2	2.81 ± 0.29	70.82 ± 0.62	4.94 ± 0.13	5.64 ± 0.09	34.68	288.22	60.93	1744.17	0.88
CK1	0.61 ± 0.14	2.23 ± 0.11	1.16 ± 0.06	0.65 ± 0.03	7.56	9.07	14.28	199.40	3.12
S1	6.84 ± 0.45	20.96 ± 0.34	5.51 ± 0.13	3.53 ± 0.07	84.35	85.32	67.97	1091.49	<0.1
S3	6.87 ± 0.45	17.12 ± 0.31	4.86 ± 0.12	3.18 ± 0.06	84.74	69.70	59.91	983.10	<0.1
S4	10.99 ± 0.57	18.27 ± 0.32	8.55 ± 0.17	4.78 ± 0.08	135.55	74.35	105.47	1478.36	<0.1
KD2	2.58 ± 0.28	0.11 ± 0.02	0.57 ± 0.04	0.91 ± 0.03	31.76	0.45	6.98	279.99	<0.1
KD3	0.59 ± 0.13	0.35 ± 0.04	0.45 ± 0.04	1.09 ± 0.04	7.25	1.42	5.60	337.37	0.30
KD4	0.70 ± 0.14	3.32 ± 0.13	0.82 ± 0.03	0.50 ± 0.02	8.63	13.51	10.11	154.50	<0.1
RD1B	1.78 ± 0.23	33.35 ± 0.43	1.89 ± 0.08	5.90 ± 0.09	21.92	135.74	23.29	1824.11	<0.1
RD2C	2.59 ± 0.28	6.64 ± 0.19	1.04 ± 0.06	0.69 ± 0.03	31.98	27.04	12.86	214.60	<0.1
RD3B	0.28 ± 0.09	0.27 ± 0.04	0.79 ± 0.05	2.59 ± 0.06	3.48	1.09	9.77	801.46	<0.1
RD3C	1.54 ± 0.21	5.24 ± 0.17	2.19 ± 0.08	2.83 ± 0.06	18.96	21.34	27.06	873.36	<0.1
RD4B	1.32 ± 0.20	0.63 ± 0.06	0.48 ± 0.04	5.00 ± 0.08	16.23	2.58	5.91	1546.10	<0.1
BF72	19.92 ± 0.77	86.29 ± 0.69	21.36 ± 0.26	6.27 ± 0.09	245.56	351.20	263.40	1936.41	<0.1
BF69	29.48 ± 0.94	91.01 ± 0.71	23.93 ± 0.28	6.80 ± 0.09	363.52	370.43	295.01	2100.01	<0.1
BF66	26.03 ± 0.88	80.51 ± 0.67	19.55 ± 0.25	6.66 ± 0.09	320.89	327.66	241.02	2057.32	<0.1
BF63	14.23 ± 0.65	90.44 ± 0.70	21.33 ± 0.26	7.36 ± 0.10	175.49	368.11	262.94	2274.29	<0.1
BF60	11.47 ± 0.59	75.76 ± 0.65	16.07 ± 0.23	6.40 ± 0.09	141.48	308.33	198.13	1977.99	<0.1
BF57	25.54 ± 0.87	75.68 ± 0.64	19.57 ± 0.25	6.78 ± 0.09	314.89	308.01	241.27	2094.26	<0.1
BF54	18.68 ± 0.75	60.96 ± 0.58	19.99 ± 0.25	5.78 ± 0.09	230.31	248.10	246.43	1785.28	<0.1
BF51	25.62 ± 0.88	74.85 ± 0.64	17.56 ± 0.24	3.73 ± 0.07	315.89	304.63	216.49	1153.50	<0.1
BF48	20.97 ± 0.79	53.19 ± 0.54	21.14 ± 0.26	5.85 ± 0.09	258.59	216.48	260.60	1809.16	<0.1
BF45	21.72 ± 0.81	57.27 ± 0.56	15.06 ± 0.22	5.33 ± 0.08	267.77	233.09	185.72	1646.43	<0.1
BF42	25.26 ± 0.87	39.34 ± 0.46	9.45 ± 0.17	4.37 ± 0.07	311.48	160.10	116.51	1351.18	<0.1
BF39	10.98 ± 0.57	47.12 ± 0.51	10.87 ± 0.19	4.29 ± 0.07	135.41	191.80	133.99	1325.21	<0.1
BF36	12.80 ± 0.62	29.71 ± 0.40	8.13 ± 0.16	3.34 ± 0.07	157.84	120.92	100.29	1032.23	<0.1

BF33	4.31 ± 0.36	13.73 ± 0.27	4.32 ± 0.12	2.93 ± 0.06	53.10	55.90	53.23	904.37	<0.1
BF30	27.31 ± 0.90	53.44 ± 0.54	10.29 ± 0.18	2.51 ± 0.06	336.75	217.49	126.92	775.95	<0.1
BF27	10.04 ± 0.55	53.12 ± 0.54	10.75 ± 0.19	5.64 ± 0.09	123.80	216.21	132.59	1743.11	<0.1
BF24	11.26 ± 0.58	21.38 ± 0.34	6.61 ± 0.15	3.72 ± 0.07	138.87	87.02	81.45	1148.37	<0.1
BF21	16.20 ± 0.70	50.33 ± 0.53	11.69 ± 0.19	3.32 ± 0.07	199.77	204.83	144.14	1024.57	<0.1
BF18	8.41 ± 0.50	15.60 ± 0.29	3.72 ± 0.11	2.58 ± 0.06	103.64	63.51	45.83	797.08	<0.1
BF15	11.33 ± 0.58	21.02 ± 0.34	7.72 ± 0.16	4.43 ± 0.08	139.76	85.57	95.19	1370.30	<0.1
BF12	7.85 ±0.49	25.53 ± 0.37	6.66 ± 0.15	3.81 ± 0.07	96.85	103.93	82.13	1175.78	<0.1
BF9	11.77 ± 0.59	42.87 ± 0.49	7.53 ± 0.16	2.65 ± 0.06	145.14	174.48	92.86	817.35	<0.1

Table.7.2. Descriptive statistics of the samples activity concentration in Bq/Kg

		U^{238}	Th^{232}	Ra^{226}	K^{40}
Mean		1.43E+2	1.60E+2	1.13E+2	1.26E+3
Median		1.35E+2	1.48E+2	94.03	1.25E+3
Mode		3.48[a]	.45[a]	5.60[a]	154.50[a]
Std. Deviation		1.12E+2	1.22E+2	9.07E+1	5.97E+2
Variance		1.25E+4	1.49E+4	8.22E+3	3.56E+5
Minimum		3.48	.45	5.60	154.50
Maximum		363.52	370.43	295.01	2274.29
Sum		5134.50	5762.32	4087.12	4.55E4
Percentiles	25	32.650	57.8025	31.75	8.31E2
	50	1.35E2	1.48E2	94.03	1.25E3
	75	2.42E2	2.78E2	1.95E2	1.77E3

a. Multiple modes exist. The smallest value is shown

Table.7.3. Descriptive statistics of the BF samples (Bq/Kg)

	U^{238}	TH^{232}	Ra^{226}	K^{40}
Mean	2.08E+2	2.14E+2	1.64E+2	1.47E+3
Median	1.88E+2	2.16+2	1.39E+2	1.36E+3
Std. Deviation	9.16E+1	1.01E+2	7.83E+1	4.87E+2
Minimum	53.10	55.90	45.83	775.95
Maximum	363.52	370.43	295.01	2274.29
Sum	4576.80	4717.80	3616.14	3.23E+4

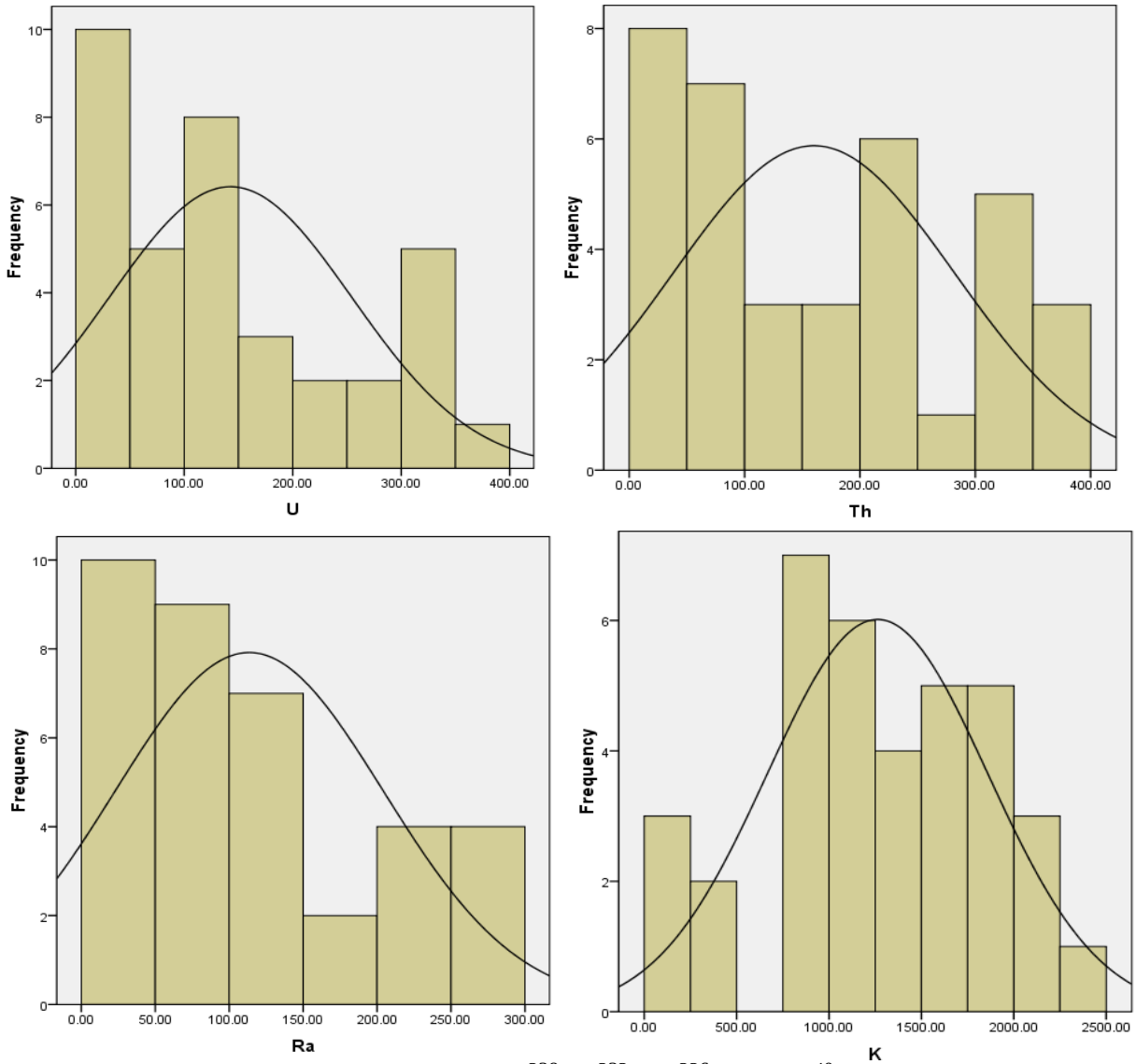

Figure 7.1. (a-d) Frequency distribution of ^{238}U, ^{232}Th, ^{226}Ra, and ^{40}K activity concentration in the Accra Plains.

The activity concentration of ^{40}K was found to be higher than the other radionuclides (Fig.7.2). The ^{40}K concentration increased with depth from 30m to 63m deep (Fig.7.3). The concentrations of ^{232}Th also increased marginally with depth from 33m to 72m. Thus suggesting there is a relatively increase in activity concentration of the radionuclides with depth.

The concentration of ^{238}U in the BF rock samples ranged from 53.1 to 363.5 Bq/kg. The KD rock samples had ^{238}U concentration ranging from 7.25 to 31.8Bq/kg whilst the RD rock samples from Ghacem factory in Tema had ^{238}U concentration ranging from 3.48 to 32Bq/kg. The rock samples from Ashiaman had ^{238}U concentration ranging from 34.7 to 70.6Bq/kg. The concentrations of ^{238}U in the shale soil (S) samples varied from 84.3 to 135.5Bq/kg whilst the clay sample (CK) collected from Okwenya had ^{238}U concentration of 7.6Bq/kg. The rock samples from GAEC and Ashiaman as well as the shale samples from Accra had higher ^{238}U concentration than the world mean ^{238}U concentration of 35Bq/kg for rock/soil as reported in the UNSCEAR Report (2000).

The BF rock samples had ^{232}Th concentration ranging from 55.90 to 370.43 Bq/kg whilst the KD samples had ^{232}Th concentrations ranging from 0.45 to 13.51Bq/kg. The RD rock samples from Tema had ^{232}Th concentration ranging from 1.09 to 135.74Bq/kg. The ASH samples from Ashiaman had ^{232}Th concentration ranging from 288.22 to 314.69/kg. The concentrations of ^{232}Th in the shale soil samples varied from 69.70 to 85.32/kg whilst the clay sample collected from Okwenya had a ^{232}Th concentration of 9.07Bq/kg. The world mean ^{232}Th concentration for rock/soil is 32Bq/kg (UNSCEAR 2000) indicating high ^{232}Th concentrations in the samples from BF, Ashiaman, Tema and the shale samples from Accra.

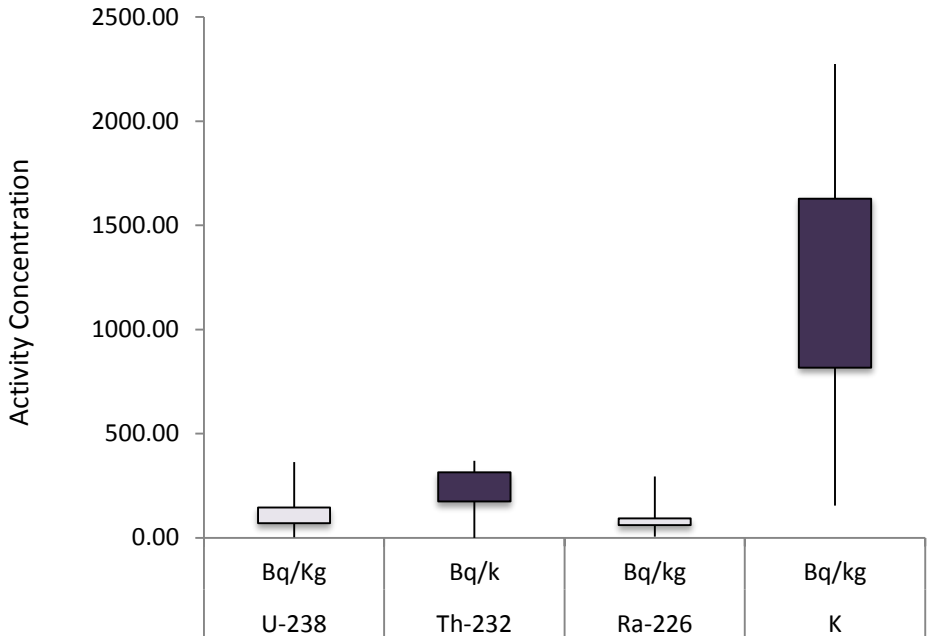

Figure 7.2 Variation in the activity concentration of ^{238}U,$^{232}Th$$^{226}Ra$ and ^{40}K

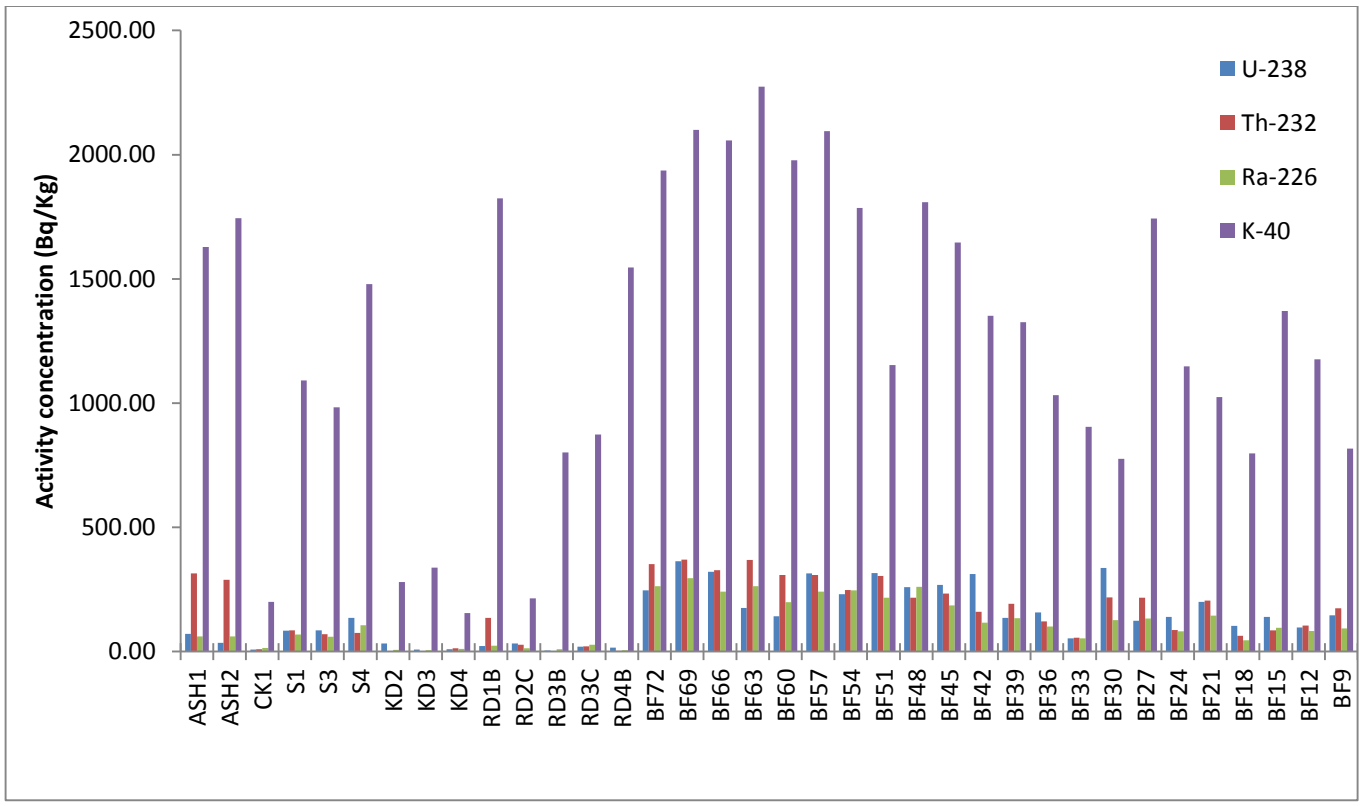

Figure.7.3. Activity concentration of ^{238}U,$^{232}Th$$^{226}Ra$ and ^{40}K at sample location

The ^{226} Ra concentrations for the BF samples ranged from 45.83 to 295.01 Bq/kg. The KD and RD samples had ^{226}Ra concentrations ranging from 4.04 to 10.11 Bq/kg and 5.91 to 27.06 Bq/kg respectively. The ASH rock samples had a mean ^{226}Ra concentration of 60.88 Bq/kg whilst the clay sample from Okwenya had a ^{226} Ra concentration of 14.28 Bq/kg. The ^{226}Ra concentration for the shale soil samples varied from 59.91 to105.47 Bq/kg.

The concentration of ^{40}K in for the BF rock samples ranged from 776.0 to 2274.3 Bq/kg. The KD samples had ^{40}K concentration ranging from 145 to 377.4 Bq/kg whilst the RD samples had concentrations ranging from 214.6 to 1824.1Bq/kg. The ASH samples had ^{40}K concentration ranging from 1628.4 to 1744.2 Bq/kg. The concentrations of ^{40} K in the shale soil samples varied from 983.1 to 1478.4 Bq/kg whilst the clay (CK) sample had a concentration of 199.3 Bq/kg. The worldwide mean ^{40}K concentration reported by UNSCEAR (2000) is 400Bq/kg. The rock types investigated had potassium values higher than the worldwide mean value except for the KD rock samples.

^{137}Cs is a man-made high specific –activity long-lived radionuclide. It does not exist naturally in soil, sand and its source rocks but as product of radioactivity fallout. It is strongly absorbed to small soil and clay particles. The concentration range for ^{137}Cs is from 10 to 1000Bq/kg (El-Dine *et al* 2004). Most of the ^{137} Cs concentrations in this study were below the lowest detection limit. However, low concentrations were found in the ASH samples and the clay (montmorillonite) sample from Okwenya as well as in one of the KD rock samples from the foothills of the Krobo Mountain.

7.1.1. Distribution of Thorium, Uranium, and Potassium

The relationship between the thorium (Th), uranium (U), radium (Ra) and potassium (K) concentrations and the total activity concentration in the samples are diagrammatically shown in figure 7.4.(a-d) and by Pearson correlation matrix in Table 7.4. Good correlation exists between ^{232}Th and the total activity concentration for all the samples with correlation coefficients of 0.955. The BF samples had correlation coefficients (R^2) of 0.965 for ^{232}Th and 0.975 for ^{226}Ra (Table 7.5). The ^{238}U and ^{40}K activity concentrations had a fairly good correlation with the total activity concentration with correlation coefficients of 0.844 and 0.846 respectively. This implies that ^{232}Th and ^{226}Ra contributed significantly to the total radioactivity in the geological formation in the Plains.

Table 7.4 Pearson correlation matrix for all the samples

	U	Th	Ra	K	Total activity
U 238	1	.723**	.856**	.537**	.844**
Th 232	.723**	1	.858**	.791**	.955**
Ra 226	.856**	.858**	1	.745**	.955**
K 40	.537**	.791**	.745**	1	.846**
Total activity	.844**	.955**	.955**	.846**	1

**. Correlation is significant at the 0.01 level (2-tailed)

Table 7.5 Pearson correlation matrix for the BF samples

	U	Th	Ra	K	Total
U	1	.651**	.672**	.386	.738**
Th	.651**	1	.919**	.777**	.965**
Ra	.672**	.919**	1	.843**	.975**
K	.386	.777**	.843**	1	.848**
Total	.738**	.965**	.975**	.848**	1

**. Correlation is significant at the 0.01 level (2-tailed).

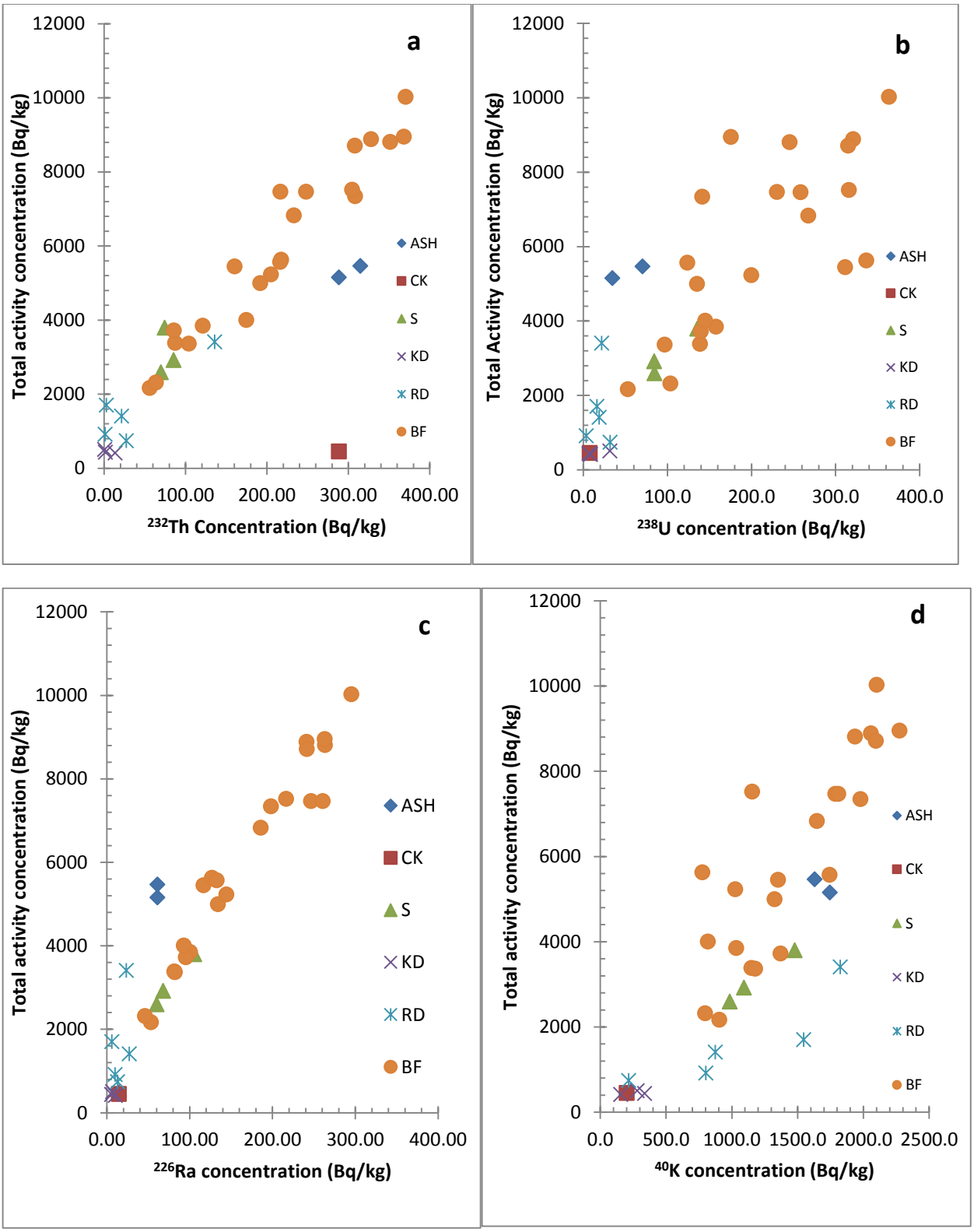

Figure7.4 (a-d) The total activity concentration vs individual radionuclide activity concentration

The thorium and uranium content binary diagram illustrated in figure 7.5 (a) show, a trend indicating relatively increase in thorium concentration with increase in uranium concentration although there is no real correlation between them. However the thorium and radium contents binary diagram (Fig 7.5 (b)) show a remarkable increase in thorium concentration with corresponding increase in radium concentration especially for the BF samples. This indicates a strong correlation between the radionuclides. There was slight increase in uranium concentration with increasing potassium concentration, but the points are very diffuse (Fig. 7.5 (d)). This behaviour suggest relatively high mobility of U isotopes due to the formation of uranyl-anion complexes such as $(UO_2)(CO_3)_3^{-4}$ (Kraemer and Kharaka, 1986; Langmuir, 1978). Uranium has an insoluble tetravalent state that is fixed under reducing conditions, but is transformed to the soluble hexavalent state which may be mobilized into solution. In contrast, thorium has a single insoluble tetravalent state which is geochemically associated with uranium and therefore is a useful standard for comparison purposes (Anjos *et al* 2005). The binary diagram (Fig.7.5 (c)) however showed increase in thorium concentration with increase in potassium concentration. This was more evident in the BF samples.

The original concentrations of uranium, thorium and potassium in rocks may vary because of alteration or metamorphic processes (Verdoya *et al.,* 2001). The Th/U ratio is useful in the recognization of geochemical facies. The ratio gives an indication of the relative depletion or enrichment of the radioisotopes (caused by primary dissolution and by secondary mineral formation). The main factors that influence the mineralogical structure of a rock are the bulk composition of the rock, the pressure and temperature conditions at the time of crystallization and the composition of the fluid phase in the rock during metamorphism. The bulk composition

of the metamorphic rock may be inherited from the original sedimentary or igneous precursor, or may be chemically altered by metasomatic activity during the metamorphic process.

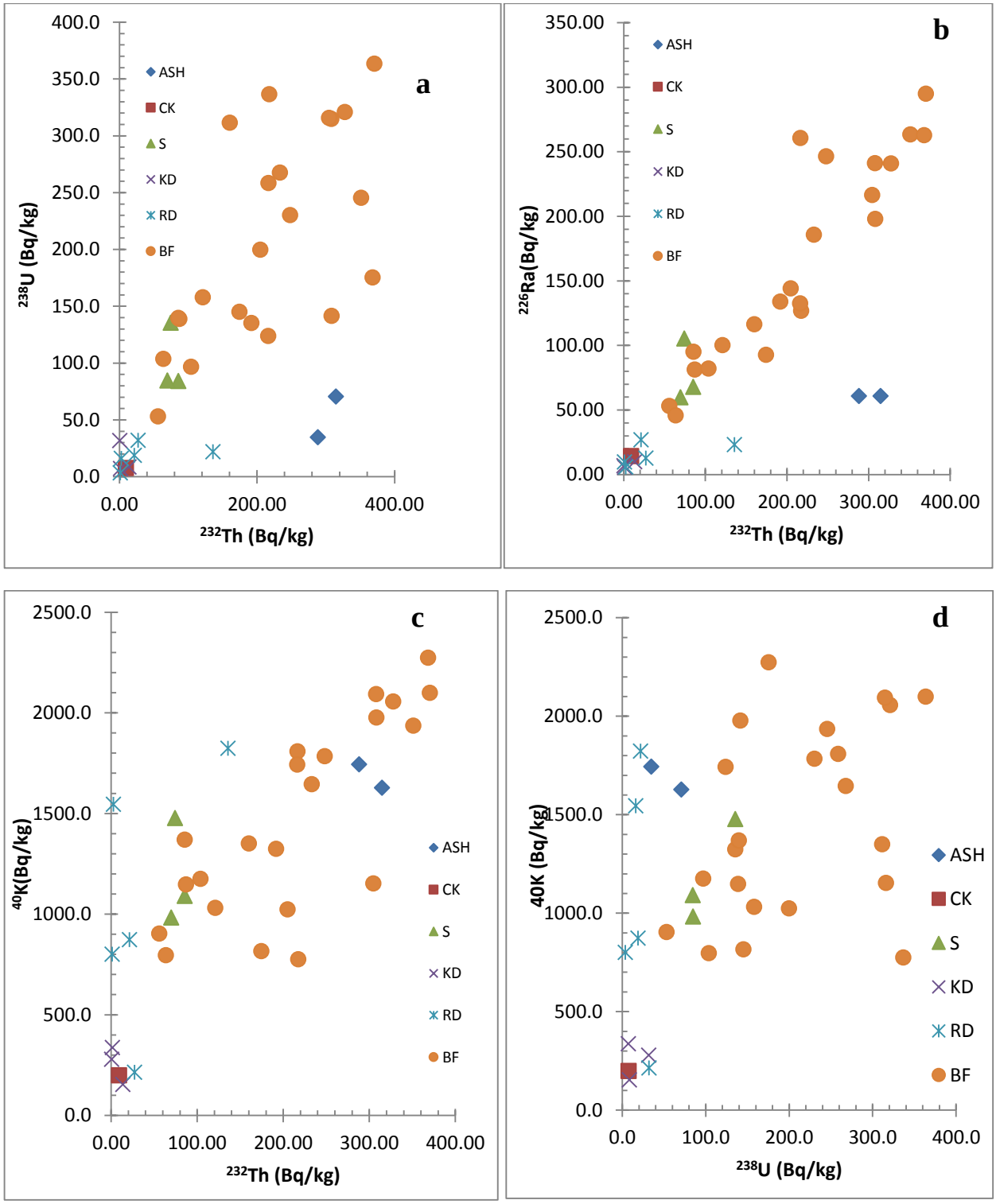

Figure 7.5. (a-d) Variation diagramms of the radionuclides

Th/U ratio for continental crust varies from 3.84–4.2 (Plant and Saunders, 1996). Adams and Weaver (1958) suggested that Th/U ratios less than 2 are highly suggestive of relative uranium enrichment and implicates reducing conditions as contrasted with ratios greater than 7, which indicates preferential removal of uranium possibly by leaching. According to Orgun *et al*. (2005), higher ^{238}U activity concentration than ^{232}Th activity concentration belongs to the category of silica-oversaturated rocks (>70 SiO_2wt %). ^{232}Th activity concentrations are generally higher than ^{238}U activity concentrations of the granitic and volcanic samples (Orgun *et al*., 2007).

The Th/U values obtained in this study are generally low except for the samples collected at Ashiaman (Table7.6) thus indicating some type of preferential enrichment of thorium in the crustal materials. The Th/U ratios for the BF samples varied from 1.56 to 6.60 with an average value of 3.27. Most of the values are generally less than the typical values for many granitic rocks of 4.2. They indicate fractures and high degree of alternation (Smellie *et al* 1986).

Table.7.6 Activity ratios for the geological samples from the Accra Plains

Sample ID	Location	Th/U	Th/Ra	Th/K	U/Ra	U/K	Ra/K
ASH1	Ashiaman	13.50	15.67	14.67	1.16	1.09	0.94
ASH2	Ashiaman	25.18	14.33	12.55	0.57	0.50	0.88
CK1	Okwenya	3.64	1.92	3.45	0.53	0.95	1.79
S1	Accra	3.06	3.80	5.93	1.24	1.94	1.56
S3	Accra	2.49	3.52	5.38	1.41	2.16	1.53
S4	Accra	1.66	2.14	3.82	1.29	2.30	1.79
KD2	Krobo Mts	0.04	0.19	0.12	4.55	2.84	0.62
KD3	Krobo Mts	0.60	0.77	0.32	1.29	0.54	0.42
KD4	Krobo Mts	4.74	4.05	6.64	0.85	1.40	1.64
RD1B	Tema	18.76	17.66	5.65	0.94	0.30	0.32
RD2C	Tema	2.56	6.37	9.57	2.49	3.73	1.50
RD3B	Tema	0.95	0.34	0.10	0.36	0.11	0.31

RD3C	Tema	3.41	2.39	1.85	0.70	0.54	0.78
RD4B	Tema	0.48	1.32	0.13	2.75	0.26	0.10
BF72	GAEC	4.33	4.04	13.77	0.93	3.18	3.41
BF69	GAEC	3.09	3.80	13.39	1.23	4.34	3.52
BF66	GAEC	3.09	4.12	12.09	1.33	3.91	2.94
BF63	GAEC	6.35	4.24	12.29	0.67	1.93	2.90
BF60	GAEC	6.60	4.71	11.83	0.71	1.79	2.51
BF57	GAEC	2.96	3.87	11.17	1.31	3.77	2.89
BF54	GAEC	3.26	3.05	10.55	0.93	3.23	3.46
BF51	GAEC	2.92	4.26	20.05	1.46	6.86	4.70
BF48	GAEC	2.54	2.52	9.08	0.99	3.58	3.61
BF45	GAEC	2.64	3.80	10.75	1.44	4.08	2.83
BF42	GAEC	1.56	4.16	9.00	2.67	5.78	2.16
BF39	GAEC	4.29	4.34	10.99	1.01	2.56	2.53
BF36	GAEC	2.32	3.65	8.89	1.57	3.83	2.43
BF33	GAEC	3.19	3.18	4.69	1.00	1.47	1.47
BF30	GAEC	1.96	5.19	21.28	2.65	10.88	4.10
BF27	GAEC	5.29	4.94	9.42	0.93	1.78	1.91
BF24	GAEC	1.90	3.24	5.75	1.71	3.03	1.78
BF21	GAEC	3.11	4.31	15.18	1.39	4.89	3.53
BF18	GAEC	1.86	4.20	6.05	2.26	3.26	1.44
BF15	GAEC	1.85	2.72	4.74	1.47	2.56	1.74
BF12	GAEC	3.25	3.83	6.71	1.18	2.06	1.75
BF9	GAEC	3.64	5.69	16.21	1.56	4.45	2.85

The KD samples had relatively high U concentration than Th and thus reflected in the generally low Th/U mass ratios except KD 4. The extreme values (0.04 and 0.60) indicate U mineralization accompanying oxidation. The shale samples had a low Th/U ratio owing to their high uranium content.

The relative U enrichment suggests reducing condition and precipitation of UO_2. Uranium is usually transported in oxidizing fluids in the hexavalent state as uranyl ion (UO_2^{2+}) and as soluble uranyl complexes including carbonate. The presence of ferric iron in the rocks (magnetite) indicates the oxidizing capacity of the rocks and will aid in the transportation of U.

In the presence of dissolved oxygen, the Fe^{2+} can be oxidized and precipitated as ferric oxyhydroxide.

In the near surface environment, where the samples were collected, an open geochemical system may prevail due to low temperature alteration, weathering and groundwater infiltration. Thus the U has been enriched at a lower level relative to Th due to weathering, high alteration of the near surface rocks and under the prevailing oxidizing environment.

The samples from Ashiaman had high Th/U with an average value of 19.34 reflecting high Th concentration and preferential removal of uranium by leaching through groundwater infiltration.

Plots of thorium against potassium are almost invariably quite linear. Thorium occurs in nature only as the tetravalent ion. The close association of thorium and potassium in a wide variety of rocks, however, together with the concentration of all radioactive materials toward the outer part of the earth indicates that thorium is probably closely coordinated with oxygen ions (Bayer *et al*, 1969). This coordination complex provides the low density necessary for upward migration which the individual thorium ions would not show. The potassium – thorium plot is widely used for the recognition of clay minerals associations and the discrimination of micas and feldspars (Anjos *et al* 2005). As both thorium (by adsorption) and potassium(chemical composition) are associated with clay minerals, the ratio Th/K expresses relative potassium enrichment as an indicator of clay minerals species, and as might be diagnostics of other radioactive minerals. Low ratio (high potassium) feldspars and micas are contrasted with high ratio illite, smectite, kaolinite and chlorite. The Th/K ratios for the BF and ASH samples composed of felsic gneiss

were high whilst the ratios for KD and some of the RD samples are low. The extremely high concentration of thorium is noteworthy in view of the general tendency for thorium and potassium to occur together.

7.1.2. Radiological effects

The main objective of measuring radioactivity is to make an estimate of radiation doses likely to be delivered externally to the general public. The contribution of natural radionuclides to the absorbed dose rate in air depends on the concentrations of the radionuclides in the rock and soil.

The calculated absorbed dose rates are presented in Table 7.7. The absorbed dose rates varied from 96.00 to 479.26 nGy/h for the BF samples, 262.84 to 290.59 nGy/h for the ASH samples, 122.24 to 169.17 nGy/h for the shale soil samples, 18.27 to 26.62 nGy/h for the KD samples and from 35.68 to 168.18nGy/h for the RD samples. According to UNSCEAR (2000) report, the dose rate in air outdoors from terrestrial gamma-ray in normal circumstances is about 57nGy/h. Thus the absorbed dose rate values for the samples were higher except for the KD samples. The largest contributor to the absorbed dose in air was from ^{232}Th. Figure 7.6. illustrates the measured relative contribution to the total dose outdoors for the BF samples which had the highest dose rates.

The annual effective dose equivalent (AEDE) was calculated from the absorbed gamma dose rate using the conversion coefficient from absorbed dose in air to the effective dose (0.7Sv/Gy) and

the outdoor occupancy factor (0.2). The AEDE values for the samples were high (Table 7.7.) as the world average annual effective dose is approximately 70Sμv/y (UNSCEAR, 2000).

Table. 7.7. Absorbed dose rate (D), Annual effective dose equivalent (AEDE), External hazard index (H_{ex}) and Radium equivalent activity (Ra_{eq}) for the rock and soil samples

ID	Absorbed dose rate (D) nGy/h	Annual Effective Dose equivalent (AEDE) mSv/y	External hazard index (Hex)	Radium equivalent activity Ra_{eq} Bq/kg
ASH1	290.59	0.36	1.72	636.23
ASH2	262.84	0.32	1.64	607.39
CK1	17.28	0.02	0.11	42.6
S1	136.01	0.17	0.74	274.02
S3	122.24	0.15	0.63	235.27
S4	169.17	0.21	0.88	325.62
KD2	26.62	0.03	0.08	29.18
KD3	18.27	0.02	0.09	33.61
KD4	18.59	0.02	0.11	41.33
RD1B	168.18	0.21	0.97	357.86
RD2C	40.05	0.05	0.18	68.05
RD3B	35.68	0.04	0.2	73.03
RD3C	58.06	0.07	0.34	124.81
RD4B	73.53	0.09	0.35	128.64
BF72	406.32	0.50	2.47	914.73
BF69	479.26	0.59	2.66	986.43
BF66	431.95	0.53	2.34	867.99
BF63	398.25	0.49	2.6	964.45
BF60	334.07	0.41	2.14	791.34
BF57	418.85	0.51	2.28	842.98
BF54	330.7	0.41	1.99	738.68
BF51	378.04	0.46	2.00	740.93
BF48	325.67	0.40	1.92	709.47
BF45	333.15	0.41	1.74	645.81
BF42	296.95	0.36	1.21	449.49
BF39	233.66	0.29	1.38	510.3
BF36	189.01	0.23	0.95	352.7
BF33	96.00	0.12	0.55	202.8
BF30	319.3	0.39	1.34	497.68
BF27	260.47	0.32	1.55	575.98
BF24	164.6	0.20	0.79	294.31
BF21	258.73	0.32	1.39	515.93

BF18	119.48	0.15	0.53	198.02
BF15	173.39	0.21	0.87	323.06
BF12	156.55	0.19	0.87	321.28
BF9	206.52	0.25	1.09	405.3

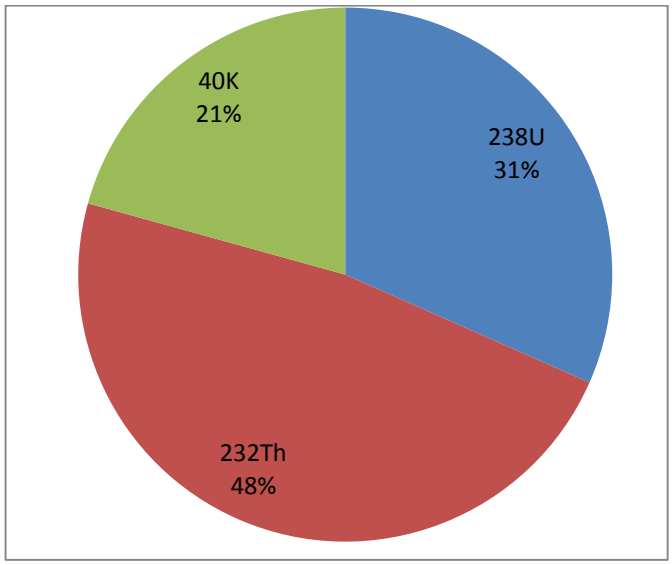

Figure 7.6. Relative contribution to absorbed dose rate in air outdoors for the BF samples

Despite the high AEDE values, the Accra Plains can be classified as a low-level natural radiation area (LLNRA) in accordance with the classification scheme proposed by Sohrabi (1998). According to the classification scheme, a LLNRA is an area or a complex of dwelling where potential public exposure fails below or equal to twice the average global annual effective dose from natural sources, i.e. by UNSCEAR report 1993,

$$2 \times 2.4 = 4.8 \text{ mSv/y or} \approx 5\text{mSv/y}. \quad (7.1)$$

In areas with the normal background radiation, the average annual external effective dose rate from the terrestrial radionuclides is 0.46 mSv/year (Mohanty *et al.*,2004; Bennett, 1997)

The calculated gamma ray radiation hazards due to the specified radionuclides assessed by two different indices, the radium-equivalent activity and external radiation hazard are shown in table. The permissible value of Ra_{eq} is ≤ 370 Bq/kg (El-Galy *et al*, 2008). The mean calculate Ra_{eq}values for GAEC and Ashiaman samples were higher than the permissible values. The GAEC values increased with depth indicating increase in the risk hazard with depth.

The external hazard index (H_{ex}) was used to measure the external hazard due to the emitted gamma radiation. It indicated high external hazard indices for the BF samples which increased with increase in depth. The samples from Ashiaman also had external hazard indices greater than one (1).

7.2. Conclusion

The relative enrichment of the radionuclides is K > Th > U > Ra. The median activity of ^{238}U, ^{232}Th, and ^{40}K for the samples were higher than world median value of rocks except for the activity concentrations of the rock samples collected around the Krobo Mountains and Tema which may be due to high alteration and weathering of the rocks. The activity concentration of ^{40}K was found to be higher than the other radionuclides. The high ^{40}K concentration may be due to high potassium feldspar mineral contents in the samples. The highest radionuclide concentrations were measured in the rock samples collected from GAEC (BF) premises which were composed mainly of felsic gneisses. The samples collected around the foothills of the Krobo Mountains (KD) composed of mafic gneiss had the lowest radionuclide concentrations.

Minimum concentrations of ^{137}Cs were only found in the samples collected at Ashiaman, Okwenya as well as in one of the rock samples from the foothill of the Krobo Mountains.

^{232}Th and ^{226}Ra contributed significantly to the total radioactivity in the geological formation in the Plains. The Th/U values obtained in this study are generally low except for the samples collected at Ashiaman thus indicating preferential enrichment of thorium in the crustal materials. The Th/U ratios for the samples collected from the borehole drilled at GAEC varied from 1.56 to 6.60 with an average value of 3.27. The relative U enrichment suggests reducing condition and precipitation of UO_2.

The samples from Ashiaman had high Th/U with an average value of 19.34 reflecting high Th concentration and preferential removal of uranium by leaching through groundwater infiltration. The possible loss of uranium may due to oxidation of uranium to the uranyl ion during the evolution of suites of the rocks. This conclusion is based on the assumed greater solubility of uranyl ion than of tetravalent uranium or thorium in the volatile igneous phase. It is however possible that fractionation occurs between the tetravalent U and Th ions, for the two ions are not identical, though they are quite similar. The presence of ferric iron (magnetite) in the rocks indicate the oxidizing capacity of the rocks which will aid in the transportation of U.

The dominant U removal process was probably leaching from the minerals into the groundwater whilst the U gain displayed may be a result of the interaction of groundwater enriched in uranium. The results provide a qualitative assessment of radionuclide behaviour and indicate that groundwater form the principal pathways for radionuclide mobilization. As analogues of the

actinides, the mobilization of U and Th implies that they cannot be assumed to be immobile in the far-field of a geological formation in a repository environment. The sites of rock/radionuclide interaction in the repository environment may be influenced by the mineralogical assemblages which are present and the physico-chemical processes which are imposed by the specific geochemical conditions of the repository. The iron minerals phases in the geological formation will create an oxidizing environment.

Groundwater natural radioactivity investigation need to be carried out to determine the degree of disequilibrium which defines the time elapsed since the disequilibrium formed. The nature of rock-radionuclide interaction and the geochemical processes which determine the radionuclide behavior and cause of the disequilibrium between the naturally occurring isotopes need to be studied in details.

Chapter Eight

8.0. Conclusion

The aim of this dissertation is to characterize the hydrogeochemical conditions of the rocks of the Accra Plains and to verify their desired favourable and stable hydrogeochemical conditions for a repository. A combined study of the mineralogical composition of the rocks, groundwater chemistry, mineral saturation of the groundwater, and distribution of stable isotopes were used to characterize the hydrogeochemical processes that control the chemistry of the groundwater. The major ions of the groundwater contain signatures of the whole history of the groundwater and the reaction of the groundwater with the surrounding mineral assemblages over the long period of time.

The nature and distribution of rock formations and the hydrogeological system have an important influence in the spatial distribution and geochemistry of the groundwaters. The mineralogical composition of the geological formation in the Accra Plains was carried out to deduce its influence on the groundwater geochemistry as well as alternation of the individual minerals.

Geochemical investigations provide valuable information on the groundwater conditions. The geochemical characterisation of the groundwaters aided in the evaluation of

- the chemical composition of the groundwaters in the rocks; and
- the geochemical processes affecting groundwaters (water/rock interaction,)

The stability of the buffer and backfill material of a radioactive waste repository are influenced by the concentrations of Na^+, Ca^{2+} and Mg^{2+} in the groundwater. Analyses of the groundwaters in Accra Plains show that, the concentrations of calcium and magnesium which together constitute 48% of the total cations in the groundwater will provide a stable chemical environment for a backfill and buffer materials.

The dominance of Cl and Na and the low concentration of HCO_3 in the major ion composition of the groundwaters were typical characteristics of the Scandinavian and Canadian Shields groundwaters which is being investigated as a host rock for a radioactive waste repository.

The hydrogeochemical characteristics of the groundwater are as a result of water-rock interaction (silicate weathering) along the flow path. The groundwaters pick up and increase dissolved load through mineral dissolution and hydrolysis of primary the minerals (plagioclase and the ferromagnesium minerals) with the generation of clays (kaolinite and montmorillonite) and other minerals as well as ionic compounds. Reverse ion exchange also controlled the chemical composition of the groundwater especially along the coastal areas of the Plain.

The stability diagram shows that the groundwater plots in the stability fields of kaolinite and montmorillonite. At low concentrations, the cationic species are associated with kaolinite. However with increasing ionic content and TDS, the groundwaters tend to reach and follow the kaolinite-montmorillonite boundary and eventually to the montmorillonite stability field. This implies that the chemistry of the groundwater favours the formation of kaolinite and montmorillonite which are suitable backfill and buffer materials for a radioactive waste repository.

Environmental stable isotopes (oxygen-18 and hydrogen-2) analyses were used to evaluate the hydrogeological characteristics of the aquifer systems of the crystalline basement rocks setting of the Accra Plains. The relation between $\delta^{2}H$ and $\delta^{18}O$ with respect to the global meteoric water (GMWL) line and the local meteoric water line (LMWL) shows majority of the samples plotting between the GMWL and the LMWL with the others plotting away from these lines. This suggests that meteoric water is the main recharge source to the groundwater system. The recharge takes place in fracture in the geologic formation but under the semi-arid conditions, the groundwaters undergo evaporation where the water can be lost from the unsaturated zone or from the water table. Thus the recharge of partially evaporated water, with an enriched isotopic signature takes place in some areas. The groundwater is also affected by the mixing of various rainfall events and/or surface runoff. In contrast recharge in other areas seems to take place rapidly, possibly via preferred pathways, preventing any significant evaporation.

Gamma spectrometry was used to determine the abundance and distribution of natural occurring radionuclides (U, Th and K) in the geological formation in the Accra Plains. Analyses of the natural radionuclide distribution were used in the prediction of the radionuclide behavior in the aquifer. Understanding of the geochemical processes which determine the distribution of the natural radionuclide assist in the prediction of radionuclide behaviour in the waste disposal environment

The hydrogeochemical conditions of the rocks of the Accra Plains indicate that, the area between the Akwapim Togo and the Valley View University is unsuitable for a radioactive waste repository due to the presence of preferential channels or routes that will lead to easy saturation of a radioactive waste repository developed in that area with groundwater recharged at the

Akwapim Togo Mountains. Secondly, the pH of the groundwater measured at the Valley View University was lower than the required pH conditions for a radioactive waste repository. The pH condition of the groundwaters will facilitate the corrosion of the waste containers, degradation of the engineered barriers as well as sorption and solubilities leaking radionuclides.

The hydrogeochemical conditions of the rocks at Okwenya and the foothills of the Krobo Mountains were found to be favourable for a radioactive waste repository. Reducing condition is a requirement for the repository environment. The mafic gneiss at Okwenya and the foothills of the Krobo Mountains contains redox-sensitive minerals, such as magnetite, biotite, chlorite, and amphiboles. Reactions involving these minerals with groundwater would provide a reducing conditions in the aquifer required for a repository.

The clay mineral, montmorillonite identified in the rock at Okwenya and the foothills of the Krobo Mountains will remain stable for a long period of time. The long time stability of these minerals together with their ion exchange properties which can retard the migration of long-lived radionuclides makes them a useful backfill and or buffer material for a radioactive waste repository. The groundwater conditions will also provide a stable chemical environment for the montmorillonite clay minerals as a backfill and buffer materials.

8.1. Recommendation

The structural geology of the Plains needs to be investigated in details to determine site within the Plains with dual permeability, dual porosity and high hydraulic conductivity. This is will help avoid developing radioactive waste repository on those sites. An example is the Valley View University site at Oyibi.

Weathering of the primary alumino-silicate minerals will results in the production of clay minerals, montmorillonite and kaolinites. In view of the importance of these clay minerals, as a good buffer and backfill materials, weathering of the primary alumino-silicate minerals and the hydrogeochemical characteristics of all the clay formations of the clay Accra Plains should be studied.

The radiation releases of Na, K, Ca and Cs increase constantly with an increase in absorbed dose of water. The most abundant minerals in the geological formation are feldspar and ferromagnesium minerals. They contribute to the Na and Ca content of the groundwater due to weathering of the minerals. The gamma-rays produced by the waste may accelerate the weathering of these minerals by interaction with the groundwater and thus increase their concentration in the groundwater. Radiolysis may cause changes in the mineralogical composition of these minerals and reduce their longlife time dissolution rate. Thus the effect of radiolysis on the geological formation needs to be investigated.

The use of geochemistry to predict the possible long-term movement of radionuclides over distances of several kilometers is far from straightforward, particularly in fractured rocks.

Certainly, the mere presence of brackish groundwater, water with a high pH, etc., suggests a sluggish groundwater system. These geochemical conditions do not develop rapidly and suggest water ages in thousands of years. This would be a useful qualitative conclusion for many purposes. But quantitative conclusions should be provided. This requires detailed studies with reliable indicators of water age, rates and directions of regional groundwater flow such as ^{3}H, ^{14}C, ^{39}Ar, and ^{36}CI,

Sorption can occur on the surfaces of microfractures inside the rock matrix, i.e. combined with matrix diffusion, and on larger fracture surfaces in direct contact with the flowing water. These mechanisms are a prerequisite in order for the rock to provide meaningful retardation of radionuclides released from defective waste containers. The sorption of radionuclides dissolved in the groundwater is described by the sorption coefficient K_d, which indicates the distribution of radionuclides between the water and the rock. The K_d values are radionuclide-specific and are furthermore dependent on the groundwater chemistry. In principle, they are also dependent on the composition of the rock, The K_d values are thereby only indirectly site-specific, via the composition of the groundwater. Hence sorption studies on the geological formation in the Plains should be carried out.

REFERENCES

1. Adams, J.A., Osmond, J. K. and Rogers, J. J. W., (1959). The geochemistry of uranium and thorium. *Phys. Chern. Earth* 3, 298.

2. Adams, J.A. and Weaver, C.E. (1958). Thorium-uranium ratios as indicators of sedimentary processes: example of concept of geochemical facies. *Bulletin American Association of Petroleum Geologists* 42(2), 387-430.

3. Akiti, T.T., (1980). Etude Géochimique et Isotopique de quelques aquifères au Ghana: gneiss de la Plaine d'Accra, calcaire de la Plaine SE de la Volta, granite de la Haute Région PhD Thesis, Université Paris-Sud, Orsay France, 345 pp

4. Akiti, T. T**., (**1977). Groundwater flow in weathered granite in the Tamne basin, North Eastern Ghana.

5. Akiti, T.T., Bondesen, E., and van Landewijk, J.E.J.M., (1972). Pseudo conglomerates and carbonatitic rocks of the Kpong area, East Ghana. Paper read at the 8th biennial conference of the *West African Science Association* at Lagos

6. Allard, B., (1982). Sorption of actinides in granitic rock, Swedish Nuclear Fuel and Waste Management Co (SKB), Stockholm, TR-82-21.

7. Allen, B.L. and Hajek, B.F. (1989). Mineral occurrence in soil environments. In: Dixon JB & Weed SB (eds) *Soils in Mineral Environments*, 2nd edn. Soil Science Society of America, Madison, Wisc. pp 199-278,

8. Andersson, J., Ström, A., Svemar, C., Almén, K.-E., Ericsson, L. O. 2000. What requirements does the KBS-3 repository make on the host rock? *Geoscientific suitability indicators and criteria for siting and site evaluation*. Swedish Nuclear Fuel and Waste Management Co (SKB), Stockholm, 189, TR-00-12, 148 p.

9. Anjos, R., Veiga, R., Soares, T., Santos, A., Aguiar, J., Frascac, M., Brage, J.,Uzeda, D., Mangia, L., Facure, A., Mosquera, B., Carvalho, C.and Gomes, P. (2005). Natural radionuclide distribution in Brazilian commercial granites. *Radiat. Meas*. 39, 245–253.

10. Appelo C.A.J. and Postma,D. (2005). Geochemistry, groundwater and pollution, Balkema, The Netherlands

11. AquaChem software vers.4.0, (2003). Hydrochemical data analysis, plotting and modelling, Waterloo Hydrogeologic

12. Attoh, K., Corfu, F., Prosper M. Nude, P.M., (2007). U-Pb zircon age of deformed carbonatite and alkaline rocks in the Pan-African Dahomeyide suture zone, West Africa, *Precambrian Research* 155, 251–260

13. Attoh, K., (1998). High-pressure granulite facies metamorphism in the Pan-African Dahomeyide orogen, *West Africa. J. Geol*. 106, 236–246.

14. Attoh, K., Dallmeyer, R.D. and Affaton, P., (1997). Chronology of nappe assembly in the Pan-African Dahomeyide orogen: evidence from 40Ar/39Ar mineral ages. *Precambrian Res.* 82, 153–171.

15. Beaucaire, C., Michelot, J.-L., Savoye, S. and Cabrera, J. (2008). Groundwater characterisation and modelling of water–rock interaction in an argillaceous formation (Tournemire, France) *Applied Geochemistry* 23, 2182–2197

16. Bennett, B.G. (1997). Exposure to natural radiation worldwide. In: Proceedings of the Fourth International Conference on High Levels of Natural Radiation: *Radiation Doses and Health Effects*, 1996. Elsevier, Beijing, China, Tokyo, pp. 15–23.

17. Beretka, J. and Mathew, P.J. (1985). Natural radioactivity of Australian building materials, industrial wastes and by-products. *Health Phys*. 48, 87.

18. Berner, R.A., (1995). Chemical weathering and its effect on atmospheric CO_2 and climate. In: White AF & Brantley SL (eds) Chemical Weathering Rates of Silicate Minerals, *Rev Min* 31: 565–583. Mineralogical Society of America, Washington

19. Bourdon, B., Turner, S., Henderson, G.M. and Lundstrom, C.C., (2003) Introduction to U series Geochemistry *Reviews in mineralogy and geochemistry* Vol. 52, 1-21

20. Bullen, T., White, A., Blum, A., Harden, J. and Schulz, M. (1997). Chemical weathering of soil chronosequence on a granitoid alluvium: 11. Mineralogical and isotopic constraints on the behaviour of strontium. *Geochimica et Cosmochimica Acta*, 61, pp. 291-306.

21. Bullen, T.D., Krabbenhoft, D.P. and Kendall, C. (1996). Kinetic and mineralogic controls on the evolution of ground water chemistry and $^{87}Sr/^{86}Sr$ in a sandy aquifer, northern Wisconsin, USA. *Geochimica et Cosmochimica Acta*, 60, pp.1807-1821.

22. Carbol, P. and Engkvist, I. (1997). Compilation of radionuclide sorption coefficients for performance assessment, *SKB Report R-97-13*. Svensk Kärnbränslehantering AB, Stockholm.

23. Cember, H. (1996). Introduction to Health Physics, 3rd Edition, McGraw-Hill, New York

24. Ceryan, S., Tudes,S. and Ceryan N. (2008). Influence of weathering on the engineering properties of Harsit granitic rocks (NE Turkey) *Bull Eng Geol Environ*.,67:97–104

25. Chadha, D.K. (1999). A proposed new diagram for geochemical classification of natural waters and interpretation of chemical data, *Hydrogeology journal*, 7 pp 431-439

26. Chapman, N.A. and McKinley, I.G., (1987). The Geological Disposal of Nuclear Waste. John Wiley & Sons (publ), Chichester. 252 pps.

27. Chebotarev, I.I., (1955). Metamorphism of natural waters in crust of weathering-1. *Geochimica et Cosmochimica Acta* ,8, 22-48

28. Clark, I.D. and Fritz, P. (1997). Environmental isotope in hydrogeology, CRC Boca Raton, Lewis, Fl

29. Coleman, L.M, Shepherd, T.J., Durham, J.J., Rouse, J.E. and Moore, G.R. (1982). Reduction of water with zinc for hydrogen isotope analysis. *Analytical Chemistry* 54: 993–995.

30. Coplen, T.B., Herczeg, A.L. and Barnes, C. (2000). Isotope engineering—using stable isotopes of the water molecule to solve practical problems. In Environmental Tracers in Subsurface Hydrology, Cook PG, Herczeg AL (eds). Kluwer Academic Publishers: Boston; 79–110.

31. Craig, H. (1961). Isotope variation in meteoric waters. *Science* 133, 1702–1703.

32. Crooks, J.P., Kesse, G.O., Holms,R.F. and Abbey, D.T., 2003. Geology of the ¼º field sheets Nos. 101, 102, 103, 104, Akuse, Archive Report No. 23- Second Edition, Ghana Geological Survey Department Accra, Ghana

33. Curtis, D.B. and Gancarz, A.J., (1983). Radiolysis in nature: evidence from the Oklo natural reactors. KBS Tech. Rep. (TR 83-10), Stockholm, Sweden.

34. Curtis, D.B. (1985). The chemical coherence of natural spent fuel at the Oklo nuclear reactors Swedish Nuclear Fuel and Waste Management Company Report, *SKB TR-85-04*. Stockholm, Sweden.

35. Dansgaard, W. (1964). Stable isotopes in precipitation. Tellus XVI 4:436–468

36. Darko, P. K., (2001). Quantitative Aspects of Hard Rock Aquifers: Regional Evaluation of Groundwater Resources in Ghana. Ph.D Thesis, Charles University, Prague, Czech Republic.

37. Darko, P.K., Barnes, E.A. and Sekpey, N.K.(1995). Groundwater assessment report on the Accra Plains. Unpublished Technical Report, Water Resources Research Institute (CSIR) Accra

38. Datta,P.S., and Tyagi,S.K., (1996), Major ion chemistry of groundwater in Delhi area: Chemical weathering process and groundwater regime. *Journal of the Geological Society of India*, 47, 179-188.

39. Deer, W.A., Howie, R.A. and Zussman, J. (1992). An Introduction to the Rock Forming Minerals. Longmans, London.

40. Deshpande, R.D., Bhattacharya, S.K., Jani, R.A. and Gupta, S.K. (2003). Distribution of oxygen and hydrogen isotopes in shallow groundwaters from southern India: influence of a dual monsoon system. *Journal of Hydrology* 271: 226–239.

41. Deutsch, W.J., (1997). Groundwater geochemistry–fundamentals and applications to contamination. Lewis Publishers, Boca Raton, p 221

42. Domenico PA, Schwartz FW (1998) Physical and chemical hydrology,2nd edn, Wiley, New York

43. Dongarra,G., Manno,E.,Sabatino,G and Varrica,D. (2009). Geochemical characteristics of waters in mimeralised area of Peloritani Mountains (Sicily, Italy), *Applied Geochemistry* 24,900-914

44. Drake, J. J., (1983). The effects of geomorphology and seasonality on the chemistry of carbonate groundwater. *Journal of hydrology* 61, 223-236

45. Drever J.I. (1997). The geochemistry of natural water: surface and groundwater, environments, 3rd edn. Prentice Hall, Englewood Cliffs, NJ, p 436

46. Drever, J. I. and Smrth. C. L. (1978). Cyclic wetting and drying of the soil zone as an influence on the chemistry of groundwater and terrains. *American Journal Science* 278, 1448-1454.

47. Efa,E N., Martin,N. and Muff, R., (2006). Explanatory Notes for the Hydrogeological Map for Urban Planning 1:100 000 of Greater Accra Metropolitan Area Ghana–Germany Technical Cooperation Project:Environmental and Engineering Geology for Urban Planning in the Accra-Tema Accra, January

48. Eggleton, R.A., Foudoulis, C. and Varkevisser, D., (1987). Weathering of Basalt: Changes in Rock Chemistry and Mineralogy *Clays and Clay Minerals*, Vol. 35, No. 3. 161-169.

49. Eggleton, R.A. (1986). The relation between crystal structure and silicate weathering rates. In: Colman SM & Dethier DP (eds) *Rates of Chemical Weathering of Rocks and Minerals*, pp 21–40. Academic Press, Orlando, F

50. Egidi,P., (1998), Background, 26 January 1998 _http://www.normis.com/bkgrnd.htm

51. Elango, L., Kannan, R. and Senthil K. (2003). Major ion chemistry and identification of hydrogeochemical processes of groundwater in a part of Kancheepuram District, Tamil Nadu, India. *Journal Environmental Geosciences*, 10–4, 157–166.

52. El-Dine, W., El-Shershaby, A., Ahmed, F. and Abdel-Haleem, A.S. (2001). Measurement of radioactivity and radon exhalation rate in different kinds of marbles and granites. *Appl. Radiat. Isot*. 55, 853–860.

53. El-Galy,M.M., El-Mezayn, A.M., Said,A.F., Mowafy,A.A. and Mohamed,M.S., (2008). Distribution and environmental impact of some radionuclides in sedimentary rocks at Wadi Naseib area, southwest Sinai,Egypt, *J. Environ. Radioact*, 99,pp 1075-1082.

54. Epstein, S. and Mayeda, T.K. (1953). Variations of the $^{18}O/^{16}O$ ratio in natural water. *Geochim Cosmochim Acta* 4:213–220

55. Faanhof, A., (1999). The measurement of natural radioactivity and the impact on humans. *Cesk. Cas. Fys*. 49, 281-296.

56. Fischer,S.R. and Mullican,W.F. (1997). Hydrogeochemical evolution of sodium-sulphate and sodium-chloride groundwater beneath the northern Chihuahua desert, Trans-Pecos, Texas, U.S.A., *Hydrogeology Jornal*,5, 4-16

57. Fontes, J.-Ch. (1980). Environmental isotopes in isotope hydrology. In: Fritz, P., Fontes, J.-Ch. (Eds.), Handbook of Environmental Isotope Geochemistry, Elsevier, Amsterdam

58. Fontes, J.-Ch.and Zuppi, G.M. (1976). Isotopes and Water Chemistry in Sulphide-Bearing Springs of Central Italy. Interpretation of Environmental Isotope and Hydrochemical Data in Ground Water Hydrology, Proc. Advisory Group Meeting. IAEA, Vienna, Austria, pp. 143–158.

59. Frape, S.K., Fritz, P. and McNutt, R. H. (1984).Water-rock interaction and chemistry of groundwaters from the Canadian Shield *Geochimica et Cosmochimica Acta* Vol. 48. pp. 1617 – 1627

60. Freeze, R.A. and Cherry, J.A. (1979). *Groundwater*. Prentice Hall,New Jersey.

61. Friedman, O., Machta, L. and Soller, R. (1962). Water vapour exchange between a water droplet and its environment. *J Geophys Res* 67:2761–2766

62. Fritz, P. (1981). River water, In: Gat, J.R., Gonfiantini, R. (Eds.), Stable Isotope Hydrology, Deuterium and Oxygen-18 in the Water Cycle. Technical Report Series no. 210.International Atomic Energy Agency, Vienna, Austria,pp. 196–198.

63. Garcia, M.G., Hidalgo M Del V. and Blesa, M.A. (2001). Geochemistry of groundwater in the alluvial plain of Tucuman province, Argentina. *Hydrogeology Journal* 9(6), 597-610

64. Garrels, R.M., (1967). Genesis of Some Groundwaters from Igneous Rocks. In: Abelson, P.H. (Ed.), Researches in Geochemistry, vol. 2. John Wiley & sons, pp. 405–420.

65. Gascoyne, M., (2004). Hydrogeochemistry, groundwater ages and sources of salts in a granitic batholith on the Canadian Shield, southeastern Manitoba, *Applied Geochemistry* 19,519–560

66. Gascoyne,M,. Miller,N.H. and Neymark L.A., (2002) Uranium-series disequilibrium in tuffs from Yucca Mountain, Nevada, as evidence of pore-fluid flow over the last million years, *Applied Geochemistry* 17, 781–792

67. Gascoyne, M., (1997). Evolution of redox conditions and groundwater composition in recharge discharge environments on the Canadian Shield. *Hydrogeological Journal* 5, 4-18.

68. Gat,J.R., Bowser, C.J. and Kendall, C. (1994). The contribution of evaporation from the Great Lakes to the continental atmosphere: estimate based on stable isotope data. *Geophysical Research Letters* 21: 557 – 560

69. Gat, J.R. and Matsui, E., (1991). Atmospheric water balance in the Amazon basin: an isotopic evapotranspiration model. *Journal of Geophysical Research*, 96, 13179 – 13188

70. Gat, J.R. (1981). Isotopic fractionation, In: *Stable isotope hydrology, deuterium and oxygen-18 in water cycle,* Technical Reports Series 210, IAEA, Vienna pp21-34

71. Gat, J.R., (1970). Environmental isotope balance of Lake Tiberias. In: *Isotope Hydrology*. International Atomic Energy Agency, Vienna, pp. 109–127.

72. Gat, J.R. and Tzur, Y. (1967). Modification of the isotopic composition of rainwater in processes which occur before groundwater recharge In *Isotopes in Hydrology* International Atomic Energy Agency, Vienna pp 49-61

73. Gibbs, R. J. (1970). Mechanism controlling world water chemistry. *Science* 170, 1088-1090.

74. Giblin, A.M., Batts, B.D. and Swaine, D.J., (1981). Laboratory simulation studies of uranium mobility in natural waters. *Geochim. Cosmochim. Acta* 45, 699-709.

75. Goldich, S.S. (1938). A study in rock-weathering. *J. Geol*. 46 (1), 17–58.

76. Gonfiantin,i R., Roche, M.A., Olivry, J.C., Fontes, J-Ch. and Zuppi, G.M. (2001). The altitude effect on the isotopic composition of tropical rains. *Chem Geol* 181:147–167

77. Grassa, F., Favara, R.and Valenza, M., (2006) Moisture source in the Hyblean Mountains region (south-eastern Sicily, Italy): Evidence from stable isotopes signature *Applied Geochemistry* 21 2082–2095

78. Hagros, A., (2006). Host Rock Classification (HRC) System for Nuclear Waste Disposal in Crystalline Bedrock, PhD-thesis No. 191 of the Department of Geology, University of Helsinki

79. Harley, A.D. and Gilkes, R.J. (2000). Factors influencing the release of plant nutrient elements from silicate rock powders: a geochemical overview, *Nutrient Cycling in Agroecosystems* **56:** 11–36,

80. Harris, N. (1970). Geology of the Devonian Rocks of Accra with special reference to subsurface investigations. Geological Survey Bulletin No. 38, pp.47-70, Geological Survey Department, Accra.

81. Hidalgo, M.C.-L. and Cruz-Sanjulian, J., (2001). Groundwater composition, hydrochemical evolution and mass transfer in a regional detrital aquifer Baza basin, southern Spain. *Appl. Geochem*. 16, 745–758.

82. Hiscock, K.M., (2005). Hydrogeology: Principles and Practice, Blackwell Publishing

83. Holm R.F., (1973). On the metamorphic facies of the Dahomeyan gneiss in the western Accra Plains, Ghana *Mineralogical Magazine,* June I973, vol. 39, pp. 224-32

84. Holmqvist, J., (2001). Modelling Chemical Weathering in Different Scales, Doctoral Thesis, Department of Chemical Engineering II Lund University, Sweden

85. Hu Z. and Chen J. (1992). An introduction to chemistry for geology. Beijing: Higher Education Press, 1-141.

86. International Atomic Energy Agency, (2011) Geological Disposal Facilities for Radioactive Waste, IAEA Safety Standards Series No. SSR-5, IAEA, Vienna.

87. International Atomic Energy Agency, (2009) Classification of Radioactive Waste, IAEA Safety Standards Series No. GSG-1, IAEA, Vienna.

88. International Atomic Energy Agency, (2003). Scientific and Technical Basis for Geological Disposal of Radioactive Wastes, IAEA Technical Reports Series No. 413, IAEA, Vienna

89. International Atomic Energy Agency, (1999). Hydrogeological Investigation of Sites for the Geological Disposal of Radioactive Waste, IAEA Technical Reports Series No. 391, IAEA, Vienna.

90. International Atomic Energy Agency, (1989). Measurement of radionuclides in food and the environment. IAEA Technical Report, Series No. 295, IAEA, Vienna.

91. International Atomic Energy Agency (1983). Isotope Techniques in the Hydrogeological Assessment of Potential Sites for the Disposal of High-Level Radioactive Wastes. Technical Reports Series No.228. IAEA, Vienna.

92. International Atomic Energy Agency, (1981a). Underground disposal of radioactive wastes: Basic guidance, Safety Series No. 54, IAEA, Vienna

93. International Atomic Energy Agency (1981b). Stable isotope hydrology, Deuterium and oxygen-18 in the water cycle. Tech Rep Series No 210 IAEA, Vienna

94. Ivanovich, M. and Harmon, R.S., (1982). Uranium Series Disequilibrium, Applications to Environmental Problems. Clarendon Press, Oxford 1982, 571 p.

95. Iwatsuki, T. and Yoshida, H. (1999). Characterizing the chemical containment properties of the deep geosphere: water–rock interaction analysis in relation to fracture systems in deep crystalline rock at the Tono area, Japan. In: Metcalfe, R., Rochelle, C.A. (Eds.), Chemical Containment of Waste in the Geosphere. Geol. Soc. Spec. Publ. No.157. Geological Society of London, London, UK, pp. 71–84.

96. Jankowski,J. and Acworth,R.I.(1997). Impact of debris-flow deposits on hydrogeochemical process and the development of dry land salinity in the Yass River catchment, New South Wales, Australia, *Hydrogeology journal*,**5**,71-88

97. Jantzen, C.M. and Bibler, N.E. (1985). The Role of Groundwater Oxidation Potential and Radiolysis on Waste Glass Performance in Crystalline Repository Environments, MRS Proceedings, Volume50

98. Junner, N.R and Bates D.A., (1945) Reports on the Geology and hydrology of the coastal area east of the Akwapim Range, Accra Geological Survey Memoir No 7

99. Karnland, O., (1997). Bentonite swelling pressure in strong NaCl solutions. Correlation between model calculation and experimentally determined data. SKB Technical Report TR 97-31.

100. Kathren, R.L. (1998), NORM sources and their origins, *Appl. Radiat. Isot.*, 49 pp149-168

101. KBS-3, 1983. Final Storage of Spent Nuclear Fuel, KBS-3, SKBF/KBS, Svensk kärnbränsleförsörjning AB.

102. Kendall, C. and Coplen, T.B. (2001). Distribution of oxygen-18 and deuterium in river waters across the United States. *Hydrological Processes* 15:1363–1393.

103. Kendal, C. and McDonnell, J.J. (1998). Isotope Tracers in Catchment Hydrology USGS Elsevier Science B.V., Amsterdam

104. Kesse, G.O. (1985). The mineral and rock resources of Ghana. A.A. Balkema, Rotterdam, 610 p.

105. Knight, J.L., (1998). Use of natural analogues in waste disposal, *Interdisciplinary Science Review* Vol 23 No3 pp233

106. Kortatsi, B.K. (2006). Hydrochemical characterization of groundwater in the Accra Plains of Ghana, *Environ Geol* ,50, 299-311

107. Krabbenhoft, D.P., Bowser, C.J., Anderson, M.P. and Valley, J.W. (1990). Estimating groundwater exchange with lakes: the stable isotope mass balance method. *Water Resour. Res.* 26, 2445–2453.

108. Kraemer, T. F. and Kharaka, Y. K. (1986) Uranium geochemistry in U.S. Gulf coast geopressured-geothermal systems. *Geochim. Cosmochim. Acta* 50, 1233–1238.

109. Krass, A.A. and Nobayev, (1980). The geochemistry and origin of Zirconia in kimberlite Translated by Chu Hebao.*Geology-Geochemistry*. 12, 41-46.

110. Krauskopf, K.B., (1986). Thorium and rare-earth elements as analogs for actinide elements. *Chem. Geol*. 55, 323-335.

111. Krishnamurthy, R.V. (1984). Stable isotope studies on sedimentary deposits and groundwaters and their climatic implications. PhD Thesis, Gujarat Univ. India.

112. Kronberg, B.I., Nesbitt H.W. and Fyfe, W.S., (1987). Mobilities of Alkalis, Alkaline Earths And Halogens During Weathering, *Chemical Geology*, 60, 41-49

113. Laaksoharju, M., Gurban, I. and Skårman, C. (1998). Summary of hydrochemical Conditions at Aberg, Beberg and Ceberg. *SKB Technical Report TR-98-03*. Swedish Nuclear fuel and Waste Management Co, Stockholm.

114. Laaksoharju, M., Smellie, J., Nilsson, A.C., Skarman, C., (1995). Groundwater sampling and chemical characterisation of the Laxemar deep borehole KLX02. *SKB Technical Report 95-05*, Stockholm.

115. Laaksoharju, M., Smellie, J., Routsalainen, P. and Snellman, M., (1993). An approach to quality classification of deep groundwaters in Sweden and Finland, *SKB TR 93-27*.

116. Langmuir, D. (1978). Uranium-solution-mineral equilibria at low temperatures with applications to sedimentary ores deposits. *Geochim.Cosmochim. Acta* **42,** 547–569

117. Langmuir, D. and Herman, J.S. (1980). The mobility of thorium in natural waters at low temperatures. *Geochim. Cosmochim. Acta* 44, 1753-1766.

118. Larsson I., (1984). Groundwater in hard rocks: Project8.6 of the international Hydrological Programme, Unesco, Paris pp228

119. Lasaga, A.C. (1984). Chemical kinetics of water–rock interactions. *Journal of Geophysical Research* 89(B6): 4009–4025.

120. Lasaga, A.C., Soler, J.M., Gapjor, J., Burch, T.E. and Nagy, K.L. (1994). Chemical weathering rate laws and global geochemical cycles, *Geochimica et Cosmochimica Acta*, Vol. 58, pp. 2361-2386,

121. Leake, B.E., Woolley, A.R., Arps, C.E.S., Birch, W.D., Gilbert, M.C., Grice, J.D., Hawthorne, F.C., Kato, A., Kisch, H., Krivovivhev, V.G., Linthout, K., Laird, J., Mandarino, J.A., Maresch, W.V., Nickel, E.H., Rock, N.M.S., Schumacher, J.C., Smith, D.C., Stephenson, N.C.N., Ungaretti, L., Whittaker, E.J.W., Guo, Y., (1997). Nomenclature of amphiboles: report of the Subcommittee on Amphiboles of the International Mineralogical Association, Commission on New Minerals and Mineral Names. Am Mineral 82:1019–1037

122. Leontiadis, I.L., Vergis, S. and Christodoulou, T. (1996). Isotope hydrology study of areas in Eastern Macedonia and Thrace, Northern Greece. *J. Hydrol*. 182, 1–17.

123. Liu Yingjun, 1984. Element geochemistry. Beijing: Science Press, 1-228.

124. Locsey, K.L., Grigorescu, M. and Cox, M.E. (2012).Water–Rock Interactions: An Investigation of the Relationships between Mineralogy and Groundwater Composition and Flow in a Subtropical Basalt Aquifer *Aquat Geochem* 18:45–75

125. Locsey, K.L. (2004). Hydrogeochemistry and hydrology of a basalt aquifer system, the Arherton Tablelands, North Queensland, Ph.D. thesis, Queensland University of Technology, Queensland

126. Luo, S., Ku,T-L., Roback,R., L Murrell, M. and Mcling T.L. (2000). In-situ radionuclide transport and preferential groundwater flows at INEEL (Idaho): Decay-series disequilibrium studies *Geochimica et Cosmochimica Acta,* Vol. 64, No. 5, pp. 867–881.

127. Maloszewski, P., Moser, H., Stichler, W., Bertleff, B. and Hedin, K. (1990). Modelling of groundwater pollution by river bank infiltration using oxygen-18 data. In: Groundwater Monitoring and Management, Proceedings of the Dresden Symposium, March 1987. IAHS Publication no. 173, pp. 153–161

128. Mathieu, R. and Bariac, T. (1996). An isotopic study (^{2}H and ^{18}O) on water movements in clayey soils under a semiarid climate. *Water Resour. Res*. 32, 779–789.

129. McMurry, J., Dixon, D.A., Garroni, J.D., Ikeda, B.M., Stroes-Gascoyne, S., Baumgartner, P. and Melnyk, T.W. (2003). Evolution Of A Canadian Deep Geologic Repository: Base Scenario, Atomic Energy of Canada Limited Report No: 06819-REP-01200-10092-R00, November

130. McMurry, J., (1995). Preliminary modelling study of geochemical interactions between a used fuel disposal vault and the surrounding geosphere. Atomic Energy of Canada Limited Report, AECL-11197, COG-94-506. Pinawa, Canada.

131. Meng, S.X. and Maynard, J.B. (2001) Use of statistical analysis to formulate conceptual models of geochemical behavior: water chemical data from the Botucatu aquifer in Sao Paulo state, Brazil. *J Hydrol* 250:78–97

132. Merlivat L. and Jouzel, J. (1979) Global Interpretation of the Deuterium-Oxygen 18 Relationship for Precipitation, *J. Geophys. Res.* **84**, 5029.

133. Milnes, A. G. (2002). Swedish deep repository siting programme: Guide to the documentation of 25 years of geoscientific research (1976-2000). Swedish Nuclear Fuel and Waste Management Co (SKB), *Stockholm, TR-02-18*, 190 p.

134. Mohanty, A.K., Sengupta, D., Das, S.K., Vijayan, V. and Saha,S.K.(2004). Natural radioactivity in the newly discovered high background radiation area on the eastern coast of Orissa, India. *Radiat. Meas*. 38, 153–165.

135. Moser, H., Wolf, M., Fritz, P., Fontes, J. Ch., Florkowsky, T. and Payne, B. R. (1989) Deuterium, oxygen-18 and tritium in Stripa groundwaters. *Geochimica et Cosmochimica. Acta* 53, 1756-1764.

136. Muff, R., and Efa, E. (2006). Explanatory Notes for the Geological Map for Urban Planning 1:50 000 of Greater Accra Metropolitan Area, Ghana–Germany Technical Cooperation Project: Environmental and Engineering Geology for Urban Planning in the Accra-Tema Area Accra, March 2006

137. Nagra, (1994). Kristallin-I, Safety assessment report. *Technical Report NTB-93-22*, Nagra, Wettingen, 396 p

138. Nesbitt, H. W., Markovics, G. and Price, R.C., (1980). Chemical processes affecting alkalis and alkalme earths during continental weathering. *Geochimica et Cosmochimica Acta* . 44, 1659-1666.

139. Niini, H., Hakkarainen, V. and Patrikainen, P. (1982). Geological factors in the final disposal of highlevel nuclear waste. Nuclear Waste Commission of Finnish Power Companies, Helsinki, YJT-82-36, 189 p + App.

140. Nirex Report N/011, (2000). The Nirex Repository Concept: Evaluating Performance , United Kingdom Nirex Limited

141. Nkotagu, H. (1996a). The groundwater geochemistry in a semi-arid,fractured crystalline basement. Area of Dodoma, Tanzania *Journal of African Earth Sciences.* Vol. 23, No. 4 pp593-505,

142. Nkotagu, H. (1996b). Application of environmental isotopes to groundwater recharge studies in a semi-arid fractured crystalline basement area of Dodoma, Tanzania, *Journal of African Earth Sciences*.Vol. 22, No. 4. pp. 443-457,

143. Nordstrom, D., Olsson T., Carlsson, L. and Fritz, P., (1989a). Introduction to the hydrogeochemical investigations within the International Stripa Project, *Geochimica et Cosmochimica Acta* Vol. 53. pp. 1717-1726

144. Nordstrom, K., Lindblom, S., Donahoe, R.J. and Barton, C., (1989b).Fluid inclusion in the Stripa granite and their possible influence on the groundwater chemistry. *Geochim. Cosmochim.Acta* 53, 1741–1755.

145. Nordstrom, D.K., Ball, J.W., Donahoe,R.J. and Whittemore, D., (1989c). Groundwater chemistry and water-rock interactions at Stripa, *Geochimica et Cosmochimica Acta*. Vol 53,pp.1727-1740

146. Nordstrom, D.K., (1986). Hydrogeochemical interpretation of the groundwater at the Hästholmen site, Finland. Nuclear Waste Commission of Finnish Power Companies, Report YJT-86-32.

147. Nordstrom, D.K. (ed.), Andrews, J.N., Carlsson, L., Fontes, J-Ch., Fritz, P., Moser, H. and Olsson, T. (1985). Hydrogeological and hydrogeochemical investigations in boreholes – final report of the phase I geochemical investigations of the Stripa groundwaters. Swedish Nuclear Fuel and Waste Management Co. (SKB), Stripa Project, Technical Report 85-06.

148. NRC. (1999). Evaluation of Guidelines for exposures to Technologically Enhanced Naturally Occurring Radioactive Materials, National Research Council , Washington, DC.

149. Nude, P.M. (2006). Petrology and geochemistry of deformed carbonatite and nepheline syenite gneiss in the Pan-African Dahomeyide orogeny, southeastern Ghana, West Africa PhD Thesis, University of Ghana

150. OECD, Nuclear Energy Agency, (1984). Long-term radiation protection objectives for radioactive waste disposal. OECD Nuclear Energy Agency (NEA), Paris, 97 p.

151. Orgun, Y., Altınsoy, N., Gultekin, A.H., Karahan, G. and Celebi, N. (2005).Natural radioactivity levels in granitic plutons and groundwaters in southeast part of Eskisehir, Turkey. *Appl. Radiat. Isot.* 63, 267–275.

152. Orgun Y., Altınsoy, N., Sahin, S.Y,. Gungor Y.,, Gultekin, A.H., Karahan, G. and Karacık, Z., (2007). Natural and anthropogenic radionuclides in rocks and beach sands from Ezine region (Canakkale), Western Anatolia, Turkey, *Applied Radiation and Isotopes* 65, 739–747

153. Parkhurst, D.L., Appelo, C.A.J., (1999). User's guide to PHREEQC (version 2)—a computer program for speciation,batch-reaction, one-dimensional transport, and inverse geochemical calculations. United States Geological Survey Water-Resources Investigations Report 99–4259, p 312

154. Payne, B R (1988). The status of isotope hydrology today, *J. Hydrol* 100, 207 – 237

155. Piper, A. M. (1944). A graphic procedure in the geochemical interpretation of water analyses. *Trans. Am. Geophys. Union* 25, 914–923.

156. Pitkänen, P., Partamies, S.and Luukkonen, A. (2004).. Hydrogeochemical interpretation of baseline groundwater conditions at the Olkiluoto site. Helsinki, Finland: Posiva Oy. 159 p. Posiva-2003-07. ISBN 951-652-121-5.

157. Pitkanen, P., Snellman, M., Leino-Forsman, H. and Vuorinen, U. (1994). Geochemical modelling of the groundwater at the Olkiluoto site. Helsinki, Finland: Nuclear Waste Commission of Finnish Power Companies. 89 p. YJT -94-10.

158. Plant, J.A. and Saunders, A.D. (1996). The radioactive earth. *Radiat. Prot.Dosim*. 68 (1/2), 25–36.

159. Posiva (2000). Disposal of spent fuel in Olkiluoto bedrock – Programme for research, development and technical design for the pre-construction phase. Posiva Oy, Helsinki, POSIVA 2000-14, 147 p.

160. Rajmohan N. and Elango, L. (2004). Identification and evolution of hydrogeochemical processes in the groundwater environment in a part of Palar and Cheyyar River Basins, southern India. *Environ Geol* 46:47–61

161. Rogers, J.J.W. and Adams, J. A. S., (1969). Uranium. In: Wedepohl, K. H. (Ed.), Handbook of Geochemistry, Vol. 11 (13). Springer, Berlin.

162. Rogers, J.J.W. and Ragland, P.C., (1961). Variation of thorium and uranium in selected granitic rocks, *Geochimica et Cosmochimica Acta*, 25, 99-109

163. Salem, Z. E., Sakura Y. and Aslam, M.A.M., (2004) The use of temperature, stable isotopes and water quality to determine the pattern and spatial extent of groundwater flow:Nagaoka area, Japan *Hydrogeology Journal* 12:563–575

164. Sami, K. (1992). Recharge mechanisms and geochemical processes in a semi-arid sedimentary basin, Eastern Cape, South Africa. *Journal of Hydrology* 139, 27–48.

165. Sato, J. and Endo, M., (2001). Activity ratios of uranium isotopes in Volcanic Rocks from Izu-Mariana Island-Arc Volcanoes, *Journal of Nuclear and Nuclear and Radiochemical Sciences*, Vol. 2, No 1-2, pp. N1-N2, Japan

166. Schoeller, H. (1977). Geochemistry of groundwater.In Groundwater studies-An International guide for research and practice (Ch. 15, pp. 1–18). Paris: UNESCO.

167. Scholl, M.A, Ingebritsen, S.E., Janik, C.J. and Kauahikaua, J.P. (1996). Use of precipitation and groundwater isotopes to interpret regional hydrology on a tropical volcanic island: Kilauea volcano area, Hawaii, *Water Resour Res*32:3525-3537

168. Shivanna,K., Kulkarni, U.P., Joseph, T.B. and Navada S.V. (2004). Contribution of storms to groundwater recharges in the semi-arid region of Karnataka, India, *Hydrol. Process.* 18, 473–485 (2004)

169. Siever, R. and Woodford, N. (1979). Dissolution kinetics and the weathering of mafic minerals. *Geochimica et Cosmochimica Acta*, 43, 717-724.

170. SKB 2005. Preliminary safety evaluation for the Forsmark area. Based on data and site descriptions after the initial site investigation stage. Swedish Nuclear Fuel and Waste Management Co (SKB), Stockholm, TR-05-16, 105 p.

171. SKB, 2004. Interim main report of the safety assessment SR-Can. Swedish Nuclear Fuel and Waste Management Co (SKB), Stockholm, TR-04-11, 378 p.

172. SKB, 1999. Deep repository for spent nuclear fuel. SR 97- Post-closure safety, SKB-TR-99-06, Swedish Nucl. Fuel Waste Manag. Co., Stockholm, Sweden.

173. SKI (2002) The Swedish Nuclear Power Inspectorate's Regulations concerning safety in connection with the Disposal of Nuclear Material and Nuclear Waste. General Recommendations concerning the Application of the Swedish Nuclear Power Inspectorate's Regulations above. SKIFS 2002:1. ISSN 1400-1187. Swedish Nuclear Power Inspectorate, Stockholm.

174. Smellie J. A. T., Bath A. H., and Karlsson F. (1999) Applications of hydrogeochemistry in performance assessment. In *Use of Hydrogeochemical lnformation in Testing Groundwater Flow Models, Workshop Proceedings. Borgholm, Sweden 1-3 Sept.1997* (ed. OECD NEA), pp. 43-62. OECD, Nuclear Energy Agency, Paris, France.

175. Smellie, J.A.T., MacKenzie, A.B. and Scott, R.D., (1986). An analogue validation study of natural radionuclide migration crystalline rocks using uranium-series disequilibrium studies. *Chem. Geol.* 55, 233–254.

176. Sohrabi, M., (1998). The state of the art on worldwide studies in some environments with elevated naturally occurring radioactive materials (NORM), *Appl. Radia. Isot.*,49 pp169 – 188

177. SPSS 16.0., (2007)., SPSS Inc., Chicago Ill, Raynald Levesque

178. STUK (2001). Long-term safety of disposal of spent nuclear fuel. Guide YVL 8.4. Finnish Radiation and Nuclear Safety Authority (STUK), 23.5.2001, 9 p.

179. Suk, H. and Lee, K.K. (1999) Characterization of a ground water hydrochemical system through multivariate analysis: clustering into ground water zones. *Ground Water* 37(3):358–366

180. Suksi, J., (2001) Natural Uranium As A Tracer In Radionuclide Geosphere Transport Studies, Academic Dissertation, Faculty of Science, University of Helsinki, ISSN 0358-7746

181. Stumm,W.,and Morgan, J.J. (1981). Aquatic Chemistry, An Introduction Emphasizing Chemical Equilibria in Natural Watersheds. John Wiley & Sons, New York

182. Sumerling, T. and Smith, P. (1998). Disposal of nuclear fuel waste: Geological alternatives, designs, implementation, and long term safety, Interdisciplinary Science Review Vol 23 No3 pp214

183. Tardy Y. (1971). Characterization of the principal weathering types by the geochemistry of waters from European and African crystalline massifs. *Chem Geol* 7:253–271

184. Torstenfelt, B., Ittner, T., Allard, B., Andersson, K. and Olofsson, U. (1982). Mobilities of radionuclides in fresh and fractured crystalline rock SKBF/KBS Technical Report 82-26.

185. Tóth, J. (1999). Groundwater as a geologic agent: An overview of the causes, processes, and manifestations, *Hydrogeology Journal*, 7:1–14

186. UNSCEAR, (2000). Sources and Effect of Ionizing Radiation, United Nations Scientific Committee on the Effect of Atomic Radiation, Report to General Assembly with scientific Annexes, United Nations, New York

187. UNSCEAR (1993). Sources and Effect of Ionizing Radiation, United Nations Scientific Committee on the Effect of Atomic Radiation, Report to General Assembly with scientific Annexes, United Nations, New York

188. Vandergraaf, T.T., (1987). The role of isotope geochemistry studies in the Canadian Nuclear Fuel Waste Management Program, *Applied Geochemistry* vol, 2 pp 5-9

189. Verdoya, M., Chiozzi, P. and Pasquale, V., (2001). Heat-producing radionuclides in metamorphic rocks of the Brianconnais–Piedmont Zone (Maritime Alps). *Eclogae. Geol. Helv.* 94, 1–7.

190. Wahlström, R. and Grünthal, G., (2001). Probabilistic seismic hazard assessment (horizontal PGA) for Fennoscandia using the logic tree approach for regionalization and nonregionalization models. *Seismological research letters* 72(1), 33-45.

191. Waterwatch Australia National Technical Manual, 2005. Module 6 Groundwater Monitoring. Department of the Environment and Heritage, Canberra.

192. White, A.F. and Blum, A.E. (1995). Effects of climate on chemical-weathering in watersheds. *Geochim. Cosmochim. Acta* 59 (9), 1729–1747.

193. Whitfield, J.M., Roger, J.J.W. and Adams, J.A.S. (1959). The relationship between the petrology and the thorium and uranium contents of some granitic rocks. *Geochim. Cosmochim. Acta*, 17: 248--271Wilson, M.J. (1975). Chemical weathering of some primary rock-forming minerals. *Soil Sci* 119: 349–355

194. Yonezawa, C.,Tanaka, T., Kamioka, H., (1996) Water-rock reactions during gamma-ray irradiation, *Applied Geochemistry*, Vol. 11, pp. 461-469, 1996

195. Yurtsever, Y. and Gat, J.R., (1981): Atmospheric waters. In Stable Isotope Hydrology. IAEA, Vienna, Technical Rep. No. 210, 103-142.

196. Zack, T., Kronz, A., Foley, S.F. and Rivers, T. (2002). Trace element abundances in rutiles from eclogites and associated garnet mica schists. *Chem. Geol* 184: 97–122

197. Zhu, G.F., Li, Z.Z., Su, Y.H., Ma, J.Z. and Zhang, Y.Y. (2006). Hydrogeochemical and isotope evidence of groundwater evolution and recharge in Minqin Basin, northwest China. *J Hydrol*.333(2–3):239–251

APPENDICES

APPENDIX I

Mineral Analyses

A1.1. X-Ray Diffraction

X-Ray diffraction (XRD) is a widely used technique for studying the characteristics of crystalline structures and to determine the mineralogy of fine grained materials where the grain size is too small to be analysed with the optical microscope. X-ray diffraction is based on constructive interference of monochromatic X-rays and a crystalline sample. Constructive interference is a type of interference that occurs at any location along the medium where the two interfering waves have a displacement in the same direction.

Powder diffraction is commonly used to identify unknown substances, by comparing diffraction data against a database maintained by the International Centre for Diffraction Data (ICDD)(Ruan and. Ward,2002; Ottner *et al* 2000). It may also be used to characterize heterogeneous solid mixtures to determine relative abundance of crystalline compounds and, when coupled with lattice refinement techniques, such as Rietveld refinement, can provide structural information on unknown materials (Moore *et al* 1997)

X-rays are electromagnetic radiation similar to light, but with a much shorter wavelength. They are produced when electrically charged particles of sufficient energy are decelerated. These X-rays are generated by a cathode ray tube, filtered to produce monochromatic radiation, collimated to concentrate, and directed toward the sample. The interaction of the incident rays with the sample produces constructive interference (and a diffracted ray) when conditions satisfy Bragg's Law ($n\lambda=2d \sin \theta$). This law relates the wavelength of electromagnetic radiation to the diffraction angle and the lattice spacing in a crystalline sample. These diffracted X-rays are then detected, processed and counted. By scanning the sample through a range of 2θangles, all possible diffraction directions of the lattice should be attained due to the random orientation of the powdered material. Conversion of the diffraction peaks to d-spacings allows identification of the mineral because each mineral has a set of unique d-spacings. Typically, this is achieved by

comparison of d-spacings with standard reference patterns. Copper is the most common target material for single-crystal diffraction, with CuK_{α} radiation = 1.5418Å.

Quantification is based on the fact that the peak intensities from an individual mineral are proportional to the latter's content in the sample. Inasmuch as no two crystal structures are identical, no two structures will give all reflections at the same angles. Minerals can therefore be identified by their pattern of diffraction peak.

Measurement of peak intensities, therefore, provides information regarding the relative amount of the corresponding mineral phase. However, factors other than the mineral content such as varying absorption coefficient of different mineral phases in a mixture, particle size, degree of crystallinity, preferred orientation of the sample, etc., also affect the peak intensities (Al-Jaroudi et al, 2007).

The intensities of the XRD pattern of an individual mineral are known to be proportional to the concentrations of the different minerals present. Therefore, by measuring the intensities of patterns, some idea of the relative amounts of each phase can be achieved. The peak/ line positions and relative intensities of the diffractogram are compared with the reference 'fingerprint' patterns of known compounds available in the International Centre for Diffraction Data (ICDD) powder diffraction file (PDF) database and the phases identified. The PDF published by the (ICDD, the principal source of data for identification of phases by XRD, contains data for more than 115,000 compounds.

As a method, XRD is attractive because of its speed and ease of performance, it requires only small amounts of material, it is non-destructive and can be used to perform semi-quantitative analyses

Although well accepted as a definitive tool for mineral identification, XRD is traditionally regarded as having limitations in the evaluation of mineralogical data on a quantitative basis. The limitations include identification of only crystalline materials changes and the components of the

same mineral series (i.e. micas, feldspars, amphiboles) which have very similar crystallographic structures are difficult to separate due to their very similar XRD patterns.

The identification and quantification of the mineral phases were done using computer programs –Jade (search-match program) and Siroquant (quantification program which expresses the composition of crystalline material within a sample in percentage of dry weight).
The program Jade searches a large database (ICDD) of mineral XRD intensity patterns and matches those ideal patterns with the experimental ones. The limitation of this search-match process is that similar crystallographic structures result in similar XRD patterns and this can make mineral identification questionable, especially of minerals belonging to the same series such as plagioclase or pyroxenes. The Siroquant program provides quantitative analyses of mineral phases

References

Al-Jaroudi, S.S., Ul-Hami, A., Mohammed, A-R.I. and Saner. S., (2007), Use of X-ray powder diffraction for quantitative analysis of carbonate rock reservoir samples Powder Technology 175, 115–121

Moore, D.M. and Reynolds Jr. R.C. (1997) X-ray Diffraction and the Identification and Analysis of Clay Minerals, 2nd ed., Oxford University Press, Oxford, p. 378.

Ottner, F., Gier, S., Kuderna,M. and Schwaighofer,B. (2000) Results of an interlaboratory comparison of methods for quantitative clay analysis, *Applied Clay Science* 17, 223–243.

Ruan, C.D. and Ward, C.R. (2002) Quantitative X-ray powder diffraction analysis of clay minerals in Australian coals using Rietveld methods, Applied Clay Science 21, 227–240.

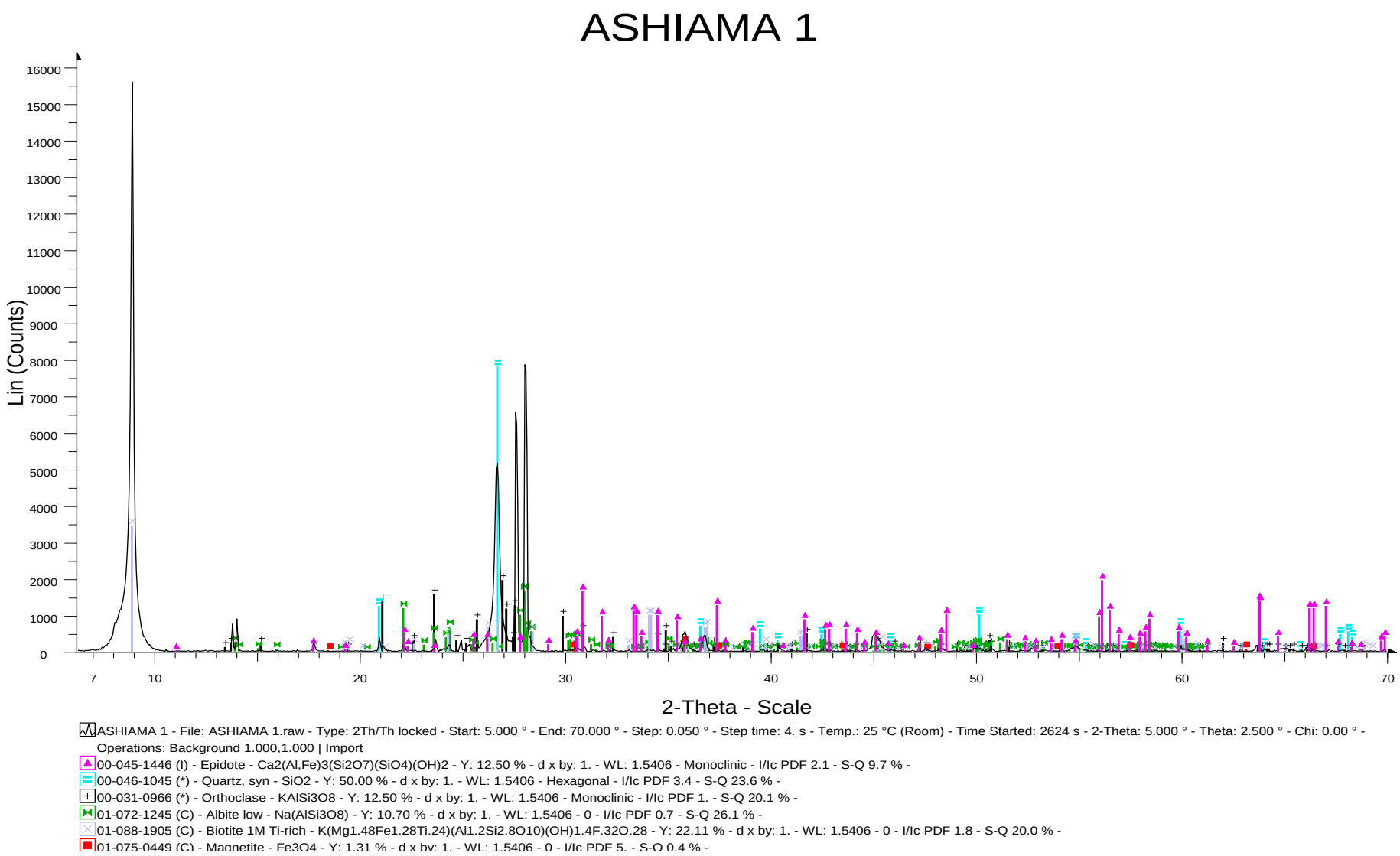

Figure A1.1 XRD pattern of ASH -1 sample

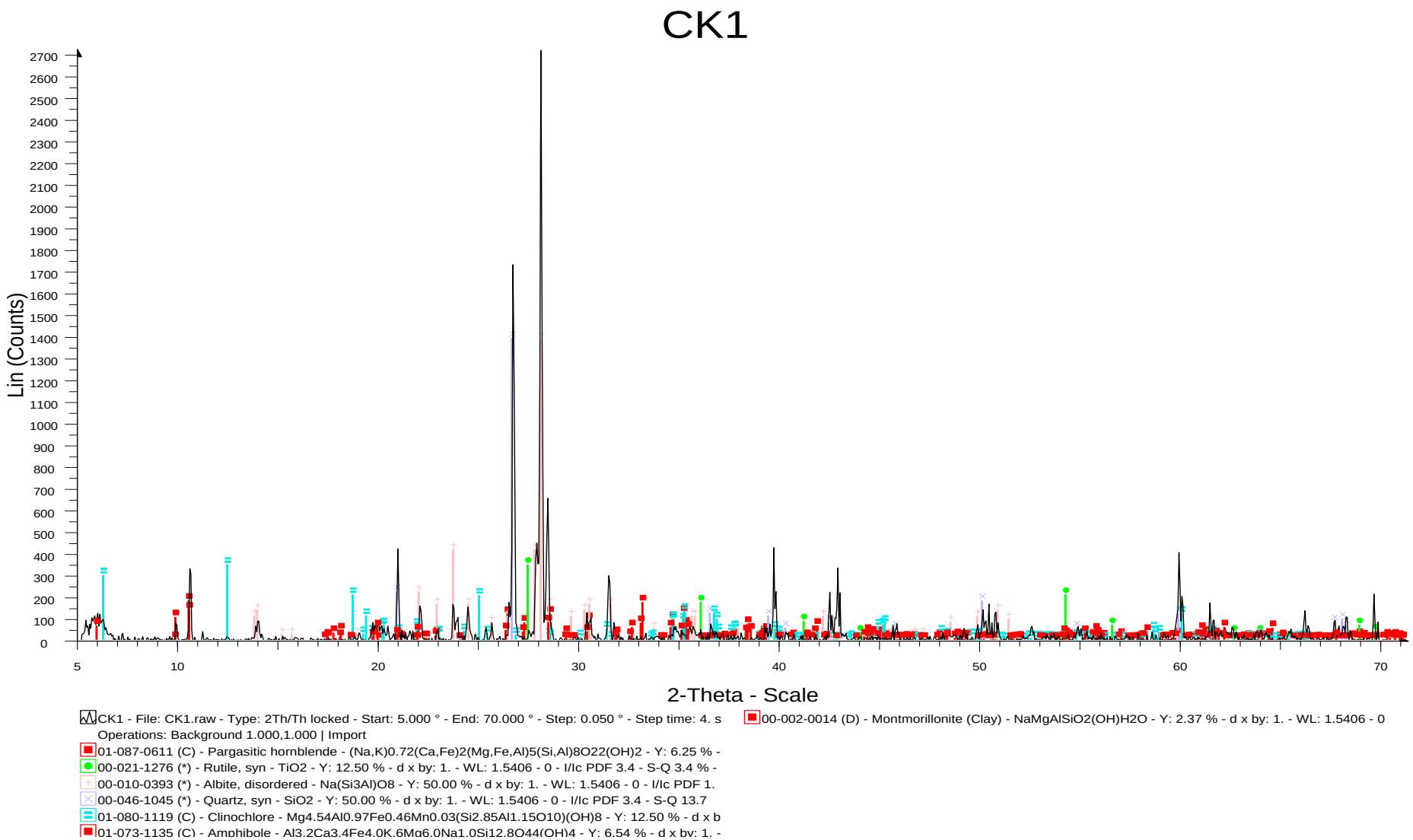

Figure A1.2 XRD patterns of CK1 sample

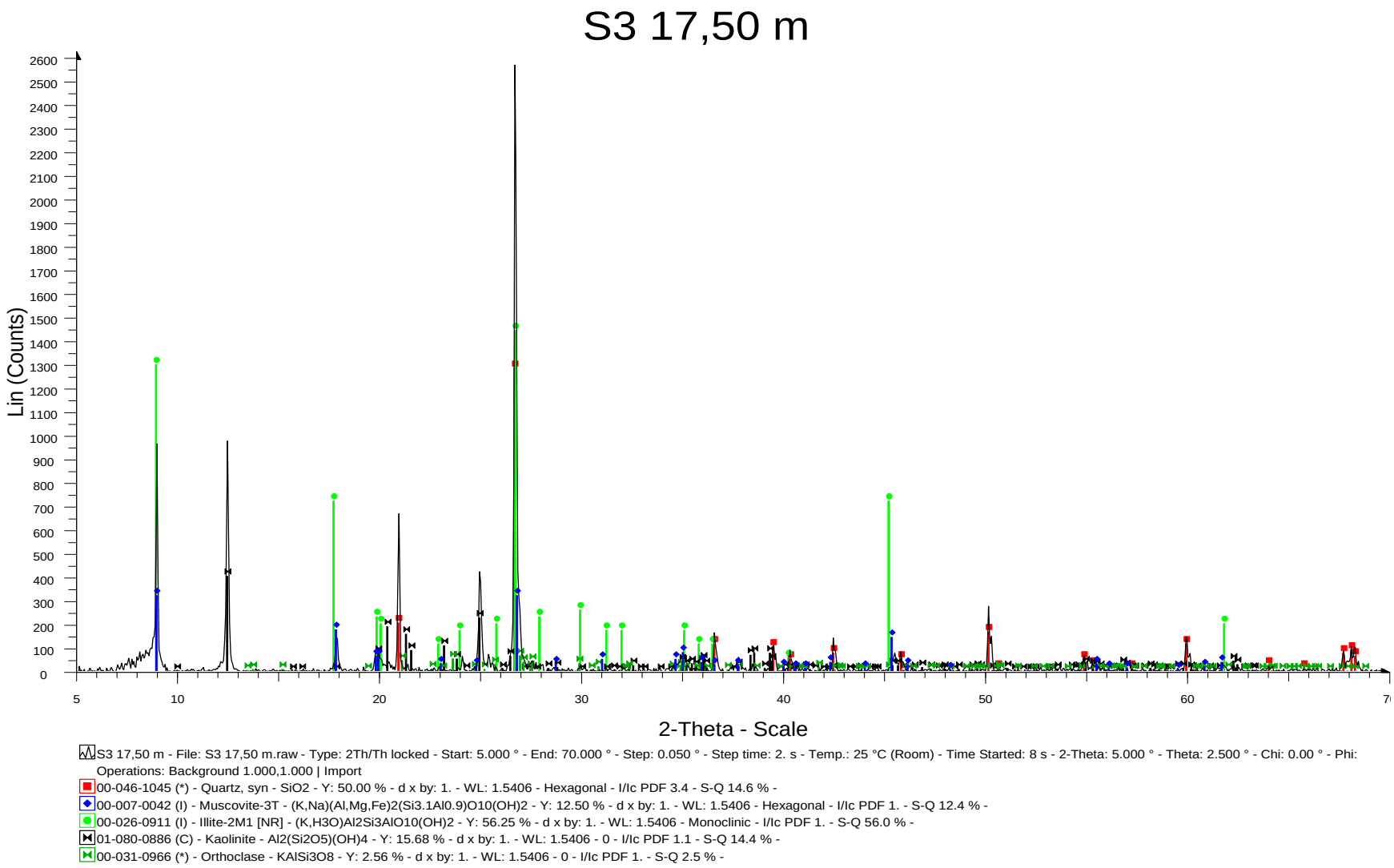

Figure A 1.3 XRD patterns of S3 samples

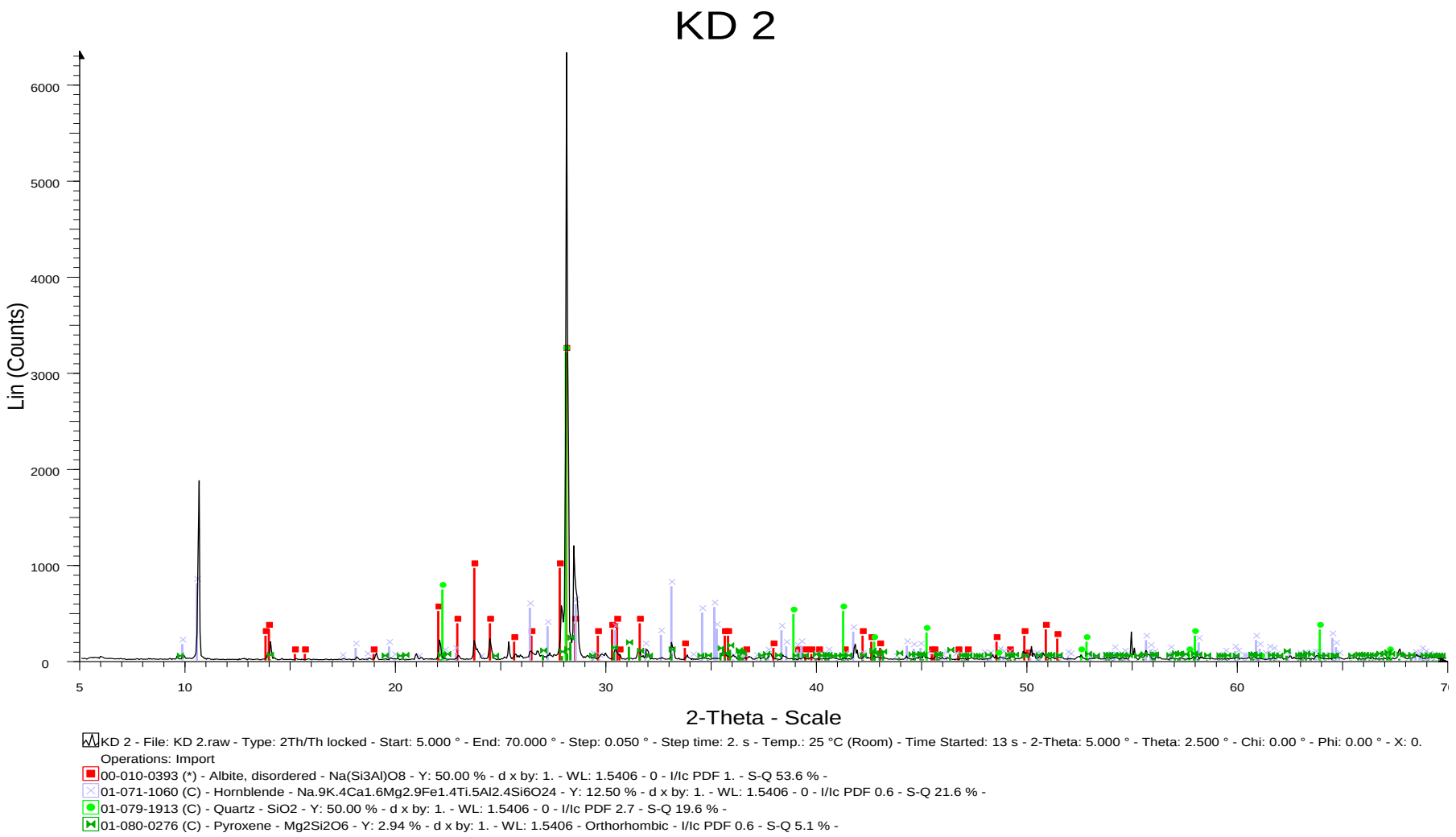

Figure A 1.4 XRD patterns of KD 2 samples

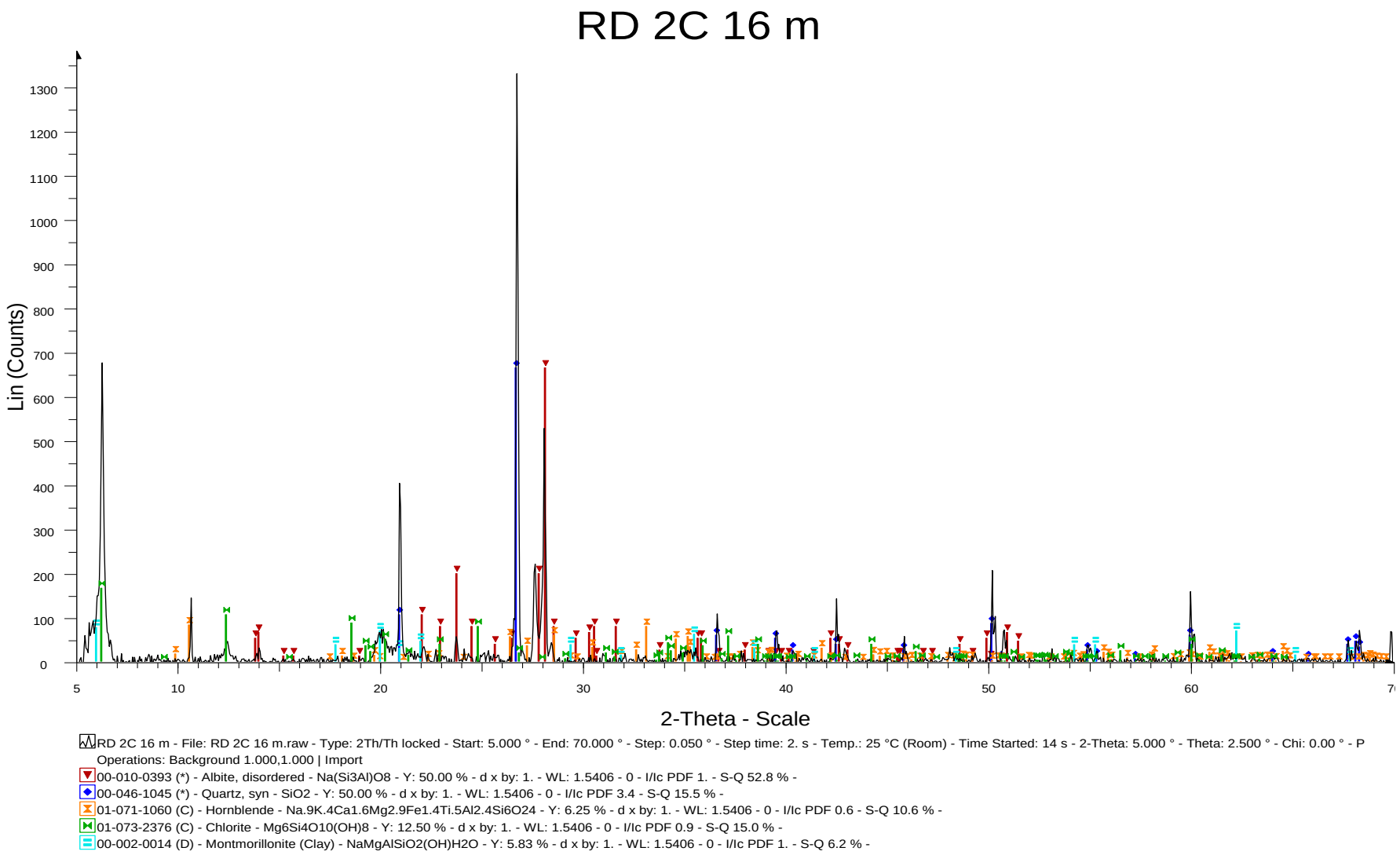

Figure A 1.5 XRD patterns of RD2C sample

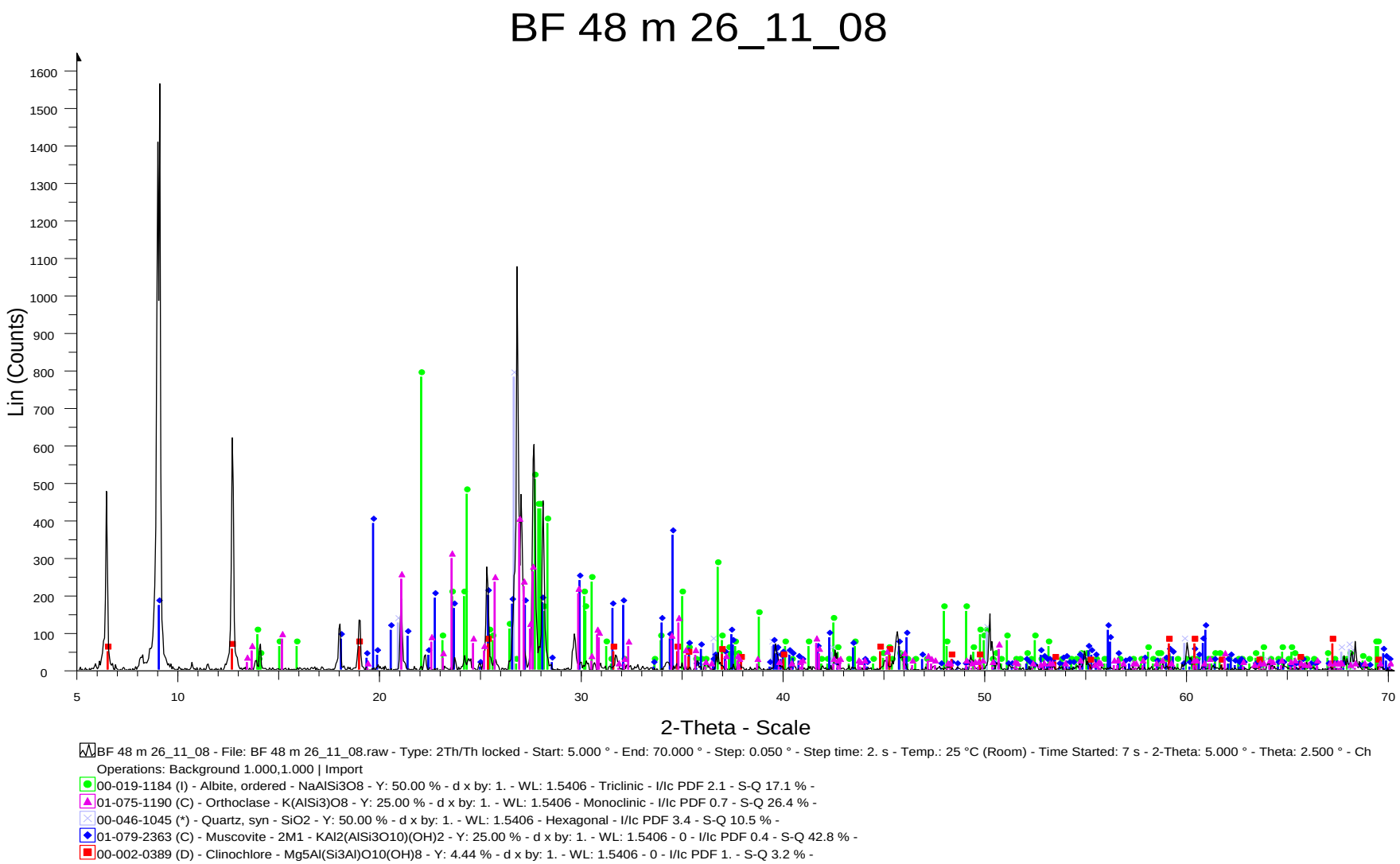

Figure A 1.6 XRD patterns of BF 48 samples

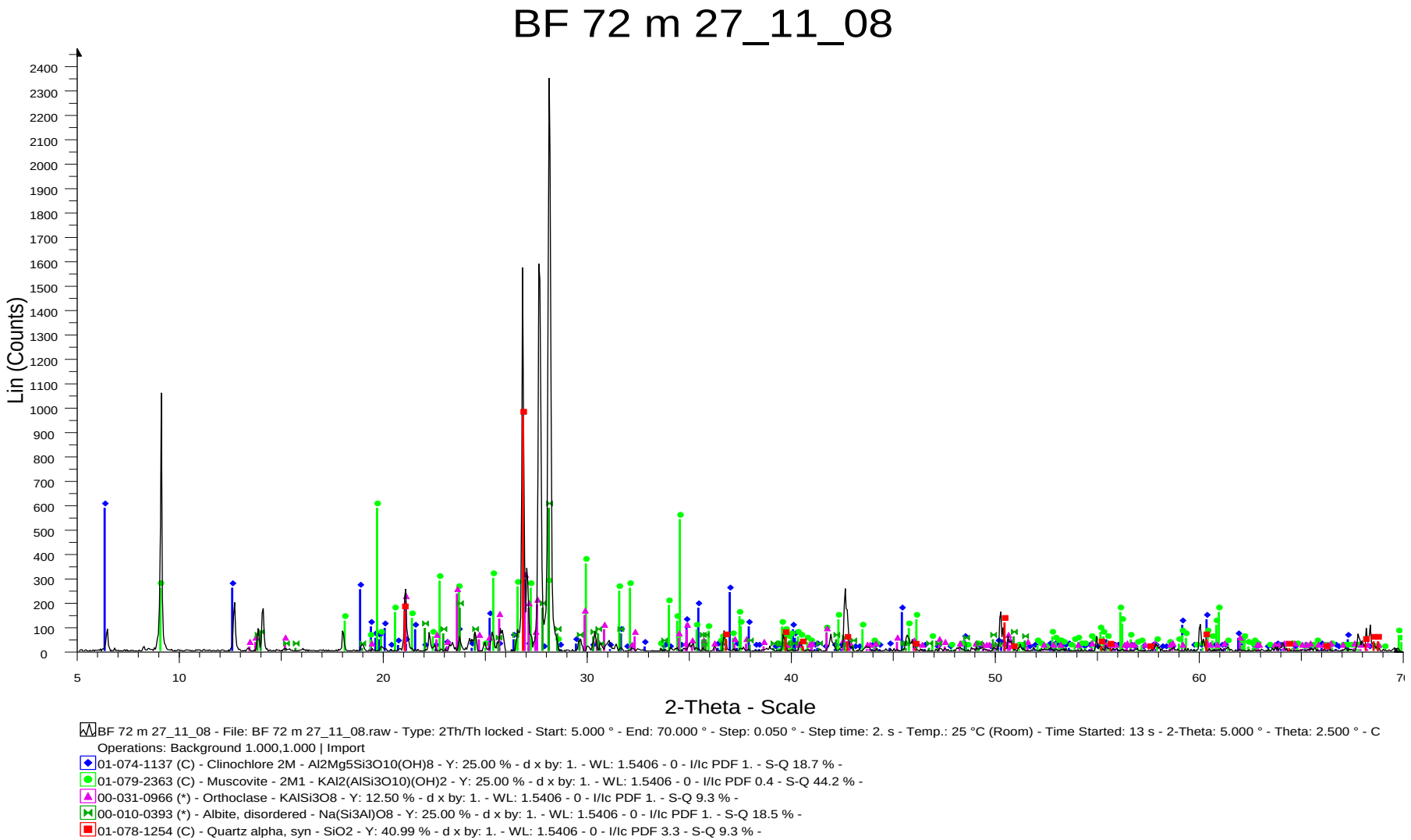

Figure A 1.7 XRD patterns of BF 72 samples

A2.1. Scanning Electron Microscopy

The Scanning Electron Microscopy (SEM) is routinely used to generate high-resolution images of shapes of objects and to show spatial variations in chemical compositions. This technique is also widely used to identify phases based on qualitative chemical analysis and/or crystalline structure.

A2.2 Fundamental Principles of Scanning Electron Microscopy

The scanning electron microscope (SEM) uses a focused beam of high-energy electrons to generate a variety of signals at the surface of solid specimens. The signals that derive from electron-sample interactions reveal information about the sample including external morphology (texture), chemical composition, and crystalline structure and orientation of materials making up the sample. Accelerated electrons in an SEM carry significant amounts of kinetic energy, and this energy is dissipated as a variety of signals produced by electron-sample interactions when the incident electrons are decelerated in the solid sample. These signals include secondary electrons (that produce SEM images), backscattered electrons (BSE), diffracted backscattered electrons (EBSD that are used to determine crystal structures and orientations of minerals), photons-particles that transmit light (characteristic X-rays that are used for elemental analysis and continuum X-rays), visible light (cathodoluminescence–CL), and heat. Secondary electrons and backscattered electrons are commonly used for imaging samples: secondary electrons are most valuable for showing morphology and topography on samples and backscattered electrons are most valuable for illustrating contrasts in composition in multiphase samples (i.e. for rapid phase discrimination).

X-ray generation is produced by inelastic collisions of the incident electrons with electrons in discrete ortitals (shells) of atoms in the sample. As the excited electrons return to lower energy states, they yield X-rays that are of a fixed wavelength (that is related to the difference in energy levels of electrons in different shells for a given element). Thus, characteristic X-rays are produced for each element in a mineral that is "excited" by the electron beam. SEM analysis is considered to be "non-destructive"; that is, x-rays generated by electron interactions do not lead to volume loss of the sample, so it is possible to analyze the same materials repeatedly.

Most SEM's are comparatively easy to operate, with user-friendly "intuitive" interfaces. Many applications require minimal sample preparation. For many applications, data acquisition is rapid (less than 5 minutes/image for SEI, BSE, spot EDS analyses.) Modern SEMs generate data in digital formats, which are highly portable. The SEM is also capable of performing analyses of selected point locations on the sample; this approach is especially useful in qualitatively or semi-quantitatively determining chemical compositions, crystalline structure, and crystal orientations.

SEM's cannot detect very light elements (H, He, and Li). Most SEMs use solid state x-ray detector (EDS), and while these detectors are very fast and easy to utilize, they have relatively poor energy resolution and sensitivity to elements present in low abundances when compared to wavelength dispersive x-ray detectors (WDS) on most electron probe microanalyzers (EPMA).

The petro-texture and the mineralogy of the rocks utilized in the lab tests and the chemistry, and the morphology of the minerals were performed on polished sections carried out from selected samples. Observations were firstly taken by using a scanning electron microprobe (SEM) (FEI Quanta 400 MK2 model) at 15 kV and point-beam 1-5 µm in size operative conditions. The operating conditions (magnification, chamber pressure, spot diameter, voltage, detector type, sample distance from detector) are reported in the sections photos

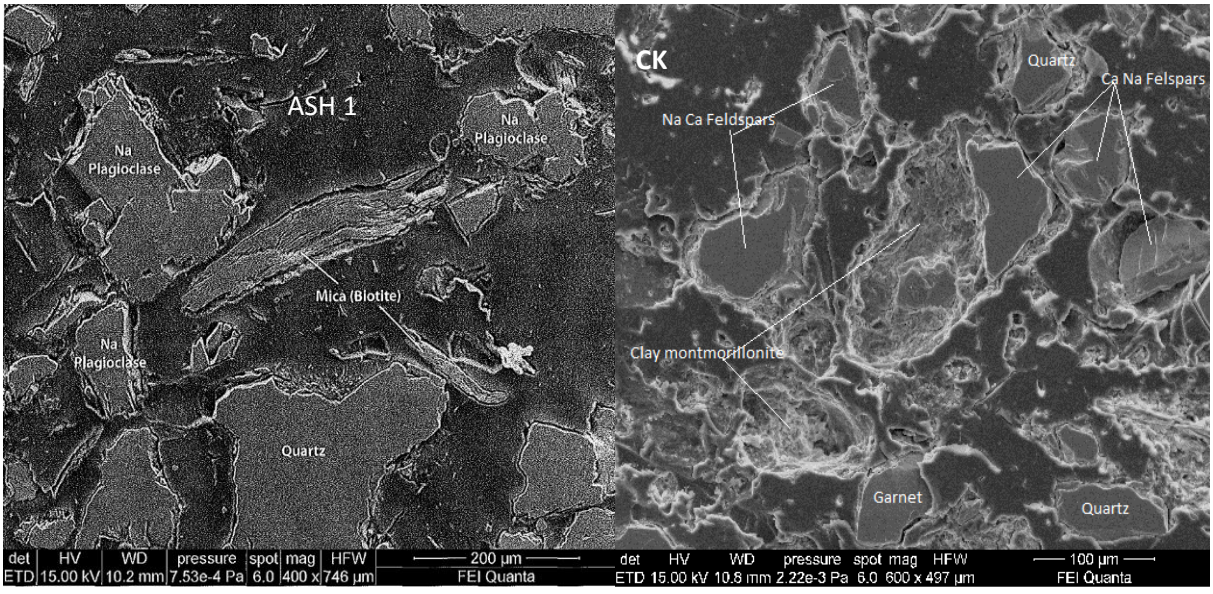

Figure B1.1 SEM pattern of ASH 1 and CK samples

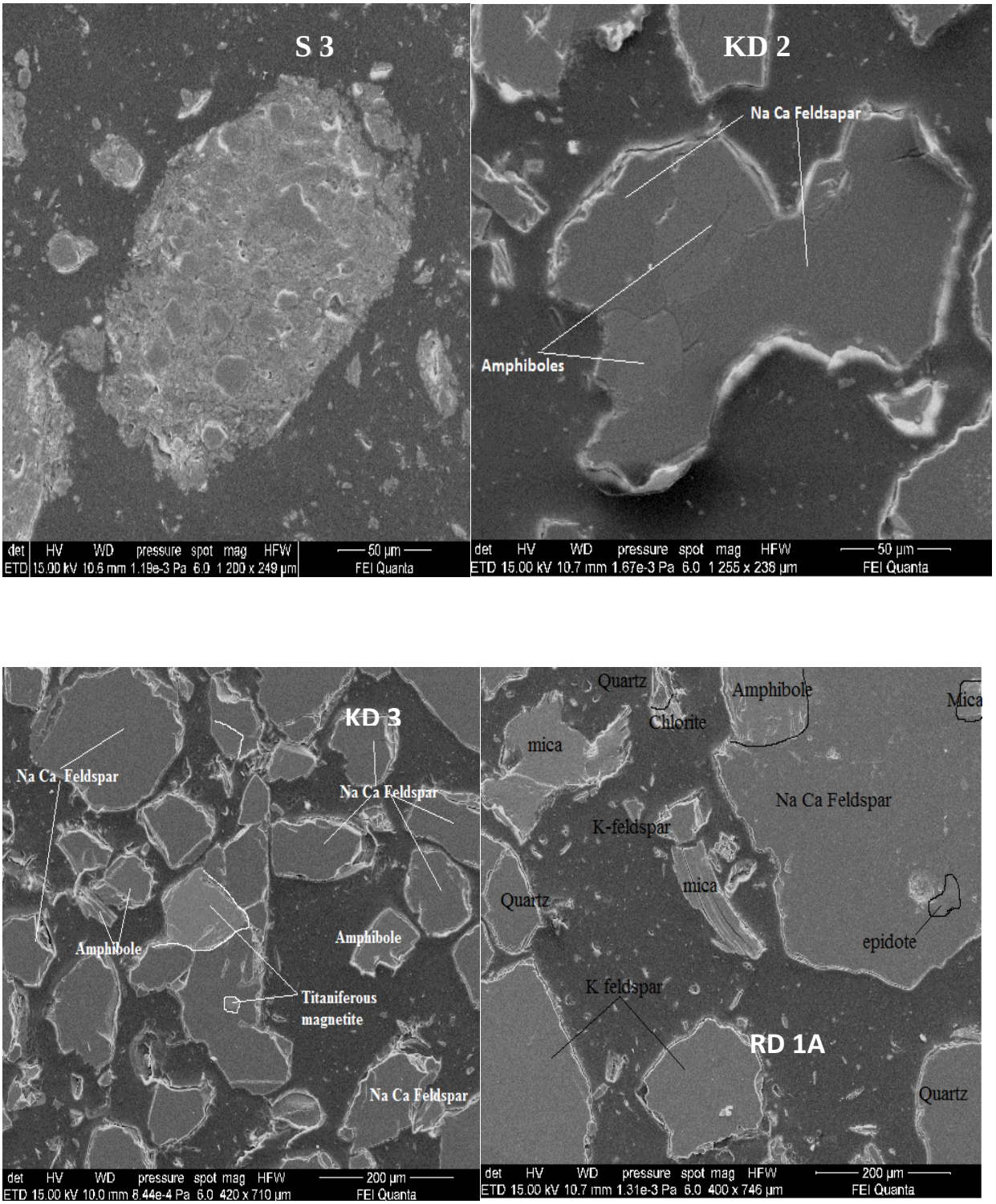

Figure B1.2 SEM pattern of S3, KD 2, KD3 and RD 1A samples

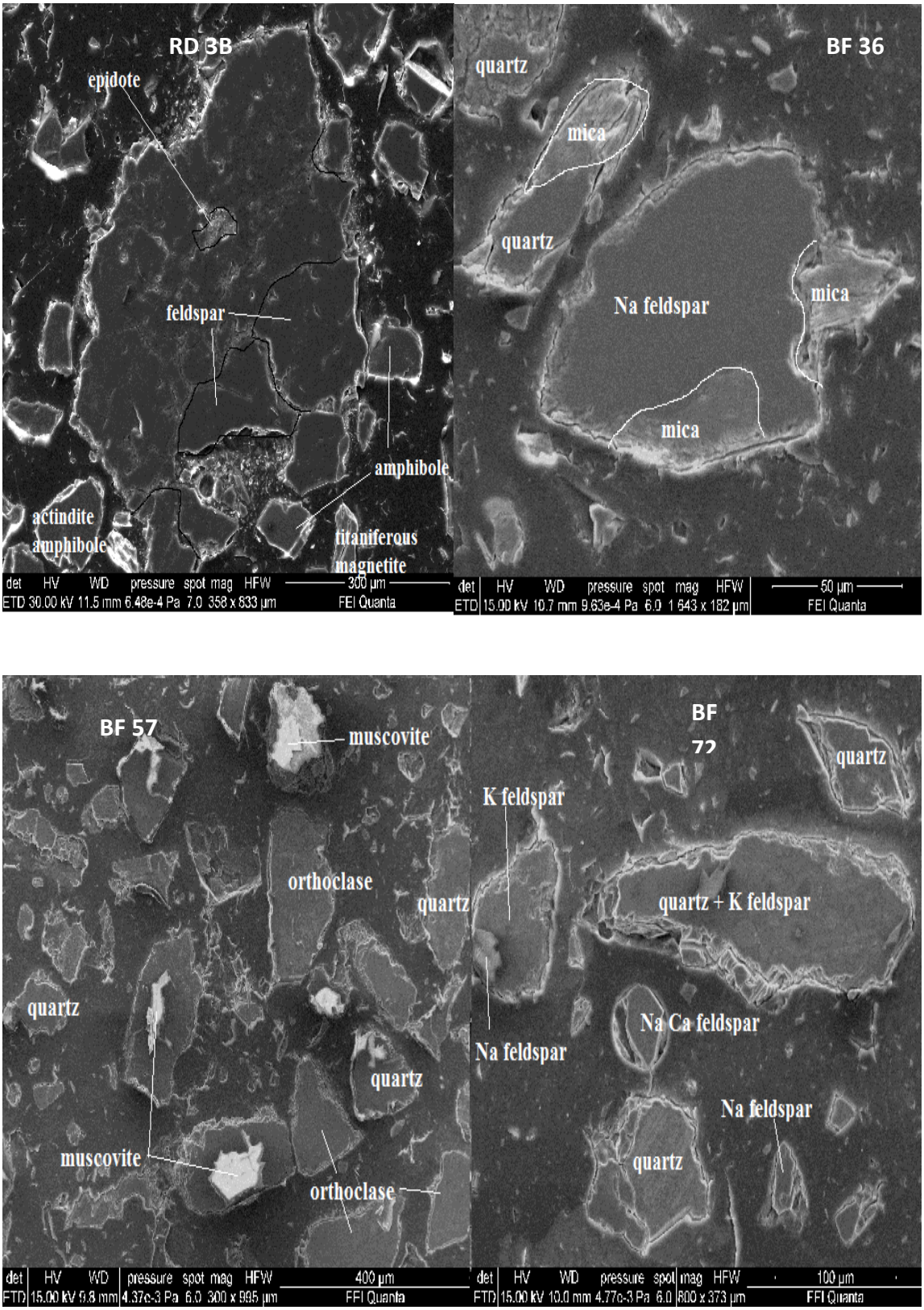

Figure B 1.3 SEM patterns of RD 3B, BF 36, BF 57 and BF 72 samples

A3.1. Electron Microprobe Analysis

Electron microprobe analysis (EMPA), or electron probe microanalysis, is an analytical technique that is used to establish the chemical composition of small areas on solid-state materials at the micron scale. The specimen is bombarded with a beam of accelerated electrons. The electron beam is focused on the surface of the specimen using a series of electromagnetic lenses and the energetic electrons produce characteristic X-rays within a small volume (typically between one and nine cubic microns) of the specimen. This volume is known as the interaction volume of the electrons. The electrons are scattered elastically, resulting in an 'excitation volume' much larger than the actual diameter of the beam. This volume usually has a diameter on the order a several microns. The characteristic X-rays are detected at particular wavelengths, and their intensities are measured to determine concentrations. All elements (except hydrogen, helium, and lithium) can be detected because each element has a specific set of X-rays that it emits. A variety of inelastic scattering event also occurs, yielding information about the chemistry and structure of the target.

Electron microprobes are outfitted with wavelength dispersive spectrometers (WDS), and in many if not most cases have an energy dispersive one (EDS) as well. WDS operates with a small fraction of the X-rays that escape from the sample, reaching a crystal, and a particular wavelength will be diffracted at a particular angle (the Bragg angle) into a gas-filled amplification tube, where a pulse is produced that is proportional to the energy of the X-ray. A WDS spectrometer is tuned to one wavelength and sits there and counts the numbers of X-rays. You might compare it to a serial information source, getting one channel of information at a time.

EDS, on the other hand, looks at all the X-rays coming off the sample, and stretching the analogy, is a parallel information gathering device, collecting all the different wavelengths. The EDS detector is a solid-state device, where electron-hole pairs are produced for each x-ray that hits it, with the number of pairs a function of the total x-ray energy divided by the energy needed to produce one pair. This small signal is amplified, and then becomes one bit of information in a spectrum gathered for the sample ('multi-channel analyzer').

This analytical technique has a high spatial resolution and sensitivity, and individual analyses are reasonably short, requiring only a minute or two in most cases. Additionally, the electron microprobe can function like a scanning electron microscope (SEM) and obtain highly magnified images of a sample. The small interaction volume of EMPA permits the collection of highly localized compositional data and to examine specimens too small to be studied with other analytical techniques. In addition, it allows for the determination of the chemical variability over the surface of a sample. Consequently, EMPA is well-suited to study specimens composed of mixed phases that one wishes to resolve and analyze in situ, leaving the contextual relationships of the phases unaltered and visible.

Although electron probes have the ability to analyze for almost all elements, they are unable to detect the lightest elements (H, He and Li); as a result, for example, the "water" in hydrous minerals cannot be analyzed. Some elements generate x-rays with overlapping peak positions (by both energy and wavelength) that must be separated. Microprobe analyses are reported as oxides of elements, not as cations; therefore, cation proportions and mineral formulae must be recalculated following stoichiometric rules. Probe analysis also cannot distinguish between the different valence states of Fe, so the ferric/ferrous ratio cannot be determined and must be evaluated by other techniques

A3.2 Sample Preparation

Mineral grains or rock chips were mounted in 1-inch epoxy disk. and then polished to expose a cross-section of the material. The sample is fine polish so that surface imperfections do not interfere with electron-sample interactions. This is particularly important for samples containing minerals with different hardnesses. The polishing yields a flat surface of uniform smoothness.

Most silicate minerals are electrical insulators. Directing an electron beam at the sample can lead to electrical charging of the sample, which must be dissipated. Therefore prior to analyses, the samples were coated with a thin film of a conducting material (carbon) by means of evaporative deposition. The carbon coating is thin and light enough that interference with the electron beam and emitted X-rays is minimal.

Samples were then loaded into the sample chamber via a vacuum interlock and mounted on the sample stage. The sample chamber is then pumped to obtain a high vacuum. A CAMECA SX 50 electron microprobe, equipped with five spectometers (EMPA-WDS, Electro Probe X-Ray Microanalyzer and BSE-back-scattered electron) was used to determine the mineral chemistry of the samples.

TableA1.1: EPMA of magnetite in the samples

	KD 1		KD 2	RD 1A		BF 57	BF 72	ASH 1		
SiO_2	0.031	0.064	0.367	6.306	8.449	0.153	0.124	0.011	0.038	0.261
TiO_2	0.068	0.021	0.183	0.000	0.247	0.000	0.000	0.349	1.045	0.276
Al_2O_3	0.152	0.264	0.092	0.716	2.125	0.090	0.017	0.062	0.030	0.135
Cr_2O_3	0.007	0.069	0.109	0.000	0.015	0.201	0.000	0.010	0.017	0.012
MgO	1.894	0.01	0.026	0.287	1.610	0.002	0.000	0.000	0.000	0.020
CaO	0.168	0.122	0.220	0.130	0.149	0.000	0.000	0.014	0.025	0.056
MnO	0.593	0.000	0.077	0.129	0.131	0.022	0.000	0.042	0.025	0.017
FeO	89.717	89.994	87.098	71.130	67.28	91.488	88.168	88.225	87.821	85.841
Na_2O	0.015	0.032	0.006	0.019	0.046	0.000	0.006	0.004	0.019	0.022
K_2O	0.000	0.000	0.000	0.046	1.046	0.074	0.010	0.053	0.013	0.037
Total	92.645	90.576	88.178	78.763	81.098	92.03	88.325	88.77	89.033	86.677
Cations				Based on 24 Oxygens						
Si	0.009	0.020	0.118	2.043	2.513	0.048	0.040	0.004	0.012	0.086
Ti	0.015	0.005	0.044	0.000	0.055	0.000	0.000	0.085	0.251	0.068
Al^{iv}	0.000	0.000	0.000	0.274	0.745	0.033	0.007	0.023	0.011	0.052
Al^{vi}	0.054	0.098	0.035	0.000	0.000	0.000	0.000	0.000	0.000	0.000
Cr	0.002	0.017	0.028	0.000	0.004	0.049	0.000	0.003	0.004	0.003
Mg	0.858	0.005	0.012	0.138	0.714	0.001	0.000	0.000	0.000	0.010
Ca	0.055	0.041	0.076	0.045	0.047	0.000	0.000	0.005	0.009	0.020
Mn	0.153	0.000	0.021	0.035	0.033	0.006	0.000	0.011	0.007	0.005
Fe^{3+}	0.119	0.103	0.158	0.121	0.395	0.000	0.000	0.020	0.003	0.012
Fe^{2+}	22.678	23.618	23.311	19.149	16.340	23.760	23.906	23.736	23.425	23.552
Na	0.009	0.020	0.003	0.012	0.027	0.000	0.004	0.003	0.012	0.011
K	0.000	0.000	0.000	0.019	0.397	0.029	0.004	0.022	0.005	0.014
Total	23.952	23.927	23.806	21.836	21.270	23.926	23.961	23.912	23.739	23.833

Table A1.2: EPMA of titaniferous magnetite in the samples

	KD 2				RD 3	CK 1
SiO_2	0.046	0.001	0.045	0.010	0.000	0.096
TiO_2	27.769	24.964	20.215	36.710	24.422	26.754
Al_2O_3	0.096	0.101	0.230	0.000	0.158	0.230
Cr_2O_3	0.070	0.107	0.128	0.027	0.143	0.102
MgO	0.109	0.202	0.032	0.461	0.105	0.207
CaO	0.079	0.042	0.059	0.035	0.000	0.040
MnO	0.130	0.062	0.065	0.327	0.000	0.143
FeO	72.079	74.036	78.842	61.862	75.021	72.158
Na_2O	0.020	0.053	0.000	0.011	0.003	0.000
K_2O	0.000	0.000	0.000	0.004	0.000	0.000
Total	100.398	99.568	99.616	99.447	99.852	99.73
Cations	Based on 24 Oxygens					
Si	0.013	0.000	0.012	0.002	0.000	0.025
Ti	3.878	3.171	4.202	6.539	4.004	5.263
Al^{iv}	0.000	0.000	0.000	0.000	0.000	0.000
Al^{vi}	0.033	0.034	0.075	0.000	0.051	0.071
Cr	0.016	0.024	0.028	0.005	0.031	0.021
Mg	0.047	0.085	0.013	0.163	0.043	0.081
Ca	0.025	0.013	0.017	0.009	0.000	0.011
Mn	0.032	0.015	0.015	0.066	0.000	0.032
Fe^{3+}	0.059	0.053	0.038	0.024	0.002	0.021
Fe^{2+}	15.977	17.392	15.332	10.645	15.823	13.141
Na	0.011	0.029	0.000	0.005	0.001	0.000
K	0.000	0.000	0.000	0.001	0.000	0.000
Total	20.091	20.816	19.732	17.459	19.955	18.666

TableA1.3: EPMA of rutile in the samples

	RD 2C		BF 57	BF 72	CK 1		
SiO_2	0.024	0.000	1.643	0.751	0.000	0.048	0.030
TiO_2	99.885	99.526	95.997	96.683	98.947	98.026	98.849
Al_2O_3	0.000	0.000	0.000	0.204	0.000	0.000	0.000
Cr_2O_3	0.043	0.120	0.031	0.042	0.152	0.208	0.128
MgO	0.000	0.012	0.014	0.025	0.000	0.011	0.000
CaO	0.017	0.021	0.620	0.148	0.023	0.157	0.086
MnO	0.000	0.000	0.000	0.000	0.041	0.052	0.017
FeO	0.178	0.190	1.067	1.982	0.073	0.641	0.334
Na_2O	0.007	0.000	0.021	0.033	0.015	0.006	0.000
K_2O	0.000	0.000	0.016	0.027	0.000	0.000	0.000
Total	100.154	99.869	99.409	99.895	99.251	99.149	99.444
Cations				Based on 24 oxygens			
Si	0.004	0.000	0.269	0.126	0.000	0.008	0.005
Ti	11.978	11.972	11.596	11.680	11.974	11.909	11.951
Al^{iv}	0.000	0.000	0.000	0.000	0.000	0.000	0.000
Al^{vi}	0.000	0.000	0.000	0.040	0.000	0.000	0.000
Cr	0.005	0.015	0.004	0.006	0.020	0.027	0.017
Mg	0.000	0.003	0.004	0.006	0.000	0.003	0.000
Ca	0.003	0.004	0.109	0.027	0.004	0.027	0.015
Mn	0.000	0.000	0.000	0.000	0.006	0.007	0.002
Fe^{3+}	0.009	0.008	0.000	0.000	0.000	0.002	0.000
Fe^{2+}	0.015	0.018	0.146	0.278	0.010	0.085	0.046
Na	0.002	0.000	0.007	0.011	0.005	0.002	0.000
K	0.000	0.000	0.003	0.006	0.000	0.000	0.000
Total	12.016	12.020	12.138	12.180	12.019	12.070	12.036

Table A1.4: EPMA of sphene in the samples

	RD 1A				BF 36	ASH 1	
SiO_2	30.59	30.622	30.449	30.694	30.767	30.461	30.894
TiO_2	37.757	37.405	34.558	31.939	35.965	35.608	35.697
Al_2O_3	0.977	1.143	2.983	4.772	1.484	2.130	2.081
Cr_2O_3	0.024	0.012	0.012	0.043	0.000	0.002	0.017
MgO	0.000	0.011	0.000	0.043	0.01	0.000	0.023
CaO	28.642	28.857	28.947	29.391	28.853	29.174	29.183
MnO	0.050	0.074	0.050	0.071	0.018	0.113	0.065
FeO	0.666	0.993	1.181	1.814	1.053	1.173	1.041
Na_2O	0.029	0.022	0.028	0.015	0.042	0.040	0.000
K_2O	0.015	0.006	0.004	0.028	0.098	0.000	0.004
Total	98.75	99.145	98.212	98.81	98.29	98.701	99.005
Cations					Based on 24 Oxygens		
Si	4.860	4.854	4.864	4.876	4.917	4.854	4.897
Ti	4.511	4.459	4.152	3.816	4.322	4.267	4.255
Al^{iv}	0.183	0.214	0.562	0.894	0.279	0.400	0.389
Al^{vi}	0.000	0.000	0.000	0.000	0.000	0.000	0.000
Cr	0.003	0.002	0.002	0.005	0.000	0.000	0.002
Mg	0.000	0.003	0.000	0.010	0.002	0.000	0.005
Ca	4.876	4.901	4.955	5.003	4.940	4.981	4.956
Mn	0.007	0.010	0.007	0.010	0.002	0.015	0.009
Fe^{3+}	0.006	0.000	0.000	0.000	0.004	0.001	0.003
Fe^{2+}	0.082	0.132	0.158	0.241	0.137	0.155	0.135
Na	0.009	0.007	0.009	0.005	0.013	0.012	0.000
K	0.003	0.001	0.001	0.006	0.020	0.000	0.001
Total	14.540	14.583	14.710	14.866	14.636	14.685	14.652

Table 1.5: EPMA of Spinel in the samples

	RD 2C						BF 12	BF 72	CK 1
SiO_2	6.441	6.015	14.996	2.464	5.027	2.212	1.631	1.831	10.544
TiO_2	0.185	0.133	0.225	0.175	0.503	0.472	0.079	0.086	0.574
Al_2O_3	9.903	9.856	18.238	11.04	20.838	10.596	0.137	0.183	12.570
Cr_2O_3	0.062	0.073	0.673	0.322	0.407	0.127	23.790	29.991	0.000
MgO	0.023	0.087	0.077	0.193	0.19	0.351	0.024	0.267	0.765
CaO	0.009	0.135	0.061	0.041	0.204	0.095	0.053	1.018	0.934
MnO	0.023	0.000	0.07	0.036	0.013	0.000	1.708	1.758	45.572
FeO	62.827	63.568	48.126	62.231	52.933	64.21	78.215	70.919	5.443
Na_2O	0.004	0.003	0.013	0.038	0.036	0.006	0.000	0.013	0.130
K_2O	0.004	0.042	0.004	0.020	0.025	0.024	0.042	0.078	0.074
Total	79.481	79.912	82.483	76.56	80.176	78.093	105.679	106.144	76.606
Cations						Based on 24 Oxygens			
Si	1.854	1.735	3.465	0.763	1.298	0.677	0.396	0.431	2.823
Ti	0.040	0.029	0.039	0.041	0.098	0.109	0.014	0.015	0.116
Al^{iv}	0.000	0.000	0.000	0.000	0.000	0.000	0.000	0.051	0.000
Al^{vi}	3.361	3.351	4.966	4.027	6.340	3.825	0.039	0.000	3.966
Cr	0.014	0.017	0.123	0.079	0.083	0.031	4.568	5.577	0.000
Mg	0.010	0.038	0.027	0.089	0.073	0.160	0.009	0.094	0.305
Ca	0.003	0.042	0.015	0.014	0.056	0.031	0.014	0.257	0.268
Mn	0.006	0.000	0.014	0.009	0.003	0.000	0.351	0.350	10.335
Fe^{3+}	0.008	0.096	0.037	0.057	0.140	0.076	0.044	0.000	0.628
Fe^{2+}	15.121	15.238	9.262	16.050	11.288	16.370	15.843	13.951	0.591
Na	0.002	0.001	0.006	0.023	0.018	0.004	0.000	0.006	0.067
K	0.001	0.015	0.001	0.008	0.008	0.010	0.013	0.023	0.025
Total	20.420	20.562	17.955	21.160	19.405	21.293	21.291	20.755	19.124

APPENDIX II
GEOCHEMICAL ANALYSES

B1.1 Chemical Analysis of Groundwater

The physical parameters of the groundwater were measured in the field and included the parameters electrical conductivity, pH, temperature and total dissolved solids. The samples were collected in 250ml polyethylene, acid washed bottles for analysis of chemical parameters in the laboratory. The samples were transported to the laboratory in an ice chest maintained at a temperature of 4 ^{o}C. The samples were subsequently filtered in the laboratory with a 0.45µm pore size filters. Each sample was divided into two samples. One sample was acidified with nitric acid for cation analysis whilst the one was preserved for anion analysis.

The groundwater samples were analysed for the major cations using inductively coupled plasma atomic emission spectrometer (ICP-AES) whilst the anions (Cl^{-},SO_4^{2-},NO_3^{-}) were analysed by Ion chromatography. The anion HCO_3, was analysed by titration. The analyses were checked by calculating the cation-anion balance for each sample.

B1.2. Cation Analyses

The major cations analysed were Na, K, Ca and Mg. They were analysed by a Perkin Elmer inductively coupled plasma emission spectrometer (ICP-ES).Silica although not in ionic form in groundwater, was also analysed with this suite of cations. The instrument was calibrated using synthetic standards. The detection limits used are shown in table B1.1.

B1.2.1 Sample Preparation

No sample preparation was required as the groundwater samples were prefiltered and acidified and therefore did not need acid digestion

Table B1.1 Cation Detection limits

Elements	Minimum Detection Limits
Na	0.015 mg/L
K	0.20mg/L
Mg	0.009mg/L
Ca	0.06mg/L
Si	0.18mg/L

B1.2.2.Theory of Operation

Inductively Coupled Plasma-Atomic Emission Spectrometry (ICP-AES) is one of the most common techniques for elemental analysis. Its high specificity, multi-element capability and good detection limits result in the use of the technique in a large variety of applications (Warra and Jimoh, 2011). ICP-AES utilizes plasma as the atomization and excitation source (MiPlaza Materials Analysis 2008). Plasma is an electrically neutral, highly ionized gas that consists of ions, electrons, and atoms.

The technique involves the groundwater sample being aspirated into plasma. The intensity of characteristics wavelength emitted by the excited analyte ions in the plasma are measured by a spectrophotometer. The measured intensity is proportional to the concentration of the ion in the sample being determined

B1.3. Anion Analyses

The anions –Chloride, sulfate and nitrate were determined by ion chromatography (IC) using a Dionex DX300 ion chromatograph with suppressed conductivity detection. The system utilized Dionex AS14 analytical column and AG14 guard column. Conductivity suppression was by a micromembrane suppressor, Dionex CMMS-II. The detection limits used are shown in table 2.2. The working range was based on a combination of standard concentration range and instrument working range.

Table B 1.2 Anion Detection Limit

Element	Detection Limits
Cl	0.5 mg/L
SO^{2-}_4	0.5mg/L
NO_3^-	0.05mg/L

B.1.3.1. Ion Chromatographic Process

Chromatography is a separation method based on the affinity difference between two phases, the stationary and mobile phases. A sample is injected into a column, either packed or coated with the stationary phase, and separated by the mobile phase based on the difference in interaction (distribution or adsorption) between compounds and the stationary phase. Compounds with a low affinity for the stationary phase move more quickly through the column and elute earlier. The compounds that elute from the end of the column are determined by a suitable detector. Colorimetric, electrometric or titrimetric detectors can be used for determining individual anions. In suppressed ion chromatography, anions are converted to their highly conductive acid forms; in the carbonate bicarbonate eluant, anions are converted to weakly conductive carbonic acid. The separated acid forms are measured by conductivity and identified on the basis of retention time as compared with their standards (Omar, 2000; Alsudani, *et al*., 2009).

In ion chromatography, an ion exchanger is used as the stationary phase, and the eluant for determination of anions is typically a dilute solution of sodium hydrogen carbonate and sodium carbonate.

The sample is introduced in the flowing stream and carried into the anion exchange column. Ions interact with the ion exchange sites on the stationary phase in the column. Mobile phase ions compete with the sample ions for ion exchange sites on the column. Separation depends upon the different ions having different affinities for phases. In the case of anion separations the differing affinities for stationary and mobile phases are due to the ionic charge and ion size of each anion species. Once anions are separated the concentration of each species present in the sample is

measured using a conductivity detector. A chromatograph displays peaks in conductivity at various retention times. Each anionic species is identified by its retention time which remains constant throughout successive runs.

B1.3.2. Sample Preparation

Disposable syringe filters with 0.45 mm membrane were used to filter the samples were filtered before analyses to ensure that any particulate material from the samples don't make their way onto the injection valve or the analytical column where they can cause blockages and considerably reduce the lifetime of the column(s).

B1.3.3. Reagent

3.5 mM Na_2CO_3/1.0mM $NaHCO_3$. Prepare diluting the 100x concentrate 100 fold (i.e. pipette 10mL of 100x concentrate into 1000mL volumetric flask and dilute to the mark with ultra-pure water). Fill eluent bottle with this solution and sparge with argon for at least ten minutes before starting eluent pump.

Regenerant solution: Add 2.4mL of concn H_2SO_4 to 1000mL of ultra-pure water and dilute further to 2000mLs. Fill regen bottle with this solution recap and allow to pressurize. After several minutes ensure regen solution is flowing through suppressor.

References

Alsudani, H.M.L., Al-Bayati, R.I. and Barbooti, M.M. (2009) Determination of anions by ion chromatography in water samples of Baghdad city, African Journal of Pure and Applied Chemistry Vol. 3 (9), pp. 165-169

MiPlaza Materials Analysis (2008) *Inductively Coupled Plasma- Atomic Emission Spectrometry. (ICP- AES). Koninklijke Philips Electronics. N.V.* P1-4.

Omar MA (2000). MSc. Thesis in Environmental Engineering, Institute of Environmental Science and Engineering, National University of Sciences and Technology, Rawalpindi.

Warra A.A. and Jimoh W.L.O. (2011) Overview of an Inductively Coupled Plasma (ICP) System, International Journal of Chemical Research, ISSN: 0975-3699 & E-ISSN: 0975–9131, Vol. 3, Issue 2, 2011, pp-41-48

APPENDIX III

C 1.1. Gamma ray spectrometry

Gamma ray spectrometry is an analytical method that allows the identification and quantification of gamma emitting isotopes in a variety of matrices. In one single measurement and with little sample preparation, gamma ray spectrometry allows you to detect several gamma emitting radionuclei in the sample. The measurement gives a spectrum of lines, the amplitude of which is proportional to the activity of the radionuclide and its position on the horizontal axis gives an idea on its energy.

C 1.2 Theory and concepts:

A gamma spectroscopy system consists of a detector, electronics to collect and process the signals produced by the detector, and a computer with processing software to generate, display, and store the spectrum. Other components, such as rate meters and peak position stabilizers, may also be included. To minimize the effects of background gamma radiation, the detector is surrounded by a thick lead shielding tube with the desired gamma rays entering at the scintillator end of the tube.

The incident photons create fast electrons which is used to understand the nature the of photon itself. These electrons have maximum energy that is equal to the energy of the incident gamma-ray on that electron. The detection of gamma rays occurs through its interaction with the detecting medium. A gamma-ray will interact with its medium in one of three different ways: photoelectric absorption, Compton scattering, and pair production. These different interactions change their probability of occurring depending on the energy of the gamma-ray and the atomic number of the material.

Because of the fact that the photons themselves are invisible to the detector, a detector needs to have a couple of specific functions. The first is to act as a medium that will have a high probability that an incident gamma-ray will interact within that medium. The second function of the detector is to accurately detect the fast electrons that are created.

C 1.3 Advantages

Gamma ray spectroscopy is rapid analysis technique that requires either no or minimal sample preparation under optimized conditions, provide the required selectivity and sensitivity to quantify in environmental samples, such as soils and sediments. It focuses on nuclear reaction with hydrogen, less noisesigal reactions occur when neutrons slowdown to thermal neutron, this makes it sensitive to material beneath the surface.

C1.4 Disadvantages:

Due to high energy and high penetrating power of gamma rays they are more dangerous because it difficult to prevent them from reaching the researchers body.

APPENDIX IV

PUBLICATIONS

Paper 1

Environmental Stable Isotope Studies of Groundwater in the Accra Plains

E.T.Glover, T.T.Akiti and S. Osae

Elixir Pollution 55 (2013) 12813-12819

ABSTRACT

The environmental stable isotopic (oxygen-18 and hydrogen-2) composition of groundwater in the crystalline geological formation underlying the Accra Plains of South-east Ghana were studied to obtain information on the recharge process. The groundwater had an average isotopic value of –3.19‰ ^{18}O and –14.36‰ ^{2}H. The groundwater recharge takes place in fractures with the occurrence of minor evaporation. The groundwater was also affected by the mixing of various rainfall events and or surface runoff. The groundwaters at Valley View University were more depleted than the other groundwaters in the Plains indicating that the groundwater was recharge at the Akwapim Togo Mountains through preferential channels.

Paper 2

Natural radioactivity in some geological formation in the Accra Plains

E.T.Glover, T.T.Akiti and S. Osae

Elixir Geoscience 50 (2012) 10186-10192

ABSTRACT

The activity concentrations of naturally occurring radionuclides, uranium (^{238}U), thorium (^{232}Th), radium (^{226}Ra) and potassium (^{40}K) were measured in the geological samples collected from the Accra Plains using a high resolution hyper pure germanium (HPGe) detector. The radiological parameters were also calculated. ^{238}U concentration was found to vary from below detection limit to 363.5 Bq/kg. Activity concentration of ^{232}Th varied from below detection limit to 370.41 Bq/kg. The activity concentration of ^{226}Ra ranged from 4.04 Bq/kg to 295.01Bq/kg, whereas, the 40K activity concentration varied from 145 Bq/kg to 2274.3 Bq/kg. The absorbed dose rates varied from 18.27 to 479.26 nGy/h. The annual external effective dose rates ranged from 0.02 to 0.51 mSv/y. The radium equivalent activity (Raeq) varied from 29.15 to 986.42 Bq/kg. Value of external hazard index (Hex) varied from 0.11 to 2.66. Good correlations existed between 232Th and 226Ra activity concentrations and the total activity concentration. The Th/U ratios obtained indicate the metasomatic activity of analyzed radionuclides. The gamma ray radiation hazards due to the radionuclides increased with depth.

Paper 3

Major ion chemistry and identification of hydrogeochemical processes of groundwater in the Accra Plains

E.T.Glover, T.T.Akiti and S. Osae

Elixir Geoscience 50 (2012) 10279-10288

ABSTRACT

Major ion geochemistry was used to characterize the chemical composition of the groundwater in the Accra Plains and to understand its geochemical evolution. Sodium and chloride were the dominant ions in the groundwater. The TDS values increase south eastwards through the central part of the Plains towards the coast. Three hydrochemical facies which evolves from Na-Mg-Ca-Cl-HCO3 to Na-Ca-Cl was identified using the Piper diagram and Chadha proposed rectangular plot. The R-mode factor analysis result show that three factors account for 83.65% of the total variance in the hydrochemistry. Interpretation of the hydrochemical data suggested that mineral (silicate) weathering, cation-exchange and reverse ion–exchange control the chemical composition of the groundwater. The thermodynamic plots indicate that the groundwater is in equilibrium with kaolinite and montmorillonite minerals. The saturation index also indicated that about 47% of the groundwater samples were oversaturated with respect to calcite and dolomite.